# Aerosol effects on microphysical properties of Amazonian clouds

## Dissertation

zur Erlangung des Grades ”Doktor rerum naturalium (Dr. rer. nat.)”
des Fachbereichs 09
Chemie, Pharmazie, Geographie und Geowissenschaften,

verfasst und vorgelegt von
Oliver Lauer
geb. in Frankenthal

Johannes Gutenberg-Universität Mainz

angefertigt am Max-Planck-Institut für Chemie

Mainz, 2022


I hereby declare that I wrote the dissertation submitted without any unauthorized external assistance and used only sources acknowledged in the work. All textual passages which are appropriated verbatim or paraphrased from published and unpublished texts as well as all information obtained from oral sources are duly indicated and listed in accordance with bibliographical rules. In carrying out this research, I complied with the rules of standard scientific practice as formulated in the statutes of Johannes-Gutenberg-Universität Mainz to ensure standard scientific practice.

Mainz, 07.11.2022, Oliver Lauer

# Abstract

Atmospheric aerosol particles fundamentally affect cloud formation and properties by acting as cloud condensation nuclei (CCN) at cloud base and beyond. The effects of aerosols on clouds in theory and processes on small scale are well understood. For real clouds and for a range of atmospheric pollution states, however, the understanding of microphysical processes across the entire cloud structure still bears major open questions. Aircraft studies have accurately measured the aerosol effects on clouds on local scales and for short time periods. Satellite investigations cover large scales for extended periods, but with limited accuracy on microphysical processes at different cloud levels, often covering the cloud tops only. A combination of both,provides a comprehensive picture of aerosol and cloud microphysics on large geographic scales across multiple years, which is crucial to understand the current state and future development of the climate system.

In this thesis, in situ aerosol data and high-resolution satellite observations across multiple years were combined for the atmosphere over the remote Amazon rain forest. Satellite retrieved profiles of the temperature and the effective radius of cloud droplets were used to resolve seasonal changes in fundamental cloud properties. A clear seasonality was found in aerosol and cloud parameters. The fraction of aerosol particles being activated into cloud droplets was high during the pristine wet season, but also during the polluted dry season. It was higher than expected from previous studies. The results show that the cloud formation in the Amazon is both, aerosol- and updraft-sensitive, not just for the low aerosol concentrations in the wet season, but also under the heavy biomass burning smoke influence in the dry season. Our findings shed light on the aerosol-driven changes in fundamental parameters of tropical convective clouds and suggest that the buffering effect of updraft-limited droplet activation at high aerosol concentrations is smaller than expected.

The effects of aerosol particles on cloud properties are not limited to cloud base, but cover the entire vertical cloud structure. Seasonal patterns in the vertical cloud structure were investigated by resolving the distinct microphysical zones of condensational droplet growth, collision and coalescence, secondary droplet activation, the mixed phase of water and ice particles as well as the ice phase. The vertical profiles of the effective radius of cloud particles as a function of temperature differ strongly between the low aerosol conditions during the wet season and the biomass burning smoke dominated dry season. The vertical depth of the cloud microphysical zones is strongly seasonal as well. The seasonality is most pronounced for the condensational growth zone, which is much deeper in the dry season. In contrast, the secondary activation zone plays a more significant role in the wet season. These findings underline that the widely variable aerosol population in the Amazon has profound effects on microphysical processes across the entire vertical profile of convective clouds.

# Zusammenfassung

Atmosphärische Aerosolpartikel beeinflussen die Wolkenbildung und -eigenschaften grundlegend, indem sie als Wolkenkondensationskerne (CCN) an der Wolkenbasis und darüber hinaus wirken. Die Auswirkungen von Aerosolen auf Wolken sind in der Theorie und auf kleinen Prozessskalen gut verstanden. Für reale Wolken und für eine Reihe von atmosphärischen Verschmutzungszuständen ist das Verständnis der mikrophysikalischen Prozesse über die gesamte Wolkenstruktur jedoch noch mit grundlegenden offenen Fragen verbunden. Flugzeugstudien haben die Aerosoleffekte auf Wolken auf lokalen Skalen und für kurze Zeiträume genau gemessen. Satellitenuntersuchungen decken große Skalen über längere Zeiträume ab, jedoch mit begrenzter Genauigkeit auf der Prozessebene, da sie oft nur die Wolkenoberseiten erfassen. Eine Kombination aus beidem, heißt ein Prozessverständnis der Aerosol- und Wolkenmikrophysik auf großen geografischen Skalen über mehrere Jahre hinweg, ist für das Verständnis des aktuellen Zustands und der künftigen Entwicklung des Klimasystems von entscheidender Bedeutung.

In dieser Arbeit wurden In-situ-Aerosoldaten und hochauflösende Satellitenbeobachtungen über mehrere Jahre für die Atmosphäre über dem abgelegenen Amazonasregenwald kombiniert. Mit Hilfe von satellitenbasierten Profilen der Temperatur und des effektiven Radius von Wolkentropfen wurden saisonale Veränderungen grundlegender Wolkeneigenschaften aufgezeigt. Bei den Aerosol- und Wolkenparametern wurde eine deutliche Saisonabhängigkeit festgestellt. Der Anteil der Aerosolpartikel, die in Wolkentropfen aktiviert werden, war sowohl während der sauberen Regenzeit als auch während der verschmutzten Trockenzeit hoch. Er war höher als in früheren Studien erwartet. Die Ergebnisse zeigen, dass die Wolkenbildung im Amazonasgebiet sowohl aerosol- als auch aufwindabhängig ist, und zwar nicht nur bei niedrigen Aerosolkonzentrationen in der Regenzeit, sondern auch unter dem Einfluss von starkem Biomasseverbrennungsrauch in der Trockenzeit. Unsere Ergebnisse geben Aufschluss über die aerosolbedingten Veränderungen grundlegender Parameter tropischer Konvektionswolken und deuten darauf hin, dass der Puffereffekt der aufwindbegrenzten Tropfenaktivierung bei hohen Aerosolkonzentrationen geringer ist als erwartet.

Die Auswirkungen von Aerosolpartikeln auf die Wolkeneigenschaften sind nicht auf die Wolkenbasis beschränkt, sondern umfassen die gesamte vertikale Wolkenstruktur. Die saisonalen Muster in der vertikalen Wolkenstruktur wurden untersucht, indem die verschiedenen mikrophysikalischen Zonen des Kondensationswachstums, der Kollision und Koaleszenz, der sekundären Tropfenaktivierung, der gemischten Phase aus Wasser- und Eispartikeln sowie der Eisphase aufgelöst wurden. Die vertikalen Profile des effektiven Radius von Wolkenpartikeln als Funktion der Temperatur unterscheiden sich stark zwischen den aerosolarmen Bedingungen der Regenzeit und der von Biomasseverbrennung und Rauch dominierten Trockenzeit. Die vertikale

Ausdehnung der mikrophysikalischen Wolkenzonen ist ebenfalls stark saisonabhängig. Am stärksten ausgeprägt ist die Saisonabhängigkeit für die Zone des Kondensationswachstums, die in der Trockenzeit eine tiefere vertikale Ausdehung hat. Im Gegensatz dazu spielt die sekundäre Aktivierungszone in der Regenzeit eine wichtigere Rolle. Diese Ergebnisse unterstreichen, dass die stark variierende Aerosolpopulation im Amazonasgebiet tiefgreifende Auswirkungen auf die mikrophysikalischen Prozesse im gesamten Vertikalprofil der konvektiven Wolken hat.

# Contents

CHAPTER 1

# Introduction

# 1.1 Aerosol particles and cloud condensation nuclei

Aerosols are commonly distinguished by their physical properties (size, shape, hygroscopicity), chemical composition or origin. All of them are intertwined with each other in manifold ways. When classifying aerosols by size the aerosol particle size distribution (PSD) is commonly split in 4 major modes (e.g. Pöschl, 2005; see Fig. 1.1). All of this modes often contain a maximum in their size range, but this is subject to constant change and depends heavily on location, daytime, altitude, precipitation and other environmental factors. When distinguishing aerosols by size, the particles in the different modes often share a similar origin and therefore similar chemical properties.

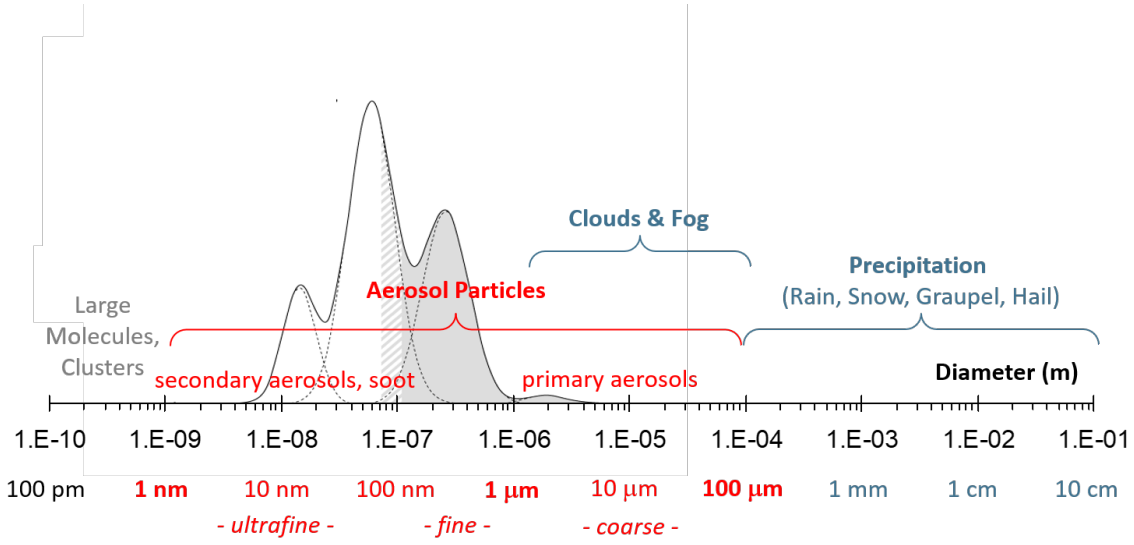


**Figure 1.1:** Illustration of the size range and a typical particle size distribution of atmospheric aerosol particles, cloud droplets and precipitation (Pöschl et al.2005)

.

Starting from smallest to biggest the Nucleation mode covers the smallest aerosols with lifetimes of only seconds to minutes at maximum before particles in this size range accumulate to bigger particles, in this size range secondary aerosols are dominant. Secondary aerosols particles (SAP) describes particles that form in the atmosphere from chemical compounds that react in the gas phase and form molecule structures that eventually grow by further condensation of compounds into a solid particle (e.g. Kulmala et al., 2001; Kulmala et al., 2004). The nucleation modes often refers to particles $< 10\,\mathrm{nm}$.

Next follows the Aitken mode with a size range of up to $100\,\mathrm{nm}$, this includes aged secondary aerosols that grow by conglomeration, as well as soot and other combustion products, like exhaust car emissions. Aitken mode particles typically do not get activated to cloud droplets, but can participate in cloud formation under specific circumstances, for example when supersaturation is high at cloud base and secondary activation above cloud base (e.g. Rosenfeld et al., 2002; Braga et al., 2021; Fan et al., 2018b).

Following next is the accumulation mode. It includes particles up to a size of $1000\,\mathrm{nm}$. In the Accumulation mode secondary particles stop growing quickly and form stable conglomerations that don't undergo more major changes. More primary aerosols are found in this size range, as well as bio aerosols in the form of viruses. Aerosols in this size range are chemically stable and their aerodynamic properties allow them the longest airborne lifetime out of all the Aerosol size range, resulting in them being numerically the biggest fraction of aerosols and play a decisive roe in cloud formation, with their ability to act as cloud condensation nuclei (CCN) (e.g. Williamson et al., 2019; Andreae et al., 2018; Dusek et al., 2010). Convection within clouds can transport this aerosols to the upper troposphere or even the stratosphere, where they can have airborne lifetimes of several month up to years (Kristiansen et al., 2016).

Last is the Coarse mode which covers all aerosols $> 1000\,\mathrm{nm}$, Aerosols in this size range are chemically most diverse and range from sea-spray, minerals, bio aerosols, pollen, to non exhaust car emissions, like break dust and tyre wear. Their longevity in the airborne state is limited by their size, but Coarse mode particle are the biggest mass fraction out of all aerosols even though their number fraction is low. They play an important roll in rain formation as giant aerosols, or ice formation, where especially dust and bio aerosols act as ice nucleating particles (INP) (e.g. Schnell and Vali, 1972; Spracklen and Heald, 2014; Tobo et al., 2013).

Aerosols are removed from the atmosphere in two ways either by wet or dry deposition. Dry deposition means deposition by gravity and mostly effects large aerosols, that do no longer experience enough aerodynamic drag compared to their gravitational pull to stay airborne. Wet deposition on the other hand includes 2 major mechanisms, direct and indirect wet deposition. Direct wet deposition includes CCN, aerosols that activated to cloud droplets and deposit in form of precipitation, while indirect wet deposition includes the aerosols that get collected by precipitation on their way to the ground.

The interaction of aerosol particles with water vapor is described by the Köhler theory (Köhler, 1936). It combines the curvature (Kelvin) effect describing the enhancement of water vapor pressure above a curved particle surface, and the solute (Raoult) effect accounting for water uptake by hygroscopic particle mass, which is often parameterized by the hygroscopicity parameter $\kappa$ (Petters and Kreidenweis, 2007). The maximum of the Köhler curve represents the critical supersaturation ($S_{\mathrm{crit}}$) above which a particle of a given composition and dry size (critical diameter, $D_{\mathrm{crit}}$) can activate into cloud droplets:

$$S_{crit} = \frac{D_{wet}^3 - D_{crit}^3}{D_{wet}^3 - (1-\kappa)D_{crit}^3} \exp\left(\frac{4\sigma_{s/a}M_w}{RT\rho_w D_{wet}}\right). \tag{1.1}$$

While $D_{\mathrm{wet}}$ is the wet diameter of the particle R is the Rainold number, $\sigma$ is the surface tension where typically the surface tension of water is used, and $\rho$ is the density. Dependent on the shape of the particle size distribution (PSD) in the atmosphere a distinct cutoff particle diameter $D_{\mathrm{crit}}(S,\kappa)$, assuming constant supersaturation and hygroscopicity, exists. In reality the droplet activation is not an ideal step function, due to different particle shapes and different aerosols composition (Pöhlker et al., 2016). The CCN number concentration $N_{\mathrm{CCN}}$ of, especially in the lower troposphere,

has a profound influence on the microphysical processes in clouds, and consequently on many aspects of weather and climate. These interactions have been summarized in a number of review articles addressing in particular the effects of aerosols on climate (e.g. Penner, 1994; Lohmann and Feichter, 2005) as well as on cloud processes and precipitation (McFiggans et al., 2006; D Rosenfeld, 2006; Andreae and Rosenfeld, 2008). Aerosol size distributions are typically described by a log normal function according to Heintzenberg (1994):

$$f_H(D) = \sum_{i=1}^{n} \frac{C_i}{\sqrt{2\pi}\ln(\sigma_i)} \exp\left\{-\left[\frac{\ln\left(\frac{D}{D_i}\right)}{\sqrt{2}\ln(\sigma_i)}\right]^2\right\} \tag{1.2}$$

with $D_i$ as the mode mean geometric diameter, $C_i$ as the integral particle number concentration of the mode, and $\sigma_i$ as the modal geometric standard deviation.

Aerosols that got activated as CCN at cloud base can be processed in clouds by absorption of soluble matter, chemical reactions or collision coalescence. In case the processed aerosol is not removed from the atmosphere by wet deposition and the droplet fully evaporates at cloud top or due to dry air entrainment the resulting cloud processed aerosol particle increased in mass compared to their previous state. Could processing shifts the size of processed particles to larger sizes, widening the accumulation mode and leaving a gap between the aerosols to small to activate as CCN at cloud base in the Aitken mode and the cloud processed aerosols in the accumulation mode. The resulting characteristic gap between the Aitken and the accumulation mode is called the Hoppel minimum (e.g. Hoppel et al., 1996; Krüger et al., 2014).

## 1.2 Cloud microphysics

Coupled cumulus clouds are one of the most common clouds around the globe, as well as over the amazon basin and have a significant impact on radiative forcing. They form at the top of the planetary boundary layer (PBL) as a result of atmospheric instabilities that allow air to rise above the PBL with increasing altitude the pressure of the transported air parcel decreases the resulting expansion cooling reduces the maximum partial pressure of water vapor in said air parcel resulting in an increase of relative humidity. When the humidity increases above the maximum saturation the water vapor starts to condense on present aerosols starting with the biggest, most hydrophilic as described by Equation 1.1.

The amount of water vapor in the atmosphere is limited and particles at cloud base 'compete' for the available water vapor. Consequently the supersaturation decrease after reaching a maximum $S_{\text{max}}$ at cloud base and particles with $S_{\text{crit}}$ higher than $S_{\text{max}}$ shrink again above cloud base as a result to the reduced in-cloud supersaturation . At approx. $100\,\text{m}$ above cloud base the number of droplets become stable and droplets grow adiabatic. A second consequence of the limit of water vapor in air is that the maximum supersaturation at cloud base $S_{\text{max}}$ is generally higher in clean conditions, compared to polluted conditions. This is called the Twomey effect and it fundamentally influences cloud development and cloud properties (Twomey, 1959).The relation between droplet radius ($r_{\text{max}}$) at the maximum supersaturation, the updraft ($w$) and the number concentration of droplets ($N_{\text{d}}$) is described by Pinsky et al. (2012) using the following equation:

$$r_{max} = C\frac{w^{\frac{1}{4}}}{\sqrt{N_d}} \tag{1.3}$$

while $C$ is constant for a specific temperature and density of the particles and water, $r_{\text{max}} = 3.28\,\mu\text{m}$ for $N_{\text{CN}} = 100\,\text{cm}^{-}3$ and $r_{\text{max}} =$ |SI1.04 for a aerosol number concentration $N_{\text{CN}} = 1000\,\text{cm}^{-}3$ (Pinsky et al., 2012). The relation between particles and cloud droplets is often estimated according to Pruppacher and Klett (1997):

$$N_d = N_{CN}S^k \tag{1.4}$$

while $S$ is the supersaturation in the cloud and $k$ depends on the particles size distribution. However the relation between activated droplets and total particles are more accurate by taking into account the aerosol size distribution and the sensitivity of clouds to the particle load. Reutter et al. (2009) have shown that clouds are most sensible to a change in aerosol load for low aerosol number concentrations and high updraft (aerosol limited regime). Clouds are most sensitive to updraft for high aerosol concentrations and low updraft (updraft limited regime). However, Pöhlker et al. (2021) have shown, that also the shape of the aerosol size distribution can plays a important role, in particular for low number concentrations of large particles. While the effect of $\kappa$ again depends on the shape of the aerosol size distribution and the total number concentration, which makes the system even more complex (see Figure 1.2). Following it is useful to calculate droplet number concentrations according to Pöhlker et al. (2021) using a bin resolved micro physical model based

on equation 1.1 and 1.2 instead of using a simple approximation.

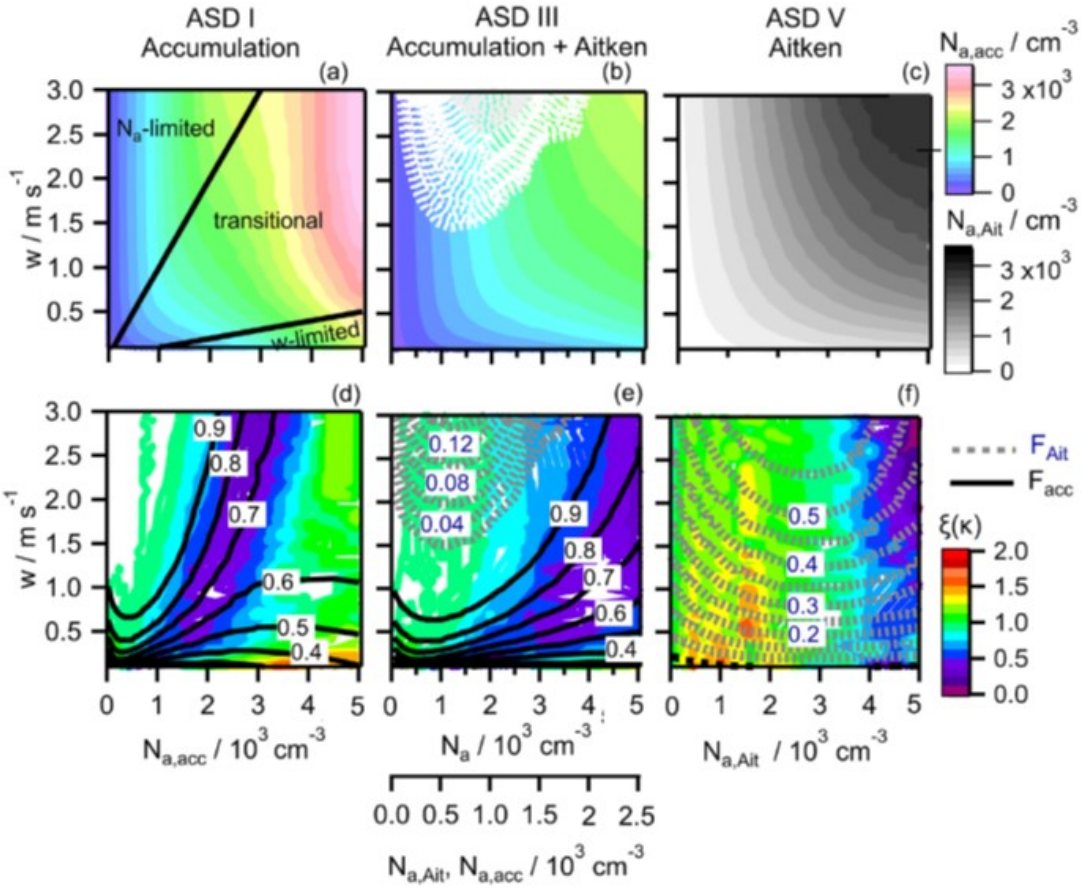


**Figure 1.2:** Figure adopted from Pöhlker et al. (2021). (a)–(c) $N_\mathrm{d}$ as a function of $w$ and $N_\mathrm{CN}$ for $\kappa = 0.7$ (a) only accumulation mode, (b) particles equally distributed between Aitken and accumulation mode, and (c) only Aitken mode. Color scale: $N_\mathrm{CN,acc}$ is the number of particles in the accumulation mode, black/white scale: $N_\mathrm{a,Ait}$ the number of particles in the Aitken mode. (d)–(f) Corresponding sensitivity of $N_\mathrm{d}$ to $N_\mathrm{CN}$ $\xi(N_\mathrm{CN})$. Solid black lines show contours of activated fraction of the accumulation mode ($F_\mathrm{act,acc}$) and dashed grey lines show contours of activated fraction of the Aitken mode ($F_\mathrm{act,Ait}$)

.

The number concentration of natural aerosol sources is low enough that effect on clouds is comparatively high. As described in Section 1.1 aerosol new particle formation is a important source for anthropogenic pollution, but also depending on preexisting particles (Stevens and Feingold, 2009). Following, a low anthropogenic emissions have a larger effect on the aerosol number concentration. Carslaw et al. (2013) show that also the radiative forcing is highest anthropogenic emissions and in addition the uncertainty on modelling the current and future climate largely depends on the uncertainty on understanding the aerosol sensitive cloud regime (1.3). Note that the numbers for the forcing is related to a specific region and differs from a global mean.

While the fundamental physics of the influence of added aerosol particles on $N_\mathrm{d}$ is well described by established theory at the particle scale the effect is poorly investigated at the large-scale (hundreds of kilometres) [Quaas et al. (2020)). This is

one aspect the work done in the scope of this PhD helps to understand the relation between aerosols and clouds using experimental data on a regional scale.

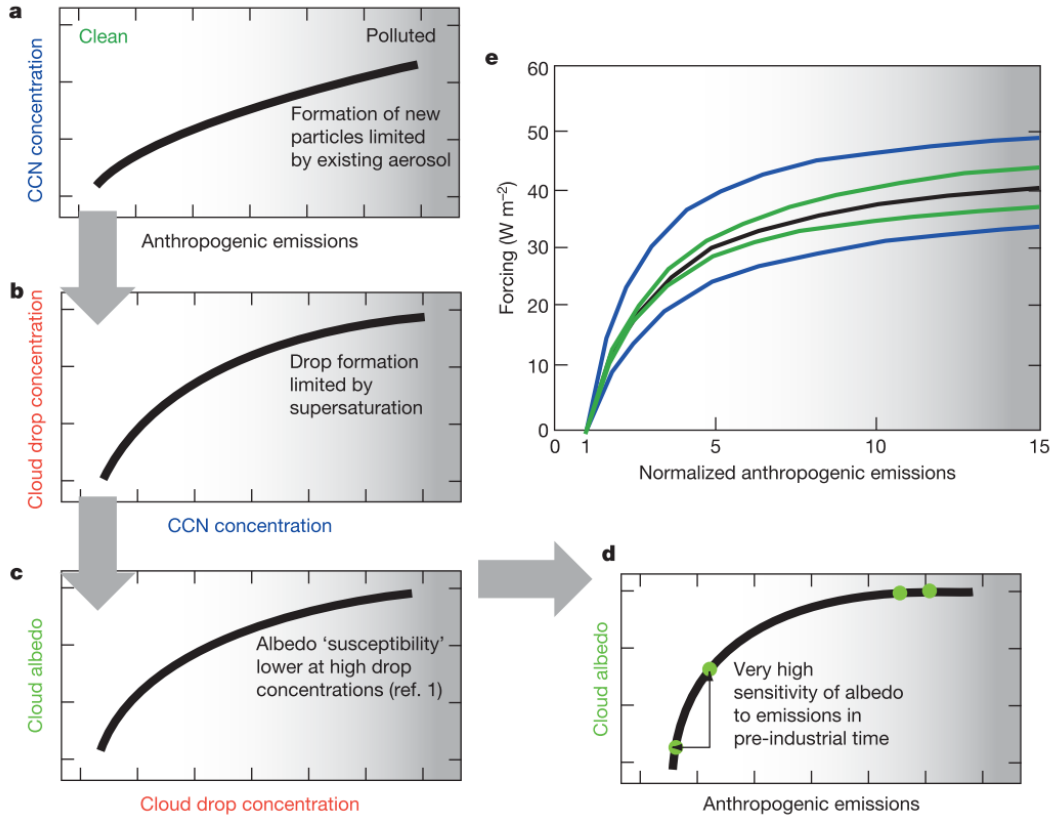


**Figure 1.3:** Adopted from Carslaw et al. (2013), (a) addect of Anthropogenic emissions on total aerosol and CCN number concentration, (b) effect of CCN cumber concentration on $N_{\mathrm{d}}$, (c) effect of $N_{\mathrm{d}}$ on $r_{\mathrm{max}}$ and with this on cloud albedo. (d) summarizes the effects shown in a-c and show the effect of anthropogenic emissions on cloud albedo. (e) shows the related forcing for a specific region and the effect of the error in modeling recent and future climate for a small error in low aerosol regimes in green and blue for a bigger error in low aerosol regimes

.

Aerosol not only influence the properties at cloud base, but also influence the cloud evolution above cloud base (Derksen et al., 2009). At cloud base the maximum supersaturation marks the point in the cloud where water flux of excess water vapor as a result of expansion cooling and surface area available for condensation are in equilibrium. Above the level where the maximum supersaturation is reached the supersaturation drops again, because the growing droplets provide more than enough surface area for continuous condensation. The continuous condensation in the cloud constantly releases latent heat stabilizing the updraft in return, securing the supply with humid air form the boundary layer (Rosenfeld and Lensky, 1998).

After activation the adiabatic droplet growth is characterized by a stable droplet number, a narrow droplet size distribution and constant droplet growth, because no new droplet activation happens above the cloud base. It is called the condensation or diffusion zone (see Fig. 1.4) and reaches from the cloud base to the height where the median droplet size exceeds $14-15\,\mu\mathrm{m}$. At this size coalescence becomes the

dominating microphysical process and droplets will merge into much bigger droplets widening the droplet size distribution and reducing the total droplet number. Due to the merging the median droplet size in the T-Re profile (temperature vs. effective radius) in the coalescence zone growth faster than expected from adiabatic behavior. In the coalescence zone droplets grow to a size that their aerodynamic drag is lower than their gravitational pull leading to warm rain out (Rosenfeld and Lensky, 1998). Therefore the rain onset height typically correlates with the altitude of the coalescence zone. In case a cloud shows warm rain-out, the surface available for condensation at the top of the coalescence zone is strongly depleted, reducing updraft speeds, but also leading to a increase in supersaturation. This new surge of supersaturation at higher altitude can exceed the maximum supersaturation at cloud base, enabling new activation of droplets that couldn't be activated at cloud base or got entrained into the cloud above the cloud base (Fan et al., 2018a; Khain et al., 2012): This effect is mainly investigated in theory and by models and is contend of this PhD by using satellite data in combination with field measurements and models.

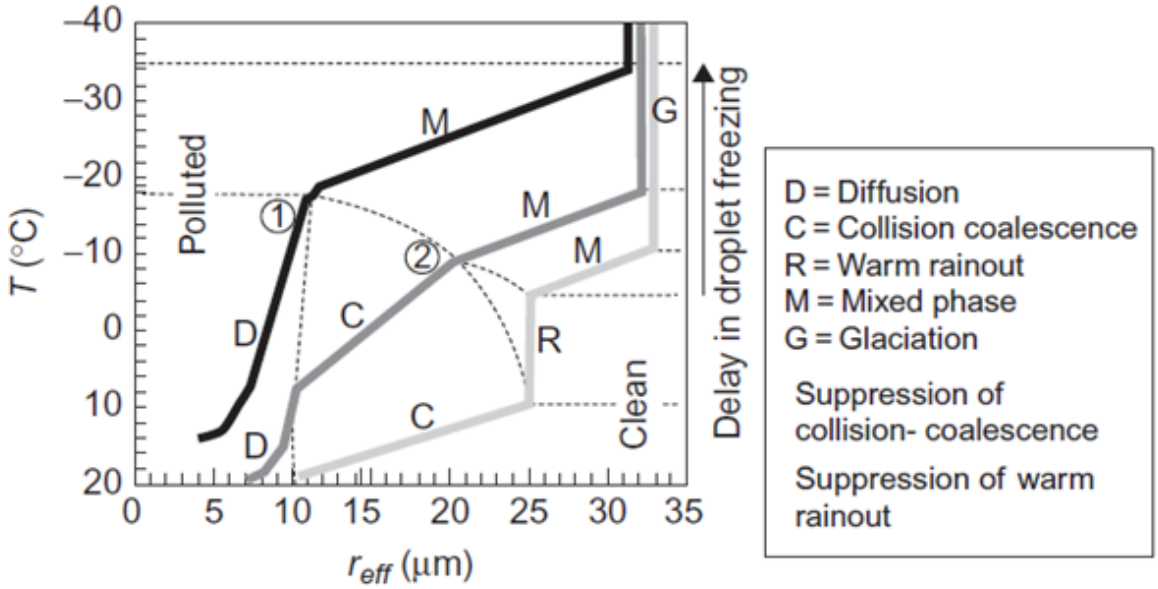


**Figure 1.4:** Figure adopted from Rosenfeld and Lensky (1998), Conceptual diagram of the microphysical zones in convective clouds the vertical evolution of the effective radius with the Temperature.

Clouds do not rain out and rise up to temperatures below $-10\,°C$, ice formation starts. The onset of ice formation largely defence on the availability of particles that can act as ice nuclei (INP) and differs for different regions e.g. Baustian et al., 2012; Hoose et al., 2010). Biologic and dust particles are known to effectively act as INP and following the INP concentration is larger over the continent in comparison to the ocean (e.g. Kunert et al., 2019). As soon as INP initiate the formation of ice crystals the cloud consists of liquid supercooled droplets and ice crystals. This zone is called mix phase zone. The ICE activation initiate an additional updraft and ice crystals can take up water from droplets and not from the gas phase only (Bergeron-Findeisen-Prozess). A large number of small droplets can suppress the rain out in the mix phase

zone and lead to heavy weather (Fan et al., 2018a). On the other hand, enhancement of coalescence in supercooled droplets can enhance the ice precipitation processes. The larger drops freeze faster and at warmer temperatures (Bigg, 1953), and grow faster by riming than drops of comparable mass would have grown by coalescence (Braham, 1964; Johnson, 1987; Pinsky and Khain, 1998) Clouds raising up to $-35\,^{\circ}\mathrm{C}$ start to glaciate also without INP because homogeneous freezing of droplets appears at this temperature. Ice clouds and the effect of INP on clouds and the effect of secondary ice formation is a large field which is not scope of this PhD and therefore only mentioned shortly at this point.

The amount of factors that influence cloud development and behavior make clouds still the biggest contributor to overall uncertainties in global modelling. In addition to the aerosol effect on clouds, clouds are influenced by meteorological parameters like pressure, humidity, temperature, radiation, as well as big and small scale dynamic movement (Lohmann, 2017). However, the effect of aerosols on clouds is still the largest uncertainty (Forster et al., 2021), because these large scale atmospheric systems are well understood and models yields have a high degree of accuracy. Therefore separating aerosol and meteorological influence is not the right approach to quantify cloud radiative effects (Lohmann, 2017). Aerosol effects on clouds influence global circulation systems and the thermodynamic and radiative energy budgets on local and global scale (Rosenfeld et al., 2014a).

The high number of independent parameters on cloud properties make cloud observation especially challenging and limits detailed cloud studies in time and scale, consequently large scale analysis are limited by the accessibility and accuracy of large scale satellite measurements. Satellite measurements of Aerosol properties are lacking in detail compared the meteorological measurements. It is not possible to receive information about the chemical or size composition of aerosols via satellite, while the aerosol concentration can be inferred from the Aerosol optical depth (AOD), the uncertainty of the aerosol concentration be as high as one order of magnitude (e.g. Shinozuka et al., 2009; Andreae, 2009; Colarco et al., 2010). The uncertainty is especially large at low aerosol concentrations, when the aerosol influence on clouds is most prominent. The limited aerosol information from satellite remote sensing is propagated in the unclear influence of clouds in global radiative forcing (Lohmann, 2017). Therefore, satellite investigations of clouds are combined with ground based aerosol observations in the scope of this PhD.

## 1.3 Aerosols and clouds in the Amazon rain forest

The Amazon Basin is one of the view regions on our polluted planed where pristine aerosol conditions can be fined frequently during the wet season (Pöhlker et al., 2018, Hamilton et al., 2014). The understanding of pristine aerosole condition is essential to understand aerosles also in a polluted region (Hamilton, 2015). The Amazon is also a region with massive deforestation and high aerosol pollution related to Biomass Burning in the dray season. The unique rain forest ecosystem and the intense and large-scale (re)circulation of water between biosphere and atmosphere make the Amazon rain forest to a natural laboratory to study the life cycle of shallow and deep convective clouds and the effect of different aerosol on convective clouds (e.g., Andreae et al., 2004; Freud et al., 2008; Rosenfeld et al., 2016; Wendisch et al., 2016; Braga et al., 2017). Not only the aerosole emissions, but also the changes in land cover, e.g., conversion of forest to pasture, alter the amount and type of clouds (e.g., Heiblum et al., 2014; Avissar et al., 2002; Davidson et al., 2012; Machado et al., 2018). This in turn changes local and regional circulation and rainfall patterns, and consequently deforestation has been predicted to reduce the potential for hydropower generation in the Amazon This effect and the water and carbon cycle in the Amazon is well described by Andreae et al. (2015). FISCH et al. (1998) present a general description of Amazonian climate, pointing out the paleoclimate, the characteristics of rainfall and field observations of atmospheric phenomena. Molion (1993), studying the large scale and mesoscale circulations in Amazonia depicts the following main convective mechanisms acting in Amazonia: diurnal convection, squall lines and the organized convective systems associated with the penetration of cold fronts from the South that interact with tropical convection.

To explore the atmospheric processes is this unique ecosystem, such as aerosol–cloud interactions, the Amazon Tall Tower Observatory (ATTO) was established in 2010/11 (Andreae et al., 2015). ATTO has been set up in a pristine rain forest region in the central Amazon Basin, about 150km northeast of the city of Manaus. Two 80m towers have been operated at the site since 2012, and a 325m tower since 2015. During the wet season, ATTO receives comparatively clear air masses of marine origin from the northeast that travel over mostly untouched rain forest, whereas during the dry season strongly polluted air masses are advected from the southeast, originating from numerous fires in the Amazon's arc of deforestation (Pöhlker et al., 2019). Detailed information on characteristic differences in the atmosphere for the contrasting wet and dry season conditions at ATTO can be found in a number of studies (e.g., Nölscher et al., 2016; Pöhlker et al., 2016; Moran-Zuloaga et al., 2018; Saturno et al., 2017). However, Holanda et al. (2020), shows that also Biomass Burning blooms from Africa entering the Amazonian atmosphere and get entrained. Figure 1.5 shows the frequency of pristine conditions at ATTO and the effect on aerosol and cloud properties, with lowest aerosol emissions and for lowest anthropogenic activities and largest effective radius.

Strong forest fires lead to reduction of cloud droplet size and the delay of precipitation onset from $1.5$ above cloud base in pristine clouds to more than $5$ in polluted clouds and more than $7$ in pyro-clouds is presented by Andreae et al. (2004), measured by aircraft. Cecchini et al. (2017), show that $N_{\mathrm{CN}}$ is the primary driver for the vertical profiles of effective diameter and droplet concentration in the warm phase

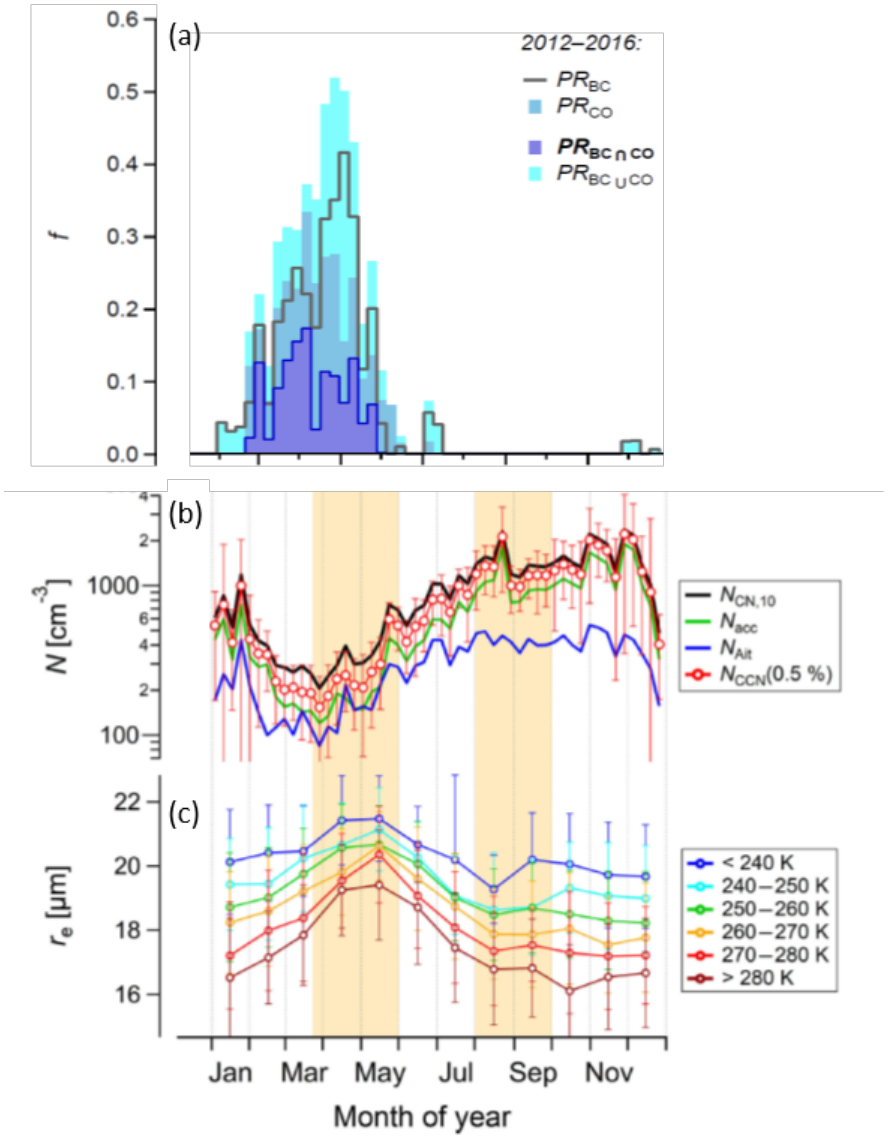


**Figure 1.5:** Figure from Pöhlker et al. (2018). (a) The appearance of pristine aerosol conditions at the Amazon Tall Tower Observatory (ATTO) calculated from black carbon and CO data, the different color symbolised different methods for detecting the pristine aerosol conditions. (b) Aerosol and CCN number concentrations measured at ATTO, and (c) effective radius for different cloud top temperatures.

of Amazonian convective clouds, while $w$ have a modulating role in the latter and in total condensed water, this work was done by aircraft measurements. Rosenfeld et al. (2016) demonstrated, that also satellite data can be used to investigate aerosol cloud interactions and CCN on a microphysical scale. However, systematic analysis of the relation between aerosols and clouds on a large scale using ling term aerosol observations and satellite data is missing, the results summarized above are based on short term aircraft campaign. Therefore in the scope of this PhD aerosol cloud interactions are investigated in the Amazon using satellite and long term ATTO data, to achieve a large scale.

## 1.4 Research objectives and thesis outline

In the scope of this PhD the aerosol cloud interactions at cloud base and on the development of convective clouds was investigated on a regional scale for a long time combining in-situ measurements at ATTO and satellite data.

The satellite retrievals of cloud properties were performed using the Visible Infrared Imaging Radiometer Suite (VIIRS) passive sensor, onboard the Suomi National Polarorbiting Partnership (NPP) satellite. The VIIRS sensor has a very high spatial resolution of $375\,\mathrm{m}$ at the nadir in five optical channels which enable the observation of clouds in different development states and obtaining a T-$r_e$ profile (Figure 1.4 shows a theoretical T-$r_e$ profile) (Efraim et al., 2022b; Rosenfeld et al. (2014c); Rosenfeld et al. (2014b)). Satellite remote sensing allows to measure the median droplet size over the temperature profile of clouds in an investigated area. Assuming that clouds at different development states have comparable properties at the same altitude it is possible to create a representative T-$r_e$ profile for the given area. Treating the cloud as a adiabatic chamber with a continuous updraft it is possible to use the droplet growth rate over temperature to fit an adiabatic curve. The pressure at cloud base can be calculated from the delta of the cloud base temperature and the average air temperature at ground level. This enables the possibility to recalculate the CCN number concentration at cloud base, with the limitation that only the part of the cloud that behaves adiabatic can be considered.

Being able to generate conclusive T-$r_e$ profiles allows to get better understanding of in cloud microphysical processes and helps to specify aerosol influence on convective clouds at cloud base and even at higher altitude. This research is done in order to help reducing the high uncertainty that aerosol cloud interactions introduce in global climate models and subsequently global radiative forcing. Investigation aerosol, cloud interactions by satellites only, are limited to large particles using the aerosol optical depth (AOD) or the aerosol index (AI) (Shinozuka et al., 2009; Andreae, 2009; Colarco et al., 2010). Direct optical measurements like AOD need a clear, cloud free sky to measure the aerosol load and the interpretation of the results needs additional context in form of regional average aerosol size distribution or the average chemical composition of the aerosols in the investigated region, both of which can vary significant on a annual or diurnal basis. Using T-Re profiles received by satellite remote sensing it is possible to achieve the same spacial and temporal resolution than with direct optical aerosol measurements, but with the benefit of only taking the aerosols into account that interact with clouds and actively take part in the cloud forming processes as CCN. This method has its own limitations but it bypasses a lot of uncertainty factors that can not be eliminated in directly analyzing the optical properties of atmospheric aerosol.

In order to determine the viability of T-Re profiles a comparison with long therm data at ATTO was conducted. The ATTO side offered strong arguments to be chosen as a test site for this task. The proximity of the ATTO to the equator reduces the correction needed for solar and viewing angles, the central Amazon basin does not feature any major or abrupt elevation changes, which could influence The T-Re method negatively by introducing terrain forced updrafts that can not be accounted for in this method. The homogeneous background provided by the dense vegetation

also increases contrast against the clouds reducing the difficulty to determine cloud base heights. All this factors combined render ATTO to be ideal for satellite remote sensing all year round. But not only the environmental factors at ATTO are ideal for remote sensing, it is also one of the view places in the world where aerosol number concentrations get so low that droplet activation at cloud base is purely aerosol limited during the wet season. This are conditions where cloud properties are most sensitive to aerosol concentrations and therefore accurate measurements are most important. Combining well documented and well established long therm ground measurements of aerosol, with ideal conditions for satellite remote sensing methods ATTO offers a worldwide unique opportunity to systematically investigate and validate T-Re profiles as an option to improve the understanding of aerosol cloud interactions globally.

Models suggested that a secondary cloud droplet activation is taking place at altitudes way above cloud base when war rain-out is occurring. T-Re profiles offered the possibility for better insight into vertical cloud development and the microphysical processes at deeper cloud levels. Secondary activation above cloud base in the amazon, was detected and investigated over a long time and regional scale first time in the scope if this PhD. T-Re profiles were found to allow a more detailed look into cloud microphysics and vertical development of clouds on a macro scale. The vertical development of the median droplet radius defines distinct microphysical zones within coupled cumulus clouds. The detection of this microphysical zones can be atomized enabling large scale or in the case of this study long therm investigation of seasonal trends and influences in cloud development.

This more detailed information is vital to interpret and understand the overall influence aerosols have on cloud development at cloud base and beyond. The long therm studies also emphasized that the strong seasonality of aerosol load and distribution is not crucial for basic cloud parameters like cloud base height and temperature, but instead is essential for in cloud developments and microphysics, resulting in distinct seasonal differences in the microphysic cloud structure and subsequently cloud longevity, liquid water content, rain onset height, ice fraction and radiative properties of coupled clouds over the amazon.
This dissertation is based on four publications while two are focused on the theoretical background and the methods used and two are concentrated on the application of the method:

1. *Satellite-Based Detection of Secondary Droplet Activation in Convective Clouds*. A new approach of analyzing and interpreting the vertical cloud microstructure obtained by satellite remote sensing is presented. Spectral bin microphysics adiabatic parcel model was used to interpreted T-$r_e$ profiles. The classification of different cloud microphysical zones includes the (a) condensational growth of droplets, (b) growth by coalescence, (c) rain-out, (d) secondary droplet activation zone (SAZ), (e) mixed-phase of ice particles and water droplets, and (f) glaciation of the cloud. The detection of the SAZ is introduced here for the first time and is strongest for low aerosol load and highly depends on the aerosol size distribution at cloud base. This method allows to identify the activation of aerosol particles above cloud base and their role in invigorating deep convective clouds. This was demonstrated using case studies of aerosol size distributions and cloud profiles from ATTO.

2. *Satellite-based detection of secondary droplet activation during condensational growth in convective clouds*. This study concentrates on highly polluted clouds, where the secondary activation appears already in the condensational growth zone before collision calescence. A method detecting SAZ for highly polluted clouds is proposed by spectral bin microphysics adiabatic parcel model runs. The SAZ in the condensational growth zone results in an overestimation of $N_{\mathrm{d}}$ at cloud base and is used in the application of the method as a filter of data not been used for scientific analysis. The method is based on the model; however, case studies using aerosol size distribution from ATTO and cloud profiles from the satellite was used to evaluate the method.
3. *High aerosol sensitivity of Amazonian clouds throughout the seasons*. The paper presents the long-term effect of aerosol on clouds using tree years aerosol data from ATTO in combination with cloud properties retreated from satellite. A clear seasonality was observed in aerosol and cloud properties which well correlates, a remarkably high fraction of aerosol particles acts as CCN in clouds also in the highly polluted dry season, this is higher than expected from prior studies. The cloud formation in the Amazon is both, aerosol- and updraft-sensitive, not just in the predominately low aerosol abundance during the wet season, as previously assumed, but also in the dry season with heavy biomass burning smoke present. Our findings shed light on the aerosol-driven changes in fundamental parameters of tropical convective clouds and suggest that the buffering effect of updraft limited droplet activation at high aerosol concentrations is weaker than expected.
4. *Cloud Microphysical Zones in the Amazon*. The effect of aerosols on clouds are not limited to cloud base. This study shows the effect of aerosols on the vertical evolution of clouds using long-term data of aerosol properties measured at ATTO and cloud microphysical structure from satellite. hase. The vertical profiles of the effective radius of cloud particles as a function of temperature differ strongly between the low aerosol conditions during the wet season and the biomass burning smoke dominated dry season. Also the vertical depth of the cloud microphysical zones is strongly seasonal. The condensational growth zone is much deeper in the dry than in the wet season and the secondary activation zone plays a more significant role in the wet season. My findings underline the profound effects of aerosol population in the Amazon microphysical processes and vertical profiles of convective clouds.

CHAPTER 2

# Results

# 2.1 Satellite-based detection of secondary droplet activation in convective clouds

**This chapter has been published as:**

Efraim, A.; Lauer, O.; Rosenfeld, D.; Braga, R. C.; Franco, M. A.; Kremper, L. A.; Zhu, Y.; Pöschl, U.; Pöhlker, C.; Andreae, M. O.; Artaxo, P.; Araújo, A. C. de, and Pöhlker, M. L.: "Satellite-Based Detection of Secondary Droplet Activation in Convective Clouds". *Journal of Geophysical Research: Atmospheres*, 127, 12. (2022). DOI: 10.1029/2022JD036519

**Contribution to this publication by Oliver Lauer:** Avichay Efraim and I have contributed equally to this paper. I was mainly responsible for the conceptual design of the manuscript and the analysis of the satellite data. Further, I contributed significantly to the writing of this paper. Particular focal point of my contribution to the satellite analysis were: (i) improving the analysis code to approximate cloud base droplet number concentrations and the retrieved $T$-$r_{\mathrm{e}}$ profiles to prepare them for microphysical zone discrimination; (ii) developing the analysis code to automatize the microphysical zone detection for all zones distinguished in the paper; (iii) preparing and selecting the example cases used in the study, along with suitable fitting of the $T$-$r_{\mathrm{e}}$ profiles and cloud microphysical structure to highlight the potential of the approach.

JGR Atmospheres

RESEARCH ARTICLE
10.1029/2022JD036519

# Satellite-Based Detection of Secondary Droplet Activation in Convective Clouds

**Avichay Efraim[1], Oliver Lauer[2], Daniel Rosenfeld[1], Ramon C. Braga[3], Marco A. Franco[2,4], Leslie A. Kremper[2], Yannian Zhu[5,6], Ulrich Pöschl[2], Christopher Pöhlker[2], Meinrat O. Andreae[2,7,8], Paulo Artaxo[3], Alessandro C. de Araújo[9,10], and Mira L. Pöhlker[2,9,11]**

[1]Institute of Earth Sciences, The Hebrew University of Jerusalem, Jerusalem, Israel, [2]Multiphase Chemistry Department, Max Planck Institute for Chemistry, Mainz, Germany, [3]National Marine Science Centre, Southern Cross University, Coffs Harbour, Australia, [4]Institute of Physics, University of São Paulo, São Paulo, Brazil, [5]School of Atmospheric Sciences, Nanjing University, Nanjing, China, [6]Joint International Research Laboratory of Atmospheric and Earth System Sciences & Institute for Climate and Global Change Research, Nanjing University, Nanjing, China, [7]Department of Geology and Geophysics, King Saud University, Riyadh, Saudi Arabia, [8]Scripps Institution of Oceanography, UCSD, La Jolla, CA, USA, [9]Faculty of Physics and Earth Sciences, Leipzig Institute for Meteorology, University of Leipzig, Leipzig, Germany, [10]Brazilian Agricultural Research Corporation (EMBRAPA), Belém, Brazil, [11]Experimental Aerosol and Cloud Microphysics Department, Leibniz Institute for Tropospheric Research, Leipzig, Germany

**Abstract** We present a new approach of analyzing and interpreting vertical profiles of cloud microstructure obtained by satellite remote sensing. The method is based on a spectral bin microphysics adiabatic parcel model and aims to elucidate the effects of aerosols on the evolution of convective clouds and related microphysical processes, including the activation of cloud condensation nuclei (CCN), the growth of cloud droplets, and the formation of precipitation. Characteristic features in the vertical profiles of effective radius ($r_e$) and temperature ($T$) reveal different microphysical zones in convective clouds related to the change increase of $r_e$ with decreasing $T$. The classification of the different microphysical zones includes the (a) condensational growth of droplets, (b) growth by coalescence, (c) rainout, (d) secondary droplet activation zone (SAZ), (e) mixed-phase of ice particles and water droplets, and (f) glaciation of the cloud. The detection of the SAZ is introduced here for the first time. This method allows us to identify the activation of aerosol particles above cloud base and their role in the invigoration of deep convective clouds.

**Plain Language Summary** Using satellite remote sensing, we can obtain the vertical profiles of cloud microphysical processes in developed clouds. In this study, we present a new way of analyzing these profiles and understand the different processes that cloud droplets undergo during the development of the cloud. These processes include the turning of aerosols into cloud droplets, and the droplets' coalescence into rain drops. The change of droplets' size with height, as obtained by the satellite, reflect the different microphysical processes inside the cloud. While expecting the droplets to grow with height, a decrease of the droplets size suggests either rainout of the larger droplets from the cloud; or creation of small new droplets at much greater heights than the cloud base, where they are usually created. Those processes can be related to the extent of decrease of cloud drop size with height. The detection of new droplet formation above the cloud base with satellite is introduced here for the first time and it allows to understand this microphysical process and its effect of the development of the clouds and precipitation.

**Key Points:**

- A new method to interpret the cloud microstructure of deep convective clouds from satellite remote sensing is presented in this study
- The microphysical process of secondary activation of droplets above cloud bases is demonstrated with a model and detected in observations
- The satellite detection of the secondary activation microphysical zone is introduced here for the first time

**Supporting Information:**

Supporting Information may be found in the online version of this article.

**Correspondence to:**

A. Efraim and M. L. Pöhlker,
Avichay.Efraim@mail.huji.ac.il;
m.pohlker@mpic.de

**Citation:**

Efraim, A., Lauer, O., Rosenfeld, D., Braga, R. C., Franco, M. A., Kremper, L. A., et al. (2022). Satellite-based detection of secondary droplet activation in convective clouds. *Journal of Geophysical Research: Atmospheres*, *127*, e2022JD036519. https://doi.org/10.1029/2022JD036519

Received 19 JAN 2022
Accepted 28 MAY 2022

**Author Contributions:**

**Conceptualization:** Avichay Efraim, Oliver Lauer, Daniel Rosenfeld, Mira L. Pöhlker
**Formal analysis:** Avichay Efraim, Oliver Lauer
**Investigation:** Avichay Efraim, Oliver Lauer
**Methodology:** Avichay Efraim, Oliver Lauer, Daniel Rosenfeld, Ramon C. Braga, Marco A. Franco, Leslie A. Kremper, Yannian Zhu
**Resources:** Avichay Efraim, Ramon C. Braga, Marco A. Franco, Leslie A. Kremper, Alessandro C. de Araújo, Mira L. Pöhlker



## 1. Introduction

### 1.1. Background

The effects of aerosols on clouds and climate are among the largest uncertainties in the assessment and modeling of climate change (IPCC, 2013, 2021). The investigation of aerosols and clouds using remote sensing techniques allows global monitoring and analysis of aerosol-cloud interactions (e.g., Bréon et al., 2002; Grosvenor et al., 2018; Rosenfeld et al., 2016; Rosenfeld and Lensky, 1998). A main challenge, however, is to investigate aerosol and cloud properties at an accuracy that suffices to quantify the response of cloud microstructure and the corresponding radiative effects to aerosol perturbations. Aerosols serving as cloud condensation nuclei (CCN) determine the droplet number concentration ($N_d$) at cloud base for a given cloud base updraft speed ($w_b$), and

Journal of Geophysical Research: Atmospheres 10.1029/2022JD036519

**Software:** Avichay Efraim, Oliver Lauer, Yannian Zhu
**Supervision:** Daniel Rosenfeld, Mira L. Pöhlker
**Visualization:** Avichay Efraim
**Writing – original draft:** Avichay Efraim, Oliver Lauer
**Writing – review & editing:** Avichay Efraim, Oliver Lauer, Daniel Rosenfeld, Ramon C. Braga, Marco A. Franco, Leslie A. Kremper, Yannian Zhu, Ulrich Pöschl, Christopher Pöhlker, Meinrat O. Andreae, Paulo Artaxo, Mira L. Pöhlker

subsequently dominate the cloud microphysical and precipitation processes. The impact of fine ($d < 1$ μm) and ultrafine ($d < 0.1$ μm) aerosol particles (UAP) on deep convective clouds can be substantial through the following two mechanisms:

1. Suppression of warm rain: For a given updraft speed, polluted conditions with high CCN number concentrations ($N_{CCN}$) lead to the formation of clouds with high $N_d$ and small $r_e$ at cloud base (Twomey, 1977). In such conditions, collision and coalescence processes are inhibited, thus delaying the droplets' growth into rain drops (Gunn and Phillips, 1957; Squires, 1958). Hence, extra latent heat is caused by the air parcels' ability to hold more liquid water content (LWC). This increases the updraft speed and maintains the clouds at a higher altitude. When postponing the rain initiation while the cloud continues to grow vertically, the cloud droplets are transported to above the zero-isotherm and freeze into ice hydrometeors (Braga et al., 2017). As a result, latent heat of freezing is released and increases the buoyancy, causing an invigoration of the cloud toward the tropopause, where it spreads aside into wide anvils (Rosenfeld, Lohmann, et al., 2008).
2. Invigoration by activation of droplets above cloud base: This is typically found in clean air masses with relatively low $N_{CCN}$, which result in large $r_e$ and a corresponding high coalescence efficiency. The drop coalescence reduces the integrated droplets' surface area, which reduces the condensation rate. As a result, the supersaturation ($S$) increases to the point where it exceeds the $S$ at cloud base allowing activation of CCN with high critical $S$ (typically UAP) that were not activated at cloud base. The activation of particles into cloud droplets high above the cloud base releases additional latent heat, increases the buoyancy, and invigorates the clouds (Fan et al., 2018; Khain et al., 2012).

The invigoration caused by these mechanisms creates larger and colder anvils (Fan et al., 2013; Pan et al., 2021), which may emit less longwave radiation to space and thus creates a positive radiative forcing and warms the Earth (Cotton et al., 2011; Slingo & Slingo, 1988). In addition, the evaporation of tiny ice crystals from these high anvils is likely to enrich the upper troposphere with water vapor, which is a strong greenhouse gas and thus likely to increase the positive radiative forcing.

Aerosol optical depth (AOD) has been extensively used as a proxy for $N_{CCN}$ (Feingold et al., 2001; Quaas et al., 2009). The Aerosol Index (AI), which is the product of AOD and Angström exponent (Nakajima et al., 2001), provides a better estimation for $N_{CCN}$. However, Shinozuka et al. (2015), showed that such optically retrieved $N_{CCN}$ could vary by an order of magnitude compared to the directly measured $N_{CCN}$. Furthermore, the satellite-retrieved AOD and AI become insensitive to $N_{CCN} < 150$ cm$^{-3}$ due to the small signal-to-noise ratio. This threshold varies greatly depending on the size of the CCN and their activation supersaturation (Shinozuka et al., 2015).

The $N_d$ can also be retrieved based on the vertical evolution of $r_e$ in the growing convective towers. This approach relies on the remarkable aircraft observations, which show that $r_e$ increases with height above cloud base almost as if the clouds were adiabatic, despite the fact that the cloud LWC is mostly smaller than adiabatic (Freud et al., 2011). This pattern is caused by the nearly inhomogeneous mixing behavior of the convective clouds with the ambient air. Based on in-cloud aircraft measurements, Freud et al. (2011) showed that the cloud base $N_d$ could be approximated by dividing the adiabatic LWC by the mass of a single droplet having an adiabatic $r_e$. Since both, $r_e$ and cloud top temperature, can be retrieved by satellites, $N_d$ could be calculated based on the assumption of adiabatic $r_e$ and LWC (Rosenfeld, Fischman, et al., 2014; Rosenfeld, Liu, et al., 2014). The adiabatic LWC as a function of temperature can be calculated based on the retrieved cloud base temperature and pressure (Freud et al., 2011). The knowledge of the cloud base height above the surface, $H_b$, also allows estimating $w_b$, which can be obtained as $w_b = 0.9H_b$, with $H_b$ in km, and $w_b$ in ms$^{-1}$ (Zheng and Rosenfeld, 2015). The cloud base maximum $S$ ($S_{max}$) can be calculated based on $N_d$ and $w_b$ (Pinsky et al., 2012). The $N_d$ is then by definition $N_{CCN}(S)$. All these considerations were combined by Rosenfeld et al. (2016) into a satellite methodology to retrieve cloud base $N_d$ and $S$, which further yields $N_{CCN}(S)$ with an accuracy of ±30%.

However, $N_d$ and $N_{CCN}$ can be retrieved from vertical $T$-$r_e$ profiles only as long as condensation dominates the cloud droplets' growth (i.e., for $r_e < 14$ μm). Drop coalescence increases $dr_e/dT$ beyond the condensational growth rate. Rosenfeld and Lensky (1998) provided a conceptual model of the vertical evolution of $T$-$r_e$ in deep convective clouds. They hypothesized that a stabilization or moderation of $r_e$, that is, $dr_e/dT \approx 0$, after exceeding a threshold of approximately 14 μm was considered as resulting from rainout of the larger drops from the cloud. The appearance of ice particles increases the $r_e$ further because ice particles are typically much larger than

Journal of Geophysical Research: Atmospheres 10.1029/2022JD036519

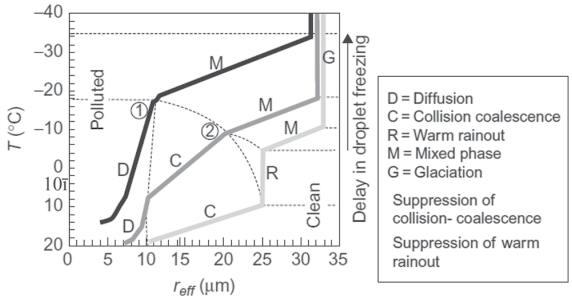


**Figure 1.** Conceptual diagram of the microphysical zones in convective clouds based on the vertical evolution of the $T$-$r_e$ relationships as developed in (Rosenfeld & Lensky, 1998), here adopted from (Rosenfeld, 2018).

water drops in the same mixed-phase clouds. Eventually the cloud reaches a full glaciation, where the indicated $r_e$ reaches a maximum. Rosenfeld and Lensky (1998) used the $T$-$r_e$ profile to partition the clouds into five vertical microphysical zones as shown in Figure 1: (a) Diffusion and condensational growth (in short "condensation"); (b) coalescence growth; (c) rainout; (d) mixed phase; (e) glaciated cloud.

### 1.2. Secondary Activation Zone

The $T$-$r_e$ conceptual model from Rosenfeld and Lensky (1998) in Figure 1, is based on the assumption of CCN activation into cloud droplets at cloud base. It does not consider the new activation of droplets in the course of cloud growth. The activation of particles into cloud droplets high above cloud base is referred to as secondary activation, as opposed to the primary activation of droplets at cloud base. Secondary activation can occur above cloud base in two ways: (a) The droplet coalescence reduces the integrated droplets' surface area available for condensation, which reduces the condensation rate. As a result, $S$ might exceed the $S_{max}$ at cloud base allowing inactivated UAP from the cloud base to nucleate into cloud droplets; (b) Additional entrained particles from the lateral and/or top boundaries of the cloud that can be activated even at the existing $S$ at that level. Both ways will result in a reduction of the observed $r_e$ with decreasing $T$ due to the nucleation of small new droplets in the environment of coalesced droplets. This has been validated with several in-cloud penetration aircraft campaigns (Bera et al., 2022; Braga et al., 2017; Paluch and Baumgardner, 1989; Paluch and Knight, 1984; Prabha et al., 2011; Warner, 1969). The vertical microphysical zone where these processes occur is defined here as the "secondary activation zone" (SAZ). Clouds with enough latent heat left after warm rainout to keep the air parcel rising and which include a sufficient number of CCN can form a SAZ. The new droplets' formation releases enough latent heat to keep the cloud growing, increasing its longevity and height.

In this study, we describe an updated method to identify the microphysical zones of convective clouds based on $T$-$r_e$ profiles, taking the SAZ into account. We used a spectral bin microphysics adiabatic parcel model to simulate the $N_d$, $S$, and the rain water fraction (RWF) profiles for four aerosol size distribution (ASD) and aerosol number concentrations below cloud base. The ASD and the simulated cloud properties are described in Section 3.1. Then, an application of the modeled cloud properties and their effect on the shape of the $T$-$r_e$ profile is described in Section 3.2, and the effect of real measured ASD on two satellite retrieved $T$-$r_e$ case studies is described in Section 3.3.

## 2. Methods

### 2.1. Model Description

In this study, we used an adiabatic cloud parcel model to describe the properties of convective clouds. The modeling was possible due to the inherent characteristic of $r_e$ in convective clouds caused by the inhomogeneous nature of turbulent mixing at the cloud edges (Rosenfeld et al., 2016). The model is a spectral bin adiabatic parcel model developed by Pinsky and Khain (2002). This parcel model explicitly describes the cloud particle spectrum evolution using a moving mass grid containing 2000 mass bins, allowing effects on droplet collisions. The model describes the processes of aerosol particle growth, particle activation into cloud droplets, the vertical evolution of the cloud microstructure and precipitation-forming processes in the water phase ($T > -10$°C). The aerosol particles are considered as spherical NaCl particles to ensure compatibility with the model construction. The effect of different chemical compositions and hygroscopicity on cloud microphysics and ASD is beyond the scope of this study and has been addressed instead in Braga et al. (2021) and Pöhlker et al. (2021). Braga et al. (2017) have shown that the vertical evolution of the $r_e$ measured by cloud probes generally agrees well with the theoretical $r_e$ driven by the adiabatic growth of droplets through water condensation. When $r_e$ exceeds 14 μm, coagulation and coalescence processes start to dominate. The coagulation process of cloud drops is calculated as proposed by Pinsky et al. (2001), who describe this process by solving stochastic collision equations according to Bott (1997). The coagulation of droplets is calculated after the initial condensational growth of particles. The drop-drop collision efficiency is calculated for each set of droplet masses allocated to the same parcel. Although

Journal of Geophysical Research: Atmospheres 10.1029/2022JD036519

the model is very detailed, and strives to describe the basic physical processes, by considering only basic cloud properties while simplifying or ignoring additional environmental factors, the resulting microphysical processes may vary from real cloud behavior. This is discussed in Section 4.

### 2.2. Satellite $T$-$r_e$ Retrieval

The satellite retrievals of cloud properties for the case studies described in this study were performed using the Visible Infrared Imaging Radiometer Suite (VIIRS) passive sensor, onboard the Suomi National Polar-orbiting Partnership (NPP) satellite. The VIIRS sensor has a very high spatial resolution of 375 m at the nadir in five optical channels for detailed spectral information (Rosenfeld, Fischman, et al., 2014; Rosenfeld, Liu, et al., 2014). High spatial resolution is required to resolve the vertical structure of convective clouds. At lower resolution only the largest individual convective clouds can be resolved, thus missing the fine structure required to detect the SAZ. A snapshot of the $T$-$r_e$ profile of a cloud cluster provides the same information as obtained by tracking a single convective cloud throughout its vertical evolution (Arakawa and Schubert., 1974; Lensky and Rosenfeld, 2006). It is also assumed that $r_e$ in the cloud top pixel has the same value as in more developed clouds at the same height, as long as precipitation does not fall through that level (Freud et al., 2008; Rosenfeld and Lensky, 1998). These assumptions enable to infer vertical $T$-$r_e$ development of clouds in a two-dimensional spatial image. Moreover, to reduce the data distortion, the satellite zenith angle of the clouds has to be between 30° and −20°, and the solar zenith angle of the clouds has to be below 65°. The wavelengths used to retrieve the $T$-$r_e$ profile include 3.7 and 10.8 μm (Rosenfeld, Fischman, et al., 2014; Rosenfeld, Liu, et al., 2014). This method assumes retrieval of water drops. However, ice particles are much larger than the droplets in the clouds, in which they are formed. They absorb more strongly the solar radiation at the 3.7 μm band. Thus, the satellite retrieved $r_e$ of ice particles appear larger than the same size water drops. Therefore, a very large $r_e$ at supercooled temperature usually indicates the existence of ice in the cloud.

A designated software produces an RGB display that highlights the cloud microphysics and $T$ and $r_e$ retrievals in each pixel. On the basis of this display, cloud scenes of interest are manually sampled to avoid or minimize obstruction by multilayer or semi-transparent clouds that can disrupt the retrieved $T$-$r_e$. A cloud mask algorithm, introduced by Zhu et al. (2014), filters out the partially filled cloudy pixels due to measurement errors in such pixels. The specific $r_e$ values for each pixel are sorted by the detected temperature for each pixel into 1°C sized bins (i.e., 9.5–10.5°C in the 10°C bin etc.). Then, the 30-percentile median for all $r_e$ values within one bin is calculated resulting in a continuous vertical cloud profile of $r_e$ as a function of $T$ (Rosenfeld et al., 2016). The effect of aerosols on the $T$-$r_e$ profile is mostly reflects in the growing clouds, rather than mature dissipating clouds. Thus, the use of the 30-percentile median is meant to capture the clouds in their growing phase (Lensky and Rosenfeld, 2006; Rosenfeld, Woodley, et al., 2008). Multilayer clouds are identified by a lack of continuity in the $T$-$r_e$ profiles. Therefore, this methodology is not valid for non-convective clouds or scenes obscured by multilayer clouds. The uncertainties of satellite-retrieved $r_e$ and $T$ are approximately 8% and 0.2–1.1°C, respectively (Rosenfeld et al., 2016). Although, the importance of those uncertainties is reduced because the method described in this study is examining the relative change of $r_e$ with $T$ and not the absolute values. $T$-$r_e$ profiles retrieved in various locations show similar results for similar environments (e.g., Huang et al., 2022; Lensky and Rosenfeld, 2006; Rosenfeld, 2007; Rosenfeld, Woodley, et al., 2008) implying the robustness of $T$-$r_e$ retrievals and the fact that this method can be applied worldwide, in any meteorology and for any convective clouds as long as a valid unperturbed $T$-$r_e$ profile is retrieved. This study analyzes the satellite retrieved $T$-$r_e$ profiles by an automatic algorithm to detect the different microphysical zones. The entire description of the algorithm is described in Section 3.2.

### 2.3. Aerosol Observations at the Amazon Tall Tower Observatory

The Amazon Tall Tower Observatory (ATTO, 2020) is located in the central Amazon Basin (2.145°S, 59.004°W at 130 m above sea level). It monitors fundamental climatic and atmospheric parameters in a vast region of pristine rainforest. Some of the meteorological measurements at ATTO include temperatures, wind profiles, and precipitation (Andreae et al., 2015). These parameters were used to determine the coupling state of the clouds scenes and to choose case studies where the air parcel that was sampled at ATTO fed the cloud that was sampled by the satellite. For each of the case studies described in Section 3.3, an ASD was measured by a Scanning Mobility Particle Sizer (SMPS, TSI Inc.) connected to an inlet line with 60 m height at an 80 m tall mast (Franco et al., 2022). An overview of the atmospheric, geographic, and ecological conditions, as well as

Journal of Geophysical Research: Atmospheres 10.1029/2022JD036519

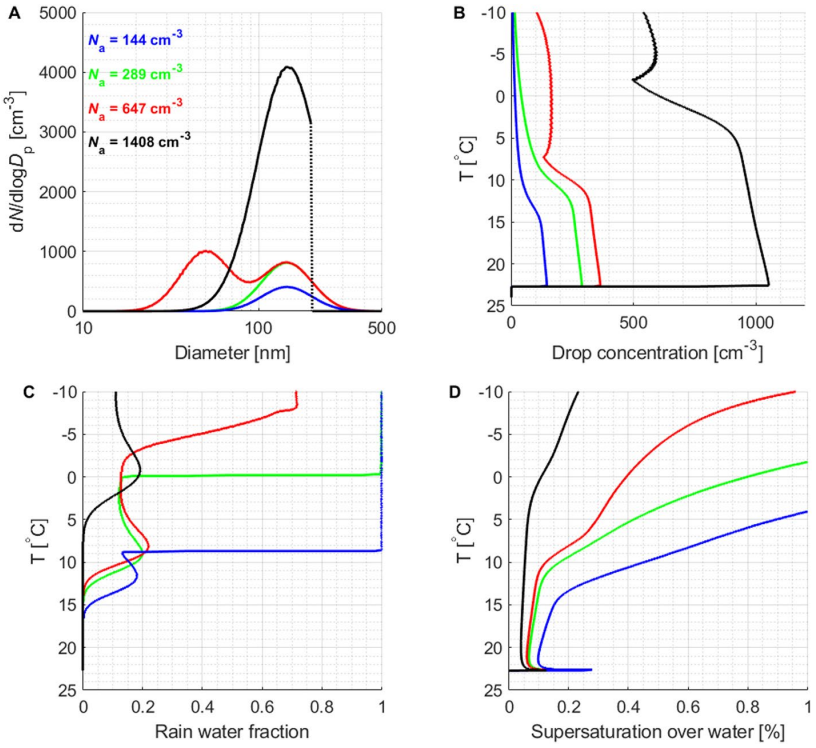


**Figure 2.** Simulations of cloud properties for four different aerosol size distributions (ASD) and total particle number concentrations ($N_a$). Panel A shows the four ASD including the cases (1) very clean unimodal (blue) with $N_a$ = 144 cm$^{-3}$, monomodal size distribution, with accumulation mode only; (2) clean unimodal (green) with $N_a$ = 289 cm$^{-3}$, monomodal size distribution, with accumulation mode only; (3) clean bimodal (red) with $N_a$ = 647 cm$^{-3}$, bimodal size distribution, the same number of accumulation mode particles as clean unimodal and additional Aitken mode particles; (4) polluted (black) with $N_a$ = 1,408 cm$^{-3}$, wide monomodal size distribution, with mostly accumulation mode reaching into the Aitken mode. The polluted ASD is truncated at 200 nm to prevent early warm rain initiation by enhanced coalescence. Panel B shows the simulated $N_d$ with decreasing $T$. Panel C shows the vertical rain water fraction (RWF) profile. RWF is defined as the ratio between rain water content to total water content, where drops with a diameter >50 μm are considered raindrops. Due to the lack of significant activation of new droplet in the very clean unimodal and clean unimodal cases (shown in Figure 3), RWF jumps to unity when the smallest drops grow beyond the threshold of 50 μm. In reality, the drop size distribution is wider, and therefore, there would not be such a sharp jump. In addition, clouds that completely rainout cannot develop due to a lack of condensation and buoyancy. The model forces the cloud to grow beyond this point in order to compare clouds profiles with and without significant new activation. Panel D shows the vertical profile of supersaturation over water.

commonly encountered air masses, can be found, for example, in Artaxo et al. (2013), Andreae et al. (2015), and Pöhlker et al. (2019). Characteristic aerosol and CCN conditions at ATTO have been described in recent studies (e.g., Moran-Zuloaga et al., 2018; Pöhlker et al., 2016, 2018).

## 3. Results

### 3.1. Simulations of Cloud Microphysical Properties

This section discusses the vertical $T$-$r_e$ profiles of convective clouds using the parcel model with various initialization values. The simulations were performed for four ASD measured in subsaturated conditions (Braga et al., 2021; Pöhlker et al., 2021) as shown in Figure 2a. The data and initial thermodynamic conditions for the simulations, such as pressure, temperature, relative humidity, and height were collected below cloud bases of convective clouds during flight AC19 of the ACRIDICON-CHUVA campaign (Wendisch et al., 2016). The ASD include three monomodal ASD and one bimodal ASD that simulates a Hoppel minimum. The Hoppel minimum is a size separation gap between two size modes, which usually indicates the size of the smallest particles that can

Journal of Geophysical Research: Atmospheres 10.1029/2022JD036519

serve as CCN for the given thermodynamical conditions due to cloud processing (Hoppel and Frick, 1986; Hudson et al., 2015). The two size modes are the Aitken mode, with particles smaller than the Hoppel minimum (from approximately 10 to 70 nm), and the accumulation mode, which includes the larger ones (from approximately 70 to 200 nm) (Seinfeld and Pandis, 1998). The three monomodal ASD have only an accumulation mode for different aerosol number concentrations (cases: very clean unimodal, clean unimodal, and polluted) and the bimodal ASD has Aitken and accumulation modes (case: clean bimodal). Even though observations show no warm rain for similarly polluted cases (Braga et al., 2017), the model still simulates rain due to its construction. Therefore, to prevent or at least delay the initiation of warm rain by nucleation of large droplets and enhanced coalescence, the polluted ASD is truncated at 200 nm and lacks particles larger than this threshold. The comparison of the polluted ASD with and without the truncation is illustrated in the supplements (Figure S1). The increase of updraft speed with height is assumed to be linear with a constant acceleration of 0.9 $ms^{-1}$ $km^{-1}$. These are typical velocities found near the base of convective clouds (Zheng and Rosenfeld, 2015). The aerosol spectra and the respective vertical profiles of cloud properties for each ASD case are presented in Figure 2, the droplet size distribution (DSD) for each $T$ bin is presented in Figure 3 and the corresponding $T$-$r_e$ profiles from the model runs are shown in Figure 4.

The number of activated drops at cloud base is mostly influenced by accumulation mode particles, which are activated first (Pöhlker et al., 2016, 2018). As can be seen in Figure 2b, $N_d$ at cloud base is almost equal to the $N_a$ for the very clean unimodal and clean unimodal cases, while for the clean bimodal and polluted cases, $N_d$ at cloud base is much smaller than the total $N_a$, meaning that a large fraction of the particles was not activated at cloud base. The inactivated particles are activated aloft when $S$ exceeds $S_{max}$ at a higher altitude (Figure 2d). Figure 3 shows the DSD in each $T$ bin, colored by the number concentration of each size bin. For all four ASDs an increase of droplet concentration appears above the cloud base. However, the number concertation of activated droplets above cloud base in the very clean unimodal and clean unimodal cases is of at least two orders of magnitude lower than in the clean bimodal and polluted cases. The ratio of the number of activated droplets with respect to the number of eliminated large drops in the clean bimodal and polluted cases is much larger, which means a much more significant SAZ. This is noticeable in the increasing drop concentration with decreasing $T$ for those cases (Figure 2b). In addition, Figure 3 shows the conversion of cloud droplets into raindrops which populate the larger size bins.

RWF is defined as the ratio between the rain water content ($d > 50$ µm) and the total water content (Figure 2c). RWF starts to increase as coalescence start and to decrease as the rain drops precipitate from the cloud parcel. This process takes place when the terminal velocity of raindrops is larger than the updraft speed within the cloud parcel. When the SAZ is negligible (very clean unimodal and clean unimodal cases) RWF increases with decreasing $T$ up to unity when the smallest drops grow beyond the threshold of 50 µm. In reality, the drop size distribution would be wider, and therefore, there would not be such a sharp jump. In addition, clouds that completely rain out cannot develop higher due to a lack of condensation and buoyancy. In this study, the model forces the cloud to grow beyond this point to illustrate how secondary activation changes the $T$-$r_e$ profile compared to the alternative that is rarely realized in nature. The height for the onset of rain formation above the cloud base (RWF > 0) increases for increasing $N_d$ at cloud base (Figures 2c and 3). This is consistent with the delayed coalescence at greater $N_d$ due to slower droplet growth with height. The $N_d$ starts to decrease sharply at the temperature of rain initiation, as the coalescence merges many cloud droplets into fewer raindrops. For simulations in which $N_d$ starts to increase above cloud base (clean bimodal and polluted) the existence of a significant SAZ is identified. This occurs at the height where $S$ exceeds the $S_{max}$ at the cloud base. In these cases, a considerable amount of aerosol particles that were not activated into droplets near the cloud base are activated at the larger $S$ aloft. This is valid for these model runs since the model does not include entrainment of additional aerosol particles. However, in nature, the origin of these particles is not necessarily inactivated aerosols from the cloud base, but they could also be from the surroundings, for which $S$ does not have to exceed $S_{max}$. The significant activation of the new droplets in these cases replenishes the cloud water content; therefore, RWF values do not go up to 1.

### 3.2. Detection of Microphysical Zones Based on Modeled $T$-$r_e$ Profiles

Different microphysical processes determine the shape of the $T$-$r_e$ profiles of convective clouds. These processes were investigated using the model results described in Section 3.1. Figure 4 shows the $T$-$r_e$ profiles of the four simulated clouds with varying shapes and colors representing the different microphysical zones. The gray lines in the background of the plot are the theoretical adiabatic $r_e$ curves under the assumption of condensational growth for different cloud base $N_d$. The adiabatic curves are calculated based on the adiabatic LWC and the correspond-

Journal of Geophysical Research: Atmospheres 10.1029/2022JD036519

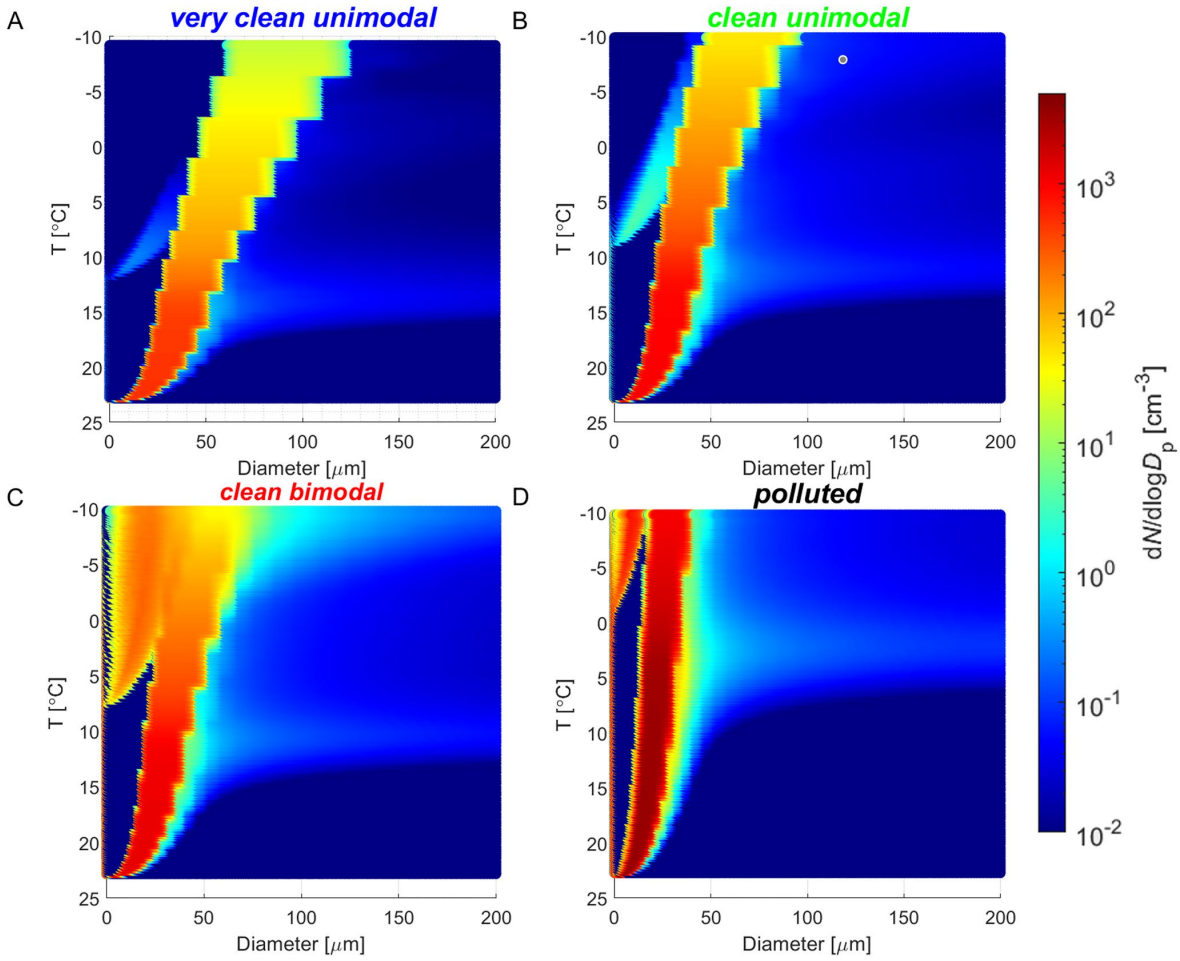


**Figure 3.** The droplet size distribution (DSD) in each $T$ bin, colored by the number concentration of each size bin, for the four model runs presented in Figure 2. It is inferred from this figure that SAZ occurs in all four ASD. However, in Panel A and B (very clean unimodal and clean unimodal cases) the number concentration of activated droplets above cloud base is at least two orders of magnitude lower than the clean bimodal and polluted cases shown in panels C and D. Therefore, the ratio of droplets activation to large drops elimination in the clean bimodal and polluted cases is larger, which means a much more significant SAZ. This causes an increase in drop concentration with deceasing $T$ (Figure 2b). It is also shown here that the rain initiation is higher for cases with higher initial $N_d$.

ing development of $r_e$. The adiabatic LWC is computed using an adiabatic parcel model that rises from the cloud base temperature and pressure obtained from reanalysis (Rosenfeld et al., 2016). The deviations between the actual and the theoretic adiabatic $T$-$r_e$ profiles define the dominant microphysical zones, as follows:

1. **Condensation:** The first zone after droplets nucleation at cloud base (red lines in Figure 4). The $r_e$ growth is similar to an adiabatic $r_e$ curve originating at cloud base. Therefore, the $T$-$r_e$ line is nearly parallel to the background $T$-$r_e$ curve with the same cloud base $N_d$. During the condensational growth phase, no rain is expected, and thus, no rain was modeled.
2. **Adiabatic growth:** There are cases where the $T$-$r_e$ growth continues adiabatically well beyond the $r_e$ threshold of rain initiation, which is commonly recognized near 14 μm (e.g., Rosenfeld et al., 2006). Beyond this threshold, the microphysical zone can no longer be defined as dominantly condensational since coalescence has become very efficient and likely plays a significant role here as well. Accordingly, the continuation of the adiabatic increase in $r_e$ beyond 14 μm is defined as adiabatic growth here (orange lines in Figure 4) to be differentiated from the condensational growth. Such behavior may result from strong updrafts, where there is not enough time to form rain in the fast-rising parcels.

Journal of Geophysical Research: Atmospheres 10.1029/2022JD036519

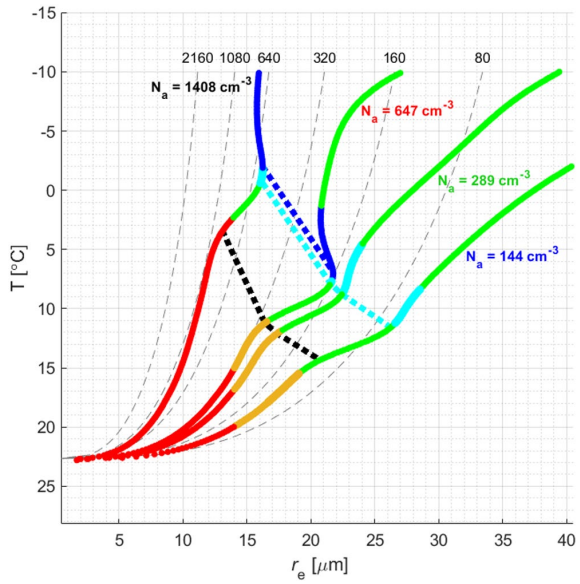


**Figure 4.** $T$-$r_e$ profiles of the four cloud simulations presented Figure 2, color-coded by different microphysical zones based on the growth rate of $r_e$ with decreasing $T$. The thin gray dashed lines in the background are the theoretical adiabatic curves. The red lines are the condensational growth phase. The orange lines mark the adiabatic growth. The green lines mark the coalescence growth. The cyan lines mark the rainout, and the blue lines mark the secondary activation zone (SAZ). The thick dashed black, cyan and blue lines indicate the rain onset, maximum rainout, and the SAZ onset, respectively.

3. **Coalescence:** Drop coalescence increases the cloud drop size due to the drops merging. Therefore, a growth rate of $r_e$ that exceeds the adiabatic growth rate marks the coalescence zone (green lines in Figure 4). The model shows the initiation of rain (Figure 2c) at the bottom of the coalescence zone. Consequently, $N_d$ sharply reduces.
4. **Rainout:** Moderation of the growth rate of $r_e$ with decreasing $T$ above the coalescence zone indicates rainout of the larger raindrops from the cloud parcel/top (cyan lines in Figure 4).
5. **Secondary activation zone:** A significant activation of new droplets after the occurrence of coalescence and/or rainout is indicated by negative $dr_e/dT$ (blue lines in Figure 4).

Figure 4 shows that the microphysical zones are distinguished from each other by the shape of the $T$-$r_e$ profiles. In all the four cloud simulations, the condensational part of the cloud (marked by red lines) behaves adiabatically and follows the theoretical adiabatic curves, depending on the $N_a$ of each case. Then, the coalescence that comes after the adiabatic part indicates the cloud droplets' transition to raindrops. The depth of rain initiation ($D_r$, in meters above cloud base) is linearly correlated with $N_d$ at cloud base, according to $D_r \sim 4 \cdot N_d$ (Freud & Rosenfeld, 2012; Konwar et al., 2012). For example, in the very clean unimodal case, $r_e$ increases fastest with decreasing $T$ and reaches rain initiation at the warmest $T$. The maximum conversion rate of cloud into raindrops (maximum rainout, marked by the thick cyan dashed line) occurs at approximately 12°C. For cases with higher initial $N_d$, the temperature of rain initiation (marked by the dashed black line) and maximum rainout occur at colder temperatures (see Figures 2–4). Coalescence and precipitation lead to a strong reduction in the droplets' integrated surface area, causing limitations to the condensation rate. This increases $S$ with decreasing $T$. In the clean and very clean unimodal cases, which have an accumulation mode only, all the aerosols get activated at cloud base, as seen in Figure 2b. The cloud droplets are larger, and their precipitation causes only a slight decrease of $dr_e/dT$, which remains positive. However, in the clean bimodal and polluted cases, the significant amount of Aitken mode particles that were not activated at cloud base get activated above cloud base because of the increase of $S$ beyond $S_{max}$ at cloud base. This results in a decrease of $r_e$ with decreasing $T$ (SAZ, marked by the blue lines). Such a pattern is observed due to the relative increase of the newly activated small droplet concentrations in the cloud parcel. This signature in $T$-$r_e$ profiles is not observed in the negligible secondary droplet activation above cloud base (see very clean unimodal and clean unimodal cases), because very little to no aerosols are left available for nucleation even at the very large $S$ values aloft. Since the updraft in the model is forced to a linear increase of 0.9 $ms^{-1}$ $km^{-1}$, the cloud continues to grow vertically, leading to regrowth of $r_e$ due to the ongoing coalescence of the remaining cloud droplets. As mentioned above, in nature, clouds with no new activation will rainout almost completely. They will reach very high $S$, but due to a lack of condensational heating, they will not develop any further. The practical impact of these results is to document the occurrence of secondary droplet activation well above the base of convective clouds with warm rain. The negative $dr_e/dT$ in the modeled $T$-$r_e$ profile indicates the secondary activation of aerosols that were not activated at cloud base and implies that the SAZ can be detected by remote sensing. Nevertheless, the appearance of SAZ in nature is not necessarily connected to inactivated Aitken mode particles. It could also be caused by the entrainment of aerosols of any size that can be activated even at $S$ below $S_{max}$.

### 3.3. Detection of Microphysical Zones Based on Satellite $T$-$r_e$ Profiles

There are unique relationships between the microphysical zones and their manifestation in the $T$-$r_e$ profiles. Accordingly, satellite-retrieved $T$-$r_e$ profiles can be used to infer microphysical zones, including the newly defined

Journal of Geophysical Research: Atmospheres 10.1029/2022JD036519

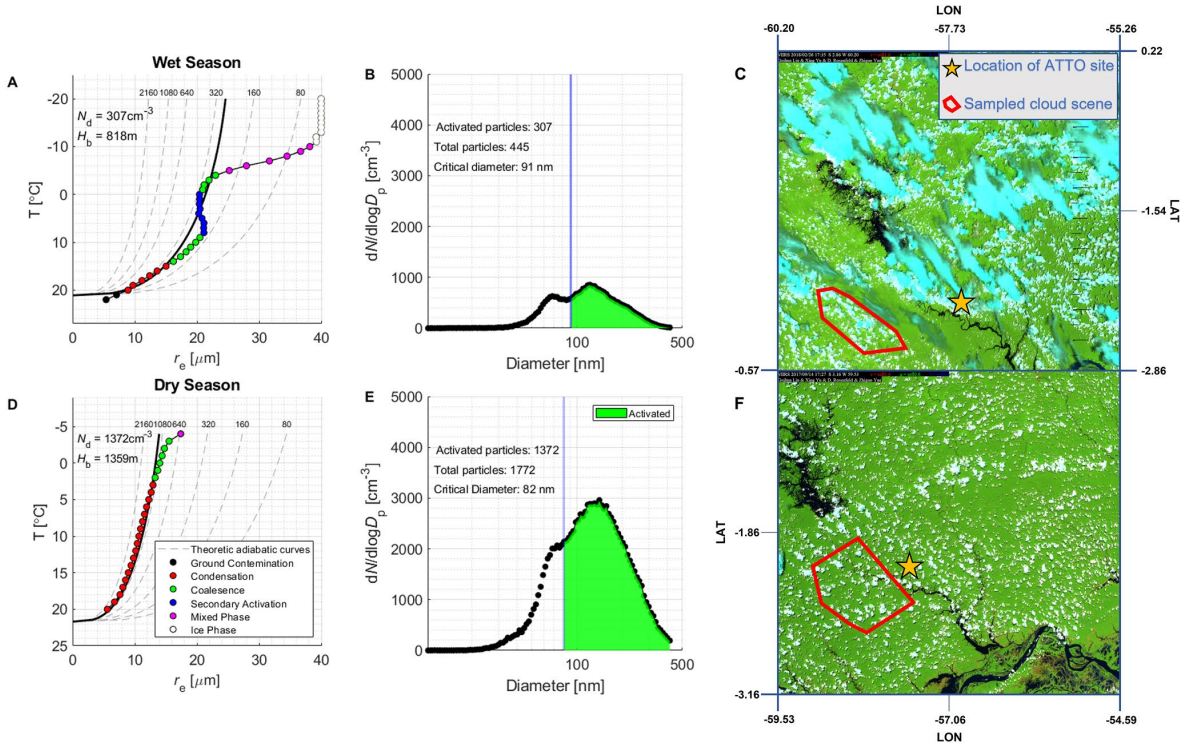


**Figure 5.** Satellite retrieved $T$-$r_e$ profiles of exemplary cloud scenes during the Amazonian wet and dry seasons close to the ATTO region, color-coded by different microphysical zones (panels A and D); and the 1-hr average ASD before the satellite overpass of each case study as measured by the SMPS on the ATTO mast (Panels B and E). Panels C and F show the true-color satellite image of each case. The ATTO location is marked by a star and the sampled cloud scene by the red polygon.

SAZ. Two cloud scenes close to ATTO were used as case studies to investigate and demonstrate the applicability of satellite $T$-$r_e$ profiles. Cloud scene A (red polygon in Figure 5a) is a cumulonimbus cloud that was taken within approximately 69 km from the ATTO site during the wet season (26 February 2018 at 17:22 UTC). This season is characterized by relatively low CCN concentrations (Pöhlker et al., 2016). The retrieved $N_d$ is 307 cm$^{-3}$ and cloud base height is 818 m, as estimated by the lifting condensation level. The first two points of this $T$-$r_e$ profile are semi-transparent cloud pixels that might cause a distortion of the retrieval and are considered as ground contamination. The 1-hr average ASD before the satellite overpass (Figure 5b) clearly shows a Hoppel minimum at 88 nm. The number of activated particles at cloud base (Figure 5b) is equal to $N_d$. Accumulating the $N_d$ largest particles on the ASD yields the smallest diameter to be activated, that is, the critical diameter. In this case the critical diameter is 91 nm. This result suggests that the activated particles at cloud base are accumulation mode particles down to that threshold. The SAZ is clearly identified above the coalescence zone at the 8°C isotherm. The activation of either remaining Aitken mode particles from cloud base and/or entrained aerosols at higher levels, causes a reduction of $r_e$ with decreasing $T$. The new droplets are added to the preexisting large cloud drops undergoing coalescence, which leads to a renewed growth of $r_e$ with decreasing $T$ above the 0°C isotherm. This means that the coalescence microphysical zone is again dominant there. The rapid growth of $r_e$ toward colder subzero temperatures can also be interpreted as a mixed phase of liquid and ice and eventually full glaciation of the cloud (Rosenfeld and Lensky, 1998). Cloud scene B (red polygon Figure 5d) is a cluster of cumulus congestus clouds that was taken within approximately 26 km from ATTO during the dry season (14 September 2017 at 17:27 UTC), which is characterized by relatively high concentrations of CCN (Pöhlker et al., 2016). The retrieved $N_d$ for the dry season case is 1,372 cm$^{-3}$ and the cloud base height is 1,359 m. The 1-hr average ASD (Figure 5e) of this case is unimodal with an inflection point instead of a clear Hoppel minimum. Thus, the separation of modes is less clear in comparison with Cloud scene A. Higher $N_d$ at cloud base with smaller $r_e$ (compared to Cloud scene A), decrease the condensational growth rate of droplets with decreasing $T$ and strongly suppress the coalescence

Journal of Geophysical Research: Atmospheres 10.1029/2022JD036519

processes, therefore a SAZ signature is not identified. At the 2°C isotherm, the $r_e$ becomes sufficiently large for the coalescence process to dominate up to the cloud's top.

## 4. Discussion

The SAZ signature allows us to identify a significant occurrence of new droplets nucleation above the cloud base. The origins of the particles on which the new droplets are formed can either be Aitken mode particles that were not activated at cloud base or entrained particles of all size aloft. In the first case, $S$ aloft has to exceed the $S_{max}$ near cloud base. A stronger SAZ, which means lower $-dr_e/dT$, can imply an increased nucleation of smaller droplets, hence a greater latent heat release that increases the buoyancy. A deeper SAZ means that the top of the SAZ reaches lower temperatures. It can imply a deeper layer of aerosol activation above cloud base; thus the latent heat release occurs higher in the cloud. Increased buoyancy due to enhanced and/or higher occurrence of latent heat release leads to cloud invigoration. The invigoration of deep convective clouds may also lead to enhanced lightning activity (Thornton et al., 2017; Yuan et al., 2011).

As mentioned in Section 2.2, the parcel model is limited to cloud processes in the water phase only ($T > -10$°C). However, satellite retrieved cloud scenes can be more vertically developed than represented in the model, growing well above the −10°C isotherm (see Cloud scene A). The rapid growth of $r_e$ above the subzero temperatures indicates a mixed phase of ice and water particles. At a maximum threshold $r_e$ of 40 μm and/or temperatures colder than −38°C, the ice phase is dominant, and the cloud is considered fully glaciated (Rosenfeld and Lensky, 1998). As mentioned in Section 3.1, another limitation of the model compared to observations is manifested in the polluted case. For example, cloud scene B compared to the modeled polluted case: Both cases represent highly polluted situations with high CCN concentration at cloud base. The parcel model initiates coalescence and warm rain at the 5°C isotherm and later on allows secondary activation, even with the truncation of the larger particles. However, in nature this does not happen in such polluted situations. Andreae et al. (2004), Rosenfeld, Fischman, et al. (2014), Rosenfeld, Liu, et al. (2014) and Braga et al. (2017) showed in different aircraft campaigns in deep tropical convective clouds that, when the air is highly polluted, the coalescence zone is mostly delayed to the mixed-phase zone or suppressed altogether. As can be seen in Cloud scene B, the coalescence is much weaker and leads into the beginning of the mixed phased zone with no secondary activation. Whether the origins of the particles are from the cloud base or entrainment aloft, the SAZ described in this study requires a large $S$, which is caused by the preceding coalescence. With that being said, in some cases secondary nucleation of droplets might also occur before coalescence dominates, during the condensational growth of the cloud. It might happen either due to entrainment, or in highly polluted clouds that are updraft limited. In those clouds the $S_{max}$ at the cloud base is rather small due to the activation of many particles. When the updraft increases with height to the extent that $S$ exceeds the $S_{max}$ at cloud base, a SAZ might occur even during the condensational growth phase. This type of SAZ differs from the SAZ discussed in this paper and will be addressed in a subsequent study.

Figure 6 shows the updated conceptual $T$-$r_e$ model with the addition of the line of SAZ for clean and polluted clouds. The clean state (blue and cyan lines) is characterized by low aerosol concentration, thus the $r_e$ increases rapidly above cloud base. The coalescence process is enhanced and leads to early warm rain. In the case where the cloud approaches supercooled temperatures and ice particles start to form, the observed $r_e$ increases sharply with height until all droplets have frozen and $r_e$ is stabilized. The cloud is then considered fully glaciated. The coalescence and rainout decrease the integrated surface area available for condensation, thus $S$ increases. High $S$ allows activation of additional cloud droplets if additional CCN are available, either from cloud base or entrained from aloft. In nature, clouds that undergo significant coalescence and/or warm rainout almost always experience SAZ (blue line). Otherwise, clouds would have difficulty developing further, due to the high $S$ and a lack of sufficient condensational latent heating (cyan line).

In the polluted case (black line), there is a larger number of CCN at cloud base. That leads to a small rate of increase of $r_e$ with height and suppression of the coalescence process. If the coalescence is suppressed up to the freezing level, rainout and SAZ will not appear on the $T$-$r_e$ profile.

Journal of Geophysical Research: Atmospheres 10.1029/2022JD036519

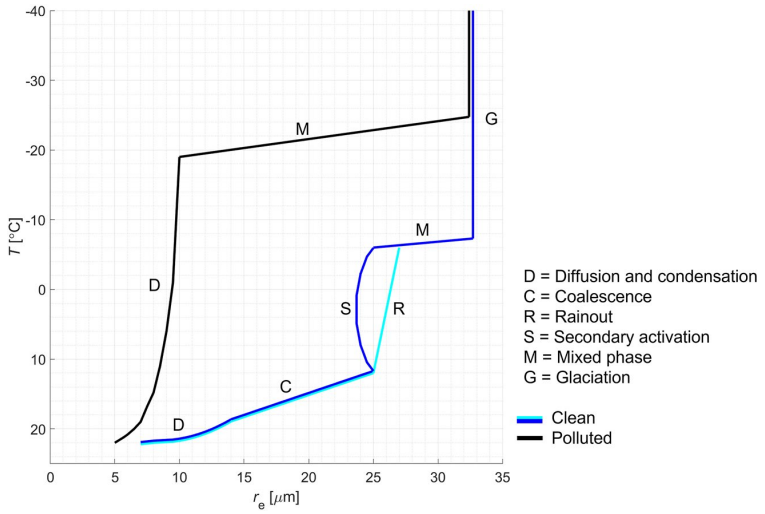


**Figure 6.** An updated conceptual diagram of the microphysical zones for clean and polluted clouds based on the vertical evolution of the $T$-$r_e$ relationships including the secondary activation of droplets above cloud base. The clean cloud (blue and cyan lines) has low $N_d$ and large $r_e$ at cloud base. The enhanced coalescence leads to early warm rain. When the cloud reaches the subzero temperatures and start to glaciate, $r_e$ is increased sharply with height. The coalescence and rainout decrease the integrated surface area available for condensation. The increased $S$ allows activation of additional available CCN into cloud droplets. In nature, clouds with significant coalescence and/or warm rainout usually experience SAZ (blue line). Otherwise, clouds would have difficulty developing further, because of the high $S$ and a lack of sufficient condensational latent heating (cyan line). The polluted case (black line) is characterized by larger $N_d$ and a smaller $r_e$ at cloud base. Suppression of the coalescence process occurs. If the suppression is all the way up to the freezing level, rainout and SAZ will not appear on the $T$-$r_e$ profile.

## 5. Summary

A method to identify the occurrence of secondary activation of droplets above deep convective cloud bases by satellite measurements was introduced in this paper. The earlier $T$-$r_e$ conceptual model by Rosenfeld and Lensky (1998) assumes CCN activation into cloud droplets at cloud base. Thus, a stabilization or moderation of $r_e$ after exceeding a threshold of approximately 14 μm with decreasing $T$ was considered as resulting from rainout of the larger drops from the cloud. However, considering additional nucleation of droplets above cloud base, in the present study the moderation or inversion of $dr_e/dT$ is ascribed to the existence of a significant secondary drop activation zone (SAZ). When pronounced coalescence and warm rain forming processes dominate during the cloud vertical growth, the droplets' integrated surface area is reduced. The reduction of the water surface area available for condensation decreases the condensation rate and increases the supersaturation to high values beyond the maximum supersaturation at cloud base. As a result, particles within the cloud parcel that could not be activated at cloud base due to their lower critical supersaturation are activated aloft. If the rate of large drops elimination is lower than the rate of new droplets activation, there is a decrease of $r_e$ with decreasing $T$ and increasing height. The origins of the newly activated particles can be either UAP from the cloud base and/or entrained particles aloft from the boundaries of the clouds.

The method presented in this study is an updated version of the previous conceptual $T$-$r_e$ model. The detection of SAZ signature on a $T$-$r_e$ profile, is introduced here for the first time. This conceptual model was demonstrated with adiabatic parcel model simulations for different scenarios of aerosol concentrations and size distributions. The SAZ signature was also observed in satellite-retrieved $T$-$r_e$ profiles. The possibility to apply this methodology to satellite retrieved $T$-$r_e$ profiles allows a detailed analysis of cloud microphysics in large areas and over long periods of time. This will increase the understanding of cloud-aerosol interactions at the micro and macro scale. The occurrence of the SAZ signature has climatic importance in shaping cloud microstructure aloft and a possible propagation to cloud radiative forcing.

Journal of Geophysical Research: Atmospheres 10.1029/2022JD036519

## Disclaimer

This paper contains results of research conducted under the Technical/Scientific Cooperation Agreement between the National Institute for Amazonian Research, the State University of Amazonas, and the Max-Planck-Gesellschaft e.V.; the opinions expressed are the entire responsibility of the authors and not of the participating institutions.

## Conflict of Interest

The authors declare no conflicts of interest relevant to this study.

## Data Availability Statement

The satellite data of the case studies presented in this study is available on the VIIRS data set found at the NOAA's Comprehensive Large Array-data Stewardship System (2022; https://www.avl.class.noaa.gov/). The ATTO data used in this study are available via the ATTO data portal through https://www.attoproject.org/. The output data from the IDL program of the sampled cloud scenes have been deposited in supplementary data files for use in follow-up studies (Efraim et al., 2022; https://doi.org/10.5061/dryad.h44j0zpnr). For data requests beyond the available data, please refer to the corresponding author.

**Acknowledgments**
The authors acknowledge the support by the Instituto Nacional de Pesquisas da Amazônia (INPA). The authors would like to thank all people involved in the technical, logistical, and scientific support within the ATTO project. The authors acknowledge the Meteorological Institute of Shaanxi Province, China, for the IDL program for retrieving the cloud microphysical parameters from NPP/VIIRS. For the operation of the ATTO site, we acknowledge the support by the Max Planck Society (MPG), the German Federal Ministry of Education and Research (BMBF contracts 01LB1001A, 01LK1602B, and 01LK2101B) and the Brazilian Ministério da Ciência, Tecnologia e Inovação (MCTI/FINEP contract 01.11.01248.00) as well as the Amazon State University (UEA), FAPEAM, LBA/INPA and SDS/CEUC/RDS-Uatumã. This work has been funded by the Max Planck Society (MPG) and FAPESP - Fundação de Amparo à Pesquisa do Estado de São Paulo, Grant No. 2017/17047-0. Marco A. Franco acknowledges the financial support of CNPq for the Ph.D. scholarship, project number 169842/2017-7, CAPES, for a sandwich doctorate at the Max Planck Institute for Chemistry, project number 88887.368025/2019-00, and FAPESP, Grant No. 2021/13610-8. Leslie A. Kremper acknowledges the financial support by the Max Planck Graduate Center with the Johannes-Gutenberg University, Mainz. In addition, this study was partially supported by the BSF Grant No. 2020809.

## References

Andreae, M. O., Acevedo, O. C., Araùjo, A., Artaxo, P., Barbosa, C. G. G., Barbosa, H. M. J., et al. (2015). The Amazon Tall Tower Observatory (ATTO): Overview of pilot measurements on ecosystem ecology, meteorology, trace gases, and aerosols. *Atmospheric Chemistry and Physics*, *15*(18), 10723–10776. https://doi.org/10.5194/acp-15-10723-2015

Andreae, M. O., Rosenfeld, D., Artaxo, P., Costa, A. A., Frank, G. P., Longo, K. M., & Silva-Dias, M. A. F. (2004). Smoking rain clouds over the Amazon. *Science*, *303*(5662), 1337–1342. https://doi.org/10.1126/science.1092779

Arakawa, A., & Schubert, W. H. (1974). Interaction of a cumulus cloud ensemble with the large-scale environment, part I. *Journal of the Atmospheric Sciences*, *31*(3), 674–701. https://doi.org/10.1175/1520-0469(1974)031<0674:ioacce>2.0.co;2

Artaxo, P., Rizzo, L. V., Brito, J. F., Barbosa, H. M. J., Arana, A., Sena, E. T., et al. (2013). Atmospheric aerosols in Amazonia and land use change: From natural biogenic to biomass burning conditions. *Faraday Discussions*, *165*, 203. https://doi.org/10.1039/c3fd00052d

ATTO - Amazon Tall Tower Observatory. (2020). *ATTO - Amazon tall tower observatory*. Retrieved from https://www.attoproject.org/

Bera, S., Chowdhuri, S., & Prabha, T. V. (2022). A new methodology for the statistical descriptions of particle-by-particle measurements of liquid droplets in cumulus clouds. *Quarterly Journal of the Royal Meteorological Society*, *148*(743), 842–859. https://doi.org/10.1002/qj.4234

Bott, A. (1997). An efficient numerical flux method for the solution of the stochastic collection equation. *Journal of Aerosol Science*, *28*, S745–S746. https://doi.org/10.1016/s0021-8502(97)85371-2

Braga, R. C., Rosenfeld, D., Krüger, O. O., Ervens, B., Holanda, B. A., Wendisch, M., et al. (2021). Linear relationship between effective radius and precipitation water content near the top of convective clouds: Measurement results from ACRIDICON–CHUVA campaign. *Atmospheric Chemistry and Physics*, *21*(18), 14079–14088. https://doi.org/10.5194/acp-21-14079-2021

Braga, R. C., Rosenfeld, D., Weigel, R., Jurkat, T., Andreae, M. O., Wendisch, M., et al. (2017). Further evidence for CCN aerosol concentrations determining the height of warm rain and ice initiation in convective clouds over the Amazon basin. *Atmospheric Chemistry and Physics*, *17*(23), 14433–14456. https://doi.org/10.5194/acp-17-14433-2017

Bréon, F. M., Tanré, D., & Generoso, S. (2002). Aerosol effect on cloud droplet size monitored from satellite. *Science*, *295*(5556), 834–838. https://doi.org/10.1126/science.1066434

Cotton, W. R., Bryan, G., & van den Heever, S. C. (2011). The mesoscale structure of extratropical cyclones and middle and high clouds. *International Geophysics*, *99*, 527–672. https://doi.org/10.1016/s0074-6142(10)09916-x

Efraim, A., Oliver, L., Daniel, R., Ramon, B., Marco, F., Leslie, K., et al. (2022). Satellite processed data [Dataset]. Dryad. https://doi.org/10.5061/dryad.h44j0zpnr

Fan, J., Leung, L. R., Rosenfeld, D., Chen, Q., Li, Z., Zhang, J., & Yan, H. (2013). Microphysical effects determine macrophysical response for aerosol impacts on deep convective clouds. *Proceedings of the National Academy of Sciences*, *110*(48), E4581–E4590. https://doi.org/10.1073/pnas.1316830110

Fan, J., Rosenfeld, D., Zhang, Y., Giangrande, S. E., Li, Z., Machado, L. A. T., et al. (2018). Substantial convection and precipitation enhancements by ultrafineaerosol particles. *Science*, *359*(6374), 411–418. https://doi.org/10.1126/science.aan8461

Feingold, G., Remer, L. A., Ramaprasad, J., & Kaufman, Y. J. (2001). Analysis of smoke impact on clouds in Brazilian biomass burning regions: An extension of Twomey's approach. *Journal of Geophysical Research*, *106*(D19), 22907–22922. https://doi.org/10.1029/2001jd000732

Franco, M. A., Ditas, F., Kremper, L. A., Machado, L. A. T., Andreae, M. O., Araújo, A., et al. (2022). Occurrence and growth of sub-50 nm aerosol particles in the Amazonian boundary layer. *Atmospheric Chemistry and Physics*, *22*(5), 3469–3492. https://doi.org/10.5194/acp-22-3469-2022

Freud, E., & Rosenfeld, D. (2012). Linear relation between convective cloud drop number concentration and depth for rain initiation: Drop concentration and rain initiation. *Journal of Geophysical Research*, *117*(D2). https://doi.org/10.1029/2011JD016457

Freud, E., Rosenfeld, D., Andreae, M. O., Costa, A. A., & Artaxo, P. (2008). Robust relations between CCN and the vertical evolution of cloud drop size distribution in deep convective clouds. *Atmospheric Chemistry and Physics*, *8*(6), 1661–1675. https://doi.org/10.5194/acp-8-1661-2008

Freud, E., Rosenfeld, D., & Kulkarni, J. R. (2011). Resolving both entrainment-mixing and number of activated CCN in deep convective clouds. *Atmospheric Chemistry and Physics*, *11*(24), 12887–12900. https://doi.org/10.5194/acp-11-12887-2011

Journal of Geophysical Research: Atmospheres 10.1029/2022JD036519


Grosvenor, D. P., Sourdeval, O., Zuidema, P., Ackerman, A., Alexandrov, M. D., Bennartz, R., et al. (2018). Remote sensing of droplet number concentration in warm clouds: A review of the current state of knowledge and perspectives. *Reviews of Geophysics*, *56*(2), 409–453. https://doi.org/10.1029/2017rg000593

Gunn, R., & Phillips, B. B. (1957). An experimental investigation of the effect of air pollution on the initiation of rain. *Journal of the Atmospheric Sciences*, *14*(3), 272–280. https://doi.org/10.1175/1520-0469(1957)014<0272:aeiote>2.0.co;2

Hoppel, W. A., & Frick, G. M. (1986). Ion-Aerosol attachment coefficients and the steady-state charge distribution on aerosols in a bipolar ion environment. *Aerosol Science and Technology*, *5*(1), 1–21. https://doi.org/10.1080/02786828608959073

Huang, T., Zhu, Y., Rosenfeld, D., Yang, Y., Lam, D. H. Y., Leung, W. H., et al. (2022). Regime-dependent impacts of aerosol particles and updrafts on the cloud condensation nuclei and the enhanced warm rain suppression: Evidence from synergistic satellite and LiDAR observations. *Geophysical Research Letters*, *49*(3). e2021GL097315. https://doi.org/10.1029/2021gl097315

Hudson, J. G., Noble, S., & Tabor, S. (2015). Cloud supersaturations from CCN spectra Hoppel m*inima. Journal of Geophysical Research: Atmospheres*, *120*(8), 3436–3452. https://doi.org/10.1002/2014jd022669

IPCC. (2013). Summary for Policymakers. In *Climate Change 2013: The Physical Science Basis* (pp. 1–30). Contribution of Working Group I to the Fifth Assessment report of the Intergovernmental Panel on Climate Change [T. F., Stocker, D., Qin, G.-K., Plattner, M., Tignor, S. K., Allen, J. , Boschung, et al. (Eds.)]. Cambridge University Press, Cambridge, United Kingdom and New York, NY, USA. https://doi.org/10.1017/CBO9781107415324.004

IPCC. (2021). Summary for policymakers. In *Climate change 2021: The physical science basis* (pp. 3–32). Contribution of Working Group I to the Sixth Assessment Report of the Intergovernmental Panel on Climate Change [V., MassonDelmotte, P., Zhai, A., Pirani, S. L., Connors, C., Péan, S., Berger, N., Caud, Y., Chen, L., Goldfarb, M. I., Gomis, M., Huang, K., Leitzell, E., Lonnoy, J. B. R., Matthews, et al. (Eds.)]. Cambridge University Press, Cambridge, United Kingdom and New York, NY, USA. https://doi.org/10.1017/9781009157896.001

Khain, A. P., Phillips, V., Benmoshe, N., & Pokrovsky, A. (2012). The role of small soluble aerosols in the microphysics of deep maritime clouds. *Journal of the Atmospheric Sciences*, *69*(9), 2787–2807. https://doi.org/10.1175/2011jas3649.1

Konwar, M., Maheskumar, R. S., Kulkarni, J. R., Freud, E., Goswami, B. N., & Rosenfeld, D. (2012). Aerosol control on depth of warm rain in convective clouds: Aerosol control on depth of warm rain. *Journal of Geophysical Research*, *117*(D13). https://doi.org/10.1029/2012jd017585

Lensky, I. M., & Rosenfeld, D. (2006). The time-space exchangeability of satellite retrieved relations between cloud top temperature and particle effective radius. *Atmospheric Chemistry and Physics*, *6*(10), 2887–2894. https://doi.org/10.5194/acp-6-2887-2006

Moran-Zuloaga, D., Ditas, F., Walter, D., Saturno, J., Brito, J., Carbone, S., et al. (2018). Long-term study on coarse mode aerosols in the Amazon rain forest with the frequent intrusion of Saharan dust plumes. *Atmospheric Chemistry and Physics*, *18*(13), 10055–10088. https://doi.org/10.5194/acp-18-10055-2018

Nakajima, T., Higurashi, A., Kawamoto, K., & Penner, J. E. (2001). A possible correlation between satellite-derived cloud and aerosol microphysical parameters. *Geophysical Research Letters*, *28*(7), 1171–1174. https://doi.org/10.1029/2000gl012186

NOAANOAANOAA's Comprehensive Large Array-data Steward*ship Sy*stem. (2022). Noaa.Gov. Retrieved from https://www.avl.class.noaa.gov/saa/products/search?sub_id=0&datatype_family=VIIRS_SDR&submit.x=22&submit.y=4

Paluch, I. R., & Baumgardner, D. G. (1989). Entrainment and fine-scale mixing in a continental convective cloud. *Journal of the Atmospheric Sciences*, *46*(2), 261–278. https://doi.org/10.1175/1520-0469(1989)046<0261:eafsmi>2.0.co;2

Paluch, I. R., & Knight, C. A. (1984). Mixing and the evolution of cloud droplet size spectra in a vigorous continental cumulus. *Journal of the Atmospheric Sciences*, *41*(11), 1801–1815. https://doi.org/10.1175/1520-0469(1984)041<1801:mateoc>2.0.co;2

Pan, Z., Rosenfeld, D., Zhu, Y., Mao, F., Gong, W., Zang, L., & Lu, X. (2021). Observational quantification of aerosol invigoration for deep convective cloud lifecycle properties based on geostationary satellite. *Journal of Geophysical Research: Atmospheres*, *126*(9). e2020JD034275. https://doi.org/10.1029/2020jd034275

Pinsky, M., Khain, A., Mazin, I., & Korolev, A. (2012). Analytical estimation of droplet concentration at cloud base: Droplet concentration at cloud base. *Journal of Geophysical Research: Atmospheres*, *117*(D18), https://doi.org/10.1029/2012jd017753

Pinsky, M., Khain, A., & Shapiro, M. (2001). Collision efficiency of drops in a wide range of Reynolds numbers: Effects of pressure on spectrum evolution. *Journal of the Atmospheric Sciences*, *58*(7), 742–764. https://doi.org/10.1175/1520-0469(2001)058<0742:ceodia>2.0.co;2

Pinsky, M. B., & Khain, A. P. (2002). Effects of in-cloud nucleation and turbulence on droplet spectrum formation in cumulus clouds. *Quarterly Journal of the Royal Meteorological Society*, *128*(580), 501–533. https://doi.org/10.1256/003590002321042072

Pöhlker, C., Walter, D., Paulsen, H., Könemann, T., Rodríguez-Caballero, E., Moran-Zuloaga, D., et al. (2019). Land cover and its transformation in the backward trajectory footprint region of the Amazon Tall Tower Observatory. *Atmospheric Chemistry and Physics*, *19*(13), 8425–8470. https://doi.org/10.5194/acp-19-8425-2019

Pöhlker, M. L., Ditas, F., Saturno, J., Klimach, T., Hrabě de Angelis, I., Araùjo, A. C., et al. (2018). Long-term observations of cloud condensation nuclei over the Amazon rain forest – Part 2: Variability and characteristics of biomass burning, long-range transport, and pristine rain forest aerosols. *Atmospheric Chemistry and Physics*, *18*(14), 10289–10331. https://doi.org/10.5194/acp-18-10289-2018

Pöhlker, M. L., Pöhlker, C., Ditas, F., Klimach, T., Hrabe de Angelis, I., Araújo, A., et al. (2016). Long-term observations of cloud condensation nuclei in the Amazon rain forest – Part 1: Aerosol size distribution, hygroscopicity, and new model parametrizations for CCN prediction. *Atmospheric Chemistry and Physics*, *16*(24), 15709–15740. https://doi.org/10.5194/acp-16-15709-2016

Pöhlker, M. L., Zhang, M., Campos Braga, R., Krüger, O. O., Pöschl, U., & Ervens, B. (2021). Aitken mode particles as CCN in aerosol- and updraft-sensitive regimes of cloud droplet formation. *Atmospheric Chemistry and Physics*, *21*(15), 11723–11740. https://doi.org/10.5194/acp-21-11723-2021

Prabha, T. V., Khain, A., Maheshkumar, R. S., Pandithurai, G., Kulkarni, J. R., Konwar, M., & Goswami, B. N. (2011). Microphysics of premonsoon and monsoon clouds as seen from in situ measurements during the cloud aerosol interaction and precipitation enhancement experiment (CAIPEEX). *Journal of the Atmospheric Sciences*, *68*(9), 1882–1901. https://doi.org/10.1175/2011jas3707.1

Quaas, J., Ming, Y., Menon, S., Takemura, T., Wang, M., Penner, J. E., et al. (2009). Aerosol indirect effects – General circulation model intercomparison and evaluation with satellite data. *Atmospheric Chemistry and Physics*, *9*(22), 8697–8717. https://doi.org/10.5194/acp-9-8697-2009

Rosenfeld, D. (2007). New insights to cloud seeding for enhancing precipitation and for hail suppression. *Journal of Weather Modification*, *39*, 61–69. https://doi.org/10.1007/978-1-4020-5835-6_6

Rosenfeld, D. (2018). Cloud-aerosol-precipitation interactions based of satellite retrieved vertical profiles of cloud microstructure. In *Remote sensing of aerosols, clouds, and precipitation* (pp. 129–152). https://doi.org/10.1016/b978-0-12-810437-8.00006-2

Rosenfeld, D., Fischman, B., Zheng, Y., Goren, T., & Giguzin, D. (2014). Combined satellite and radar retrievals of drop concentration and CCN at convective cloud base: Rosenfeld et al.; retrieving convective cloud base CCN. *Geophysical Research Letters*, *41*(9), 3259–3265. https://doi.org/10.1002/2014gl059453

Rosenfeld, D., Kaufman, Y. J., & Koren, I. (2006). Switching cloud cover and dynamical regimes from open to closed Benard cells in response to the suppression of precipitation by aerosols. *Atmospheric Chemistry and Physics*, *6*(9), 2503–2511. https://doi.org/10.5194/acp-6-2503-2006

Journal of Geophysical Research: Atmospheres 10.1029/2022JD036519

Rosenfeld, D., & Lensky, I. M. (1998). Satellite-based insights into precipitation formation processes in continental and maritime convective clouds. *Bulletin of the American Meteorological Society*, *79*(11), 2457–2476. https://doi.org/10.1175/1520-0477(1998)079<2457:sbiipf>2.0.co;2

Rosenfeld, D., Liu, G., Yu, X., Zhu, Y., Dai, J., Xu, X., & Yue, Z. (2014). High-resolution (375 m) cloud microstructure as seen from the NPP/VIIRS satellite imager. *Atmospheric Chemistry and Physics*, *14*(5), 2479–2496. https://doi.org/10.5194/acp-14-2479-2014

Rosenfeld, D., Lohmann, U., Raga, G. B., O'Dowd, C. D., Kulmala, M., Fuzzi, S., et al. (2008). Flood or drought: How do aerosols affect precipitation? *Science*, *321*(5894), 1309–1313. https://doi.org/10.1126/science.1160606

Rosenfeld, D., Woodley, W. L., Lerner, A., Kelman, G., & Lindsey, D. T. (2008). Satellite detection of severe convective storms by their retrieved vertical profiles of cloud particle effective radius and thermodynamic phase. *Journal of Geophysical Research*, *113*(D4), D04208. https://doi.org/10.1029/2007jd008600

Rosenfeld, D., Zheng, Y., Hashimshoni, E., Pöhlker, M. L., Jefferson, A., Pöhlker, C., et al. (2016). Satellite retrieval of cloud condensation nuclei concentrations by using clouds as CCN chambers. *Proceedings of the National Academy of Sciences*, *113*(21), 5828–5834. https://doi.org/10.1073/pnas.1514044113

Seinfeld, J. H., & Pandis, S. N. (1998). *Atmospheric chemistry and physics: From air pollution to climate change*. Wiley.

Shinozuka, Y., Clarke, A. D., Nenes, A., Jefferson, A., Wood, R., McNaughton, C. S., et al. (2015). The relationship between cloud condensation nuclei (CCN) concentration and light extinction of dried particles: Indications of underlying aerosol processes and implications for satellite-based CCN estimates. *Atmospheric Chemistry and Physics*, *15*(13), 7585–7604. https://doi.org/10.5194/acp-15-7585-2015

Slingo, A., & Slingo, J. M. (1988). The response of a general circulation model to cloud longwave radiative forcing. I: Introduction and initial experiments. *Quarterly Journal of the Royal Meteorological Society*, *114*(482), 1027–1062. https://doi.org/10.1002/qj.49711448209

Squires, P. (1958). The microstructure and colloidal stability of warm clouds. *Tellus*, *10*(2), 256–261. https://doi.org/10.1111/j.2153-3490.1958.tb02011.x

Thornton, J. A., Virts, K. S., Holzworth, R. H., & Mitchell, T. P. (2017). Lightning enhancement over major oceanic shipping lanes. *Geophysical Research Letters*, *44*(17), 9102–9111. https://doi.org/10.1002/2017gl074982

Twomey, S. (1977). The influence of pollution on the shortwave albedo of clouds. *Journal of the Atmospheric Sciences*, *34*(7), 1149–1152. https://doi.org/10.1175/1520-0469(1977)034<1149:tiopot>2.0.co;2

Warner, J. (1969). The microstructure of cumulus cloud. Part I. General features of the droplet spectrum. *Journal of the Atmospheric Sciences*, *26*(5), 1049–1059. https://doi.org/10.1175/1520-0469(1969)026<1049:tmoccp>2.0.co;2

Wendisch, M., Pöschl, U., Andreae, M. O., Machado, L. A. T., Albrecht, R., Schlager, H., et al. (2016). Acridicon–Chuva campaign: Studying tropical deep convective clouds and precipitation over Amazonia using the new German research aircraft Halo. *Bulletin of the American Meteorological Society*, *97*(10), 1885–1908. https://doi.org/10.1175/bams-d-14-00255.1

Yuan, T., Remer, L. A., Pickering, K. E., & Yu, H. (2011). Observational evidence of aerosol enhancement of lightning activity and convective invigoration: Aerosol enhancement of lightning. *Geophysical Research Letters*, *38*(4), https://doi.org/10.1029/2010gl046052

Zheng, Y., & Rosenfeld, D. (2015). Linear relation between convective cloud base height and updrafts and application to satellite retrievals: Satellite retrieval of cloud updrafts. *Geophysical Research Letters*, *42*(15), 6485–6491. https://doi.org/10.1002/2015gl064809

Zhu, Y., Rosenfeld, D., Yu, X., Liu, G., Dai, J., & Xu, X. (2014). Satellite retrieval of convective cloud base temperature based on the NPP/VIIRS imager. *Geophysical Research Letters*, *41*(4), 1308–1313. https://doi.org/10.1002/2013gl058970

## 2.2 Secondary droplet activation in polluted convective clouds

**This chapter will be published as:**

Efraim, A.; Campos Braga, R.; Rosenfeld, D.; Lauer, O.; Franco, M. A.; Kremper, L. A.; Pöhlker, C., and Pöhlker, M. L.: "Satellite-based detection of secondary droplet activation during condensational growth in convective clouds". *Submitted to Journal of Geophysical Research: Atmospheres*. (2022)

**Contribution to this publication by Oliver Lauer:** The effect presented in this paper was an observation of my analyses in this course of the other papers in this thesis. These cases were not used in my seasonal trend analysis in the last paper of this thesis as they erroneously overestimate $N_d$. Instead, Avichay Efraim has used my analysis and results as a basis for his case studies and the model runs in this paper. I was mainly responsible for the analysis of the satellite data and interpretation of the results in combination with the ATTO and the modeling data.

## Satellite-based detection of secondary droplet activation during condensational growth in convective clouds

Avichay Efraim[1], Ramon C. Braga[2], Daniel Rosenfeld[1], Oliver Lauer[3], Marco A. Franco[3,4,9], Leslie A. Kremper[3], Christopher Pöhlker[3], Meinrat O. Andreae[3,7,8], Cléo Q. Dias-Junior[10,11], and Mira L. Pöhlker[3,5,6]

[1]Institute of Earth Sciences, The Hebrew University of Jerusalem, Jerusalem, Israel
[2] National Marine Research Centre, Southern Cross University, 2450 Coffs Harbour, Australia
[3] Multiphase Chemistry Department, Max Planck Institute for Chemistry, 55128 Mainz, Germany
[4]Institute of Physics, University of São Paulo, São Paulo 05508-900, Brazil
[5]Leipzig Institute for Meteorology, University of Leipzig, 04103 Leipzig, Germany
[6]Atnospheric Microphysics Department, Leibniz Institute for Tropospheric Research, 04318 Leipzig, Germany
[7]Department of Geology and Geophysics, King Saud University, Riyadh, Saudi Arabia
[8]Scripps Institution of Oceanography, UCSD, La Jolla, California, USA
[9]Research Centre for Greenhouse Gas Innovation (RCGI-POLI), University of São Paulo, Av. Professor Mello Moraes, 2231, Butantã, São Paulo 05508-030, Brazil
[10]Postgraduate Program on Environmental Sciences – PPGCA, Federal University of Par´a (UFPA), Belem, PA, Brazil
[11]Postgraduate Program in Climate and Environment (CLIAMB, INPA/UEA), Manaus, AM, Brazil

Corresponding author: Avichay Efraim (Avichay.Efraim@mail.huji.ac.il)

**Abstract**

By acting as cloud condensation nuclei (CCN), aerosol particles play a key role in the climate system. The CCN can be activated into cloud droplets at the base of the cloud (primary activation), or above it (secondary activation). This study shows the conditions for the secondary aerosol activation (SA) into cloud drops above the cloud base, where the condensational growth dominates, and proposes a methodology for detecting the SA. Using a spectral bin adiabatic parcel model, we simulate the vertical profile of cloud microphysical properties and the effects of different aerosol size distributions and updraft velocities on the SA. We demonstrate that the SA decreases the cloud drop effective radius ($r_e$) with increasing height and decreasing temperature (*T)* due to the relatively larger population of smaller droplets in the cloud parcel. The SA causes $r_e$ to grow with decreasing *T* at a less than adiabatic rate. Satellite retrievals were used to calculate the adiabatic cloud drop number concentrations ($N_d$) in convective clouds over the Amazon Tall Tower Observatory (ATTO) region. The retrievals were validated against in-situ aerosol particle number concentration data obtained at ATTO. The findings of this study can be used for satellite detection of SA in convective clouds, where the retrieved $N_d$ is overestimated since the growth is no longer adiabatic. This contributes to clarifying the role of aerosol particles in the microphysics, dynamics, and precipitation behavior of convective clouds.

# 1 Introduction

## 1.1 Background

The impacts of aerosols on clouds and climate are among the most significant uncertainties in the assessment and modeling of climate change (IPCC, 2013, 2021). Remote sensing techniques for studying aerosols and clouds allow worldwide monitoring and analysis of aerosol-cloud interactions (e.g., Rosenfeld and Lensky, 1998; Bréon et al., 2002; Rosenfeld et al., 2016; Grosvenor et al., 2018). Yet, it has remained a major challenge to analyze aerosol and cloud characteristics with sufficient precision to quantify how cloud microstructure and the associated radiative properties respond to aerosol perturbations.

The number concentration of cloud droplets ($N_d$) at the cloud base mainly depends on the activation spectrum of the aerosol particles that serve as cloud condensation nuclei (CCN) as a function of supersaturation ($S$) (Köhler, 1936; Twomey, 1959). The $S$ rises when an air parcel is steadily cooled below the dew point due to existing cloud base updraft ($w_b$). When $S$ reaches a critical value ($S_c$) that is characteristic for the properties of a given CCN, it is activated and grows into a droplet. As $S$ increases, further activation of droplets occurs, and the already activated CCN continue to grow. Consequently, water vapor is removed by condensation at a steadily increasing rate, resulting in a slowing of the increase of $S$ until the effect of condensation balances the growth of $S$ due to the cooling. Under the assumption of a fixed $w_b$, the maximum $S$ at the cloud base ($S_{max}$) is reached within a small distance (a few to tens of meters) above the cloud base (Twomey, 1959; Rogers & Yau, 1996). Above the level of $S_{max}$, the existing droplets continue to grow, $S$ starts to decrease, and no further CCN are activated. The $N_d$ at the cloud base will then be determined by the number of activated $N_{CCN}$ where $S_c \leq S_{max}$ (Twomey, 1959).

Aerosol optical depth (AOD) has been widely used as a proxy for $N_{CCN}$ (Feingold et al., 2001; Andreae, 2009; Quaas et al., 2009). The Aerosol Index (AI), which is the product of AOD and Ångström exponent (Nakajima et al. 2001), provides an even better estimation for $N_{CCN}$. However, Shinozuka et al. (2015) showed that such optically retrieved $N_{CCN}$ might differ by an order of magnitude from the directly measured $N_{CCN}$. Additionally, the optical signal of aerosols used for satellite-retrieved AOD and AI decreases below the discernible level for $N_{CCN} < 150$ cm$^{-3}$. This threshold varies greatly depending on the size of the CCN and their activation supersaturation (Shinozuka et al., 2015).

Another method for remote retrieval of $N_d$ and $N_{CCN}$ in growing convective towers is based on the growth of cloud drop effective radius ($r_e$) with height or decreasing temperature ($T$). This approach relies on aircraft observations showing that the measured $r_e$ in different cloud depths above the cloud base increases almost as if the clouds were adiabatic. However, the cloud liquid water content (LWC) is mostly smaller than adiabatic state (Freud et al., 2011, Braga et al., 2017). This pattern is caused by the nearly inhomogeneous mixing behavior of the convective clouds with the ambient air. Freud et al. (2011) showed that the cloud base $N_d$ could be approximated by the ratio of adiabatic LWC ($LWC_a$) to the mass of a single droplet ($M_{droplet}$) with an adiabatic $r_e$. Rosenfeld et al. (2014a) demonstrated that the $T$-$r_e$ profiles can be retrieved by satellites and thus provide the capability of calculating the adiabatic $N_d$ based on the assumption of adiabatic $r_e$ and $LWC_a$. Using the cloud base height ($H_b$), $w_b$ can be approximated based on the empirical relation $w_b = 0.9H_b$, where $H_b$ is in km and $w_b$ is in ms$^{-1}$ (Zheng and Rosenfeld, 2015). Then, the estimated $N_d$ and $w_b$ are used to calculate $S_{max}$ (Pinsky et al., 2012),

where $N_d$ is, by definition, $N_{CCN}$ at $S_{max}$. Rosenfeld et al. (2016) combined all these considerations into a method to retrieve cloud base $N_d$ and $S_{max}$ by satellite, which is essentially the $N_{CCN}(S)$, with an accuracy of ±30%. However, as pointed out earlier, $N_d$ and $N_{CCN}$ can only be retrieved from vertical $T$-$r_e$ profiles as long as the $r_e$ behaves adiabatically. The layers of the cloud where $r_e$ is nearly adiabatic are where the condensation process dominates the cloud droplets' growth (i.e., for $r_e$ < 14 µm (Rosenfeld et al., 2006)). This occurs above the level of $S_{max}$ close to the cloud base and below the level where the coalescence process dominates. Droplet coalescence increases the growth rate of $r_e$ with decreasing $T$ beyond the adiabatic condensational growth rate; thus, the $T$-$r_e$ is not adiabatic anymore. The condensation phase of the cloud and its role in the calculation of $N_d$ will be further described in Section 1.3.

### 1.2 Secondary Activation Zone

The process of activating cloud droplets well above the cloud base (above the height of $S_{max}$) is referred to herein as secondary activation, as opposed to the primary activation of droplets at the cloud base. Secondary activation might occur in two ways:

(1) When entrained particles from the cloud's lateral and/or top boundaries get activated as their characteristic $S_c$ is lower than the actual $S$ they experience in the cloud, which is smaller than $S_{max}$.

(2) When $S$ above cloud base exceeds the $S_{max}$. This can occur either when droplet coalescence reduces the integrated droplets' surface area available for condensation, which decreases the condensation rate and increases $S$, or when there is an increase in the $w$, which increases $S$ due to a higher cooling rate. As a result, particles, which were not activated at the cloud base because their $S_c$ was greater than $S_{max}$, can now be activated into cloud droplets at this elevated $S$.

Both mechanisms will reduce the observed $r_e$ with decreasing $T$, compared to its increase rate with decreasing $T$, due to the activation of tiny new droplets in the environment of large existing droplets, as shown by several in-cloud aircraft campaigns (Warner 1969; Paluch and Knight, 1984; Paluch and Baumgardner, 1989; Prabha et al., 2011; Braga et al., 2017; Bera et al., 2022). The secondary activation process might have an important impact on climate. The released latent heat from the activation of the new cloud droplets above the cloud base increases the buoyancy and further invigorates the cloud towards the tropopause (Khain et al., 2012; Fan et al., 2018). This invigoration may lead to more extensive and colder anvils in the form of cirrus clouds (Fan et al., 2013, Pan et al., 2021). These clouds efficiently absorb outgoing longwave radiation (OLR) and marginally reflect the incoming sunlight (Stephen et al., 1990). Therefore, during the day they might not have a large albedo, but they do absorb most of the OLR during day and night, eventually resulting in a positive radiative forcing and warming effect (Slingo & Slingo, 1988; Cotton et al., 2011). Moreover, the evaporation of ice crystals from these anvils may enrich the upper troposphere with water vapor, a strong greenhouse gas. Therefore, it will likely strengthen the positive radiative forcing.

The vertical microphysical zone in the cloud where secondary activation occurs is defined as the "secondary activation zone" (*SAZ*). Efraim et al. (2022) presented a method to identify the post-coalescence *SAZ* along with

other microphysical zones from satellite observations. This method analyses the $T$-$r_e$ profile and divides the cloud into different microphysical zones based on the growth rate of $r_e$ with decreasing $T$ ($dr_e/dT$) (Fig. 1):

(1) condensational growth - $r_e$ growth rate is similar to an adiabatic $r_e$ curve originating at the cloud base;

(2) coalescence - the growth rate of $r_e$ exceeds the adiabatic growth rate;

(3) rainout - a moderation of the growth rate of $r_e$;

(4) secondary activation – a negative growth rate of $r_e$;

(5) mixed-phase of ice and water – a rapid regrowth of $r_e$ above the subzero temperatures; and

(6) glaciation – where the indicated $r_e$ reaches a maximum threshold of 40 µm and/or temperatures colder than -38 °C.

The *SAZ* signature in the $T$-$r_e$ profile, where a negative $dr_e/dT$ occurs, indicates the presence of a significant number of smaller droplets aloft either due to activation of CCN particles from the cloud base or entrainment of CCN particles from the cloud boundaries. Figure 1 shows a conceptual $T$-$r_e$ profile and the microphysical zones for clouds in low (*clean*) and high (*polluted*) aerosol concentrations regimes. In the *clean* clouds, $N_d$ is relatively low, and $r_e$ is large at the cloud base. The existence of initially large droplets enhances the probability of droplet collision and coalescence process, which decreases the integrated surface area available for condensation. As a result, $S$ increases, and allows activation of more CCN with higher $S_c$ into cloud droplets. In nature, clouds with significant coalescence and rainout experience secondary activation if there are sufficient unactivated CCN in the cloud parcel (blue line). Otherwise, clouds that have not undergone any orographic or mechanical lifting or do not have the thermodynamic conditions, would have difficulty developing further because of the high $S$ and a lack of sufficient condensational latent heating (cyan line). The *polluted* cloud (black line) has a larger $N_d$ and a smaller $r_e$ at the cloud base. In such conditions, the coalescence process is inhibited and delays the droplets' growth into raindrops (Gunn and Phillips, 1957; Squires, 1958). When this process is suppressed up to the freezing level; the warm rainout and secondary activation will not appear in the $T$-$r_e$ profile.

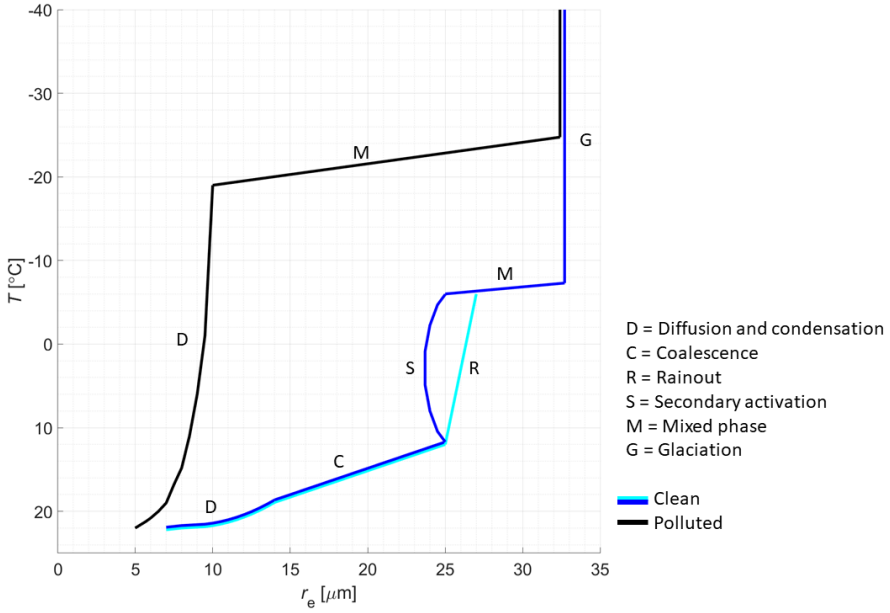


135 Figure 1. Conceptual diagram of the microphysical zones in convective clouds in low (*clean* - blue and cyan lines) and high (*polluted* – black line) aerosol concentration regimes based on the vertical evolution of the effective radius ($r_e$) with decreasing *T*. Adapted from Efraim et al., 2022.

Model runs have shown that activation of new droplets above the cloud base may occur after coalescence in both clean and polluted clouds (Efraim et al., 2022). The ratio between the droplet activation and the large drop
140 elimination due to precipitation has to be high for the *SAZ* to be significant and the $N_d$ increase to be noticeable, meaning more droplets will activate during the secondary activation above the cloud base than being eliminated due to precipitation.

However, an increase in updraft (*w*) above the cloud base may promote secondary activation also when the condensational growth takes place, even before the coalescence process dominates. This can occur when the
145 cooling rate, dictated by the *w*, increases *S* to the extent that *S* exceeds $S_{max}$ near the cloud base, where the condensational growth is still dominant. The effect of secondary activation of droplets during the condensational growth phase will be described in the following section.

Hereafter, the microphysical zone in the cloud where secondary activation during the condensational growth occurs is referred to as $SAZ_{cond,}$ and the secondary activation of droplets above the coalescence phase is indicated
150 as $SAZ_{coal}$.

### 1.3 Secondary activation during the condensational growth phase, $SAZ_{cond}$

Additional condensation of water vapor above the level of $S_{max}$ leads to a growth of the existing cloud droplets, i.e., condensational growth. This process further increases the integrated droplet surface area, decreases *S*, and

usually prevents the activation of additional cloud droplets above that level (Rosenfeld, 2018). The $LWC_a$ is divided over the single droplet mass of the existing cloud droplets ($M_{droplet}$), causing the $N_d$ to remain relatively constant with height. This is valid as long as the cloud is adiabatic and there is no droplet evaporation or activation of new CCN particles (Rosenfeld, 2018). Therefore, a linear relationship of $LWC_a$-$M_{droplet}$ ratio would mean an adiabatic part of the cloud. The adiabatic condensational growth phase is then determined by the most consecutive linear points of the $LWC_a$-$M_{droplet}$ ratio. This linear part should also be close to the cloud base and pass through the origin, because when $LWC_a$ is zero, there are no droplets. Figure 2 illustrates the $LWC_a$ [g/kg] as a function of $M_{droplet}$ [µg] for each temperature bin. The $LWC_a$ is calculated based on the retrieved cloud base pressure and temperature and increases up to the cloud top (Freud et al., 2011). Assuming the droplets are spherical, the $M_{droplet}$ is calculated by the product of the droplet volume and the water density. The droplet volume calculation uses the mean-volume radius, $r_v$, where $r_v = \frac{r_e}{1.08}$ in the adiabatic part (Freud et al., 2011). As long as the $LWC_a$-$M_{droplet}$ ratio remains linear, the adiabaticity is preserved. This means that the $LWC_a$ is divided equally between the existing cloud base $N_d$ without losing or gaining droplets. If this ratio is no longer linear, it can either mean droplet coalescence, where $M_{droplet}$ increase beyond adiabaticity; precipitation, where $M_{droplet}$ decreases due to the removal of raindrops and remaining tiny drops; or activation of new cloud droplets, which also decreases $M_{droplet}$.

As mentioned above, $N_d$ is calculated based on the linear $LWC_a$-$M_{droplet}$ ratio. Any deviation from adiabaticity due to $SAZ_{cond}$ in the defined linear part may cause an overestimation in the retrieval of cloud base $N_d$. This will be further discussed in Section 4. Another impact of $SAZ_{cond}$ is the suppression of warm rain due to the activation of tiny cloud droplets that inhibits the collision and coalescence processes and delay the droplets' growth into raindrops. In addition, several studies suggested, based on aircraft and satellite measurements, that warm rain formation requires a cloud with $r_e$ larger than 13-14 µm (Rosenfeld and Gutman, 1994; Gerber, 1996; Pinsky and Khain, 2002; VanZanten et al., 2005; Chen et al., 2008; Prabha et al., 2011; Konwar et al., 2012; Freud and Rosenfeld, 2012). The occurrence of $SAZ_{cond}$ results in a smaller $r_e$ close to the cloud base, thus suppressing warm rain formation and being prone to invigorate the cloud. This will be described by the model and with aircraft validations in Section 3.1 and Section 4, respectively.

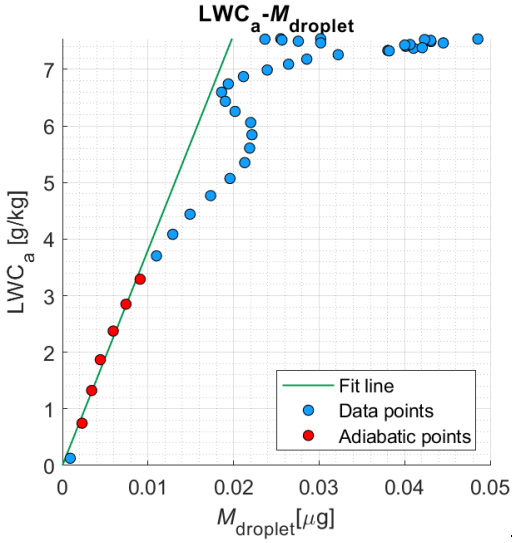


Figure 2. Illustration of the adiabatic LWC (LWC$_a$ [g/kg]) over droplet mass ($M_{droplet}$ [µg]). The data was derived from a sample case study over the Amazon from March 23rd, 2017. Each point represents the calculated LWC$_a$ and $M_{droplet}$ for each temperature bin. The LWC$_a$ is calculated based on the cloud base pressure and temperature, and the $M_{droplet}$ is based on the mean-volume radius ($r_v$), where $r_v = \frac{r_e}{1.08}$ in the adiabatic part. The red points and the green fit line mark the part where the LWC$_a$-$M_{droplet}$ ratio is most linear and passes through (0,0). These are the adiabatic points by which the $N_d$ at the cloud base is calculated. Any deviation or noise in the defined adiabatic points may cause a bias in retrieving the cloud base $N_d$.

This study describes the physical principle of secondary activation of droplets during the condensational growth of convective clouds. For this purpose, a spectral bin microphysics adiabatic parcel model was used to simulate the $r_e$, $N_d$, $w$, and $S$ profiles with decreasing $T$ for different aerosol size distribution (ASD) and $w$ schemes. In addition, a method to detect $SAZ_{cond}$ from satellite is presented, and the impact of $SAZ_{cond}$ on the satellite retrieval of $N_d$ is discussed. The simulated cloud properties are described in Section 3.1. Case studies with and without a detectable $SAZ_{cond}$ on satellite retrieved $T$-$r_e$ and discussion are described in Section 3.2 and Section 4, respectively.

## 2 Methods

### 2.1 Model Description

The model used in this study is the spectral bin adiabatic parcel model developed by Pinsky and Khain (2002), which describes the cloud microphysical properties of convective clouds. It does so by explicitly calculating the particle spectrum evolution using a moving mass grid containing 2000 mass bins and allowing effects on droplet

collisions. The model also calculates the processes of aerosol growth, their activity as CCN, the vertical evolution of cloud microstructure, and precipitation-forming processes in the water phase (temperatures warmer than -10 °C). The initialization conditions are ASD, thermodynamic properties from measurements performed over the Amazon Forest, and prescribed *w* schemes. The aerosol particles are considered spherical NaCl particles to ensure compatibility with the model construction. Braga et al. (2017) have shown that the vertical evolution of $r_e$ during the condensational growth of the cloud agrees well with the theoretical $r_e$ driven by the adiabatic growth of droplets through water condensation. The coagulation and coalescence processes start to dominate at a higher level above the cloud base. The coagulation process of cloud drops is calculated as proposed by Pinsky et al. (2001), who describe this process by solving stochastic collision equations according to Bott (1997). The drop-drop collision efficiency is calculated from the cloud base for droplet masses allocated to the same parcel. As the collision efficiency increases, the coagulation and coalescence processes become more dominant and dictate the microphysical zone in the cloud. Although this model is quite thorough and attempts to describe the fundamental physical processes by simplifying or ignoring additional environmental factors, the resulting microphysical processes may vary from actual cloud behavior. However, this model is well suited to illustrate the physical principle of $SAZ_{cond}$.

### 2.2 Satellite *T*-$r_e$ retrieval

The satellite retrievals of cloud properties described in the case studies in section 3.2 were performed using the Visible Infrared Imaging Radiometer Suite (VIIRS) passive sensor onboard the Suomi National Polar-orbiting Partnership (S-NPP) satellite. The VIIRS sensor offers a relatively high spatial resolution of 375 meters at a nadir in 5 optical channels for detailed spectral information (Rosenfeld et al., 2014a, 2014b). Such high spatial resolution is needed to accurately resolve the vertical structure of convective clouds. A snapshot of the *T*-$r_e$ profile of a cloud cluster provides the same information as obtained by tracking a single convective cloud throughout its vertical evolution (Arakawa and Schubert, 1974, Lensky and Rosenfeld, 2006). It is also assumed that for a non-precipitating cloud, $r_e$ in the cloud top pixel has the same value as within more developed clouds at the same height (Rosenfeld and Lensky, 1998; Freud et al., 2008). These assumptions enable the inference of vertical *T*-$r_e$ development of clouds in a two-dimensional spatial image. The wavelengths used to retrieve the *T*-$r_e$ profile are 3.7 µm and 10.8 µm (Rosenfeld et al., 2014b). This method assumes retrieval of water drops. However, ice particles are much larger than the droplets in the clouds in which they are formed. They absorb more strongly the solar radiation at the 3.7 µm band. Consequently, the satellite retrieved $r_e$ of ice particles appear larger than the same size water drops. Therefore, a very large $r_e$ at supercooled temperature usually indicates the existence of ice in the cloud. A designated IDL software produces an RGB display that highlights the cloud microphysics and *T* and $r_e$ retrievals in each pixel. Based on this display, cloud scenes of interest are manually selected to avoid or minimize obstruction by multilayer or semi-transparent clouds. A cloud mask algorithm, introduced by Zhu et al. (2014), filters out the partially filled cloudy pixels to avoid measurement errors in such pixels. To reduce data distortion, the cloud scenes have to be located where the satellite zenith

angle is between 30° and -20°, and the solar zenith angle is below 65°. The specific $r_e$ values for each pixel are sorted by the detected temperature for each pixel into 1 °C sized bins (i.e., 9.5 - 10.5 °C in the 10 °C bin, etc.). Then, the 30$^{th}$ percentile for all $r_e$ values within one bin is calculated, resulting in a continuous $T$-$r_e$ profile (Rosenfeld et al., 2016). The 30-percentile median is taken to capture the clouds in their growing phase since the effect of aerosols on the $T$-$r_e$ profile is mostly reflected in the growing clouds rather than in mature dissipating clouds (Lensky and Rosenfeld, 2006; Rosenfeld et al., 2008). Multilayer clouds are identified by a lack of continuity in the $T$-$r_e$ profiles. Therefore, this methodology is invalid for non-convective clouds or scenes obscured by multilayer clouds. $T$-$r_e$ profiles obtained in different locations yield similar findings for similar environments. (e.g., Lensky and Rosenfeld, 2006; Rosenfeld, 2007; Rosenfeld et al., 2008; Huang et al., 2022) implying the robustness of $T$-$r_e$ retrievals and the fact that this method can be applied worldwide, in any meteorology, and for any convective clouds as long as a valid unperturbed $T$-$r_e$ profile is retrieved. An automatic algorithm then analyzes the retrieved $T$-$r_e$ profiles to detect the different microphysical zones (Efraim et al., 2022), while this study focuses on the detected condensational growth phase.

### 2.3 Aerosol observations at the Amazon Tall Tower Observatory

The Amazon Tall Tower Observatory (ATTO) is located in the central Amazon Basin (2.145 °S, 59.004 °W at 130 m above sea level). For each of the case studies described in section 3.2, an ASD was measured by a Scanning Mobility Particle Sizer (SMPS, TSI Inc.) connected to an inlet line at 60 m height on an 80 m tall mast (for details see Franco et al., 2022). In addition, the ATTO site monitors fundamental climatic and atmospheric parameters such as temperatures, wind profiles, and precipitation (Andreae et al., 2015). These parameters were used to determine the coupling state of the cloud scenes and to choose case studies where the air parcel sampled at ATTO fed the cloud scene sampled by the satellite. An overview of the atmospheric, geographic, and ecological conditions, as well as commonly encountered air masses at the ATTO site, can be found in Andreae et al. (2015), Pöhlker et al. (2019), and Holanda et al. (2020). The typical aerosol and CCN conditions at ATTO have been described in recent studies (e.g., Pöhlker et al., 2016, 2018; Moran-Zuloaga et al., 2018; Franco et al., 2022).

## 3 Results

### 3.1 Simulations of $SAZ_{cond}$

This section presents the simulated vertical profiles of convective cloud properties from the spectral bin adiabatic parcel model and the effect of different inputs of ASD and $w$ scheme on the existence and properties of $SAZ_{cond}$ and other microphysical zones. Case studies with and without $SAZ_{cond}$ will be presented in Section 3.4. The initial thermodynamic conditions for the simulations, including pressure, temperature, relative humidity, and height, were measured below cloud bases during flight AC07 of the ACRIDICON-CHUVA campaign (Wendisch et al., 2016). The simulations are based on modified ASDs measured below cloud bases in subsaturated conditions (Braga et al., 2021, Pöhlker et al., 2021).

The cloud properties presented here are the simulated $r_e$, $N_d$, the total particle number concentration ($N_a$), $S$, rainwater fraction (RWF) and $w$ as a function of decreasing $T$ or increasing height. The $T$-$r_e$ profile for each simulation (Fig. 3D and 4D) shows the theoretical adiabatic $r_e$ curves under the assumption of condensational growth only for each cloud base $N_d$ (grey lines). The adiabatic curves are calculated based on the $LWC_a$ and the corresponding development of $r_e$ based on the cloud base temperature and pressure (Rosenfeld et al., 2016). The deviations between the actual and the theoretical adiabatic $T$-$r_e$ profiles define the dominant microphysical zones.

The RWF is defined as the ratio between the rainwater content (where drops with a diameter > 50 µm are considered raindrops) and the total water content (Fig. 3F and 4F). It increases as coalescence starts and decreases as the rain drops precipitate from the cloud. If there is no new droplet activation, RWF increases with decreasing $T$ up to unity when the smallest drops grow beyond the threshold of 50 µm in diameter. In the case of *SAZ* occurrence, the drop size distribution is wider, and the RWF stabilizes as new droplets are activated aloft before they coalesce and precipitate. Generally, clouds that completely rain out cannot develop higher due to a lack of condensation and buoyancy. However, in this study, the model forces the cloud to grow beyond the point of total rainout to illustrate how secondary activation changes the $T$-$r_e$ profile compared to the alternative that is rarely realized in nature.

To emphasize the impact of different ASD and $w$ schemes on the microstructure of the cloud and the *SAZ*, two sets of simulations were performed. The first one uses a fixed ASD and three prescribed $w$ schemes and the second one uses two ASD and a fixed $w$ scheme.

Fixed ASD

The input of the first simulation includes: (1) a representative bimodal ASD with a high concentration of accumulation mode particles that serve as CCN at a supersaturation of approx. 0.3 % and a smaller Aitken mode particle population (e.g., Pöhlker et al. 2016, 2018; Franco et al., 2022). The $N_a$ is 1782 $cm^{-3}$ (Fig. 3A); (2) Three prescribed $w$ schemes (Fig. 3B) with a typical initial speed of 1.5 m $s^{-1}$ at cloud base (Braga et al., 2017) and then different rates of increase with height. The first $w$ scheme ($w_1$, red dashed line) has the lowest slope and is close to constant $w$ with height. $w_2$ (green dashed line) has a higher increase rate than $w_1$ and $w_3$ has the strongest increase rate with height (blue dashed line). As mentioned above, clouds that completely rain out cannot develop higher due to a lack of condensation and buoyancy. However, in this study, the model's increasing $w$ schemes force the cloud to grow beyond this point to illustrate how secondary activation changes the $T$-$r_e$ profile compared to the alternative that is rarely realized in nature.

The $T$-$N_d$-$N_a$ profile (Fig. 3C) shows that for all three $w$ schemes, the primary activation of droplets at the cloud base is the same due to the same constant $w$ at the cloud base. The $N_d$ at the cloud base is smaller than the total $N_a$, meaning that not all particles were activated at the cloud base. After the primary activation, $N_d$ stays nearly constant with decreasing $T$ and only decreases slightly due to the minor coalescence process above the cloud base. This is consistent with the constant $N_a$ concentration with decreasing $T$, meaning that no new activation of droplets occurs. The $T$-$r_e$ profile (Fig. 3D) shows that, at first, $r_e$ increases at the same rate as the theoretic adiabatic curve for the same cloud base $N_d$. This means that during this phase, the dominant microphysical

process in the cloud is condensational growth. For the $w_1$ case (red dashed line in Fig. 3D), the coalescence and collision processes start to dominate at ~0 °C and lead to rainout at that level, as shown in the *T*-RWF profile (Fig. 3F). The $N_d$ starts to decrease sharply at the level of rain initiation, as the coalescence merges many cloud droplets into fewer raindrops. The coalescence and rainout reduce the integrated droplet surface area available for condensation and the exceeding of *S* above $S_{max}$. As a result, smaller particles with lower critical *S* are activated as cloud droplets. This is the $SAZ_{coal}$ defined and shown in Efraim et al. (2022). The $SAZ_{coal}$ is easily seen on the *T*-$N_d$-$N_a$ profile as the increase of $N_d$ and reduction of $N_a$ at ~-3 °C. It is also noticeable in the *T*-$r_e$ profile, as $r_e$ increases above the adiabatic curve when the coalescence becomes more dominant, and decreases with the activation of new droplets. In nature, this could also happen due to the entrainment of particles with low critical *S* from the lateral boundaries of the cloud. For the $w_2$ case, the rain initiation is delayed almost until cloud top, at ~-8 °C (green line on Fig. 3F), and the cloud remains adiabatic up to that level. When *w* increases even faster ($w_3$; blue line on Fig. 3C), the strong cooling rate causes a high enough *S* to exceed the $S_{max}$ and to activate new droplets even during the condensational growth, representing $SAZ_{cond}$. In this case, $N_d$ starts to increase during the dominant condensational growth phase at ~6 °C, and the $r_e$ reduces below the adiabatic curve (blue dashed line in Fig. 3D). The activation of new droplets during the condensational growth delays the coalescence process and the initiation of the rain. As seen in the *T*-RWF profile, no rain is initiated until cloud top (blue dashed line in Fig. 3F). Eventually, for the same ASD, the stronger *w* scheme causes $SAZ_{cond}$ while the weaker ones may keep the cloud adiabatic or cause $SAZ_{coal}$.

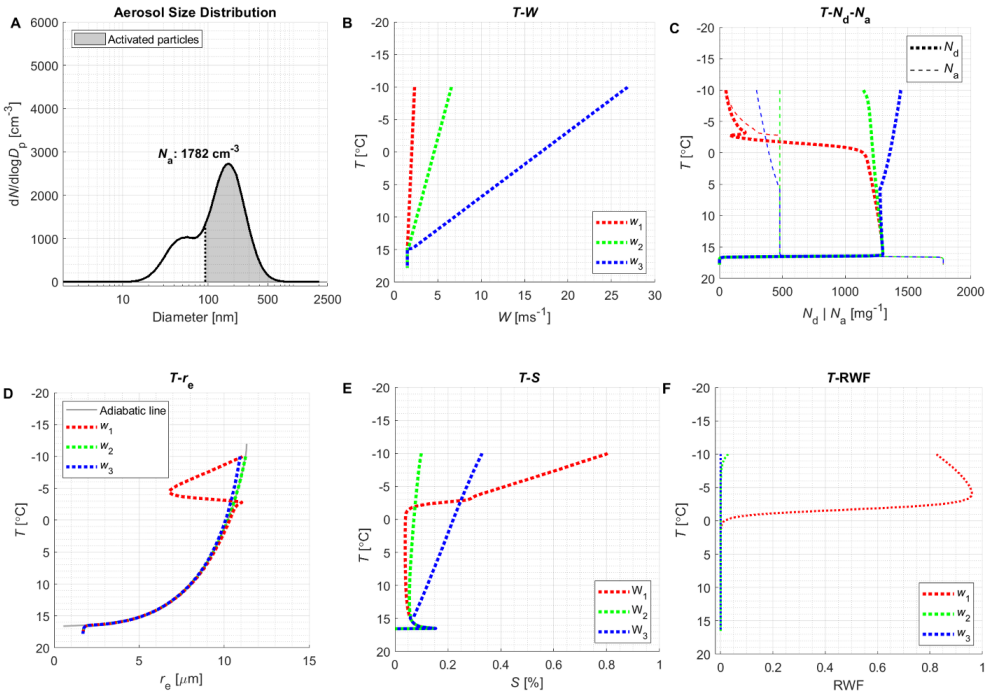

Figure 3. Simulations of cloud properties for a fixed aerosol size distribution (ASD) and three prescribed updraft schemes ($w$). Panel A shows the bimodal ASD with a high concentration of accumulation mode particles and a lower concentration of Aitken mode particles. The total particle number concentration ($N_a$) below the cloud base is 1782 $cm^{-3}$. The shaded grey marks the calculated activated particles at the cloud base. Panel B shows the prescribed $w$ schemes with a constant $w$ speed of 1.5 $ms^{-1}$ up to the cloud base and then different increase rates, where $w_1$ (red dashed line) has the lowest slope and is close to constant $w$ with height. $w_2$ (green dashed line) has a higher increase rate than $w_1$, and $w_3$ (blue dashed line) has the strongest increase rate. Panels C-F shows the different cloud properties, where the color of the lines is related to the same-colored $w$ scheme in each panel. Panel C shows the number concentration of cloud droplets ($N_d$) and $N_a$ profile in units of $mg^{-1}$ to avoid the consideration of the change of air density with height; Panel D shows the effective radius ($r_e$) profile, where the thick grey line is the theoretical adiabatic curve, calculated based on the cloud base $P$ and $T$; Panel E shows the vertical profile of supersaturation over water ($S$) and Panel F shows the vertical rainwater fraction (RWF) profile.

Fixed *w* scheme

The input of the second simulation includes: (1) two bimodal ASD, where ASD1 is identical to the ASD in the previous simulation (blue plot in Fig. 4A), whereas ASD2 has the same concentration of Aitken particles, but a lower concentration of accumulation mode particles (green plot in Fig. 4A); (2) One prescribed $w$ scheme (fig 4B) identical to the $w_3$ scheme from the first simulation. The $N_a$ is 1782 $cm^{-3}$ for ASD1 and 938 $cm^{-3}$ for ASD2.
The $T$-$N_d$-$N_a$ profile (Fig. 4C) shows a higher concentration of activated $N_d$ at the cloud base for the ASD1 case (blue dashed line), which has a higher concentration of accumulation mode particles. Therefore, $S_{max}$ for the ASD1 case (blue dashed line in Fig 4E) is smaller than for the ASD2 case (green dashed line). However, the cloud base $N_d$ is smaller than the $N_a$ for both cases, meaning that there are unactivated interstitial particles within the cloud parcel. After the primary activation, the $N_d$ stay relatively constant with height, and the $r_e$ increase at the same rate as the theoretic adiabatic curve for the same cloud base $N_d$ (Fig. 4D), indicating that condensational growth is the dominant microphysical process. For the prescribed $w$ scheme in this simulation, $SAZ_{cond}$ appears for both cases, however, the level of $SAZ_{cond}$ changes. With the constant increase of $w$ and cooling rate, $S$ exceeds the initially smaller $S_{max}$ for the ASD1 case at a lower level, causing $SAZ_{cond}$ to occur at a lower level. The critical $S$ increases as the interstitial particles' size and the air $T$ decrease. Thus, a higher critical $S$ must be reached to activate further interstitial particles in the ASD2 case. Therefore, the $SAZ_{cond}$ occurs slightly higher than the point where $S$ exceeds $S_{max}$. The $r_e$ in both cases goes below adiabatic, but for the lower-level $SAZ_{cond,}$ the reduction starts at higher $T$. The secondary activation of a higher concentration of particles in the ASD1 case (blue dashed line in Fig. 4D) results in the $r_e$ decrease to smaller values than for the ASD2 case (green dashed line). The activation of new droplets delays the coalescence process and the initiation of the rain in both cases up to the cloud top (Fig. 4F). Eventually, for the same strong $w$, a case with a more prominent accumulation mode will experience an earlier and stronger $SAZ_{cond}$ because of more available particles for activation with lower critical $S$ in the rising parcel. The cloud microstructure profiles for the simulations of the $w_1$ and $w_2$ schemes with ASD2 are shown in the supplements (Fig. S1).

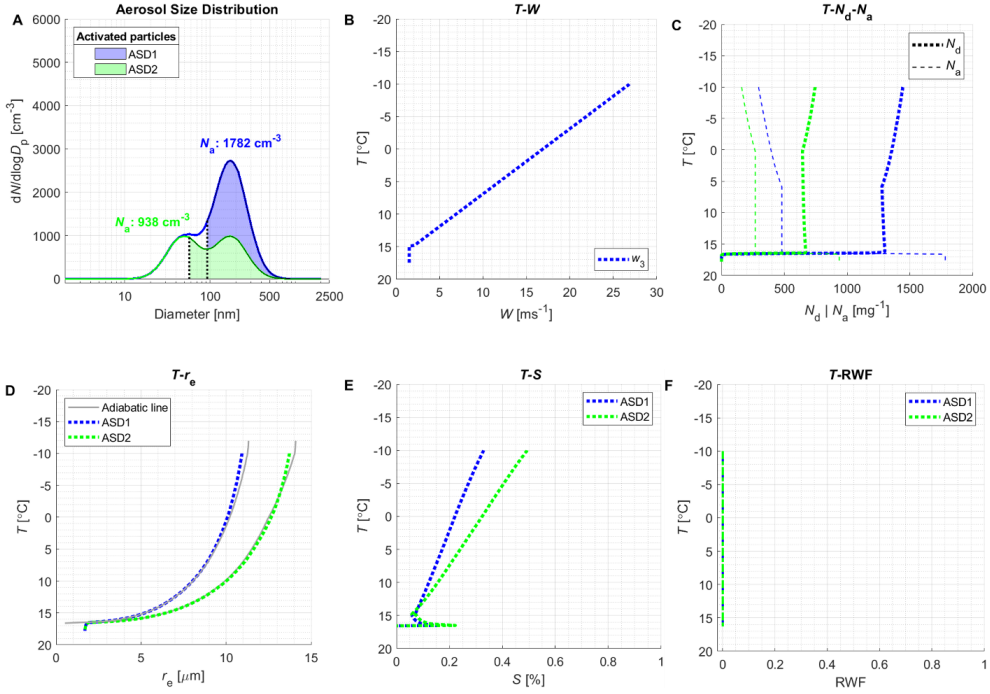


Figure 4. Simulations of cloud properties for fixed prescribed updraft scheme ($w$) (panel B) and two different aerosol size distributions (ASD) (panel A). The $w$ scheme is the same as $w_3$ in Fig. 3. The first ASD (ASD1, blue) is the same as illustrated in Fig. 3, with the same $N_a$. The second ASD (ASD2, green) has the same Aitken mode as the blue one but has a lower accumulation mode. The $N_a$ of ASD2 is 938 cm$^{-3}$. Panels C-F shows the different cloud properties where the color of the lines is related to the same-colored ASD in each panel. Panel C shows the $N_d$ and the $N_a$ concentration profile in units of mg$^{-1}$ to avoid the consideration of the change of air density with height; Panel D shows the $T$-$r_e$ profiles, where the thick grey line is the theoretical adiabatic curve, calculated based on the cloud base $P$ and $T$; Panel E shows the vertical profile of $S$ and Panel F shows the vertical RWF profile.

### 3.2 Detection of $SAZ_{cond}$ based on satellite retrieved $T$-$r_e$ profiles

Since the microphysical zones in deep convective clouds can be inferred from the $T$-$r_e$ profiles, satellite-retrieved $T$-$r_e$ profiles can be used to detect the microphysical zones within the cloud. The different microphysical zones and the method for their detection by the $T$-$r_e$ profile analysis have been fully described in Efraim et al. (2022) and also briefly in Section 1.2. However, the newly defined $SAZ_{cond}$ is less readily detected since it is a part of the defined condensational growth phase. Still, it can be identified by analyzing the small fluctuations within the condensational growth points. These small fluctuations can be either noise, as a result of the ±30% uncertainty (Freud et al., 2011; Rosenfeld et al., 2016), in which case these points should still be defined as condensational growth; or signal, representing the appearance of smaller droplets within the condensational growth phase.
To analyze the fluctuations in the condensational growth points, we used the profile of the natural logarithm of

the adiabatic $N_d$ with decreasing $T$ ($T$-ln($N_{da}$)). The value of ln($N_{da}$) is calculated by taking the natural logarithm of the $LWC_a$-$M_{droplet}$ ratio for each $T$ bin, for the adiabatic points. Using the ln($N_{da}$), instead of the absolute value of $N_{da}$, emphasizes the relative change in $N_{da}$ in the concentrations rather than the absolute change. The ln($N_{da}$) was linearly segmented by the trend of the points. Ideally, the ln($N_{da}$) should be constant or decrease during the condensational growth. Any ln($N_{da}$) increase can be either due to noise or a signal. The $SAZ_{cond}$ is then identified where a significant increase of ln($N_{da}$) occurs.

This section presents two cloud scenes as case studies with and without a detected $SAZ_{cond}$, and an application of a method to detect the $SAZ_{cond}$ by remote sensing. Both cloud scenes were taken over the ATTO region, where the ASD of the air feeding into the clouds was measured. Each case study presents the satellite overpass image, the 1-hour average ASD before the satellite overpass, the $LWC_a$-$M_{droplet}$ ratio, the $T$-$r_e$ profile, and the $T$-ln($N_{da}$) profile.

Cloud scene A (red polygon in Fig. 5A) is an example of a case without $SAZ_{cond}$. In this case, a cluster of cumulus congestus clouds was taken within ~25 km of the ATTO site. The satellite overpass was on 6 July 2017 at 17:40 UTC. The adiabatic points are marked in red on the $LWC_a$-$M_{droplet}$ profile (Fig. 5C). These points have the best linear fit with the origin ($R^2 = 0.995$) and therefore they define the condensational growth phase. The $N_d$ at the cloud base is then determined by the linear ratio of $LWC_a$-$M_{droplet}$. The thick black line on the $T$-$r_e$ profile (Fig. 5D) is the adiabatic curve calculated from the cloud base temperature and pressure of the specific retrieved $N_d$. The defined condensational growth points (red points) agree with the adiabatic curve until the coalescence begins and exceeds adiabaticity (Fig D and E). The adiabatic $T$-ln($N_{da}$) profile (Fig. 5F) shows a slight increase of 0.079 in the ln($N_{da}$) for the adiabatic points which can be either noise or signal. The calculated $N_d$ based on the linear $LWC_a$-$M_{droplet}$ ratio is 836 $cm^{-3}$. The 1-hour average ASD (Fig. 5B) has a well-defined Hoppel minimum at 85 nm. The Hoppel minimum is a size separation gap between two size modes, which usually indicates the size of the smallest particles that can serve as CCN for the given thermodynamic conditions due to cloud processing (Hoppel and Frick, 1986; Hudson et al., 2015). Summing the $N_d$ largest particles on the ASD in Fig. 5B (green shading) yields the smallest diameter to be activated, i.e., the critical diameter, since the larger particles are activated first. In this case, the critical diameter is 82 nm. This suggests that the activated particles at the cloud base are accumulation mode particles down to that threshold. The good agreement of the retrieved $N_d$ with the concentration of the accumulation mode particles implies that the fluctuations in the condensational points are likely to be noise and the case is without $SAZ_{cond}$. That is because no significant overestimation of $N_d$ was found, as opposed to the Cloud scene B, presented next. This will be further discussed in Section 4.

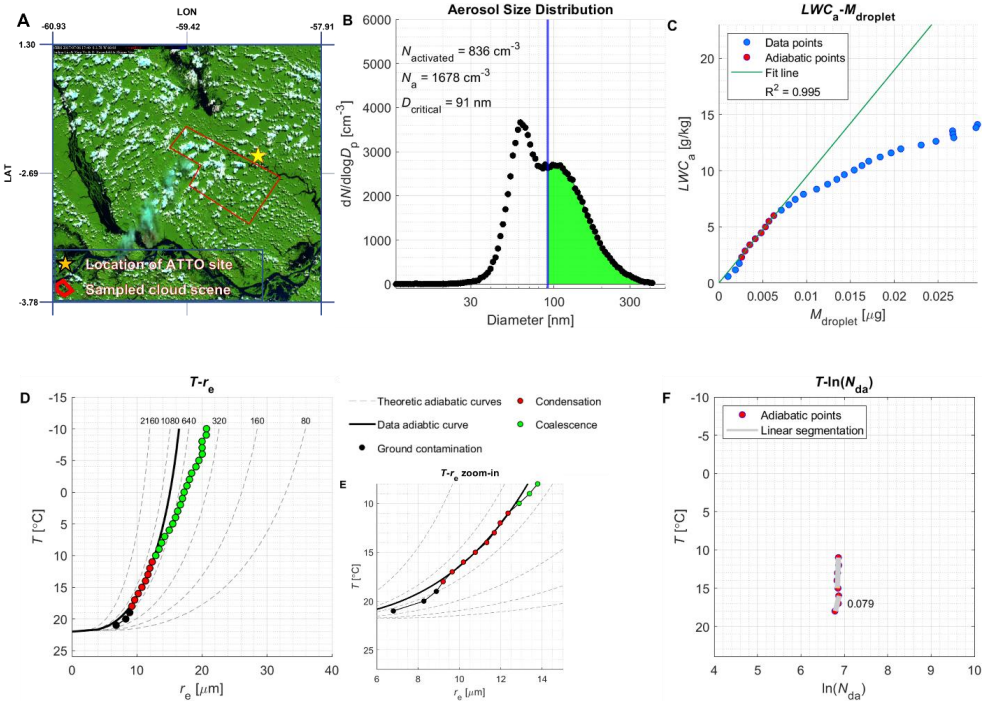


Figure 5. Satellite-retrieved cloud microphysical profiles in the ATTO region without indications for secondary activation in the condensational growth phase (Cloud scene A). Panel A shows the true-color satellite image with the ATTO site marked as the star and the sampled cloud scene shown as a red polygon. Panel B shows the 1-hour average ASD at ATTO before the satellite overpass, with the particle fraction activated as cloud droplets being shown as green shading under the curve. Panel C shows the $LWC_a$-$M_{droplet}$ ratio where the red points are defined as the adiabatic ones, with the best fit with the origin ($R^2$=0.995). The adiabatic points are marked as the condensational growth points on the $T$-$r_e$ profile (red points in Panel D). Panel E shows an enhanced $T$-$r_e$ profile focused on the adiabatic part. The $T$-ln($N_{da}$) profile (Panel F) shows only the adiabatic points (red points in Panel D) and the trend lines with decreasing $T$. The value in Panel F (0.079) is the slope of the positive trend line.

On the other hand, Cloud scene B (red polygon in Fig. 6A) is an example of a case with $SAZ_{cond}$. The sampled cloud is a developed cumulonimbus ~70 km from ATTO. The satellite overpass was on 1 July 2017 at 17:30 UTC. The 1-hour average ASD for cloud scene B (Fig. 6B) has a well-defined Hoppel minimum at 91 nm and a total $N_a$ of 932 cm$^{-3}$. The $LWC_a$-$M_{droplet}$ ratio profile (Fig. 6C) defined the adiabatic points (red points) with a linear fit of $R^2$ = 0.916. These points are also in good agreement with the adiabatic curve on the $T$-$r_e$ profile (Fig. 6D and 6E). However, the adiabatic $T$-ln($N_{da}$) (Fig. 6F) shows a larger increase in ln($N_{da}$) of 0.32, compared to Cloud scene A. This suggests larger fluctuations in the adiabatic points. The calculated $N_d$ based on the linear $LWC_a$-$M_{droplet}$ ratio is 1079 cm$^{-3}$, actually exceeding the $N_a$ measured at ATTO. Even allowing for possible differences in aerosol concentrations between ATTO and the location of the cloud as well as a potential overestimation of the retrieved

$N_d$, this would imply that all particles were activated and the critical diameter was near 10 nm, the detection limit of the SMPS. Therefore, the fluctuation in the adiabatic points, in this case, is implied to be a signal of activation of extra cloud droplets during the condensational growth. In Section 4, we will discuss how the presence of $SAZ_{cond}$ may lead to an overestimation of $N_d$.

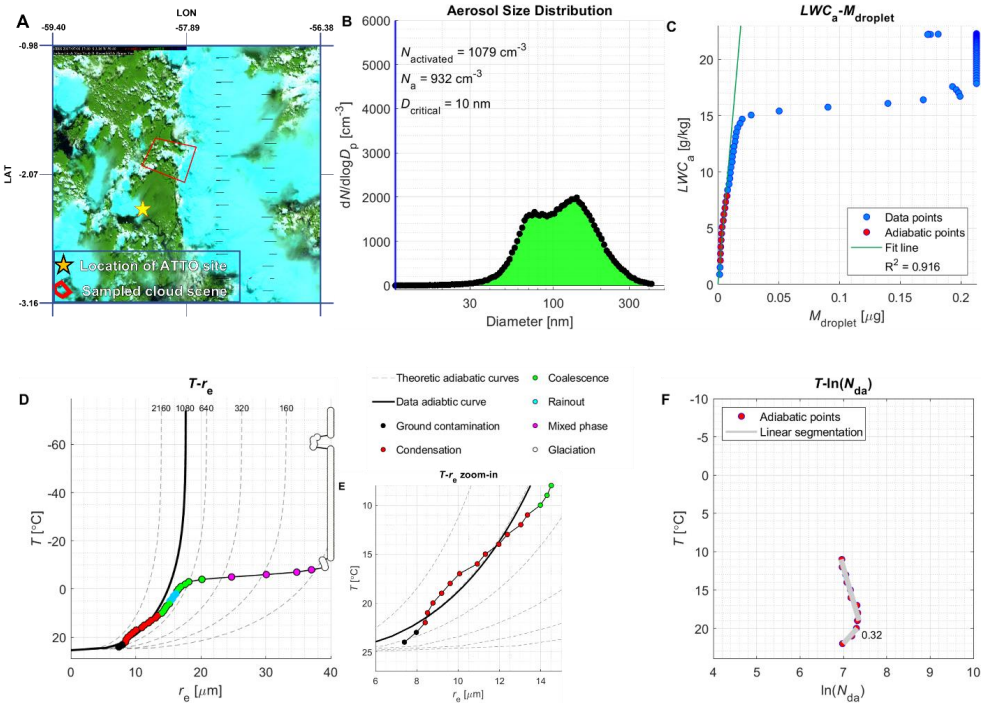


Figure 6. Satellite-retrieved cloud microphysical profiles in the ATTO region with indications for secondary activation in the condensational growth phase (Cloud scene B). Panel A shows the true-color satellite image with the ATTO site marked as the star and the sampled cloud scene shown as a red polygon. Panel B shows the 1-hour average ASD at ATTO before the satellite overpass, with the particle fraction activated as cloud droplets being shown as green shading under the curve. Panel C shows the $LWC_a$-$M_{droplet}$ ratio where the red points are defined as the adiabatic ones, with the best fit with the origin ($R^2$=0.916). The adiabatic points are marked as the condensational growth points on the $T$-$r_e$ profile (red points in Panel D). Panel E shows an enhanced $T$-$r_e$ profile focused on the adiabatic part. The $T$-ln($N_{da}$) profile (Panel F) shows only the adiabatic points (red points in Panel D) and the trend lines with decreasing $T$. The value in Panel F (0.32) is the slope of the positive trend line.

## 4 Discussion

The *SAZ* during condensational growth ($SAZ_{cond}$) may be detectable in the *T*-$r_e$ profile as a slight decrease of $r_e$ below the adiabatic $r_e$ during the condensational growth phase, as shown in Cloud scene B. It was also described by the model, in Section 3.1, where the $r_e$ was reduced below the adiabatic values in cases of droplet activation during condensational growth. This can occur due to an increase in *w* or at the same *w*, for different ASD. However, in nature, the $SAZ_{cond}$ can occur also due to the entrainment of particles with low critical *S*, which can be activated at the existing *S* during the dominant condensational growth. As seen in Cloud scene B, $SAZ_{cond}$ may cause an overestimation of the retrieved $N_d$ from the satellite. Additional droplet activation reduces the $r_e$ for the same amount of LWC, thus the $r_e$ decreases below the adiabatic curve. This results in a calculated $N_d$ above the adiabatic $N_d$ at the cloud base and thus an overestimation of $N_d$. In addition, the calculation of $N_d$ at the cloud base is based on the ratio of $LWC_a$ to $M_{droplet}$ for the defined adiabatic points. The $M_{droplet}$ relies on the assumption that $\frac{r_e}{r_v} = 1.08$ for adiabatic processes (Freud et al., 2011). The explicit formulas for the calculation $r_e$ and $r_v$ are:

$$(1)\ r_e = \frac{\int N(r) r^3 dr}{\int N(r) r^2 dr}$$

$$(2)\ r_v = \left(\frac{3 \cdot LWC}{4\pi \rho_w N}\right)^{\frac{1}{3}}$$

Where *N* and *r* are the droplet concentration and radii, respectively, and $\rho_w$ is the density of water (Freud and Rosenfeld, 2012). Adding *N* droplets with small *r* above cloud base due to $SAZ_{cond}$ would not reduce the $r_e$ as much as it would reduce $r_v$, assuming unchanged LWC. Therefore, the retrieved $N_d$ under the assumption that all droplets were activated at the cloud base would give a much larger $N_d$ compared to the actual $N_d$ at the cloud base. In addition, $SAZ_{cond}$ would cause a $\frac{r_e}{r_v}$ ratio larger than 1.08. Since the algorithm for the calculation of $N_d$ assumes adiabaticity, the 1.08 ratio is taken. When $SAZ_{cond}$ occurs the calculated $r_v$ is then smaller than its true value, causing a positive bias in $N_d$. Another reason that might cause an overestimation of the retrieved $N_d$ is the use of more adiabatic points with less certainty. Supposedly, taking only the first point on the adiabatic curve would suffice in the calculation of $N_d$, since it gives the ratio of $LWC_a$ to $M_{droplet}$. However, the uncertainty of the first points closer to the cloud base is large and sometime might be considered ground contamination (Rosenfeld et al., 2016; Efraim et al., 2022). To reduce the uncertainty, the algorithm for the calculation of $N_d$ does not rely merely on the first point but rather includes more points above, as long as they are on the adiabatic curve. In case these points include fluctuations due to $SAZ_{cond}$, this might result in a larger $LWC_a$-$M_{droplet}$ ratio, hence a larger $N_d$.

Another impact of the $SAZ_{cond}$, as shown by the model, is the suppression of warm rain. This was observed by in-situ measurements of *T*-$r_e$ profiles from clouds probes in several flights during the ACRIDICON–CHUVA campaign (Wendisch et al., 2016), which showed that the measured $N_d$ was larger above the cloud base than at the cloud base (Braga et al., 2017). During flightsAC08, AC12 and AC20 strong *w* (up to 15 $ms^{-1}$) was measured above the cloud base. The strong *w* increased *S* and allowed more CCN activation. The measured profile of $r_e$ with height was smaller than the estimated adiabatic $r_e$ profile (Fig. 7). The measured $r_e$ values were smaller than 13 µm,

indicating the suppression of raindrop formation. Measured droplet size distribution from the cloud probe on the aircraft validated that indeed no raindrops were present on these flights (Braga et al., 2017). Instead, ice particles were formed above the 0 °C isotherm. The released latent heat from the freezing increases the buoyancy and leads to the invigoration of the cloud (Rosenfeld et al., 2008).

As described in section 3.2, the minor fluctuation of the condensational growth can be defined either as noise (e.g., Cloud scene A) or an actual signal of $SAZ_{cond}$ (e.g., Cloud scene B). To distinguish between noise and signal, a threshold value of the increase in $\ln(N_{da})$ should be set. This should go along with validations of measured ASD below the cloud to determine the concentration of activated particles and the existence of overestimation of $N_d$. This requires analysis of many cases and will require further research.

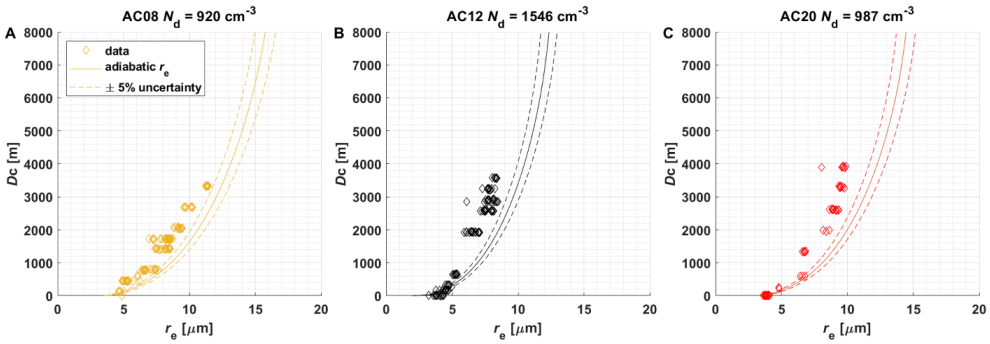


Figure 7. Cloud droplet effective radius ($r_e$) as a function of cloud depth (Dc) for flights AC08 (A), AC12 (B) and AC20 (C). The solid line indicates the $r_e$ estimated for adiabatic growth from the cloud base. The dashed lines indicate the adiabatic $r_e$ values considering the uncertainty of the estimate. The estimated adiabatic number of droplets ($N_d$) at the cloud base is shown on top of the figure. Adapted from Braga et al., 2017.

## 5 Conclusions

The microphysical zone in convective clouds where activation of droplets above the cloud base occurs is referred to as the secondary activation zone (*SAZ*). The detection of *SAZ* based on *T*-$r_e$ profiles allows identifying a significant occurrence of new droplet activation above the cloud base, either after the dominant coalescence of droplets ($SAZ_{coal}$) or during the dominant condensational growth of the cloud droplets ($SAZ_{cond}$). While the properties of $SAZ_{coal}$ were discussed in Efraim et al. (2022), the physical principle and the causes for $SAZ_{cond}$ are presented in this study. A spectral-bin adiabatic parcel model was used to describe the effect of velocity (*w*) and different aerosol size distributions (ASD) on the existence of $SAZ_{cond}$. The simulations showed that a stronger increase of *w* with decreasing *T* results in the change from unperturbed dominant condensational growth to the occurrence of $SAZ_{cond}$ when a high *w* increases *S* to the extent that it exceeds the maximum supersaturation simulated at the cloud base ($S_{max}$). The simulations also showed that, for the same *w* scheme, a more polluted case with higher CCN concentrations and resulting lower $S_{max}$ would lead to a $SAZ_{cond}$ starting at lower cloud depths and with more significant activation of interstitial particles into cloud droplets. A method to detect

$SAZ_{cond}$ from $T$-$r_e$ profiles measured by the S-NPP satellite was demonstrated using two case studies, one in which $SAZ_{cond}$ was observed and another where it was not identified. We found that the existence of $SAZ_{cond}$ may cause an overestimation of the satellite retrieved $N_d$ due to: (a) the smaller $r_e$ after $SAZ_{cond}$ for the same amount of LWC and (b) the deviation from the assumption that all droplets were activated at cloud base, (c) the reduction of adiabaticity, and (d) the consideration of more adiabatic points with less certainty. In addition, $SAZ_{cond}$ leads to a warm rain suppression and possible invigoration of the cloud by the released latent heat from ice nucleation above the 0 °C isotherm. The occurrence of *SAZ* has climatic importance by shaping the deep convective cloud microstructure with possible consequences for cloud radiative forcing. The ability to detect both $SAZ_{cond}$ and $SAZ_{coal}$ signatures from satellites allows a detailed analysis of convective cloud microphysics in large areas and over long periods. Further investigations of these signatures in convective clouds will improve our understanding of their role in aerosol-cloud interactions worldwide.

*Data availability.* The satellite data of the case studies presented in this study is available on the VIIRS dataset found at the *NOAA's Comprehensive Large Array-data Stewardship System* [https://www.avl.class.noaa.gov/]. The ATTO data used in this study are available via the ATTO data portal at https://www.attoproject.org/. The output data from the IDL program of the sampled cloud scenes have been deposited in supplementary data files for use in follow-up studies [https://doi.org/10.5061/dryad.h44j0zpnr]. For data requests beyond the available data, please refer to the corresponding author.

*Author contributions.* Conceptualization, A.E., O.L., M.L.P, R.C.B., and D.R; Formal analysis, A.E. and O.L.; Investigation, A.E. and O.L.; Methodology, A.E., O.L., R.C.B., D.R., L.A.K., and M.A.F.; Resources, A.E., R.C.B., L.A.K., M.A.F. and M.L.P.; Software, A.E. and O.L.; Supervision, D.R. and M.L.P; Visualization, A.E.; Writing – original draft, A.E.; Writing – review & editing, A.E., R.C.B., D.R., O.L., M.A.F., L.A.K., C.P., M.O.A., C.Q.D.J., and M.L.P.

*Competing interests.* The authors declare that they have no conflict of interest.

*Disclaimer.* This paper contains results of research conducted under the Technical/Scientific Cooperation Agreement between the National Institute for Amazonian Research, the State University of Amazonas, and the Max-Planck-Gesellschaft e.V.; the opinions expressed are the entire responsibility of the authors and not of the participating institutions.

*Acknowledgments.* For the operation of the ATTO site, we acknowledge the support by the Max Planck Society, the German Federal Ministry of Education and Research and the Brazilian Ministério da Ciência, Tecnologia e Inovação as well as the Amazon State University (UEA), FAPEAM, LBA/INPA, and SDS/CEUC/RDS-Uatumã. We would like to especially thank all the people involved in the technical, logistical, and scientific support of the ATTO project. Special thanks to Lior Efraim and Imri Yitzhak for their moral support.

*Financial support*. This research has been supported by the Max Planck Society, the Max Planck Graduate Center with the Johannes Gutenberg University Mainz (MPGC), the Bundesministerium für Bildung und Forschung (BMBF contracts 01LB1001A, 01LK1602B, and 01LK2101B), the Brazilian Ministério da Ciência, Tecnologia e Inovação (MCTI/FINEP contract 01.11.01248.00), the Conselho Nacional de Desenvolvimento Científico e Tecnológico (CNPq, Brazil) (process 200723/2015-4), the FAPESP (Fundação de Amparo à Pesquisa do Estado de São Paulo) (grant no. 2017/17047-0 and 2021/13610-8), the CNPq project (grant no. 169842/2017-7), and the CAPES project (grant no. 88887.368025/2019-00).

## References

Andreae, M. O. (2009). Correlation between cloud condensation nuclei concentration and aerosol optical thickness in remote and polluted regions. *Atmospheric Chemistry and Physics*, *9*(2), 543–556. https://doi.org/10.5194/acp-9-543-2009

Andreae, M. O., Acevedo, O. C., Araùjo, A., Artaxo, P., Barbosa, C. G. G., Barbosa, H. M. J., et al. (2015). The Amazon Tall Tower Observatory (ATTO): Overview of pilot measurements on ecosystem ecology, meteorology, trace gases, and aerosols. *Atmospheric Chemistry and Physics*, *15*(18), 10723–10776. https://doi.org/10.5194/acp-15-10723-2015

Arakawa, A., & Schubert, W. H. (1974). Interaction of a Cumulus Cloud Ensemble with the Large-Scale Environment, Part I. *Journal of Atmospheric Sciences*, *31*(3), 674–701. https://doi.org/10.1175/1520-0469(1974)031<0674:IOACCE>2.0.CO;2

Artaxo, P., Rizzo, L. V., Brito, J. F., Barbosa, H. M. J., Arana, A., Sena, E. T., et al. (2013). Atmospheric aerosols in Amazonia and land use change: From natural biogenic to biomass burning conditions. *Faraday Discussions*, *165*, 203. https://doi.org/10.1039/c3fd00052d

*ATTO - Amazon Tall Tower Observatory*. (2020, January 21). ATTO - Amazon Tall Tower Observatory. https://www.attoproject.org/

Bera, S., Chowdhuri, S., & Prabha, T. V. (2022). A new methodology for the statistical descriptions of Particle-by-Particle measurements of liquid droplets in cumulus clouds. *Quarterly Journal of the Royal Meteorological Society*, *148*(743), 842–859. https://doi.org/10.1002/qj.4234

Bott, A. (1997). An efficient numerical flux method for the solution of the stochastic collection equation. *Journal of Aerosol Science*, *28*, S745–S746. https://doi.org/10.1016/S0021-8502(97)85371-2

Braga, R. C., Rosenfeld, D., Krüger, O. O., Ervens, B., Holanda, B. A., Wendisch, M., et al. (2021). Linear relationship between effective radius and precipitation water content near the top of convective clouds: Measurement results from ACRIDICON–CHUVA campaign. *Atmospheric Chemistry and Physics*, *21*(18), 14079–14088. https://doi.org/10.5194/acp-21-14079-2021

Braga, R. C., Rosenfeld, D., Weigel, R., Jurkat, T., Andreae, M. O., Wendisch, M., et al. (2017). Further evidence for CCN aerosol concentrations determining the height of warm rain and ice initiation in convective clouds over the Amazon basin. *Atmospheric Chemistry and Physics*, *17*(23), 14433–14456. https://doi.org/10.5194/acp-17-14433-2017

Bréon, F.M., Tanré, D., & Generoso, S. (2002). Aerosol Effect on Cloud Droplet Size Monitored from Satellite. Science, 295(5556), 834–838. https://doi.org/10.1126/science.1066434

Chen, R., Wood, R., Li, Z., Ferraro, R., & Chang, F.-L. (2008). Studying the vertical variation of cloud droplet effective radius using ship and space-borne remote sensing data. *Journal of Geophysical Research*, *113*, D00A02. https://doi.org/10.1029/2007JD009596

Cotton, W. R., Bryan, G., & van den Heever, S. C. (2011). The Mesoscale Structure of Extratropical Cyclones and Middle and High Clouds. In *International Geophysics* (Vol. 99, pp. 527–672). Elsevier. https://doi.org/10.1016/S0074-6142(10)09916-X

Efraim, A., Lauer, O., Rosenfeld, D., Braga, R. C., Franco, M. A., Kremper, L. A., et al. (2022). Satellite-Based Detection of Secondary Droplet Activation in Convective Clouds. Journal of Geophysical Research: Atmospheres, 127(12). https://doi.org/10.1029/2022JD036519

Efraim, Avichay, et al. (2022), Satellite processed data, Dryad, [Dataset], https://doi.org/10.5061/dryad.h44j0zpnr

Fan, J., Leung, L. R., Rosenfeld, D., Chen, Q., Li, Z., Zhang, J., & Yan, H. (2013). Microphysical effects determine macrophysical response for aerosol impacts on deep convective clouds. *Proceedings of the National Academy of Sciences*, *110*(48), E4581–E4590. https://doi.org/10.1073/pnas.1316830110

Fan, J., Rosenfeld, D., Zhang, Y., Giangrande, S. E., Li, Z., Machado, L. A. T., et al. (2018). Substantial convection and precipitation enhancements by ultrafine aerosol particles. *Science*, *359*(6374), 411–418. https://doi.org/10.1126/science.aan8461

Feingold, G., Remer, L. A., Ramaprasad, J., & Kaufman, Y. J. (2001). Analysis of smoke impact on clouds in Brazilian biomass burning regions: An extension of Twomey's approach. *Journal of Geophysical Research: Atmospheres*, *106*(D19), 22907–22922. https://doi.org/10.1029/2001JD000732

Franco, M. A., Ditas, F., Kremper, L. A., Machado, L. A. T., Andreae, M. O., Araújo, A., et al. (2022). Occurrence and growth of sub-50 nm aerosol particles in the Amazonian boundary layer. Atmospheric Chemistry and Physics, 22(5), 3469–3492. https://doi.org/10.5194/acp-22-3469-2022

Freud, E., & Rosenfeld, D. (2012). Linear relation between convective cloud drop number concentration and depth for rain initiation: DROP CONCENTRATION AND RAIN INITIATION. *Journal of Geophysical Research: Atmospheres*, *117*(D2), n/a-n/a. https://doi.org/10.1029/2011JD016457

Freud, E., Rosenfeld, D., Andreae, M. O., Costa, A. A., & Artaxo, P. (2008). Robust relations between CCN and the vertical evolution of cloud drop size distribution in deep convective clouds. *Atmospheric Chemistry and Physics*, *8*(6), 1661–1675. https://doi.org/10.5194/acp-8-1661-2008

Freud, E., Rosenfeld, D., & Kulkarni, J. R. (2011). Resolving both entrainment-mixing and number of activated CCN in deep convective clouds. *Atmospheric Chemistry and Physics*, *11*(24), 12887–12900. https://doi.org/10.5194/acp-11-12887-2011

Gerber, H. (1996). Microphysics of Marine Stratocumulus Clouds with Two Drizzle Modes. *Journal of Atmospheric Sciences*, *53*(12), 1649–1662. https://doi.org/10.1175/1520-0469(1996)053<1649:MOMSCW>2.0.CO;2

Grosvenor, D. P., Sourdeval, O., Zuidema, P., Ackerman, A., Alexandrov, M. D., Bennartz, R., et al. (2018). Remote Sensing of Droplet Number Concentration in Warm Clouds: A Review of the Current State of Knowledge and Perspectives. *Reviews of Geophysics*, *56*(2), 409–453. https://doi.org/10.1029/2017RG000593

Gunn, R., & Phillips, B. B. (1957). An experimental investigation of the effect of air pollution on the initiation of rain. *Journal of Atmospheric Sciences*, *14*(3), 272–280. https://doi.org/10.1175/1520-0469(1957)014<0272:AEIOTE>2.0.CO;2

Holanda, B. A., Pöhlker, M. L., Walter, D., Saturno, J., Sörgel, M., Ditas, J., Ditas, F., Schulz, C., Franco, M. A., Wang, Q., Donth, T., Artaxo, P., Barbosa, H. M. J., Borrmann, S., Braga, R., Brito, J., Cheng, Y., Dollner, M., Kaiser, J. W., … Pöhlker, C. (2020). Influx of African biomass burning aerosol during the Amazonian dry season through layered transatlantic transport of black carbon-rich smoke. *Atmospheric Chemistry and Physics*, *20*(8), 4757–4785. https://doi.org/10.5194/acp-20-4757-2020

Hoppel, W. A., & Frick, G. M. (1986). Ion—Aerosol Attachment Coefficients and the Steady-State Charge Distribution on Aerosols in a Bipolar Ion Environment. *Aerosol Science and Technology*, *5*(1), 1–21. https://doi.org/10.1080/02786828608959073

Huang, T., Zhu, Y., Rosenfeld, D., Yang, Y., Lam, D. H. Y., Leung, W. H., Lee, H. F., Cheng, J. C. H., & Yim, S. H. L. (2022). Regime-Dependent Impacts of Aerosol Particles and Updrafts on the Cloud Condensation Nuclei and the Enhanced Warm Rain Suppression: Evidence From Synergistic Satellite and LiDAR Observations. *Geophysical Research Letters*, *49*(3). https://doi.org/10.1029/2021GL097315

Hudson, J. G., Noble, S., & Tabor, S. (2015). Cloud supersaturations from CCN spectra Hoppel minima. *Journal of Geophysical Research: Atmospheres*, *120*(8), 3436–3452. https://doi.org/10.1002/2014JD022669

IPCC, 2013: Summary for Policymakers. In: Climate Change 2013: The Physical Science Basis. Contribution of Working Group I to the Fifth Assessment Report of the Intergovernmental Panel on Climate Change [Stocker, T.F., D. Qin, G.-K. Plattner, M. Tignor, S.K. Allen, J. Boschung, A. Nauels, Y. Xia, V. Bex and P.M. Midgley (eds.)]. Cambridge University Press, Cambridge, United Kingdom and New York, NY, USA, pp. 1–30, doi:10.1017/CBO9781107415324.004.

IPCC, 2021: Summary for Policymakers. In: Climate Change 2021: The Physical Science Basis. Contribution of Working Group I to the Sixth Assessment Report of the Intergovernmental Panel on Climate Change [MassonDelmotte, V., P. Zhai, A. Pirani, S.L. Connors, C. Péan, S. Berger, N. Caud, Y. Chen, L. Goldfarb, M.I. Gomis, M. Huang, K. Leitzell, E. Lonnoy, J.B.R. Matthews, T.K. Maycock, T. Waterfield, O. Yelekçi, R. Yu, and B. Zhou

(eds.)]. Cambridge University Press, Cambridge, United Kingdom and New York, NY, USA, pp. 3–32, doi:10.1017/9781009157896.001.

Khain, A. P., Phillips, V., Benmoshe, N., & Pokrovsky, A. (2012). The Role of Small Soluble Aerosols in the Microphysics of Deep Maritime Clouds. *Journal of the Atmospheric Sciences*, *69*(9), 2787–2807. https://doi.org/10.1175/2011JAS3649.1

Köhler, H. (1936). The nucleus in and the growth of hygroscopic droplets. Trans. Faraday Soc., 32(0), 1152–1161. https://doi.org/10.1039/TF9363201152

Konwar, M., Maheskumar, R. S., Kulkarni, J. R., Freud, E., Goswami, B. N., & Rosenfeld, D. (2012). Aerosol control on depth of warm rain in convective clouds: AEROSOL CONTROL ON DEPTH OF WARM RAIN. *Journal of Geophysical Research: Atmospheres*, *117*(D13), n/a-n/a. https://doi.org/10.1029/2012JD017585

Lensky, I. M., & Rosenfeld, D. (2006). The time-space exchangeability of satellite retrieved relations between cloud top temperature and particle effective radius. *Atmospheric Chemistry and Physics*, *6*(10), 2887–2894. https://doi.org/10.5194/acp-6-2887-2006

Moran-Zuloaga, D., Ditas, F., Walter, D., Saturno, J., Brito, J., Carbone, S., et al. (2018). Long-term study on coarse mode aerosols in the Amazon rain forest with the frequent intrusion of Saharan dust plumes. *Atmospheric Chemistry and Physics*, *18*(13), 10055–10088. https://doi.org/10.5194/acp-18-10055-2018

Nakajima, T., Higurashi, A., Kawamoto, K., & Penner, J. E. (2001). A possible correlation between satellite-derived cloud and aerosol microphysical parameters. *Geophysical Research Letters*, *28*(7), 1171–1174. https://doi.org/10.1029/2000GL012186

*NOAA's Comprehensive Large Array-data Stewardship System*. (n.d.). Noaa.Gov. Retrieved May 6, 2022, from https://www.avl.class.noaa.gov/saa/products/search?sub_id=0&datatype_family=VIIRS_SDR&submit.x=22&submit.y=4

Paluch, I. R., & Baumgardner, D. G. (1989). Entrainment and Fine-Scale Mixing in a Continental Convective Cloud. *Journal of the Atmospheric Sciences*, *46*(2), 261–278. https://doi.org/10.1175/1520-0469(1989)046<0261:EAFSMI>2.0.CO;2

Paluch, I. R., & Knight, C. A. (1984). Mixing and the Evolution of Cloud Droplet Size Spectra in a Vigorous Continental Cumulus. *Journal of the Atmospheric Sciences*, *41*(11), 1801–1815. https://doi.org/10.1175/1520-0469(1984)041<1801:MATEOC>2.0.CO;2

Pan, Z., Rosenfeld, D., Zhu, Y., Mao, F., Gong, W., Zang, L., & Lu, X. (2021). Observational Quantification of Aerosol Invigoration for Deep Convective Cloud Lifecycle Properties Based on Geostationary Satellite. *Journal of Geophysical Research: Atmospheres*, *126*(9). https://doi.org/10.1029/2020JD034275

Pinsky, M. B., & Khain, A. P. (2002). Effects of in-cloud nucleation and turbulence on droplet spectrum formation in cumulus clouds. *Quarterly Journal of the Royal Meteorological Society*, *128*(580), 501–533. https://doi.org/10.1256/003590002321042072

Pinsky, M., Khain, A., Mazin, I., & Korolev, A. (2012). Analytical estimation of droplet concentration at cloud base: DROPLET CONCENTRATION AT CLOUD BASE. *Journal of Geophysical Research: Atmospheres*, *117*(D18), n/a-n/a. https://doi.org/10.1029/2012JD017753

Pinsky, M., Khain, A., & Shapiro, M. (2001). Collision Efficiency of Drops in a Wide Range of Reynolds Numbers: Effects of Pressure on Spectrum Evolution. *Journal of the Atmospheric Sciences*, *58*(7), 742–764. https://doi.org/10.1175/1520-0469(2001)058<0742:CEODIA>2.0.CO;2

Pöhlker, C., Walter, D., Paulsen, H., Könemann, T., Rodríguez-Caballero, E., Moran-Zuloaga, D., et al. (2019). Land cover and its transformation in the backward trajectory footprint region of the Amazon Tall Tower Observatory. *Atmospheric Chemistry and Physics*, *19*(13), 8425–8470. https://doi.org/10.5194/acp-19-8425-2019

Pöhlker, M. L., Ditas, F., Saturno, J., Klimach, T., Hrabě de Angelis, I., Araùjo, A. C., et al. (2018). Long-term observations of cloud condensation nuclei over the Amazon rain forest – Part 2: Variability and characteristics of biomass burning, long-range transport, and pristine rain forest aerosols. *Atmospheric Chemistry and Physics*, *18*(14), 10289–10331. https://doi.org/10.5194/acp-18-10289-2018

Pöhlker, M. L., Pöhlker, C., Ditas, F., Klimach, T., Hrabe de Angelis, I., Araújo, A., et al. (2016). Long-term observations of cloud condensation nuclei in the Amazon rain forest – Part 1: Aerosol size distribution, hygroscopicity, and new model parametrizations for CCN prediction. *Atmospheric Chemistry and Physics*, *16*(24), 15709–15740. https://doi.org/10.5194/acp-16-15709-2016

Pöhlker, M. L., Zhang, M., Campos Braga, R., Krüger, O. O., Pöschl, U., & Ervens, B. (2021). Aitken mode particles as CCN in aerosol- and updraft-sensitive regimes of cloud droplet formation. *Atmospheric Chemistry and Physics*, *21*(15), 11723–11740. https://doi.org/10.5194/acp-21-11723-2021

Prabha, T. V., Khain, A., Maheshkumar, R. S., Pandithurai, G., Kulkarni, J. R., Konwar, M., & Goswami, B. N. (2011). Microphysics of Premonsoon and Monsoon Clouds as Seen from In Situ Measurements during the Cloud Aerosol Interaction and Precipitation Enhancement Experiment (CAIPEEX). *Journal of the Atmospheric Sciences*, *68*(9), 1882–1901. https://doi.org/10.1175/2011JAS3707.1

Quaas, J., Ming, Y., Menon, S., Takemura, T., Wang, M., Penner, J. E., Gettelman, A., Lohmann, U., Bellouin, N., Boucher, O., Sayer, A. M., Thomas, G. E., McComiskey, A., Feingold, G., Hoose, C., Kristjánsson, J. E., Liu, X., Balkanski, Y., Donner, L. J., … Schulz, M. (2009). Aerosol indirect effects – general circulation model intercomparison and evaluation with satellite data. *Atmospheric Chemistry and Physics*, *9*(22), 8697–8717. https://doi.org/10.5194/acp-9-8697-2009

Rogers, R. R., & Yau, M. K. (1996). *A short course in cloud physics* (3. ed., reprint). Butterworth Heinemann.

Rosenfeld, D. (2018). Cloud-Aerosol-Precipitation Interactions Based of Satellite Retrieved Vertical Profiles of Cloud Microstructure. In *Remote Sensing of Aerosols, Clouds, and Precipitation* (pp. 129–152). Elsevier. https://doi.org/10.1016/B978-0-12-810437-8.00006-2

Rosenfeld, D., Fischman, B., Zheng, Y., Goren, T., & Giguzin, D. (2014a). Combined satellite and radar retrievals of drop concentration and CCN at convective cloud base: ROSENFELD ET. AL.; RETRIEVING CONVECTIVE CLOUD BASE CCN. *Geophysical Research Letters*, *41*(9), 3259–3265. https://doi.org/10.1002/2014GL059453

Rosenfeld, D., & Gutman, G. (1994). Retrieving microphysical properties near the tops of potential rain clouds by multispectral analysis of AVHRR data. *Atmospheric Research*, *34*(1–4), 259–283. https://doi.org/10.1016/0169-8095(94)90096-5

Rosenfeld, D., Kaufman, Y. J., & Koren, I. (2006). Switching cloud cover and dynamical regimes from open to closed Benard cells in response to the suppression of precipitation by aerosols. *Atmospheric Chemistry and Physics*, *6*(9), 2503–2511. https://doi.org/10.5194/acp-6-2503-2006

Rosenfeld, D., & Lensky, I. M. (1998). Satellite-Based Insights into Precipitation Formation Processes in Continental and Maritime Convective Clouds. *Bulletin of the American Meteorological Society*, *79*(11), 2457–2476. https://doi.org/10.1175/1520-0477(1998)079<2457:SBIIPF>2.0.CO;2

Rosenfeld, D., Liu, G., Yu, X., Zhu, Y., Dai, J., Xu, X., & Yue, Z. (2014b). High-resolution (375 m) cloud microstructure as seen from the NPP/VIIRS satellite imager. *Atmospheric Chemistry and Physics*, *14*(5), 2479–2496. https://doi.org/10.5194/acp-14-2479-2014

Rosenfeld, D., Lohmann, U., Raga, G. B., O'Dowd, C. D., Kulmala, M., Fuzzi, S., et al. (2008). Flood or Drought: How Do Aerosols Affect Precipitation? *Science*, *321*(5894), 1309–1313. https://doi.org/10.1126/science.1160606

Rosenfeld, D. (2007). New insights to cloud seeding for enhancing precipitation and for hail suppression. *The Journal of Weather Modification*, *39*(1), 61–69.

Rosenfeld, D., Zheng, Y., Hashimshoni, E., Pöhlker, M. L., Jefferson, A., Pöhlker, C., et al. (2016). Satellite retrieval of cloud condensation nuclei concentrations by using clouds as CCN chambers. *Proceedings of the National Academy of Sciences*, *113*(21), 5828–5834. https://doi.org/10.1073/pnas.1514044113

Shinozuka, Y., Clarke, A. D., Nenes, A., Jefferson, A., Wood, R., McNaughton, C. S., Ström, J., Tunved, P., Redemann, J., Thornhill, K. L., Moore, R. H., Lathem, T. L., Lin, J. J., & Yoon, Y. J. (2015). The relationship between cloud condensation nuclei (CCN) concentration and light extinction of dried particles: Indications of underlying aerosol processes and implications for satellite-based CCN estimates. *Atmospheric Chemistry and Physics*, *15*(13), 7585–7604. https://doi.org/10.5194/acp-15-7585-2015

Slingo, A., & Slingo, J. M. (1988). The response of a general circulation model to cloud longwave radiative forcing. I: Introduction and initial experiments. *Quarterly Journal of the Royal Meteorological Society*, *114*(482), 1027–1062. https://doi.org/10.1002/qj.49711448209

Stephens, G. L., Tsay, S.-C., Stackhouse, P. W., & Flatau, P. J. (1990). The Relevance of the Microphysical and Radiative Properties of Cirrus Clouds to Climate and Climatic Feedback. *Journal of the Atmospheric Sciences*, *47*(14), 1742–1754. https://doi.org/10.1175/1520-0469(1990)047<1742:TROTMA>2.0.CO;2

Squires, P. (1958). The Microstructure and Colloidal Stability of Warm Clouds. *Tellus*, *10*(2), 256–261. https://doi.org/10.1111/j.2153-3490.1958.tb02011.x

Twomey, S. (1959). The nuclei of natural cloud formation part I: The chemical diffusion method and its application to atmospheric nuclei. *Geofisica Pura e Applicata*, *43*(1), 227–242. https://doi.org/10.1007/BF01993559

Twomey, S. (1977). The Influence of Pollution on the Shortwave Albedo of Clouds. *Journal of the Atmospheric Sciences*, *34*(7), 1149–1152. https://doi.org/10.1175/1520-0469(1977)034<1149:TIOPOT>2.0.CO;2

VanZanten, M., Stevens, B., Vali, G., & Lenschow, D. (2005). Observations of drizzle in nocturnal marine stratocumulus. *Journal of the Atmospheric Sciences*, *62*(1), 88–106.

Warner, J. (1969). The Microstructure of Cumulus Cloud. Part I. General Features of the Droplet Spectrum. *Journal of the Atmospheric Sciences*, *26*(5), 1049–1059. https://doi.org/10.1175/1520-0469(1969)026<1049:TMOCCP>2.0.CO;2

Wendisch, M., Pöschl, U., Andreae, M. O., Machado, L. A. T., Albrecht, R., Schlager, H., et al. (2016). ACRIDICON–CHUVA Campaign: Studying Tropical Deep Convective Clouds and Precipitation over Amazonia Using the New German Research Aircraft HALO. *Bulletin of the American Meteorological Society*, *97*(10), 1885–1908. https://doi.org/10.1175/BAMS-D-14-00255.1

Zheng, Y., & Rosenfeld, D. (2015). Linear relation between convective cloud base height and updrafts and application to satellite retrievals: SATELLITE RETRIEVAL OF CLOUD UPDRAFTS. *Geophysical Research Letters*, *42*(15), 6485–6491. https://doi.org/10.1002/2015GL064809

Zhu, Y., Rosenfeld, D., Yu, X., Liu, G., Dai, J., & Xu, X. (2014). Satellite retrieval of convective cloud base temperature based on the NPP/VIIRS Imager. *Geophysical Research Letters*, *41*(4), 1308–1313. https://doi.org/10.1002/2013GL058970

*Supplement of*

**Satellite-based detection of secondary droplet activation during condensational growth in convective clouds**

Avichay Efraim et al.

*Correspondence to:* Avichay Efraim (Avichay.Efraim@mail.huji.ac.il)

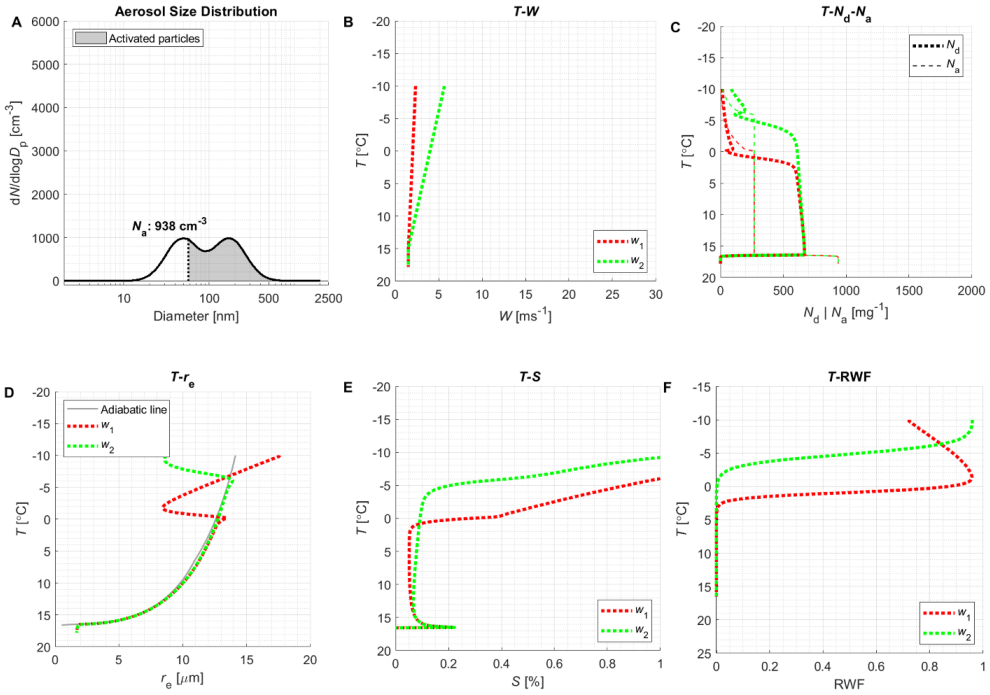


Figure S1. Simulations of cloud properties for a fixed aerosol size distribution (ASD) and two prescribed updraft schemes (*w*). Panel A shows the ASD with the same size of Aitken and accumulation modes (similar to ASD2 described in Fig. 4). The total particle number concentration ($N_a$) is 938 cm$^{-3}$. The shaded grey marks the calculated activated particles at the cloud base. Panel B shows two prescribed *w* schemes with a constant *w* speed of 1.5 ms$^{-1}$ up to cloud base and then different increase rates - $w_1$ (red dashed line) has a low slope and is close to constant *w* with height; and $w_2$ (green dashed line) with a higher increase rate than $w_1$. Panels C-F shows the different cloud properties where the color of the lines is related to the same-colored *w* scheme in each panel. Panel C shows the number concentration of cloud droplets ($N_d$) and the $N_a$ in units of mg$^{-1}$ to avoid the consideration of the change of air density with height; Panel D shows the effective radius ($r_e$) profile, where the thick black line is the theoretical adiabatic curve, calculated based on the cloud base *P* and *T*; Panel E shows the vertical profile of supersaturation over water (*S*) and Panel F shows the vertical rainwater fraction (RWF) profile. RWF is defined as the ratio between rainwater content to total water content, where drops with a diameter > 50 µm are considered raindrops. For the described ASD and *w* schemes in this figure, there is no significant secondary activation (SA) of droplets during the condensational phase. For the SA to occur, there should be either stronger *w* or more available particles for condensation, as describe in Figures 3 and 4.

## 2.3 High aerosol sensitivity of Amazonian clouds throughout the seasons

**This chapter will be submitted shortly:**
Lauer, O.; Kremper, L. A.; Rosenfeld, D.; Franco, M. A.; Andreae, M. O.; Artaxo, P.; Campos Braga, R.; Dias-Júnior, C. Q.; Araújo, A. C. de; Ditas, F.; Efraim, A.; Ervens, B.; Holanda, B. A.; Jungandreas, L.; Krüger, O. O.; Machado, L. A. T.; Hernández Pardo, L.; Pöschl, U.; Pulik, G.; Quaas, J.; Zheng, Y.; Zhu, Y.; Pöhlker, C., and Pöhlker, M. L.: "High aerosol sensitivity of Amazonian clouds throughout the seasons". *To be submitted*. (2022)

**Contribution to this publication by Oliver Lauer:** I am the first author of this publication and my contribution to this work includes the processing and analysis of the satellite data. Alongside my coauthors, I played a primary role in initiating and designing the research, analyzing the results, preparing figures, and writing the manuscript.

# High aerosol sensitivity of Amazonian clouds throughout the seasons

Oliver Lauer[1], Leslie A. Kremper[1], Daniel Rosenfeld[2], Marco A. Franco[1,3], Meinrat O. Andreae[1,4], Paulo Artaxo[3], Ramon Campos Braga[1], Cléo Quaresma Dias-Júnior[5], Alessandro C. de Araújo[6], Florian Ditas[1,a], Avichay Efraim[2], Barbara Ervens[7], Bruna A. Holanda[1], Leonore Jungandreas[8], Ovid O. Krüger[1], Luiz A. T. Machado[1,3], Lianet Hernández Pardo[1,b], Ulrich Pöschl[1], Guy Pulik[2], Johannes Quaas[9], Youtong Zheng[10], Yannian Zhu[11], Christopher Pöhlker[1], and Mira L. Pöhlker[1,9,12]

[1] Multiphase Chemistry Department, Max Planck Institute for Chemistry, Mainz, Germany
[2] Institute of Earth Sciences, The Hebrew University of Jerusalem, Jerusalem, Israel
[3] Instituto de Física, Universidade de São Paulo, São Paulo, Brazil
[4] Scripps Institution of Oceanography, University of California San Diego, La Jolla, CA 92037, USA
[5] Department of Physics, Federal Institute of Pará (IFPA), Belém, PA, Brazil
[6] Empresa Brasileira de Pesquisa Agropecuária (Embrapa) Amazonia Oriental, CEP 66095-100, Belém, Brazil
[7] Université Clermont Auvergne, CNRS, SIGMA Clermont, Institut de Chimie de Clermont-Ferrand, 63000 Clermont-Ferrand, France
[8] Helmholtz Centre for Environmental Research, Leipzig, Germany
[9] Faculty of Physics and Earth Sciences, Leipzig Institute for Meteorology, University of Leipzig, Leipzig, Germany
[10] Atmospheric and Oceanic Sciences, Princeton University, and NOAA/Geophysical Fluid Dynamics Laboratory, Princeton, New Jersey, 08544, USA
[11] Meteorological Institute of Shaanxi Province, Xi'an, China
[12] Experimental Aerosol and Cloud Microphysics Department, Leibniz Institute for Tropospheric Research, Leipzig, Germany
[a] now at: Hessian Agency for Nature Conservation, Environment and Geology, Wiesbaden, Germany
[b] now at: Institute for Atmospheric and Environmental Sciences, Goethe University Frankfurt am Main, Germany

**Correspondence:** Christopher Pöhlker (c.pohlker@mpic.de), Mira L. Pöhlker (poehlker@tropos.de)

**Abstract.** Aerosol effects on clouds and climate have remained highly uncertain. Here, we present a three-year study on aerosol-induced effects on convective clouds over remote regions in the central Amazon rain forest. The analysis combines in-situ aerosol data with satellite retrieved profiles of temperature and the effective radius of cloud droplets to resolve temporal changes in fundamental microphysical properties at a reference height above cloud base. A clear seasonality was observed, with a remarkably high fraction of aerosol particles being activated into cloud droplets, especially the activation efficiency during the dry season is higher than expected from previous studies. The cloud formation in the Amazon is both, aerosol- and updraft-sensitive, not just under the low aerosol conditions during the wet season, but also during the biomass burning smoke dominated dry season. Our findings shed light on the aerosol-driven changes in fundamental parameters of tropical convective clouds and suggest that the buffering effect of updraft limited droplet activation at high aerosol concentrations is weaker than expected.

The effects of aerosols on clouds and climate have remained widely uncertain in the assessment and modeling of climate change (Forster et al., 2021). Aerosol–cloud interactions contribute significant uncertainty to current radiative forcing estimates, especially due to a lack of knowledge of preindustrial aerosol and cloud conditions (Mülmenstädt and Feingold, 2018; Carslaw et al., 2013). Accordingly, locations that today still approximate a preindustrial atmospheric state are of particular interest to understand and constrain the anthropogenic influence on cloud abundance and properties (Andreae, 2007; Andreae et al., 2021). These locations, however, have become rare worldwide (Hamilton et al., 2014). The Amazon is one of the few remaining continental places with episodes of pristine atmospheric conditions (Martin et al., 2010; Pöhlker et al., 2018). It therefore represents a well-suited outdoor laboratory to investigate the responses and adjustments of cloud properties to aerosol perturbations across a wide range of atmospheric conditions, ranging from a widely unperturbed biosphere–atmosphere exchange in the wet season to heavy pollution in the dry season, also referred to as biomass burning season (e.g., Graham et al., 2003; Pöschl et al., 2010; Saturno et al., 2018).

The Amazonian aerosol population is characterized by a pronounced seasonality and a multimodal shape, comprising Aitken, accumulation, and coarse modes (see Table S1 with reference values) (Artaxo et al., 2013; Machado et al., 2021; Franco et al., 2022). A detailed understanding of the aerosol size distribution is a prerequisite for cloud microphysical studies as it defines the number concentration ($N_{\mathrm{CCN}}(S)$) of cloud condensation nuclei (CCN) in an aerosol population and, thus, the number of cloud droplets ($N_{\mathrm{d}}$) under a given updraft velocity ($w$) of the air masses at cloud base and the resulting water vapor supersaturation ($S$) (Köhler, 1936; Howell, 1949; Andreae and Rosenfeld, 2008; Rosenfeld et al., 2014a). The CCN efficiency ($N_{\mathrm{CCN}}(S)/N_{\mathrm{CN}}$) of an aerosol population is determined by the shape of its size distribution, the particles' hygroscopicity, and $S$. It increases with higher fractions of large particles as well as with an enhanced hygroscopicity (Dusek et al., 2006; Pöhlker et al., 2018).

Heavy biomass burning smoke affects atmospheric thermodynamics and causes adjustments in the cloud micro- and macrophysical properties, such as the cloud dynamic evolution, the vertical profile of latent heat release, and precipitation formation (e.g., Ramanathan et al., 2001; Rosenfeld et al., 2008; Martins et al., 2011). Prominent examples of aerosol-induced changes of the cloud microphysics are the so-called 'cloud albedo effect' (also Twomey effect) and 'cloud lifetime effect' (Twomey, 1977; Stevens and Feingold, 2009). The cloud albedo effect refers to an aerosol-related increase in cloud droplet number concentration ($N_{\mathrm{d}}$) and a corresponding decrease in the cloud droplet effective radius ($r_{\mathrm{e}}$), which leads to more reflective clouds for a fixed cloud macrostructure and atmospheric thermodynamic conditions (i.e., the same liquid water content). The cloud lifetime effect refers to changes in precipitation efficiency due to increased CCN and droplet numbers (e.g., Albrecht, 1989; Rotstayn, 1999). This can delay the precipitation onset in the clouds to higher altitudes, cause a corresponding suppression of low-level rainout, and prolong cloud lifetime (e.g., Andreae et al., 2004; Feingold, 2005; Lin et al., 2006; Rosenfeld et al., 2008). Beyond their fundamental role in the climate system, these processes are also critically important for the rain forest ecosystem as they directly affect the hydrological cycle in the Amazon basin.

Here, we address the effects of a biomass burning-driven increase in aerosol and CCN concentrations on the microphysics of convective clouds in the central Amazon. This experimental three-year study on aerosol-cloud interactions combines in situ aerosol data from the Amazon Tall Tower Observatory (ATTO) (Andreae et al., 2015) and high-resolution remote sensing observations of cloud microphysical properties from the Visible Infrared Imaging Radiometer Suite (VIIRS) on the Suomi National Polar-orbiting Partnership (NPP) satellite. Figure 1 shows how the comparatively high spatial resolution ($\sim 375$ m) of the VIIRS data allows to retrieve fundamental parameters, such as the cloud base height ($H_{\mathrm{cb}}$) as well as the droplet number concentration ($N_{\mathrm{d}}$) and the effective cloud droplet radius $r_{\mathrm{e}}$ at and above the base of convective clouds on large geographic scales (Rosenfeld et al., 2014b; Yue et al., 2019; Efraim et al., 2021). These parameters were examined for their seasonality

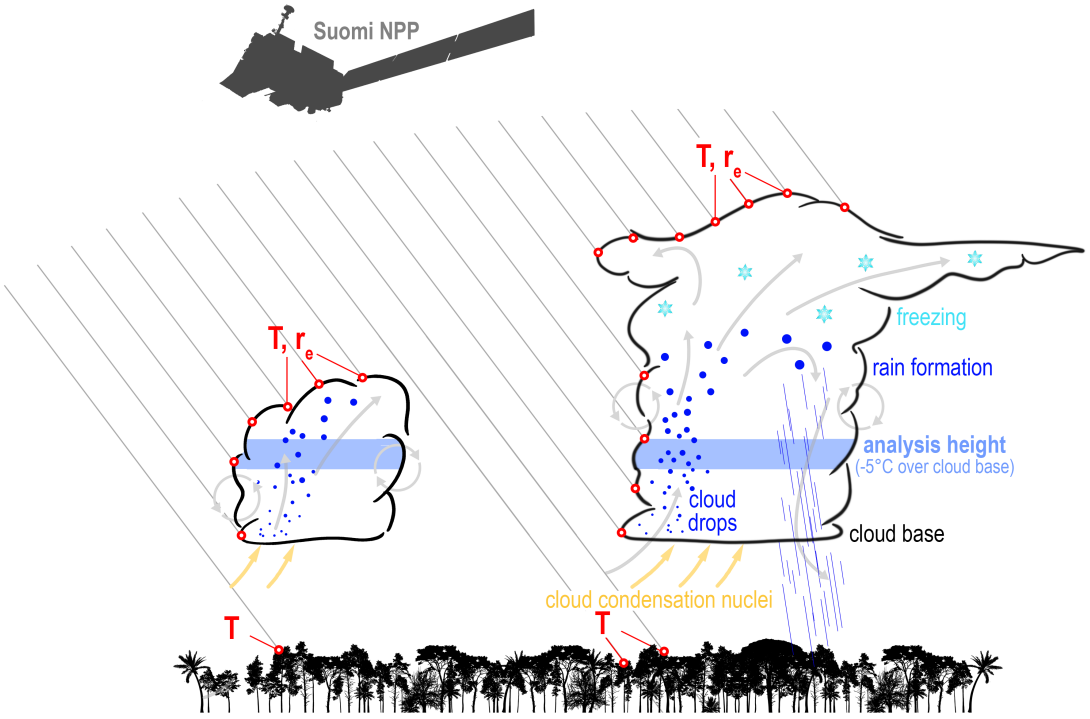


**Figure 1.** Illustration of basic microphysical processes in Amazonian convective clouds with Suomi-NPP satellite observations, covering clouds in different development states as well as side observations of fully developed cumulus clouds (see examples in Fig. 5. Temperature ($T$) and the effective radius of cloud droplets ($r_{\mathrm{e}}$) are being observed as a function of height. Under constant atmospheric conditions, the properties of clouds in different development states are interchangeable at the same temperature level, which means that a $T$-$r_{\mathrm{e}}$ profile of a cloud cluster and a profile tracking a single convective cloud throughout its evolution provide the same information (Lensky and Rosenfeld, 2006; Arakawa and Schubert, 1974). The selected analysis height of this study is located $-5$ °C over cloud base, yielding the cloud droplet effective radius ($r_{\mathrm{e,cb5}}$) at that height.

and their relation to the concentration and size distribution of the underlying aerosol field. Our findings help to understand and constrain the complex aerosol-cloud-precipitation interactions in the Amazonian hydrological cycle in order to represent these processes more accurately in numerical models (e.g., Rosenfeld et al., 2014c; Pringle et al., 2009; Quaas, 2015; Fan et al., 2016; Quaas et al., 2020).

**Seasonality of cloud microphysical properties**

A variety of meteorological, trace gas, and aerosol parameters in central Amazonia show a pronounced seasonality (e.g., Artaxo et al., 2002; Rizzo et al., 2013; Moran-Zuloaga et al., 2018a; Saturno et al., 2018). These include the total aerosol particle number concentration ($N_{\mathrm{tot}}$) and the black carbon mass concentration ($M_{\mathrm{BC}}$), which are characterized by the typical oscillation between the clean wet (Feb to May) vs polluted dry season (Aug to Nov), as shown in Fig. 2D and E. Pollution levels, here represented by $M_{\mathrm{BC}}$, are peaking around September and are lowest – episodically even below detection limit – around April and May (Pöhlker et al., 2018). We show here that also the cloud parameters $H_{\mathrm{cb}}$, $N_{\mathrm{d}}$, and $r_{\mathrm{e}}$ are strongly seasonal as well (Fig. 2A, B, and C).

The base height of the convective clouds varies between $\sim 500\,\mathrm{m}$ in the wet and $\sim 1500\,\mathrm{m}$ in the dry season (Fig. 2A). These values agree well with previously reported planetary boundary layer heights (e.g., Fisch et al., 2004; Henkes et al., 2021; Dias-Júnior et al., 2022) as well as cloud base heights (Andreae et al., 2004) in the Amazon. We obtained $H_{\mathrm{cb}}$ here through four different methods and found that the satellite-based $H_{\mathrm{cb}}$ agrees well with the other retrievals or direct measurements, which underlines the validity of the VIIRS approach. $H_{\mathrm{cb}}$ from the satellite observations and the ERA5 reanalysis data within a $50\,\mathrm{km}$ region around ATTO represent regional retrievals, whereas the ceilometer-derived $H_{\mathrm{cb}}$ as well as the lifting condensation level (LCL) calculated from ATTO meteorology data represent local retrievals. The calculated LCL-approach can be regarded as a lower limit for $H_{\mathrm{cb}}$, since cloud formation is often delayed to higher altitudes due to the influence of dry air entrainment. In fact, the LCL-based $H_{\mathrm{cb}}$ accounts for the lowest values in Fig. 2A.

The cloud parameters $N_{\mathrm{d}}$ and $r_{\mathrm{e}}$ show a clear seasonality as well (Fig. 2B and C). Due to condensational droplet growth, $r_{\mathrm{e}}$ initially increases adiabatically with height above cloud base (Efraim et al., 2021). In order to quantify the adiabatic growth rate of $r_{\mathrm{e}}$ a common reference level is chosen. Throughout this study, $r_{\mathrm{e,cb5}}$ represents the effective cloud droplet radius at $-5$°C relative to the cloud base temperature, as illustrated in Fig. 1. At this cloud level – corresponding roughly to a height of $800\,\mathrm{m}$ above cloud base – clear differences in $r_{\mathrm{e,cb5}}$ are expected for different CCN concentrations (Andreae et al., 2004; Freud et al., 2008). After reaching $S_{\mathrm{max}}$ close to the cloud base and throughout the initial phase of condensational droplet growth, $N_{\mathrm{d}}$ does not change significantly and, therefore, is not height-dependent in this range. This is valid as long as the cloud is adiabatic and no droplet evaporation or activation of new CCN occurs (Efraim et al., 2021). This level is chosen, because it is far enough from the cloud base to ensure stable adiabatic growth and at this height droplet are not yet big enough for coalescence to have a significant effect (Efraim et al., 2021).

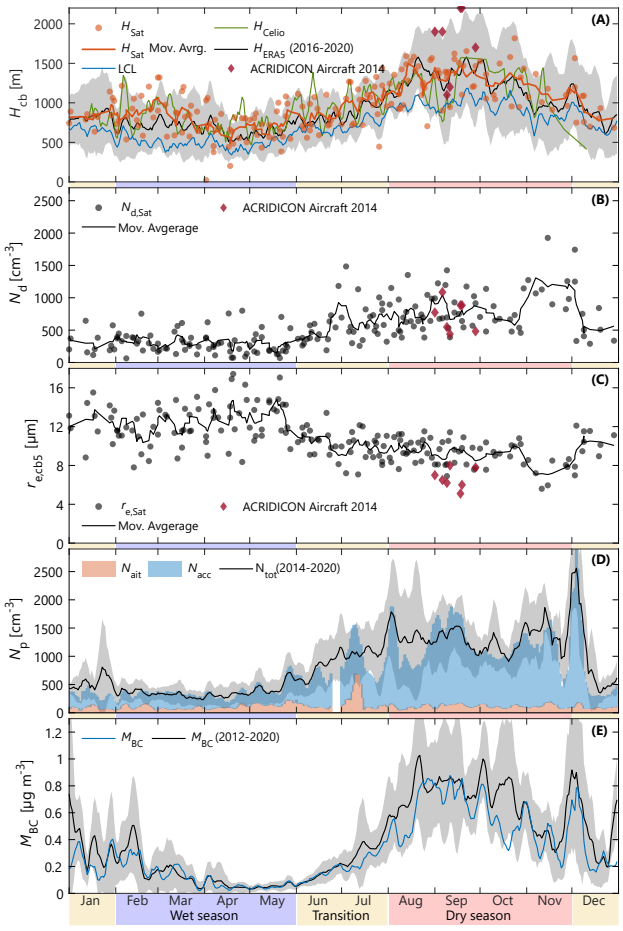


**Figure 2.** Seasonality of cloud microphysical and aerosol parameters in the ATTO region. **(A)** Cloud base height ($H_{cb}$) obtained through four different approaches: VIIRS satellite retrieval, ceilometer measurements at ATTO, lifting condensation level calculations at ATTO, and ERA5 reanalysis data. **(B,C)** The effective cloud droplet radius ($r_{e,cb5}$) and cloud droplet number concentration ($N_d$) were derived from VIIRS data. $r_{e,cb5}$ shown here was obtained at 5 °C above cloud base as a defined reference to illustrate the droplet growth rate. The markers in **(A)**, **(B)** and **(C)** represent cloud scenes on individual days while the lines are five-point floating averages. Aircraft data from Braga et al. (2016) are shown for comparison. **(D)** Aitken mode ($N_{ait}$), accumulation mode ($N_{acc}$), and total aerosol number concentrations ($N_{CN}$) from ATTO measurements. $N_{ait}$ and $N_{acc}$ are based on the two-year time frame of this study, while $N_{CN}$ is based on a seven-year period for comparison (black line as mean and gray shading as one standard deviation). **(E)** Black carbon mass concentrations ($M_{BC}$) from ATTO measurements. The three-year period of this study is shown in blue and the seven-year period in black (black line as mean and gray shading as one standard deviation).

The wet season clouds are characterized by a low droplet number concentrations (i.e., $N_d$ between ~200 and ~600 $cm^{-3}$) with growth to comparatively large droplet sizes (i.e., $r_{e,cb5}$ between ~11 and ~15 µm). Dry season clouds, in contrast, are characterized by significantly more (i.e., $N_d$ up to ~2000 $cm^{-3}$), though smaller, droplets (i.e., $r_{e,cb5}$ between ~5 and ~10 µm). Note that experimental data on $N_d$ and $r_e$ from the Amazon – especially if seasonally resolved – is still sparse. Thus, our results here help to close this fundamental knowledge gap and agree well with the few existing studies so far (e.g., Andreae et al., 2004; Freud et al., 2008; Braga et al., 2017). Andreae et al. (2004), for example, reported $r_{e,cb5}$ between $13 - 14$ µm for clean "green ocean conditions" as an upper limit and $r_{e,cb5}$ around ~7 µm for smoky conditions, with ~5 µm as an extreme value for pyrocumulus clouds. The variability in $r_{e,cb5}$ within the ATTO region ranges from even cleaner conditions with $r_{e,cb5} \approx 16$ µm to comparatively strong biomass burning pollution with $r_{e,cb5} \approx 6$ µm (Fig. 2C).

Through the cloud albedo effect, the seasonality in $N_d$ and $r_{e,cb5}$ generally follows the aerosol abundance, showing that the biomass burning-driven aerosol strongly modulates the cloud microphysical parameters (e.g., Kaufman and Nakajima, 1993). Especially, accumulation mode particles (i.e., 0.1 to 1 µm) are abundant and large enough to be the prime candidates for the majority of CCN. Under certain conditions, however, also Aitken mode particles can serve as CCN as well and, therefore, should not be neglected. In the Amazon, deep convective clouds with a comparatively high $w$ – e.g. under clean wet season conditions with a above average Aitken to accumulation mode ratio $N_{ait}/N_{acc}$ – are considered as suitable conditions under which a fraction of the Aitken mode particles can act as CCN (Pöhlker et al., 2021). Figure 2D emphasizes that the seasonality in aerosol abundance is quite different depending on the size range in the sense that the accumulation mode is characterized by a pronounced seasonality, which is mainly driven by the fire occurrence in the Amazon (Pöhlker et al., 2019; Holanda et al., 2020), whereas the strength of the Aitken mode is more constant ranging between 200 and 300 $cm^{-3}$ throughout the seasons (Franco et al., 2022; Varanda Rizzo et al., 2018; Pöhlker et al., 2016).

**Aerosol- and updraft-limited CCN regimes**

A simple yet instructive representation of the aerosol-cloud interactions under given atmospheric conditions is the relationship between the total particle number concentration ($N_{CN}$), as a routinely measured aerosol parameter, and $N_d$. The shape and slope of such $N_{CN}$ vs $N_d$ curves are determined by the interplay of $w$, $S$, as well as aerosol properties, such as concentration, composition and size distribution. Figure 3 shows the $N_{CN}$-$N_d$ relationship for the ATTO region, together with corresponding data sets from previous studies in the Amazon and worldwide. Within this $N_{CN}$ vs $N_d$ space, Reutter et al. (2009) defined regimes, in which the CCN activation and cloud droplet formation can be regarded as either aerosol-limited (high $w$ and low $N_{CN}$), updraft-limited (low $w$ and high $N_{CN}$) or falling into a transitional – meaning aerosol- and updraft-sensitive – regime (Fig. 3B).

The proximity of the $N_{CN}$-$N_d$ curve to the one-to-one line indicates the extent to which the entire aerosol population has been activated as droplets. The slope of the curve ($dN_d/dN_{CN}$) over a certain segment indicates the sensitivity of $N_d$ to a further

increase in $N_{CN}$. A purely aerosol-limited CCN activation corresponds to a slope of 1 (i.e., $dN_d/dN_{CN} \approx 1$), indicating that $N_d$ reacts sensitively to perturbations in the aerosol population. In a purely updraft-limited regime, the slope approaches zero (i.e., $dN_d/dN_{CN} \approx 0$) and additional particles can be only activated if $w$ is enhanced. Otherwise, the supersaturation is suppressed at high $N_{CN}$ as more particles compete for the same amount of water, which decreases the maximum supersaturation, $S_{max}$, at cloud base and in turn also the activation efficiency of CCN into droplets (Twomey, 1977). At some point, $w$ becomes the limiting factor for every $N_{CN}$-$N_d$ relationship and the question is in which $N_{CN}$ range $\lim_{N_{CN}\to\infty} dN_d/dN_{CN} = 0$ is reached under given conditions. The transitional regime where clouds are sensitive to changes in aerosols and updraft is characterized by a slope between unity and zero, depending on $N_{CN}$ and $w$ as well as the slope of the cumulative aerosol size distribution around the critical diameters (Pöhlker et al., 2021). Note that the $N_{CN}$ data used here was measured at 60 m assuming a well-mixed PBL with consistent aerosol size distributions over height (e.g., Adler et al., 2011).

Figure 3 shows that the $N_{CN}$-$N_d$ relationship at ATTO can be described as aerosol-limited over most of the relevant $N_{CN}$ range. The multi-year $N_{CN}$ frequency distribution ranges from clean continental air with a few hundreds of CN per $cm^3$ to polluted continental air with few thousands of CN per $cm^3$ (Andreae, 2009). High $N_{CN}$ levels above $\sim 3000 cm^{-3}$ rarely occur at ATTO and have rather been observed in the proximity of major fires, such as in the deforestation hot spots in the southeastern Amazon (e.g., Andreae, 2009; Artaxo et al., 2013; Brito et al., 2014). The $N_{CN}$ frequency distribution at ATTO is characteristic for the atmospheric conditions in central Amazonia, which implies that the aerosol-limitation of the $N_{CN}$-$N_d$ curve can probably also be regarded as representative for large parts of the basin. The highest sensitivity of $dN_d/dN_{CN} \approx 0.85$ occurs in the low $N_{CN}$ range and is lower than 0.5 at about $N_{CN} \approx 1600\,cm^{-3}$ (Fig. 3A bottom panel). While such a clear aerosol-limitation has been expected for wet season conditions (i.e., $N_{CN} \lessapprox 500\,cm^3$, see Table S1), it was found here surprisingly also for the polluted dry season (i.e., $N_{CN} \gtrapprox 1000\,cm^3$). The $N_{CN}$-$N_d$ relationship at ATTO further agrees well with data from a recent aircraft campaign (Campos Braga et al., 2021a), which resolves $N_d$ as a function of $w$ for a given $N_{CN}$ (Fig. 3A). These data illustrate the wide variability of $N_d$ depending on updraft conditions at cloud base: for $w \gtrapprox 2\,ms^{-1}$, the $N_{CN}$-$N_d$ curve is much closer to the one-to-one line and appears much stronger aerosol-limited than for $w \lessapprox 2\,ms^{-1}$. For the highest $N_{CN}$ values observed, the curve shows a tendency to level out as expected. This decrease in the slope $dN_d/dN_{CN}$ is consistent with the aircraft data in Andreae (2009) on smoky and even pyro cumulonimbus (Cb) clouds in the Amazon. All these data sets can be described well with an empirical exponential fit function as shown in Fig. 3A.

Figure 3B embeds the ATTO $N_{CN}$-$N_d$ curves into corresponding measurements from marine and continental environments worldwide. Worth noting is the comparatively close proximity of the Amazonian $N_{CN}$-$N_d$ curve to the one-to-one line, which represents high activated aerosol fractions. This agrees well with the generally high CCN efficiencies observed in the central Amazon, where 50 to 90 % of all particles can be activated as CCN at a supersaturation of $S = 0.5\,\%$ (Pöhlker et al., 2016, 2018). Such high CCN efficiencies are determined by the characteristic shape of the Amazonian aerosol size distribution, which typically has the majority of particles within the CCN-relevant size range. Specifically, sub-50 nm particles are sparse, the accumulation mode typically dominates and accounts for ~70 % of the particles in the average distribution, and the Aitken

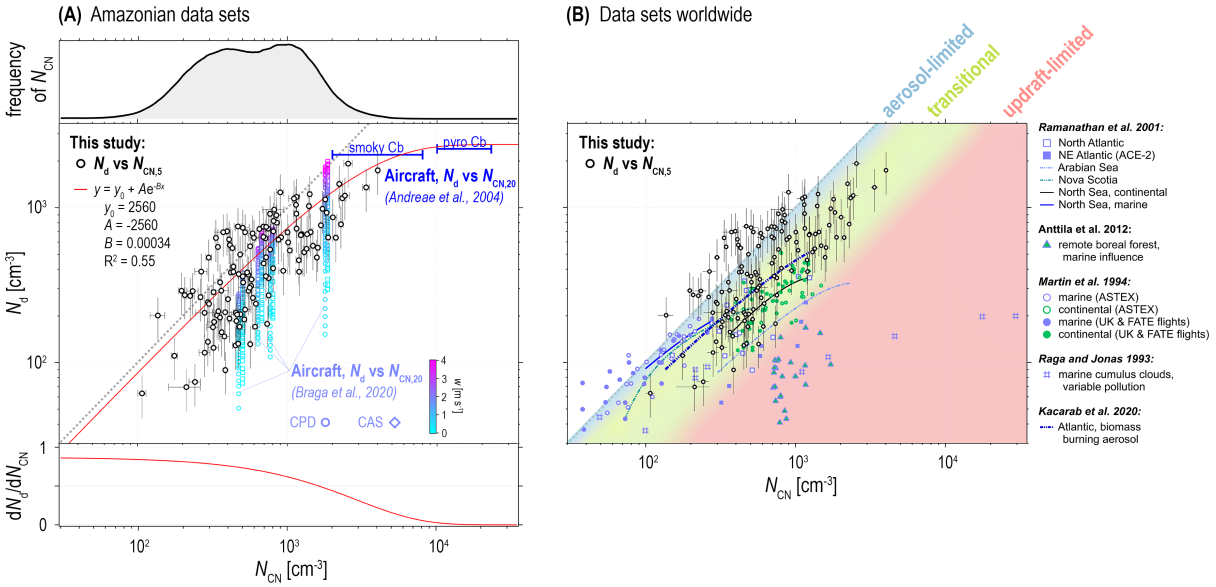


**Figure 3.** Relationship between total particle number concentration, $N_{CN}$, and droplet number concentration, $N_d$, at cloud base in the ATTO region, with data sets from previous Amazonian studies **(A)** and worldwide **(B)**. The ATTO data points (black circular markers) represent mean values with the error bars for one standard deviation in $N_{CN}$ and 30 % error bars for the uncertainty in $N_d$ according to Rosenfeld et al. (2016). Panel **(A)** combines the ATTO $N_{CN}$-$N_d$ relationship with using in situ aerosol and cloud observations from two aircraft campaigns: Campos Braga et al. (2021a) reported $N_d$ for flight average $N_{CN}$ values as a function of the updraft velocity $w$. Andreae et al. (2004) reported characteristic $N_d$ values and $N_{CN}$ ranges for highly polluted conditions over Amazonian fires. The empirical exponential fit in **(A)** includes the data from Andreae et al. (2004). Panel **(A)** also shows the $N_{CN}$ frequency distribution at ATTO from 2014 to 2021 (top) as well as the slope $dN_d/dN_{CN}$ of the empirical fit function (bottom). Panel **(B)** combines the ATTO $N_{CN}$-$N_d$ relationship with data sets worldwide (Raga and Jonas, 1993; Martin et al., 1994; Ramanathan et al., 2001; Anttila et al., 2012; Kacarab et al., 2020), which are subdivided into marine (blue) vs continental (green) environments here. The background shading in **(B)** illustrates the aerosol-limited (defined here through $N_d/N_{CN} \gtrapprox 0.9$), transitional (here $0.9 \gtrapprox N_d/N_{CN} \gtrapprox 0.2$), and updraft-limited (here $N_d/N_{CN} \lessapprox 0.2$) regimes, according to Reutter et al. (2009). The lower cut-off diameter of $N_{CN}$ is $\sim$5 nm. In both panels, the 1:1 line is shown for orientation. Cloud probes specified in **(A)** are CCP = cloud combination probe and CAS = cloud and aerosol spectrometer (see Campos Braga et al., 2021a).

mode is centered at comparatively large diameters between 67 and 71 nm (Franco et al., 2022, and Table S1). Note for comparison that most marine data sets in Fig. 3B show lower activated fractions, which could result from generally lower updrafts in marine environments $<0.5\,\mathrm{m\,s^{-1}}$ Kacarab et al. (e.g., 2020) as well as the typical shape of marine aerosol size distributions with a pronounced Aitken mode between 20 and 50 nm, which is much smaller than in the Amazon and therefore not particularly prone to act as CCN (e.g., Quinn et al., 2015; Wex et al., 2016; Gong et al., 2020). Note further that the marine $N_{CN}$-$N_d$ curves tend to level off at lower $N_{CN} \lessapprox 1000\,\mathrm{cm^{-3}}$ than the continental curves, probably also associated with lower $w$ over

ocean than over land. It can further be see that wet season $N_{CN}$ levels at ATTO overlaps with the upper range of the marine $N_{CN}$ data points, which re-emphasizes the concept of Green vs Blue Ocean conditions, in the sense that the pristine rain forest atmosphere resembles the pristine atmosphere over oceans (Roberts et al., 2001; Williams et al., 2002).

**Effective droplet radius and activation of Aitken mode particles as CCN**

Figure 4A shows the relationship between $N_{acc}$ and $N_d$. The accumulation mode represents the primary source of CCN and, therefore, accounts for the majority of the initial droplets at cloud base (Pöhlker et al., 2016, 2018). It has been retrieved here from a multimodal fitting of the overall particle number size distribution according to Franco et al. (2022), which allows to discriminate the roles of accumulation vs Aitken mode particles in the cloud droplet formation. The $N_{acc}$ vs $N_d$ scatter plot shows a comparatively tight relationship, which can be described by an empirical exponential fit. The BC mass concentration ($M_{BC}$) – as a widely used pollution marker and shown here color coding of the data points – increases with $N_{acc}$ and visualizes two clusters of data points for the clean wet vs polluted dry season. Related to Fig. 3, the $N_{acc}$-$N_d$ curve levels out at high $N_{acc}$, which implies that $w$ becomes the limiting factor and an increasingly smaller fraction of the accumulation mode particles is being activated as CCN. At low $N_{acc}$, the slope $dN_d/dN_{acc}$ approximates unity and the relationship exceeds the one-to-one line. According to the fit function in Fig. 4A, $N_{ait} \approx 70$ are activated as CCN for $N_{acc} = 0$. This corresponds to 30 to 40 % of the wet season Aitken mode population (Table S1). This experimental evidence for a contribution of the Aitken mode to cloud droplet formation is consistent with Pöhlker et al. (2021), showing that this effect is particularly strong under conditions with low $N_{CN}$ (Table S1) and a pronounced bimodal shape of the submicron aerosol population (Machado et al., 2021; Franco et al., 2022) as encountered during the Amazonian wet season. The relevance of Aitken mode particles for $N_d$ has also been emphasized in Campos Braga et al. (2021a), where aircraft data and model simulations over the Amazon region and Atlantic Ocean were compared.

Figure 4B shows the inverse relationship between $N_{acc}$ and $r_{e,cb5}$, emphasizing the relevance of the 'cloud albedo effect' in the Amazon (Twomey, 1977). The relationship can be well described with an inverse cubic relationship, which is expected since the decrease in $r_{e,cb5}$ with increasing $N_{acc}$ scales with the volume. Note that under wet season conditions (i.e., $N_{acc} < 200\,\mathrm{cm}^{-3}$), the average $r_{e,cb5}$ at the reference height $\sim 800\,\mathrm{m}$ above cloud base already reaches the threshold of $\sim 14\,\mu\mathrm{m}$, at which warm rain formations starts due to efficient droplet collision and coalescence (Rosenfeld and Gutman, 1994; Campos Braga et al., 2021b). This agrees with studies reporting a relatively low height of warm rain formation under wet season conditions in the Amazon (Braga et al., 2017; **?**). With increasing $N_{acc}$ levels, mostly driven by biomass burning smoke, $r_e$ $-5°$C above cloud base decreases substantially to about $7\,\mu\mathrm{m}$. Note in this context that a $r_e$ of $\sim 3.7\,\mu\mathrm{m}$ is the lower detection limit of the satellite retrieval.

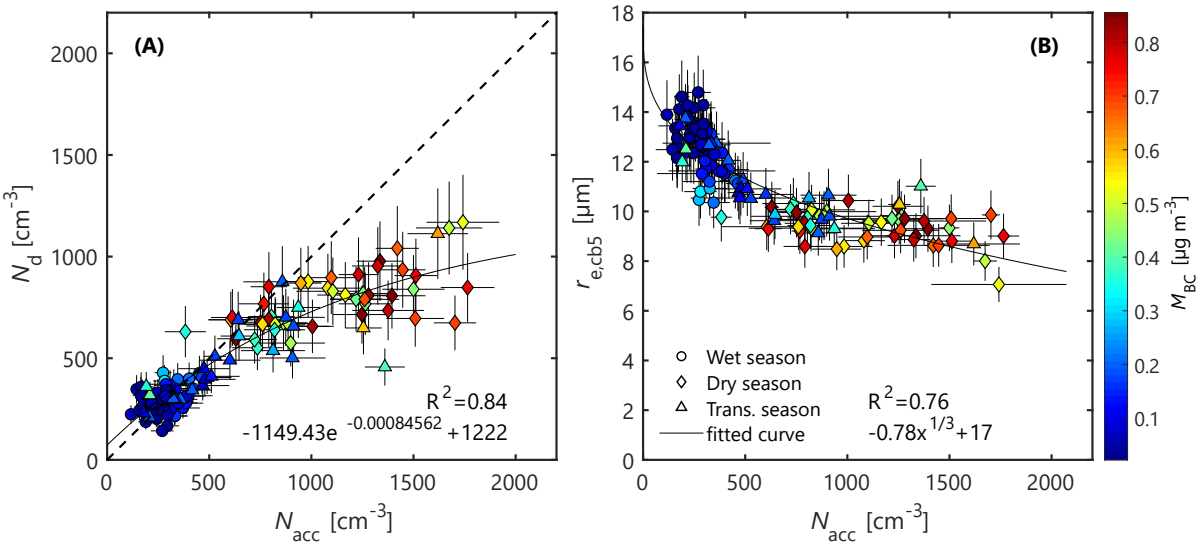


**Figure 4.** Scatter plots of accumulation mode particle number concentration ($N_{acc}$) from ATTO measurements vs droplet number concentration ($N_d$) and effective droplet radius ($r_e$) at a temperature 5 °C above the cloud base to show the droplet evolution. The $N_d$, as well as the $r_e$ are the results from satellite analysis (both 5-point floating average). The shape of the markers distinguishes between different seasons and the color of the markers scales with the black carbon (BC) mass concentration ($M_{BC}$) as a measure for biomass burning pollution. The solid black line represents an empirical exponential fit. The use of the floating average narrows the spread of the scatter diagrams significantly and emphasises the seasonal variability at the same time. The same plot with raw data without applying a floating average can be found in Fig. 8. Figures 9, 10, and 11 resolve the relationship by season.

## Conclusions

This three-year study relates measured total aerosol number concentrations ($N_{CN}$) as well as number concentrations of the Aitken and accumulation modes ($N_{ait}$, $N_{acc}$) to satellite retrievals of the cloud base height ($H_{cb}$), the droplet number concentration ($N_d$) and the effective cloud droplet radius ($r_e$) of convective clouds in the central Amazon. The results provide detailed insights into the cloud microphysics and the following can be concluded: The cloud parameters show a pronounced seasonality: The cloud base height ranged from $\sim$500 m in the wet season to $\sim$1500 m in the dry season. The wet season is further characterized by a low number ($N_d = 200 - 600\,\mathrm{cm}^{-3}$) of comparatively large droplets ($r_{e,cb5} = 11 - 15\,\mu\mathrm{m}$, at a reference height $\sim$800 m above cloud base), whereas the dry season clouds are characterized by larger numbers ($N_d$ up to $\sim$2000 cm$^{-3}$) of rather small droplets ($r_{e,cb5} = 5 - 10\,\mu\mathrm{m}$). $N_d$ in the central Amazon react sensitively to changes in $N_{CN}$ and the $N_{CN}$-$N_d$ relationship falls in between the aerosol-limited and transitional regimes. This means that even during the biomass burning season, the central Amazonian clouds are not fully buffered against changes in the aerosol population. With regard to the northwest vs southeast gradient in the Amazon basin, it can be extrapolated that clouds in the widely untouched northwest

are likewise or even more sensitive to changes in the aerosol population, whereas only clouds close to the heavy fires in the southeast reach a plateau in the $N_{CN}$-$N_d$ relationship and can be regarded as buffered. Based on the multi-year approach here, statistically robust relationships between the aerosol and cloud parameters could be obtained, which help to understand and
195 constrain the complex aerosol-cloud-precipitation interactions in the Amazonian hydrological cycle in order to represent these processes more accurately in numerical models.

## Methods

### Satellite data analysis

The approach of this study is based on the retrieval of so-called $T$-$r_e$ profiles, which estimate the vertical evolution of the effective cloud droplet radius ($r_e$) as a function of temperature ($T$) in a cluster of clouds. Satellite images were recorded by the VIIRS installed on the Suomi NPP satellite (Hillger et al., 2013, 2014). The VIIRS data are composed of 22 visible-to-infrared channels that measure the wavelength-dependent intensity of cloud-reflected sunlight and infrared emission in the spectral range from $0.6\,\mu m$ to $11.45\,\mu m$. Five out of the 22 channels provide a high spatial resolution of $375\,m$, while the other 17 channels provide a moderate resolution of $750\,m$ (Rosenfeld et al., 2014b; Hillger et al., 2014). The two high-resolution channels at $3.74\,\mu m$ and $11.45\,\mu m$ are primarily used in this study. The intensity of the emitted infrared radiation at a wavelength of $11.45\,\mu m$ is proportional to the temperature of the emitting object, approximating black body radiation (i.e., higher $T$ implies higher intensity in the $11.45\,\mu m$ channel). The intensity of the radiation at a wavelength of $3.74\,\mu m$, which comprises reflected sun light and black body emission, is inversely correlated with the effective cloud droplet radius (i.e., smaller $r_e$ entails higher radiance in the $3.74\,\mu m$ channel). The lower detection limit for $r_e$ is $3.7\,\mu m$ defined by the ratio between wavelength and $r_e$. The upper limit of $r_e$ is $40\,\mu m$ due to an exponential drop in intensity.

Figure 1 provides an illustration of cloud processes and the VIIRS satellite observations. The $T$-$r_e$ profiles were obtained from selected clouds or cloud ensembles within a certain area as shown by means of one example in Fig. 5. The overall region of interest (ROI), in which subregions (i.e., polygons) for the $T$-$r_e$ profile retrieval were selected, is centered around ATTO and covers $40\,000\,km^2$ ($200 \times 200\,km$). Note that the ROI does not include the city of Manaus and its plume, which is directed most of the time towards the west (Martin et al., 2016). Viewing angles are limited by shadows cast by the clouds if the angle between observer (satellite) and light source (sun) gets too wide. Suitable satellite zenith viewing angles (east-west direction) are limited to a range between $-10°$ and $40°$ relative to the satellite path, which eliminates 60 % of all days for investigation, on which the satellite overpass was not close enough to ATTO. Solar zenith angles are limited between $0°$ and $65°$, which makes ATTO a well-suited location as it is close to the equator and, thus, always fulfills this requirement. Further, the topography of the ATTO region is relatively flat. This largely avoids topography-forced updrafts and resulting instabilities in the planetary boundary layer (PBL), as the approach of this study requires a homogeneous temperature profile in the boundary layer. Finally, the dark forest provides an ideal homogeneous background, in strong contrast to the highly reflective clouds. These factors as well as the broad spectrum of ground-based in situ aerosol observations make ATTO a suitable location for the long-term satellite investigation.

In total, 203 days from January 2017 to December 2019 had adequate conditions that allowed a retrieval of $T$-$r_e$ profiles. Per overpass, multiple polygons were selected within the ROI (Fig. 5). All polygons were drawn by hand and meet the following requirements: (i) All clouds within the polygon are coupled with the PBL, so that the assumption of equal cloud properties at the same height for clouds in different development states is justified (Lensky and Rosenfeld, 2006). (ii) Each polygon

includes visible ground areas as the ground temperature is needed to calculate the cloud base height $H_{cb}$ (Fig. 1, Zheng and Rosenfeld (2015b)). (iii) The polygon includes clouds in different development states or fully developed clouds with a visible side profile to retrieve reliable $T$-$r_e$ profiles (see e.g. example for cloud slope in Fig. 5). (iv) Cirrus, multi-layer, decoupled and semi-transparent clouds are avoided, as they distort the $T$-$r_e$ profiles (see Fig. 6).

An exemplary VIIRS image is shown in Fig. 5a. It is a RGB-image (red, green, and blue), where each of the three base color channels represents one cloud property. Red is correlated with the cloud optical thickness (COT), green is inversely correlated with the effective cloud droplet radius ($r_e$), and blue is correlated with the temperature ($T$). The resulting color of each pixel is proportional of each property related to the three base colors. For reliable $T$-$r_e$ profiles, only coupled cumulus clouds with a clear field of view can be used. These show up as pink-colored clouds with teal edges. The pink color is a result of an average COT (medium red), high $r_e$ at the cloud top (weak green) and their warm temperature compared to higher clouds (strong blue). The teal edge is a result of small COT (weak red), small $r_e$ (strong green) and high temperature (strong blue). The ground is colored in strong blue, since it has the highest temperature. This representation of cloud properties also helps to avoid areas that can cause unwanted distortions: Clouds that are marked by bright green shading are decoupled mid-level clouds, as a result of small $r_e$ and low temperatures, while semi-transparent cirrus clouds are displayed in dark red or black. They are cold and contain ice particles, which are detected as $r_e > 40$ µm (Fig. 5A and Fig. 6A). Details on the coloring of the satellite plots can be found in Lensky and Rosenfeld (2008). For the retrieval of the $T$-$r_e$-profiles, the measured $r_e$ values are binned into 1 °C temperature intervals according to the corresponding pixel. For example, for every pixel with a temperature between 9.5 °C and 10.5 °C, the $r_e$ values get binned together into a bin centered at 10 °C. The 30$^{th}$ percentile (see explanation below) of $r_e$ for each temperature is then the $r_e$ used in the resulting $T$-$r_e$-profile for each polygon. For the $T$-$r_e$-profile retrieval within a given ROI, three different averaging methods were applied and compared:

1. *Polygons average*: Averaging of the individual $T$-$r_e$ profiles from all individual polygons in Fig. 5A, which yielded the black profile in Fig. 5B.

2. *Polygons unified*: Retrieval of the $T$-$r_e$ profile after merging all polygons in Fig. 5A and, thus, eliminating duplicated pixels, which yielded the brown profile in Fig. 5B.

3. *Total area*: Retrieval of the $T$-$r_e$ profile from the entire VIIRS image, which yielded the green profile in Fig. 5B.

Figures 5B and 6B show the comparison of the $T$-$r_e$ profiles from aforementioned methods: The $T$-$r_e$ profiles from the *averaged polygons* and *unified polygons* approaches are comparable and vary only in some aspects. The $T$-$r_e$ profile of the entire VIIRS image through the *total area* approach, however, can deviate strongly, especially when decoupled mid-level or cirrus clouds are present (Figure 6). The *unified polygons* approach yields the smoothest $T$-$r_e$ profiles, but comparing all methods to model and ground data shows that the *averaged polygons* approach yields the best approximation of cloud properties, such as $H_{cb}$ and cloud base $T$. This is expected, because the *unified polygons* use the overall warmest cloud pixel detected as cloud base, this leads to a systic overestimaton of the lcoud base T, which results in an underestimation of $H_{cb}$ for the *unified polygons*

approach, while this bias is eliminated by the *averaged polygons* approach. Therefore the *averaged polygons* $T$-$r_e$ profiles are used for all of the further analyses. Outliers within the same overpass are removed.

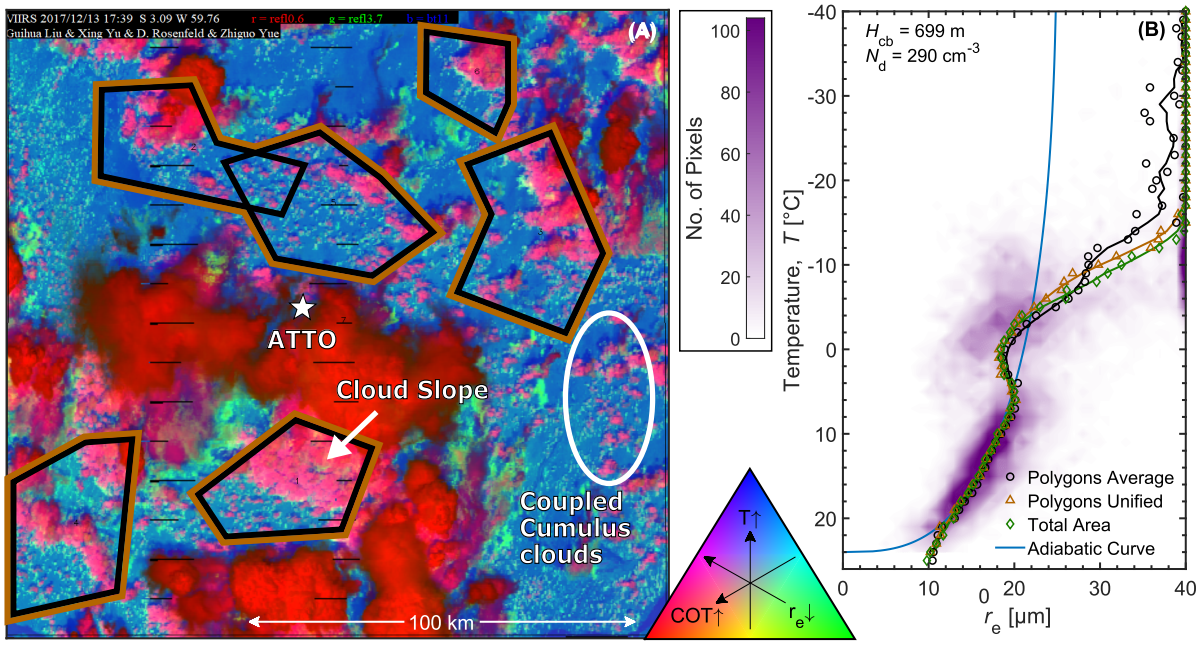


**Figure 5.** Exemplary VIIRS image of the ATTO region with the cloud scenery on 13 December 2017 **(A)** and the corresponding $T$-$r_e$ profiles **(B)**. **(A)** The VIIRS image covers 200 km x 200 km with the ATTO site being marked as the white star. In the triangular color scale, blue indicates the highest temperatures ($T$) near the surface, representing cloud-free areas. Red indicates cloud optical thickness (COT) with intense, dark red showing high COT and thus regions of deep clouds, while pink shows regions with shallow convective clouds. Green color shows the inverse effective cloud droplet radius ($r_e$) with more intense green for smaller $r_e$. In this figure the teal pixels are low level clouds with low COT, small $r_e$ and high $T$. The warmest pixels of these clouds have been interpreted as cloud base. The polygons in **(A)** show different regions that were averaged to retrieve the $T$-$r_e$ profiles shown in **(B)**: Black polygons were analysed individually to retrieve individual $T$-$r_e$ profiles that were subsequently averaged, yielding the black profile in **(B)** (averaged polygons). Brown polygons correspond to the combination of all black polygons treating it as one without overlap, yielding the brown $T$-$r_e$ profile in **(B)** (unified polygons). The green $T$-$r_e$ profile in **(B)** was obtained from the entire field of view in **(A)** (total area). The blue line in **(B)** shows the fitted adiabatic growth curve for this example case, calculated from the $T$-$r_e$ profile and the adiabatic liquid water content (LWC) from National Centers for Environmental Prediction (NCEP) reanalysis data. The average cloud base height ($H_{cb}$) is reported as $700 \pm 130$ m and $N_d$ calculated from the fitted adiabatic growth curve is $290 \pm 110\,\mathrm{cm}^{-3}$.

Here, we describe the $T$-$r_e$ data analysis briefly, while more details can be found in Rosenfeld et al. (2016), Zheng and Rosenfeld (2015b), Yue et al. (2019), and Efraim et al. (2021). Assuming a linear decrease in $T$ with height in the boundary

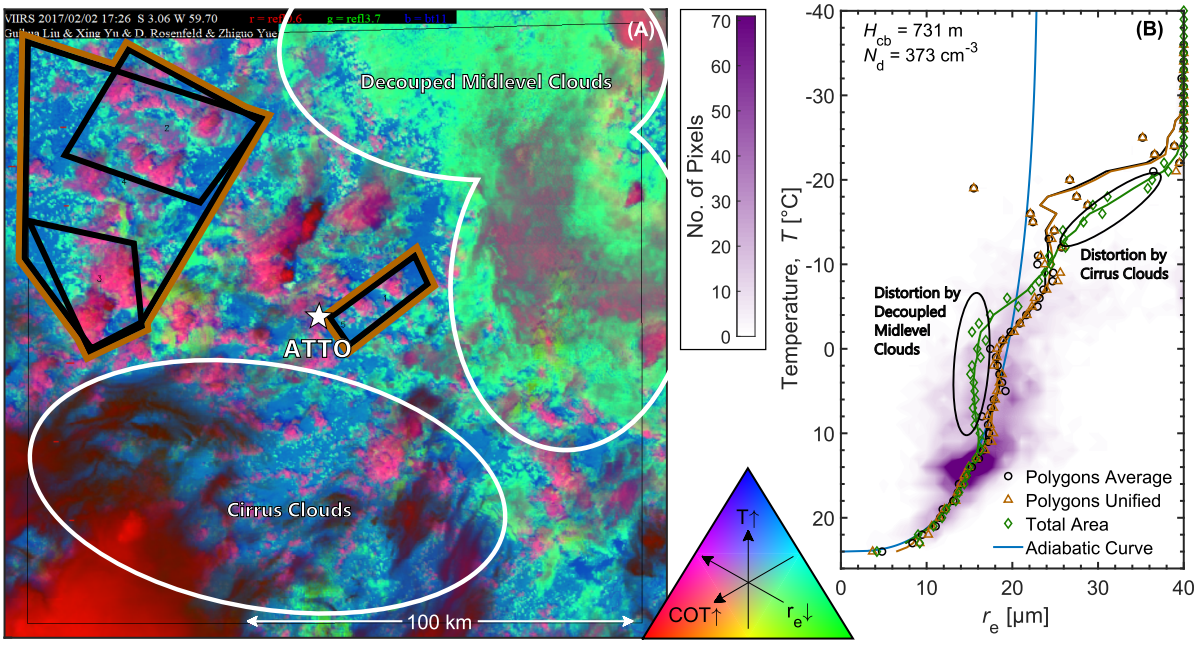


**Figure 6.** Exemplary VIIRS image of the ATTO region with the cloud scenery on 2 February 2017 **(a)** and the corresponding $T$-$r_e$ profiles **(b)**. This example emphasizes the influences of distortions, like mid-level and cirrus clouds, on the $T$-$r_e$ profiles, especially when different regions are considered (averaged polygons vs unified polygons vs total area). For details and layout aspects of this figure, refer to the caption of Fig. 5.

layer, the cloud base height ($H_{cb}$) is calculated based on the temperature difference between the cloud bin that represents the highest temperature (in which 40 % of the pixels passed the cloud mask) and the average surface temperature $T_{sfc}$ at 2 m above ground from reanalysis data (Zheng and Rosenfeld, 2015b), using the boundary layer dry lapse rate of 9.8 K/1000 m (Zheng and Rosenfeld, 2015a), with 130 m accuracy, due to the binning of $T$ to 1 °C. The comparatively low resolution of the NCEP model requires a correction of $H_{cb}$ with the satellite measured surface height. The cloud base temperature, $T_{cb}$, is crucial for the calculation of $N_d$ at cloud base. The inherent uncertainty for the VIIRS $T$ measurement is ±0.2 °C (Tobin et al., 2013), which contributes significantly to the uncertainty in the calculated $N_d$. Likewise the accuracy of the cloud mask in predicting cloud pixels contributes to the uncertainty in $N_d$ Zhu et al. (2014). Assuming adiabatic growth, $N_d$ is calculated by fitting the evolution of $r_e$ with $T$ and comparing it to the corresponding adiabatic liquid water content (LWC), based on $T_{cb}$ and the NCEP reanalysis data, as described by Rosenfeld et al. (2016). The adiabatic LWC is corrected for entrainment effects by an empirical factor of 1/1.3 following Freud et al. (2011). According to Rosenfeld et al. (2016), the uncertainty of the retrieved $N_d$ is within 30 %, which can be regarded as an upper limit. Recent improvements of the method have likely reduced the uncertainty by now. There have been no statistical analysis with aircraft data as a cross reference since the method got updated, therefore

an uncertainty below 30 % can not be quantified yet. Multiple studies reported a systematic overestimation of the satellite-retrieved $r_e$ of ∼20 % (Painemal and Zuidema, 2011; Painemal et al., 2021; Noble and Hudson, 2015), while others did not find such a systematic overestimation (Witte et al., 2018). To account for this widely recognized systematic overestimation the 30$^{th}$ percentile value of all $re$ within the same 1 °C temperature bin are used. The average deviation of $r_e$ found in this studies lie between 5 and 15 %. The $r_e$ at 5 °C above cloud base indicates the adiabatic growth rate after droplet activation. This level of 5 °C is chosen, because of the distance to the cloud base is large enough to sufficiently represent the overall trend for the growth rate, while droplets are still predominantly smaller than 14 µm, even in the wet season, to prevent the influence of starting coalescence (Rosenfeld and Gutman, 1994; Campos Braga et al., 2021b).

**The Amazon Tall Tower Observatory (ATTO)**

The Amazon Tall Tower Observatory has been established in 2011/12 in central Amazonia to explore and monitor fundamental climatic, biogeochemical, and atmospheric parameters over decades (Andreae et al., 2015). The ATTO site (2.146° S, 59.006° W, 130 m above sea level) is located ∼150 km northeast of the city of Manaus, Brazil, in a region with largely untouched primary rain forest. An overview of the atmospheric, geographic, and ecological conditions as well as commonly encountered air masses can be found in Andreae et al. (2015) and Pöhlker et al. (2019). Characteristic aerosol and CCN conditions at ATTO have been described in numerous studies (e.g., Pöhlker et al., 2016, 2018; Saturno et al., 2018; Moran-Zuloaga et al., 2018b; Holanda et al., 2020; Franco et al., 2022).

**Cloud base height and boundary layer height measurements at ATTO**

During 2017 and 2018, the lifting condensation level (LCL) was calculated from temperature and humidity measurements at 60 m height on the 80 m tall walk-up tower at the ATTO site (Andreae et al., 2015). In addition, cloud base height measurements have been conducted at ATTO since 2015 with a CHM 15k-ceilometer, which is a single-wavelength elastic-backscatter lidar, originally sold by Jenoptik AG, Jena, Germany, since 2014 sold by Lufft GmbH, Fellbach, Germany (for details, see e.g. Wiegner and Geiß, 2012; Hervo et al., 2016). Also the average boundary layer height (BLH) from ERA5 reanalysis data (https://www.ecmwf.int/en/forecasts/dataset/ecmwf-reanalysis-v5) for the region 50 km around ATTO is in good agreement with the cloud base height of coupled cumulus clouds.

**Aerosol measurements at ATTO**

Particle number size distributions were measured by a Scanning Mobility Particle Sizer (SMPS, TSI Inc., Shoreview, USA; model 3080 and later model 3082) with a condensation particle counter (CPC, model 3772). The instrument is sampling air from the 60 m inlet on the triangular mast and is located in an air-conditioned laboratory container at the foot of the tower. Sample air was transported through a stainless steel tube (finetron tubes, Dockweiler AG, Neustadt-Glewe, Germany) and dried by an automatic regenerating silica gel adsorption aerosol dryer, as described in Tuch et al. (2009), to a relative humidity (RH)

below 40 %. Values are corrected for standard conditions (Temperature 273.15 K, Pressure 1013.25 hPa and inlet transmission losses following (Von Der Weiden et al., 2009; Moran-Zuloaga et al., 2018a). The SMPS measurements cover a particle diameter range from 10 to 400 nm. Frequent size accuracy tests were performed by using monodisperse polystyrene latex particles, and the data quality was continuously verified by complementary measurements by another condensation particle counter (CPC) running in parallel. Data were acquired and exported with the Aerosol Instrument Manager Software (AIM, Version 9 & 10, TSI Inc.) and corrected for standard temperature and pressure (STP, 273.15 K, 1013.25 hPa) as well as for inlet transmission losses following the approach as described in von der Weiden et al. (2009) and Moran-Zuloaga et al. (2018b). Further, the data were checked by visual inspection for instrument malfunction events. The acquired particle size distributions were fitted by a multi-modal log-normal distribution function developed by Franco et al. (2022) to determine the Aitken and accumulation mode number concentrations. Accordingly, the Aitken mode ($N_{\mathrm{ait}}$) is defined as particles with diameters of 50 nm $< D <$ 100 nm and the accumulation mode ($N_{\mathrm{acc}}$) as particles with diameters of 100 nm $< D <$ 400 nm. The total particle concentration ($N_{\mathrm{CN}}$) here is the integral of the entire SMPS size range (i.e., 10 to 400 nm). The black carbon mass concentration ($M_{\mathrm{BC}}$) was obtained through measurements of the aerosol light absorption coefficient at a wavelength of 637 nm by a multi-angle absorption photometer, (MAAP, model 5012, Thermo Electron Group, Waltham, USA), assuming a mass absorption cross section of 6.6 $\mathrm{m^2\,g^{-1}}$ (for details, refer to Saturno et al., 2018).

**Selection and preparation of ground and satellite data**

Only ATTO ground data between 16:00 and 17:30 UTC (12:00 and 13:30 local time), which is right before and during the satellite overpass (between 17:10 and 17:45 UTC), were considered and averaged for this analysis. This represents the closest approximation of the aerosol population that had served as CCN for the cloud(s) recorded in the VIIRS images. Both, aerosol and cloud data, can vary greatly on the scale of hours. They also do not necessarily follow the same trend, as environmental influences can affect both parameters independently. Therefore, all ATTO time series were pre-processed with a 5-point moving average to filter out most of the short-term variability to emphasize the characteristic seasonal conditions and trends. The floating 5-point average has been found in the course of an iterative evaluation process as the best compromise between noise reduction and preservation of details.

*Code and data availability.* The data of the key results presented here have been deposited in supplementary data files for use in follow-up studies. The ATTO data used in this study are available via the ATTO data portal through https://www.attoproject.org/. For data requests beyond the available data, please refer to the corresponding authors. The software code for the present analysis can be found under [link].

*Author contributions.* MLP designed the study. MLP, DR, and CP led the analyses and the manuscript preparation. The satellite data analysis and synthesis with the ATTO data was done by OL. DR, YZ, AE and YZ contributed to the developed of the VIIRS analysis approach and support the analysis. The aerosol measurements at ATTO along with the data analysis was conducted by LAK, MAF, BAH, OOK, FD, LATM, ACA and CP. OL, MLP, and CP wrote the paper. All authors contributed to the discussion of the results as well as the finalization of the manuscript.

*Competing interests.* The authors declare that they have no conflict of interest.

*Disclaimer.* This paper contains results of research conducted under the Technical/Scientific Cooperation Agreement between the National Institute for Amazonian Research, the State University of Amazonas, and the Max-Planck-Gesellschaft e.V.; the opinions expressed are the entire responsibility of the authors and not of the participating institutions.

*Acknowledgements.* This research has been supported by the Max Planck Society, the Max Planck Graduate Center with the Johannes Gutenberg University Mainz (MPGC), the Bundesministerium für Bildung und Forschung (BMBF contracts 01LB1001A, 01LK1602B, and 01LK2101B), the Brazilian Ministério da Ciência, Tecnologia e Inovação (MCTI/FINEP contract 01.11.01248.00), the Conselho Nacional de Desenvolvimento Científico e Tecnológico (CNPq, Brazil) (process 200723/2015-4), the FAPESP (Fundação de Amparo à Pesquisa do Estado de São Paulo) (grant no. 2017/17047-0), the CNPq project (grant no. 169842/2017-7), the CAPES project (grant no. 88887.368025/2019-00), and the European Commission, H2020 Research Infrastructures (A-LIFE (grant no. 640458)). For the operation of the ATTO site, we acknowledge the support by the Max Planck Society, the German Federal Ministry of Education and Research and the Brazilian Ministério da Ciência, Tecnologia e Inovação as well as the Amazon State University (UEA), FAPEAM, LBA/INPA, and SDS/CEUC/RDS-Uatumã. We would like to especially thank all the people involved in the technical, logistical, and scientific support of the ATTO project.

**References**

Adler, G., Flores, J. M., Abo Riziq, A., Borrmann, S., and Rudich, Y.: Chemical, physical, and optical evolution of biomass burning aerosols: A case study, Atmospheric Chemistry and Physics, 11, 1491–1503, 2011.

Albrecht, B. A.: Aerosols, Cloud Microphysics, and Fractional Cloudiness, Science, 245, 1227–1230, 1989.

Andreae, M. and Rosenfeld, D.: Aerosol–cloud–precipitation interactions. Part 1. The nature and sources of cloud-active aerosols, Earth-Science Reviews, 89, 13–41, 2008.

Andreae, M. O.: Aerosols Before Pollution, Science, 315, 50–51, 2007.

Andreae, M. O.: Correlation between cloud condensation nuclei concentration and aerosol optical thickness in remote and polluted regions, Atmospheric Chemistry and Physics, 2009.

Andreae, M. O., Rosenfeld, D., Artaxo, P., Costa, A. A., Frank, G. P., Longo, K. M., Silva-Dias, M. A. F., MO, A., D, R., P, A., AA, C., GP, F., KM, L., MA, S.-D., Andreae, M. O., Rosenfeld, D., Artaxo, P., Costa, A. A., Frank, G. P., Longo, K. M., and Silva-Dias, M. A. F.: Smoking Rain Clouds over the Amazon, Science, 303, 1337–1342, 2004.

Andreae, M. O., Acevedo, O. C., Araùjo, A., Artaxo, P., Barbosa, C. G. G., Barbosa, H. M. J., Brito, J., Carbone, S., Chi, X., Cintra, B. B. L., da Silva, N. F., Dias, N. L., Dias-Júnior, C. Q., Ditas, F., Ditz, R., Godoi, A. F. L., Godoi, R. H. M., Heimann, M., Hoffmann, T., Kesselmeier, J., Könemann, T., Krüger, M. L., Lavric, J. V., Manzi, A. O., Lopes, A. P., Martins, D. L., Mikhailov, E. F., Moran-Zuloaga, D., Nelson, B. W., Nölscher, A. C., Santos Nogueira, D., Piedade, M. T. F., Pöhlker, C., Pöschl, U., Quesada, C. A., Rizzo, L. V., Ro, C.-U., Ruckteschler, N., Sá, L. D. A., de Oliveira Sá, M., Sales, C. B., dos Santos, R. M. N., Saturno, J., Schöngart, J., Sörgel, M., de Souza, C. M., de Souza, R. A. F., Su, H., Targhetta, N., Tóta, J., Trebs, I., Trumbore, S., van Eijck, A., Walter, D., Wang, Z., Weber, B., Williams, J., Winderlich, J., Wittmann, F., Wolff, S., and Yáñez Serrano, A. M.: The Amazon Tall Tower Observatory (ATTO): overview of pilot measurements on ecosystem ecology, meteorology, trace gases, and aerosols, Atmospheric Chemistry and Physics, 15, 10 723–10 776, 2015.

Andreae, M. O., Andreae, T. W., and Ditas, F.: Frequent new particle formation at remote sites in the temperate/boreal forest of North America, Atmospheric Chemistry and Physics Discussions, 2021, 1–30, 2021.

Anttila, T., Brus, D., Jaatinen, A., Hyvärinen, A.-P., Kivekäs, N., Romakkaniemi, S., Komppula, M., and Lihavainen, H.: Relationships between particles, cloud condensation nuclei and cloud droplet activation during the third Pallas Cloud Experiment, Atmospheric Chemistry and Physics, 12, 11 435–11 450, 2012.

Arakawa, A. and Schubert, W. H.: Interaction of a Cumulus Cloud Ensemble with the Large-Scale Environment, Part I, Journal of Atmospheric Sciences, 31, 674 – 701, 1974.

Artaxo, P., Martins, J. V., Yamasoe, M. A., Procópio, A. S., Pauliquevis, T. M., Andreae, M. O., Guyon, P., Gatti, L. V., and Leal, A. M. C.: Physical and chemical properties of aerosols in the wet and dry seasons in Rondônia, Amazonia, Journal of Geophysical Research: Atmospheres, 107, LBA 49–1–LBA 49–14, 2002.

Artaxo, P., Rizzo, L. V., Brito, J. F., Barbosa, H. M. J., Arana, A., Sena, E. T., Cirino, G. G., Bastos, W., Martin, S. T., and Andreae, M. O.: Atmospheric aerosols in Amazonia and land use change: from natural biogenic to biomass burning conditions, Faraday Discussions, 165, 203–235, 2013.

Braga, R. C., Rosenfeld, D., Weigel, R., Jurkat, T., Andreae, M., Wendisch, M., Pöhlker, M., Klimach, T., Pöschl, U., Pöhlker, C., Voigt, C., Mahnke, C., Borrmann, S., Albrecht, R., Molleker, S., Vila, D., Machado, L., and Artaxo, P.: Comparing calculated microphysical

properties of tropical convective clouds at cloud base with measurements during the ACRIDICON-CHUVA campaign, Atmospheric Chemistry and Physics Discussions, pp. 1–46, 2016.

Braga, R. C., Rosenfeld, D., Weigel, R., Jurkat, T., Andreae, M. O., Wendisch, M., Pöschl, U., Voigt, C., Mahnke, C., Borrmann, S., Albrecht, R. I., Molleker, S., Vila, D. A., Machado, L. A. T., and Grulich, L.: Further evidence for CCN aerosol concentrations determining the height of warm rain and ice initiation in convective clouds over the Amazon basin, Atmos. Chem. Phys., 17, 14 433–14 456, 2017.

Brito, J., Rizzo, L. V., Morgan, W. T., Coe, H., Johnson, B., Haywood, J., Longo, K., Freitas, S., Andreae, M. O., and Artaxo, P.: Ground-based aerosol characterization during the South American Biomass Burning Analysis (SAMBBA) field experiment, Atmospheric Chemistry and Physics, 14, 12 069–12 083, 2014.

Campos Braga, R., Ervens, B., Rosenfeld, D., Andreae, M. O., Förster, J.-D., Fütterer, D., Hernández Pardo, L., Holanda, B. A., Jurkat, T., Krüger, O. O., Lauer, O., Machado, L. A. T., Pöhlker, C., Sauer, D., Voigt, C., Walser, A., Wendisch, M., Pöschl, U., and Pöhlker, M. L.: Cloud droplet number closure for tropical convective clouds during the ACRIDICON–CHUVA campaign, Atmospheric Chemistry and Physics Discussions, 2021, 1–17, 2021a.

Campos Braga, R., Ervens, B., Rosenfeld, D., Andreae, M. O., Förster, J.-D., Fütterer, D., Hernández Pardo, L., Holanda, B. A., Jurkat, T., Krüger, O. O., Lauer, O., Machado, L. A. T., Pöhlker, C., Sauer, D., Voigt, C., Walser, A., Wendisch, M., Pöschl, U., and Pöhlker, M. L.: Cloud droplet number closure for tropical convective clouds during the ACRIDICON–CHUVA campaign, Atmospheric Chemistry and Physics Discussions, 2021, 1–17, 2021b.

Carslaw, K. S., Lee, L. A., Reddington, C. L., Pringle, K. J., Rap, A., Forster, P. M., Mann, G. W., Spracklen, D. V., Woodhouse, M. T., Regayre, L. A., and Pierce, J. R.: Large contribution of natural aerosols to uncertainty in indirect forcing, Nature, 2013.

Dias-Júnior, C. Q., Carneiro, R. G., Fisch, G., D'Oliveira, F. A. F., Sörgel, M., Botía, S., Machado, L. A. T., Wolff, S., Santos, R. M. N. d., and Pöhlker, C.: Intercomparison of Planetary Boundary Layer Heights Using Remote Sensing Retrievals and ERA5 Reanalysis over Central Amazonia, Remote Sensing, 14, 2022.

Dusek, U., Frank, G. P., Hildebrandt, L., Curtius, J., Schneider, J., Walter, S., Chand, D., Drewnick, F., Hings, S., Jung, D., Borrmann, S., and Andreae, M. O.: Size Matters More Than Chemistry for Cloud-Nucleating Ability of Aerosol Particles, Science, 312, 1375–1378, 2006.

Efraim, A., Lauer, O., Rosenfeld, D., Campos Braga, R., Kremper, L. A., M., F., Pöschl, U., Y., Z., Pöhlker, C., and Pöhlker, M. L.: Satellite detection of secondary drop activation aloft in deep convective clouds with warm rain, in prep., 2021.

Fan, J., Wang, Y., Rosenfeld, D., and Liu, X.: Review of Aerosol–Cloud Interactions: Mechanisms, Significance, and Challenges, Journal of the Atmospheric Sciences, 73, 4221 – 4252, 2016.

Feingold, G.: On smoke suppression of clouds in Amazonia, Geophysical Research Letters, 32, L02 804, 2005.

Fisch, G., Tota, J., Machado, L. A. T., Dias, M., Lyra, R. F. D., Nobre, C. A., Dolman, A. J., and Gash, J. H. C.: The convective boundary layer over pasture and forest in Amazonia, Theoretical and Applied Climatology, 78, 47–59, 2004.

Forster, P., Storelvmo, T., Armour, K., Collins, W., Dufresne, J.-L., Frame, D., Lunt, D., Mauritsen, T., Palmer, M., Watanabe, M., Wild, M., and Zhang, H.: The Earth's Energy Budget, Climate Feedbacks, and Climate Sensitivity, in: Climate Change 2021: The Physical Science Basis. Contribution of Working Group I to the Sixth Assessment Report of the Intergovernmental Panel on Climate Change, edited by Masson-Delmotte, V., Zhai, P., Pirani, A., Connors, S., Péan, C., Berger, S., Caud, N., Chen, Y., Goldfarb, L., Gomis, M., Huang, M., Leitzell, K., Lonnoy, E., Matthews, J., Maycock, T., Waterfield, T., Yelekçi, O., Yu, R., and Zhou, B., chap. 7, 2021.

Franco, M. A., Ditas, F., Kremper, L. A., Machado, L. A. T., Andreae, M. O., Araújo, A., Barbosa, H. M. J., de Brito, J. F., Carbone, S., Holanda, B. A., Morais, F. G., Nascimento, J. P., Pöhlker, M. L., Rizzo, L. V., Sá, M., Saturno, J., Walter, D., Wolff, S., Pöschl, U., Artaxo,

P., and Pöhlker, C.: Occurrence and growth of sub-50 nm aerosol particles in the Amazonian boundary layer, Atmospheric Chemistry and Physics, 22, 3469–3492, 2022.

Freud, E., Rosenfeld, D., Andreae, M. O., Costa, A. A., and Artaxo, P.: Robust relations between CCN and the vertical evolution of cloud drop size distribution in deep convective clouds, Atmospheric Chemistry and Physics, 8, 1661–1675, 2008.

Freud, E., Rosenfeld, D., and Kulkarni, J. R.: Resolving both entrainment-mixing and number of activated CCN in deep convective clouds, Atmospheric Chemistry and Physics, 11, 12 887–12 890, 2011.

Gong, X., Wex, H., Voigtländer, J., Fomba, K. W., Weinhold, K., van Pinxteren, M., Henning, S., Müller, T., Herrmann, H., and Stratmann, F.: Characterization of aerosol particles at Cabo Verde close to sea level and at the cloud level – Part 1: Particle number size distribution, cloud condensation nuclei and their origins, Atmospheric Chemistry and Physics, 20, 1431–1449, 2020.

Graham, B., Guyon, P., Maenhaut, W., Taylor, P. E., Ebert, M., Matthias-Maser, S., Mayol-Bracero, O. L., Godoi, R. H. M., Artaxo, P., Meixner, F. X., Moura, M. A. L., Rocha, C., Van Grieken, R., Glovsky, M. M., Flagan, R. C., and Andreae, M. O.: Composition and diurnal variability of the natural Amazonian aerosol, Journal of Geophysical Research-Atmospheres, 108, 4765, 2003.

Hamilton, D. S., Lee, L. A., Pringle, K. J., Reddington, C. L., Spracklen, D. V., and Carslaw, K. S.: Occurrence of pristine aerosol environments on a polluted planet, Proceedings of the National Academy of Sciences, 111, 18 466–18 471, 2014.

Henkes, A., Fisch, G., Machado, L. A. T., and Chaboureau, J.-P.: Morning boundary layer conditions for shallow to deep convective cloud evolution during the dry season in the central Amazon, Atmospheric Chemistry and Physics, 21, 13 207–13 225, 2021.

Hervo, M., Poltera, Y., and Haefele, A.: An empirical method to correct for temperature-dependent variations in the overlap function of CHM15k ceilometers, Atmospheric Measurement Techniques, 9, 2947–2959, 2016.

Hillger, D., Kopp, T., Lee, T., Lindsey, D., Seaman, C., Miller, S., Solbrig, J., Kidder, S., Bachmeier, S., Jasmin, T., and Rink, T.: First-Light Imagery from Suomi NPP VIIRS, Bulletin of the American Meteorological Society, 94, 1019 – 1029, 2013.

Hillger, D., Seaman, C., Liang, C., Miller, S., Lindsey, D., and Kopp, T.: Suomi NPP VIIRS imagery evaluation, Journal of Geophysical Research, 119, 6440–6455, 2014.

Holanda, B. A., Pöhlker, M. L., Walter, D., Saturno, J., Sörgel, M., Ditas, J., Ditas, F., Schulz, C., Franco, M. A., Wang, Q., Donth, T., Artaxo, P., Barbosa, H. M. J., Borrmann, S., Braga, R., Brito, J., Cheng, Y., Dollner, M., Kaiser, J. W., Klimach, T., Knote, C., Krüger, O. O., Fütterer, D., Lavrič, J. V., Ma, N., Machado, L. A. T., Ming, J., Morais, F. G., Paulsen, H., Sauer, D., Schlager, H., Schneider, J., Su, H., Weinzierl, B., Walser, A., Wendisch, M., Ziereis, H., Zöger, M., Pöschl, U., Andreae, M. O., and Pöhlker, C.: Influx of African biomass burning aerosol during the Amazonian dry season through layered transatlantic transport of black carbon-rich smoke, Atmospheric Chemistry and Physics, 20, 4757–4785, 2020.

Howell, W. E.: THE GROWTH OF CLOUD DROPS IN UNIFORMLY COOLED AIR, Journal of Atmospheric Sciences, 6, 134 – 149, 1949.

Kacarab, M., Thornhill, K. L., Dobracki, A., Howell, S. G., O'Brien, J. R., Freitag, S., Poellot, M. R., Wood, R., Zuidema, P., Redemann, J., and Nenes, A.: Biomass burning aerosol as a modulator of the droplet number in the southeast Atlantic region, Atmospheric Chemistry and Physics, 20, 3029–3040, 2020.

Kaufman, Y. J. and Nakajima, T.: Effect of Amazon Smoke on Cloud Microphysics and Albedo-Analysis from Satellite Imagery, Journal of Applied Meteorology and Climatology, 32, 729 – 744, 1993.

Köhler, H.: The nucleus in and the growth of hygroscopic droplets, Transactions of the Faraday Society, 1936.

Lensky, I. M. and Rosenfeld, D.: The time-space exchangeability of satellite retrieved relations between cloud top temperature and particle effective radius, Atmos. Chem. Phys., 2006.

Lensky, I. M. and Rosenfeld, D.: Clouds-Aerosols-Precipitation Satellite Analysis Tool (CAPSAT), Atmospheric Chemistry and Physics, 8, 6739–6753, 2008.

Lin, J. C., Matsui, T., Pielke, R. A., and Kummerow, C.: Effects of biomass-burning-derived aerosols on precipitation and clouds in the Amazon Basin: a satellite-based empirical study, Journal of Geophysical Research, 111, D19 204, 2006.

Machado, L. A. T., Franco, M. A., Kremper, L. A., Ditas, F., Andreae, M. O., Artaxo, P., Cecchini, M. A., Holanda, B. A., Pöhlker, M. L., Saraiva, I., Wolff, S., Pöschl, U., and Pöhlker, C.: How weather events modify aerosol particle size distributions in the Amazon boundary layer, Atmospheric Chemistry and Physics, 21, 18 065–18 086, 2021.

Martin, G. M., Johnson, D. W., and Spice, A.: The Measurement and Parameterization of Effective Radius of Droplets in Warm Stratocumulus Clouds, Journal of Atmospheric Sciences, 51, 1823 – 1842, 1994.

Martin, S. T., Andreae, M. O., Artaxo, P., Baumgardner, D., Chen, Q., Goldstein, A. H., Guenther, A., Heald, C. L., Mayol-Bracero, O. L., McMurry, P. H., Pauliquevis, T., Poschl, U., Prather, K. A., Roberts, G. C., Saleska, S. R., Dias, M. A. S., Spracklen, D. V., Swietlicki, E., and Trebs, I.: Sources and properties of Amazonian aerosol particles, Reviews of Geophysics, 48, RG2002, 2010.

Martin, S. T., Artaxo, P., Machado, L., Manzi, A. O., Souza, R. A. F., Schumacher, C., Wang, J., Biscaro, T., Brito, J., Calheiros, A., Jardine, K., Medeiros, A., Portela, B., de Sá, S. S., Adachi, K., Aiken, A. C., Albrecht, R., Alexander, L., Andreae, M. O., Barbosa, H. M. J., Buseck, P., Chand, D., Comstock, J. M., Day, D. A., Dubey, M., Fan, J., Fast, J., Fisch, G., Fortner, E., Giangrande, S., Gilles, M., Goldstein, A. H., Guenther, A., Hubbe, J., Jensen, M., Jimenez, J. L., Keutsch, F. N., Kim, S., Kuang, C., Laskin, A., McKinney, K., Mei, F., Miller, M., Nascimento, R., Pauliquevis, T., Pekour, M., Peres, J., Petäjä, T., Pöhlker, C., Pöschl, U., Rizzo, L., Schmid, B., Shilling, J. E., Dias, M. A. S., Smith, J. N., Tomlinson, J. M., Tóta, J., and Wendisch, M.: The Green Ocean Amazon Experiment (GoAmazon2014/5) Observes Pollution Affecting Gases, Aerosols, Clouds, and Rainfall over the Rain Forest, Bulletin of the American Meteorological Society, 98, 981 – 997, 2016.

Martins, J. V., Marshak, A., Remer, L. A., Rosenfeld, D., Kaufman, Y. J., Fernandez-Borda, R., Koren, I., Correia, A. L., Zubko, V., and Artaxo, P.: Remote sensing the vertical profile of cloud droplet effective radius, thermodynamic phase, and temperature, Atmospheric Chemistry and Physics, 11, 9485–9501, 2011.

Moran-Zuloaga, D., Ditas, F., Walter, D., Saturno, J., Brito, J., Carbone, S., Chi, X., Hrabě de Angelis, I., Baars, H., Godoi, R. H. M., Heese, B., Holanda, B. A., Lavrič, J. V., Martin, S. T., Ming, J., Pöhlker, M. L., Ruckteschler, N., Su, H., Wang, Y., Wang, Q., Wang, Z., Weber, B., Wolff, S., Artaxo, P., Pöschl, U., Andreae, M. O., and Pöhlker, C.: Long-term study on coarse mode aerosols in the Amazon rain forest with the frequent intrusion of Saharan dust plumes, Atmospheric Chemistry and Physics, 18, 10 055–10 088, 2018a.

Moran-Zuloaga, D., Ditas, F., Walter, D., Saturno, J., Brito, J., Carbone, S., Chi, X., Hrabě de Angelis, I., Baars, H., Godoi, R. H. M., Heese, B., Holanda, B. A., Lavrič, J. V., Martin, S. T., Ming, J., Pöhlker, M. L., Ruckteschler, N., Su, H., Wang, Y., Wang, Q., Wang, Z., Weber, B., Wolff, S., Artaxo, P., Pöschl, U., Andreae, M. O., and Pöhlker, C.: Long-term study on coarse mode aerosols in the Amazon rain forest with the frequent intrusion of Saharan dust plumes, Atmospheric Chemistry and Physics, 18, 10 055–10 088, 2018b.

Mülmenstädt, J. and Feingold, G.: The radiative forcing of aerosol–cloud interactions in liquid clouds: Wrestling and embracing uncertainty, Curr. Clim. Change Rep., 4, 23–40, 2018.

Noble, S. R. and Hudson, J. G.: MODIS comparisons with northeastern Pacific in situ stratocumulus microphysics, Journal of Geophysical Research. Atmospheres, 120, 8332, 2015.

Painemal, D. and Zuidema, P.: Assessment of MODIS cloud effective radius and optical thickness retrievals over the Southeast Pacific with VOCALS-REx in situ measurements, Journal of Geophysical Research Atmospheres, 116, 2011.

Painemal, D., Spangenberg, D., Smith, W. L., Minnis, P., Cairns, B., Moore, R. H., Crosbie, E., Robinson, C., Thornhill, K. L., Winstead, E. L., and Ziemba, L.: Evaluation of satellite retrievals of liquid clouds from the GOES-13 imager and MODIS over the midlatitude North Atlantic during the NAAMES campaign, Atmos. Meas. Tech, 14, 1–14, 2021.

Pöhlker, C., Walter, D., Paulsen, H., Könemann, T., Rodríguez-Caballero, E., Moran-Zuloaga, D., Brito, J., Carbone, S., Degrendele, C., Després, V. R., Ditas, F., Holanda, B. A., Kaiser, J. W., Lammel, G., Lavrič, J. V., Ming, J., Pickersgill, D., Pöhlker, M. L., Praß, M., Löbs, N., Saturno, J., Sörgel, M., Wang, Q., Weber, B., Wolff, S., Artaxo, P., Pöschl, U., and Andreae, M. O.: Land cover and its transformation in the backward trajectory footprint region of the Amazon Tall Tower Observatory, Atmospheric Chemistry and Physics, 19, 8425–8470, 2019.

Pöhlker, M. L., Zhang, M., Campos Braga, R., Krüger, O. O., Pöschl, U., and Ervens, B.: Aitken mode particles as CCN in aerosol- and updraft-sensitive regimes of cloud droplet formation, Atmospheric Chemistry and Physics, 21, 11 723–11 740, 2021.

Pöschl, U., Martin, S. T., Sinha, B., Chen, Q., Gunthe, S. S., Huffman, J. A., Borrmann, S., Farmer, D. K., Garland, R. M., Helas, G., Jimenez, J. L., King, S. M., Manzi, A., Mikhailov, E., Pauliquevis, T., Petters, M. D., Prenni, A. J., Roldin, P., Rose, D., Schneider, J., Su, H., Zorn, S. R., Artaxo, P., and Andreae, M. O.: Rainforest Aerosols as Biogenic Nuclei of Clouds and Precipitation in the Amazon, Science, 329, 1513–1516, 2010.

Prass, M., Andreae, M. O., de Araùjo, A. C., Artaxo, P., Ditas, F., Elbert, W., Förster, J.-D., Franco, M. A., Hrabe de Angelis, I., Kesselmeier, J., Klimach, T., Kremper, L. A., Thines, E., Walter, D., Weber, J., Weber, B., Fuchs, B. M., Pöschl, U., and Pöhlker, C.: Bioaerosols in the Amazon rain forest: temporal variations and vertical profiles of Eukarya, Bacteria, and Archaea, Biogeosciences, 18, 4873–4887, 2021.

Pringle, K. J., Carslaw, K. S., Spracklen, D. V., Mann, G. M., and Chipperfield, M. P.: The relationship between aerosol and cloud drop number concentrations in a global aerosol microphysics model, Atmospheric Chemistry and Physics, 9, 4131–4144, 2009.

Pöhlker, M. L., Pöhlker, C., Ditas, F., Klimach, T., Hrabe de Angelis, I., Araújo, A., Brito, J., Carbone, S., Cheng, Y., Chi, X., Ditz, R., Gunthe, S. S., Kesselmeier, J., Könemann, T., Lavrič, J. V., Martin, S. T., Mikhailov, E., Moran-Zuloaga, D., Rose, D., Saturno, J., Su, H., Thalman, R., Walter, D., Wang, J., Wolff, S., Barbosa, H. M. J., Artaxo, P., Andreae, M. O., and Pöschl, U.: Long-term observations of cloud condensation nuclei in the Amazon rain forest – Part 1: Aerosol size distribution, hygroscopicity, and new model parametrizations for CCN prediction, Atmos. Chem. Phys., 2016.

Pöhlker, M. L., Ditas, F., Saturno, J., Klimach, T., Hrabě de Angelis, I., Araùjo, A. C., Brito, J., Carbone, S., Cheng, Y., Chi, X., Ditz, R., Gunthe, S. S., Holanda, B. A., Kandler, K., Kesselmeier, J., Könemann, T., Krüger, O. O., Lavrič, J. V., Martin, S. T., Mikhailov, E., Moran-Zuloaga, D., Rizzo, L. V., Rose, D., Su, H., Thalman, R., Walter, D., Wang, J., Wolff, S., Barbosa, H. M. J., Artaxo, P., Andreae, M. O., Pöschl, U., and Pöhlker, C.: Long-term observations of cloud condensation nuclei over the Amazon rain forest – Part 2: Variability and characteristics of biomass burning, long-range transport, and pristine rain forest aerosols, Atmos. Chem. Phys., 2018.

Quaas, J.: Approaches to observe anthropogenic aerosol-cloud interactions, Current climate change reports, 2015.

Quaas, J., Arola, A., Cairns, B., Christensen, M., Deneke, H., Ekman, A. M. L., Feingold, G., Fridlind, A., Gryspeerdt, E., Hasekamp, O., Li, Z., Lipponen, A., Ma, P.-L., Mülmenstädt, J., Nenes, A., Penner, J. E., Rosenfeld, D., Schrödner, R., Sinclair, K., Sourdeval, O., Stier, P., Tesche, M., van Diedenhoven, B., and Wendisch, M.: Constraining the Twomey effect from satellite observations: issues and perspectives, Atmospheric Chemistry and Physics, 20, 15 079–15 099, 2020.

Quinn, P. K., Collins, D. B., Grassian, V. H., Prather, K. A., and Bates, T. S.: Chemistry and Related Properties of Freshly Emitted Sea Spray Aerosol, Chemical Reviews, 115, 4383–4399, pMID: 25844487, 2015.

Raga, G. B. and Jonas, P. R.: On the link between cloud-top radiative properties and sub-cloud aerosol concentrations, Quarterly Journal of the Royal Meteorological Society, 119, 1419–1425, 1993.

Ramanathan, V., Crutzen, P. J., Kiehl, J. T., and Rosenfeld, D.: Aerosols, Climate, and the Hydrological Cycle, Science, 294, 2119–2124, 2001.

Reutter, P., Su, H., Trentmann, J., Simmel, M., Rose, D., Gunthe, S. S., Wernli, H., Andreae, M. O., and Pöschl, U.: Aerosol- and updraft-limited regimes of cloud droplet formation: influence of particle number, size and hygroscopicity on the activation of cloud condensation nuclei (CCN), Atmospheric Chemistry and Physics, 9, 7067–7080, 2009.

Rizzo, L. V., Artaxo, P., Müller, T., Wiedensohler, A., Paixão, M., Cirino, G. G., Arana, A., Swietlicki, E., Roldin, P., Fors, E. O., Wiedemann, K. T., Leal, L. S. M., and Kulmala, M.: Long term measurements of aerosol optical properties at a primary forest site in Amazonia, Atmospheric Chemistry and Physics, 13, 2391–2413, 2013.

Roberts, G. C., Andreae, M. O., Zhou, J., and Artaxo, P.: Cloud condensation nuclei in the Amazon Basin: "marine" conditions over a continent?, Geophysical Research Letters, 28, 2807–2810, 2001.

Rosenfeld, D. and Gutman, G.: Retrieving microphysical properties near the tops of potential rain clouds by multispectral analysis of AVHRR data, Atmospheric Research, 34, 259–283, 11th conference on clouds and precipitation, 1994.

Rosenfeld, D., Lohmann, U., Raga, G. B., O'Dowd, C. D., Kulmala, M., Fuzzi, S., Reissell, A., and Andreae, M. O.: Flood or drought: How do aerosols affect precipitation?, Science, 321, 1309–1313, 2008.

Rosenfeld, D., Andreae, M. O., Asmi, A., Chin, M., de Leeuw, G., Donovan, D. P., Kahn, R., Kinne, S., Kivekäs, N., Kulmala, M., Lau, W., Schmidt, K. S., Suni, T., Wagner, T., Wild, M., and Quaas, J.: Global observations of aerosol-cloud-precipitation-climate interactions, Reviews of Geophysics, 52, 750–808, 2014a.

Rosenfeld, D., Liu, G., Yu, X., Zhu, Y., Dai, J., Xu, X., and Yue, Z.: High-resolution (375 m) cloud microstructure as seen from the NPP/VIIRS satellite imager, Atmos. Chem. Phys., 2014b.

Rosenfeld, D., Sherwood, S., Wood, R., and Donner, L.: Climate Effects of Aerosol-Cloud Interactions, Science, 343, 379–380, 2014c.

Rosenfeld, D., Zheng, Y., Hashimshoni, E., Pöhlker, M. L., Jefferson, A., Pöhlker, C., Yu, X., Zhu, Y., Liu, G., Yue, Z., Fischman, B., Li, Z., Giguzin, D., Goren, T., Artaxo, P., Barbosa, H. M. J., Pöschl, U., and Andreae, M. O.: Satellite retrieval of cloud condensation nuclei concentrations by using clouds as CCN chambers, Proceedings of the National Academy of Sciences, 2016.

Rotstayn, L. D.: Indirect forcing by anthropogenic aerosols: A global climate model calculation of the effective-radius and cloud-lifetime effects, Journal of Geophysical Research: Atmospheres, 104, 9369–9380, 1999.

Saturno, J., Holanda, B. A., Pöhlker, C., Ditas, F., Wang, Q., Moran-Zuloaga, D., Brito, J., Carbone, S., Cheng, Y., Chi, X., Ditas, J., Hoffmann, T., Hrabe de Angelis, I., Könemann, T., Lavrič, J. V., Ma, N., Ming, J., Paulsen, H., Pöhlker, M. L., Rizzo, L. V., Schlag, P., Su, H., Walter, D., Wolff, S., Zhang, Y., Artaxo, P., Pöschl, U., and Andreae, M. O.: Black and brown carbon over central Amazonia: long-term aerosol measurements at the ATTO site, Atmospheric Chemistry and Physics, 18, 12 817–12 843, 2018.

Stevens, B. and Feingold, G.: Untangling aerosol effects on clouds and precipitation in a buffered system, NATURE, 461, 607–613, 2009.

Tobin, D., Revercomb, H., Knuteson, R., Taylor, J., Best, F., Borg, L., Deslover, D., Martin, G., Buijs, H., Esplin, M., Glumb, R., Han, Y., Mooney, D., Predina, J., Strow, L., Suwinski, L., and Wang, L.: Suomi-NPP CrIS radiometric calibration uncertainty, Journal of Geophysical Research: Atmospheres, 118, 10,589–10,600, 2013.

Tuch, T. M., Haudek, A., Müller, T., Nowak, A., Wex, H., and Wiedensohler, A.: Design and performance of an automatic regenerating adsorption aerosol dryer for continuous operation at monitoring sites, Atmospheric Measurement Techniques, 2, 417–422, 2009.

Twomey, S.: The Influence of Pollution on the Shortwave Albedo of Clouds, Journal of Atmospheric Sciences, 34, 1149–1152, 1977.

Varanda Rizzo, L., Roldin, P., Brito, J., Backman, J., Swietlicki, E., Krejci, R., Tunved, P., Petäjä, T., Kulmala, M., and Artaxo, P.: Multi-year statistical and modeling analysis of submicrometer aerosol number size distributions at a rain forest site in Amazonia, Atmospheric Chemistry and Physics, 18, 10 255–10 274, 2018.

Von Der Weiden, S. L., Drewnick, F., and Borrmann, S.: Particle Loss Calculator – a new software tool for the assessment of the performance of aerosol inlet systems, Atmospheric Measurement Techniques, 2, 479–494, 2009.

von der Weiden, S.-L., Drewnick, F., and Borrmann, S.: Particle Loss Calculator – a new software tool for the assessment of the performance of aerosol inlet systems, Atmospheric Measurement Techniques, 2, 479–494, 2009.

Wex, H., Dieckmann, K., Roberts, G. C., Conrath, T., Izaguirre, M. A., Hartmann, S., Herenz, P., Schäfer, M., Ditas, F., Schmeissner, T., Henning, S., Wehner, B., Siebert, H., and Stratmann, F.: Aerosol arriving on the Caribbean island of Barbados: physical properties and origin, Atmospheric Chemistry and Physics, 16, 14 107–14 130, 2016.

Wiegner, M. and Geiß, A.: Aerosol profiling with the Jenoptik ceilometer CHM15kx, Atmospheric Measurement Techniques, 5, 1953–1964, 2012.

Williams, E., Rosenfeld, D., Madden, N., Gerlach, J., Gears, N., Atkinson, L., Dunnemann, N., Frostrom, G., Antonio, M., Biazon, B., Camargo, R., Franca, H., Gomes, A., Lima, M., Machado, R., Manhaes, S., Nachtigall, L., Piva, H., Quintiliano, W., Machado, L., Artaxo, P., Roberts, G., Renno, N., Blakeslee, R., Bailey, J., Boccippio, D., Betts, A., Wolff, D., Roy, B., Halverson, J., Rickenbach, T., Fuentes, J., and Avelino, E.: Contrasting convective regimes over the Amazon: Implications for cloud electrification, Journal of Geophysical Research: Atmospheres, 107, LBA 50–1–LBA 50–19, 2002.

Witte, M. K., Yuan, T., Chuang, P. Y., Platnick, S., Meyer, K. G., Wind, G., and Jonsson, H. H.: MODIS Retrievals of Cloud Effective Radius in Marine Stratocumulus Exhibit No Significant Bias, Geophysical Research Letters, 45, 10,656–10,664, 2018.

Yue, Z., Rosenfeld, D., Liu, G., Dai, J., Yu, X., Zhu, Y., Hashimshoni, E., Xu, X., Hui, Y., and Lauer, O.: Automated Mapping of Convective Clouds (AMCC) Thermodynamical, Microphysical, and CCN Properties from SNPP/VIIRS Satellite Data, Journal of Applied Meteorology and Climatology, 58, 887 – 902, 2019.

Zheng, Y. and Rosenfeld, D.: Linear relation between convective cloud base height and updrafts and application to satellite retrievals, Geophysical Research Letters, 2015a.

Zheng, Y. and Rosenfeld, D.: Linear relation between convective cloud base height and updrafts and application to satellite retrievals, Geophysical Research Letters, 42, 6485–6491, 2015b.

Zhu, Y., Rosenfeld, D., Yu, X., Liu, G., Dai, J., and Xu, X.: Satellite retrieval of convective cloud base temperature based on the NPP/VIIRS Imager, Geophysical Research Letters, 2014.

*Supplement of*

# High aerosol sensitivity of Amazonian clouds throughout the seasons

**Oliver Lauer et al.**

*Correspondence to:* Mira L. Pöhlker (m.pohlker@mpic.de), Christopher Pöhlker (c.pohlker@mpic.de)

**Table S1. Typical particle number concentrations under central Amazonian wet and dry season conditions. Specifically, the total number concentration of all condensation nuclei ($N_{CN}$), the particle number concentrations of Aitken, accumulation, and coarse modes ($N_{Ait}$, $N_{acc}$, $N_{coarse}$), as well as the corresponding mode peak diameters ($D_{Ait}$, $D_{acc}$, $D_{coarse}$) are summarized here.**

| Parameter | Unit | Wet season | Dry season | References |
|---|---|---|---|---|
| $N_{CN}$ | [$cm^3$] | $300-400$ | $1250-1500$ | Moran-Zuloaga et al. (2018a); Varanda Rizzo et al. (2018) |
| $N_{ait}$ | [$cm^3$] | $180-250$ | $310-480$ | Pöhlker et al. (2016); Varanda Rizzo et al. (2018) |
| $N_{acc}$ | [$cm^3$] | $150-160$ | $670-1350$ | Pöhlker et al. (2016); Varanda Rizzo et al. (2018) |
| $N_{coarse}$ | [$cm^3$] | $0.4\pm0.3$ | $1.2\pm0.8$ | Moran-Zuloaga et al. (2018a); Prass et al. (2021) |
| $D_{Ait}$ | [nm] | $67-71$ | $68-71$ | Pöhlker et al. (2016); Varanda Rizzo et al. (2018); Franco et al. (2022) |
| $D_{acc}$ | [nm] | $153-172$ | $146-161$ | Pöhlker et al. (2016); Varanda Rizzo et al. (2018); Franco et al. (2022) |
| $D_{coarse}$ | [nm] | $\sim$2000 | $\sim$1500 | Moran-Zuloaga et al. (2018a), Andreae et al. (2015) |

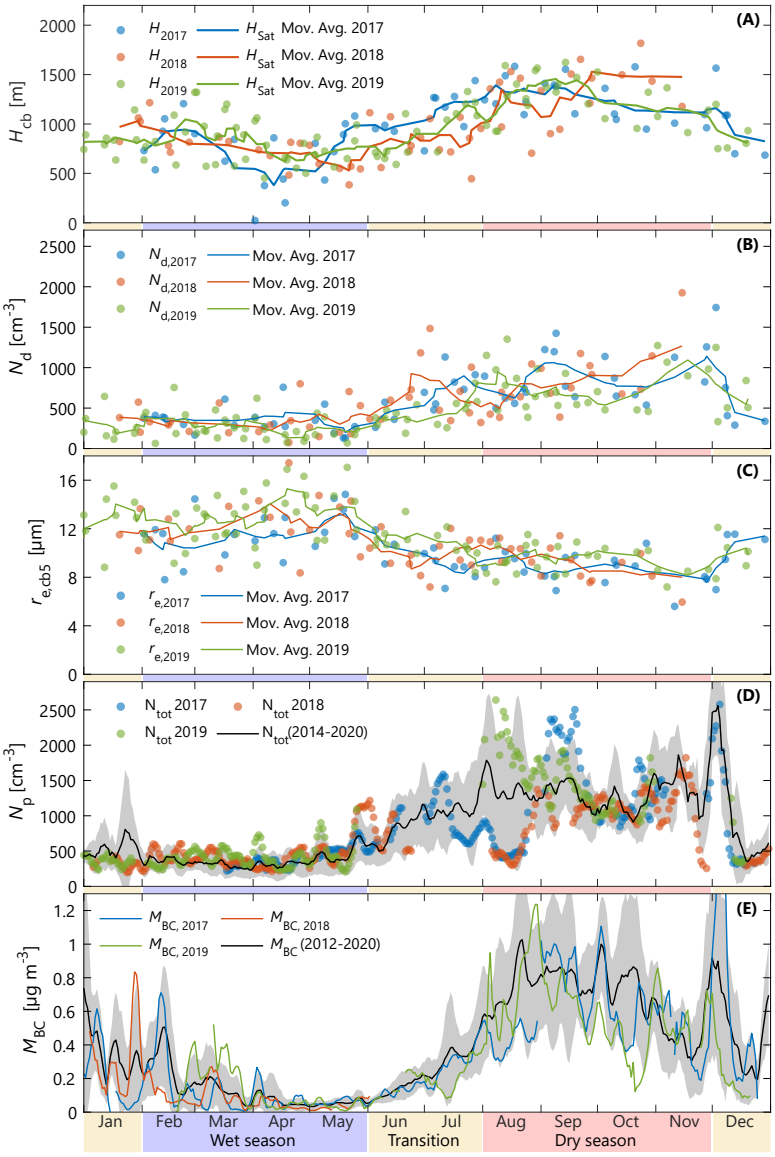


**Figure 7.** Annual data separated by year. All 3 years show the same annual trends. Significant outlier is the August aerosol data in panel D. While 2017 and 2018 have significantly lower than average aerosol concentration, August 2019 shows significantly higher concentrations. This period Also has the biggest variance of aerosol data over the 6 year period where SMPS data at ATTO is available. Even though Aerosol data is vastly increased in August 2019 the $N_d$ is only slightly increased in comparison, indicating a very low activation efficiency. This is the only occasion, in the three-year period, with wind direction directly north, carrying fresh fire plumes into the ATTO region that usually don't reach that far north.

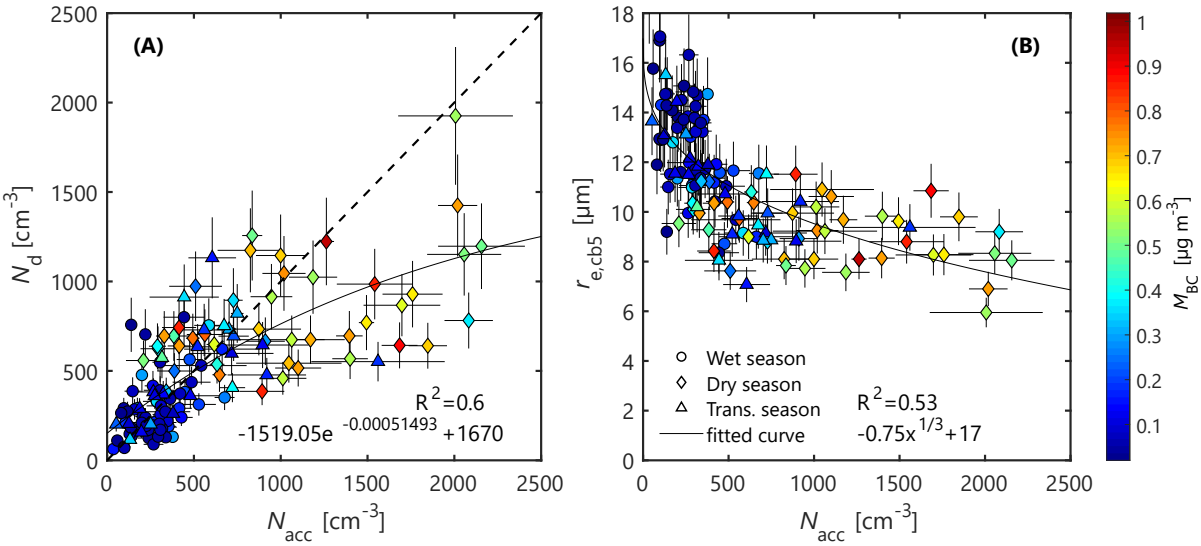


**Figure 8.** Scatter Plot raw data. Shows overall the same trend than Figure 4, the higher variability is related to the small time window of only 1.5 hours each overflight and the changing conditions especially in the dry season.

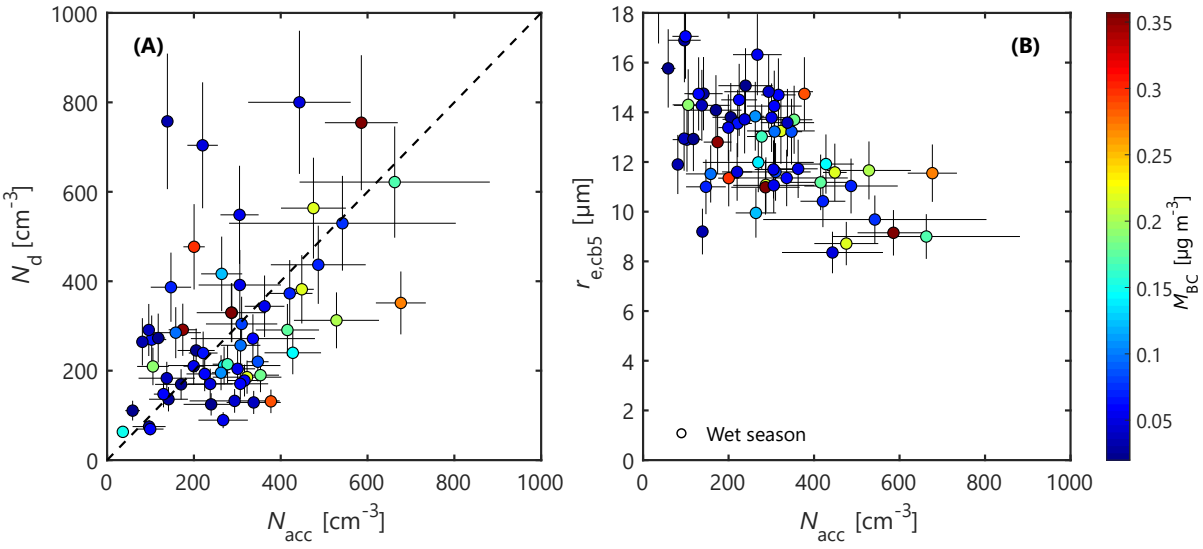


**Figure 9.** Wet season Scatter Plot. More points above the 1:1-line compared to the other seasons, due to stronger contribution of Aitken Mode Particles to $N_d$. Spread in Results origin from less robust $T$-$R_e$ fits. Because of the high growth rate fewer amount of points can be considered for ta Adiabatic fit curve.

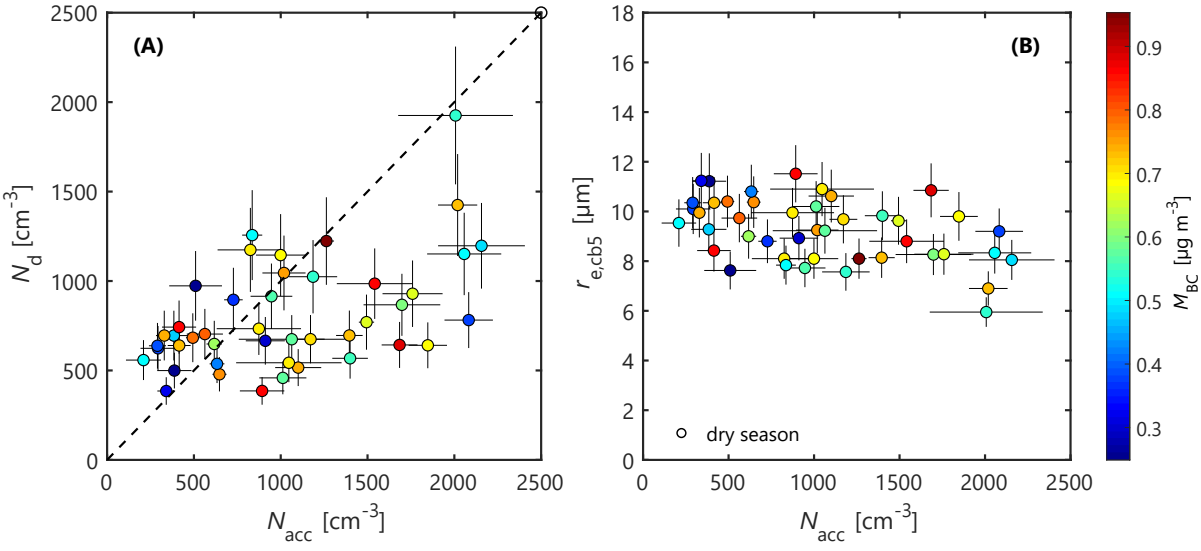


**Figure 10.** Dry season Scatter Plot. Very inconsistent conditions during this season result in large spread of results. Wind directions as well as aerosol loads and origin are constantly shifting during this time. Especially between the 3 different year 2019 showed different overall conditions compared to 2017 and 2018 especially during August. (See 7)

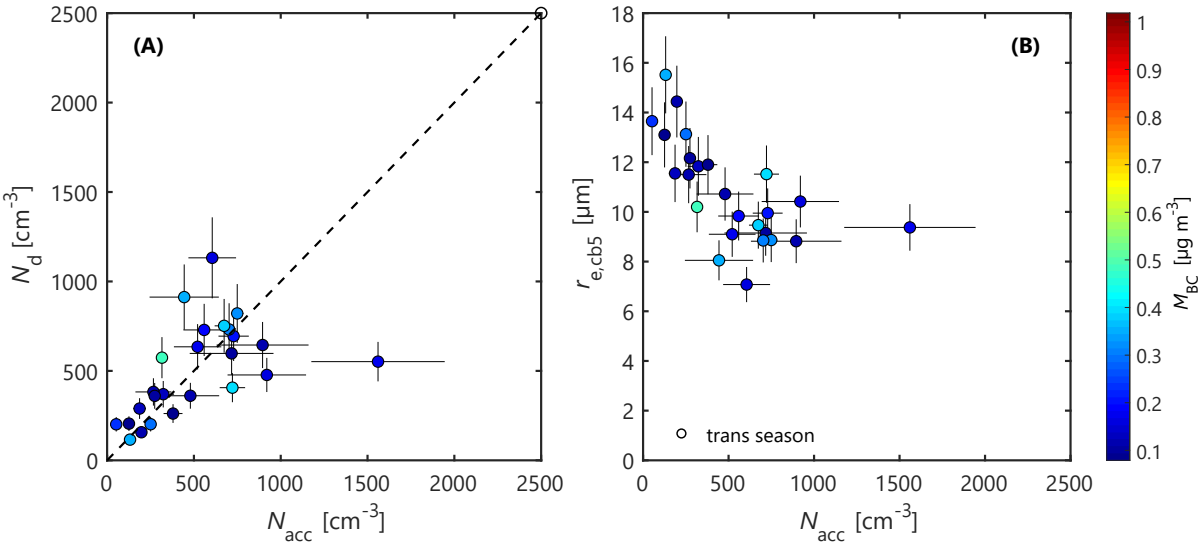


**Figure 11.** Transition season Scatter Plot. Follows closest to the theoretical expected values. Overall low black carbon mass, but stable conditions with enough $N_d$ activation for robust $T$-$R_e$ profiles.

# 2.4 Cloud microphysical zones in the Amazon

**This chapter contains a manuscript draft in a complete but still preliminary state that will be submitted to a peer-reviewed journal:**

Lauer, O.; Andreae, M. O.; Artaxo, P.; Campos Braga, R.; Efraim, A.; Kremper, L. A.; Franco Marco A.and Pöschl, U.; Zheng, Y.; Zhu, Y.; Rosenfeld, D., and Pöhlker, M. L.: "Cloud Microphysical Zones in the Amazon". *In Preparation*. (2022).

**Contribution to this chapter by Oliver Lauer:** This manuscript is currently in preparation and I am the first and main author of this manuscript. My personal contribution includes the processing, quality assurance and analysis of the satellite data. I wrote the scripts for a systematic analysis of the data. Together with my coauthors, I initiated and designed the research. I took the lead on analyzing the results, preparing figures, and writing the manuscript.

# Seasonality of microphysical zones in Amazonian convective clouds with particular focus on secondary droplet activation

Oliver Lauer[1], Daniel Rosenfeld[2], Meinrat O. Andreae[3,4], Paulo Artaxo[5], Ramon Campos Braga[1,6], Cléo Quaresma Dias-Júnior[7], Avichay Efraim[2], Leslie A. Kremper[1], Marco A. Franco[1,5], Ulrich Pöschl[1], Youtong Zheng[8], Yannian Zhu[9], Christopher Pöhlker[1], and Mira L. Pöhlker[1,10,11]

[1] Multiphase Chemistry Department, Max Planck Institute for Chemistry, Mainz, Germany
[2] Institute of Earth Sciences, The Hebrew University of Jerusalem, Jerusalem, Israel
[3] Biogeochemistry Department, Max Planck Institute for Chemistry, Mainz, Germany
[4] Scripps Institution of Oceanography, University of California San Diego, La Jolla, CA 92037, USA
[5] Instituto de Física, Universidade de São Paulo, São Paulo, Brazil
[6] National Marine Science Centre, Southern Cross University, 2450 Coffs Harbour, Australia.
[7] Department of Physics, Federal Institute of Pará (IFPA), Belém, PA, Brazil
[8] Atmospheric and Oceanic Sciences, Princeton University, and NOAA/Geophysical Fluid Dynamics Laboratory, Princeton, New Jersey, 08544, USA
[9] Meteorological Institute of Shaanxi Province, Xi'an, China
[10] Faculty of Physics and Earth Sciences, Leipzig Institute for Meteorology, University of Leipzig, Leipzig, Germany
[11] Experimental Aerosol and Cloud Microphysics Department, Leibniz Institute for Tropospheric Research, Leipzig, Germany

**Correspondence:** Christopher Pöhlker (c.pohlker@mpic.de), Mira L. Pöhlker (poehlker@tropos.de)

**Abstract.** Aerosol effects on clouds and climate have remained highly uncertain (e.g., ). Here, we present a three-year study on aerosol-induced effects on convective clouds over remote regions in the central Amazon rain forest. It combines in-situ aerosol data with high-resolution satellite retrievals. Our analysis resolves the entire vertical structure of the clouds and distinguishes the microphysical zones of condensational droplet growth, collision and coalescence, secondary droplet activation, the mixed phase of water and ice particles as well as the ice phase. The vertical profiles of the effective radius of cloud particles as a function of temperature differ strongly between the low aerosol conditions during the wet season and the biomass burning smoke dominated dry season. Also the vertical depth of the cloud microphysical zones is strongly seasonal. the seasonality is most pronounced for the condensational growth zone, which is much deeper in the dry than in the wet season. In contrast, the secondary activation zone plays a more significant role in the wet than in the dry season. Our findings underline that the strongly variable aerosol population in the Amazon has profound effects of the microphysical processes and vertical profiles of convective clouds.

## 1 Introduction

Aerosols and clouds are main factors in the climate system (Forster et al., 2021). Knowledge gaps in our process understanding of aerosol–cloud interactions, however, contribute significant uncertainty to current radiative forcing estimates (Mülmenstädt and Feingold, 2018; Carslaw et al., 2013). A particular challenge is the bridging of scales from the microphysical process levels in individual clouds to global scales to assess their role in the climate system. Coupled cumulus clouds are one of the most common cloud types worldwide. They are also in focus of the present study. Figure 1 illustrates the microphysical processes and the corresponding microphysical zones in the vertical structure of a deep convective cumulus cloud.

As a result of atmospheric instabilities, air parcels rise above the top of the planetary boundary layer (PBT) and form convective cumulus clouds. With increasing altitude, the pressure in the lifted air parcel decreases, expansion cooling reduces the maximum partial pressure of water vapor, and as a result the relative humidity (RH) increases. Water starts to condense on a fraction of the aerosol particle population, when the RH exceeds water saturation and creates a water vapor supersaturation $S$. The combination of particle size distribution and hygroscopicity defines the aerosol particle fraction that is being activated as cloud condensation nuclei (CCN) (Köhler, 1936; Howell, 1949; Andreae and Rosenfeld, 2008). The critical diameter ($D_{\text{crit}}$) marks the cutoff point for aerosol particles that get activated into cloud droplets, assuming a constant chemical composition (i.e., comparable hygroscopicity parameter $\kappa$). The $D_{\text{crit}}$ is shifted to smaller diameters for higher $S$ as a result of higher $w$ as well as for low aerosol abundance and high $\kappa$. Depending on $w$ as well as the aerosol concentration and size distribution, a stable maximum supersaturation $S_{\text{max}}$ is established at the base of the newly formed cloud, which defines the number concentration of CCN ($N_{\text{CCN}}(S)$) and the initial droplet number concentration ($N_{\text{d}}$). The altitude level of $S_{\text{max}}$ marks the point in the cloud where the flux of excess water vapor driven by expansion cooling and the available surface area for condensation are in equilibrium. Above the level of $S_{\text{max}}$, $S$ drops again as the growing droplets provide sufficient surface area for continuous condensation, which, in turn, releases latent heat, stabilizes the updraft and, therefore, secures the supply of humid air form the PBL.

After the primary cloud droplet activation at cloud base, the droplets grow adiabatically in the **condensation zone**, which is characterized by a stable $N_{\text{d}}$, a narrow droplet size distribution, and constant droplet growth rate. The condensation zone reaches from the cloud base to the altitude where the median effective droplet radius ($r_{\text{e}}$) exceeds $14-15\,\mu\text{m}$. At this size, coalescence becomes the dominating microphysical process and droplets will merge into much bigger droplets widening the droplet size distribution and reducing $N_{\text{d}}$. The growth through the merging droplets is much faster than adiabatic condensational growth. In this **coalescence zone**, droplets grow to a size that their aerodynamic drag is lower than their gravitational pull, initiating warm rain formation. Therefore, the rain onset height typically corresponds to the altitude of the coalescence zone. Coalescense and warm rain formation reduces $w$ as well as the integral surface of the droplet population as well as the rate of water vapor condensation. This process, in turn, can increase $S$ even beyond $S_{\text{max}}$ at cloud base and, therefore, initiate the activation of new particle into cloud droplets. This process is called secondary droplet activation and the can occur on the particle fraction that was either not activated at cloud base and subsequently transported upwards or on particles being entrained at the cloud

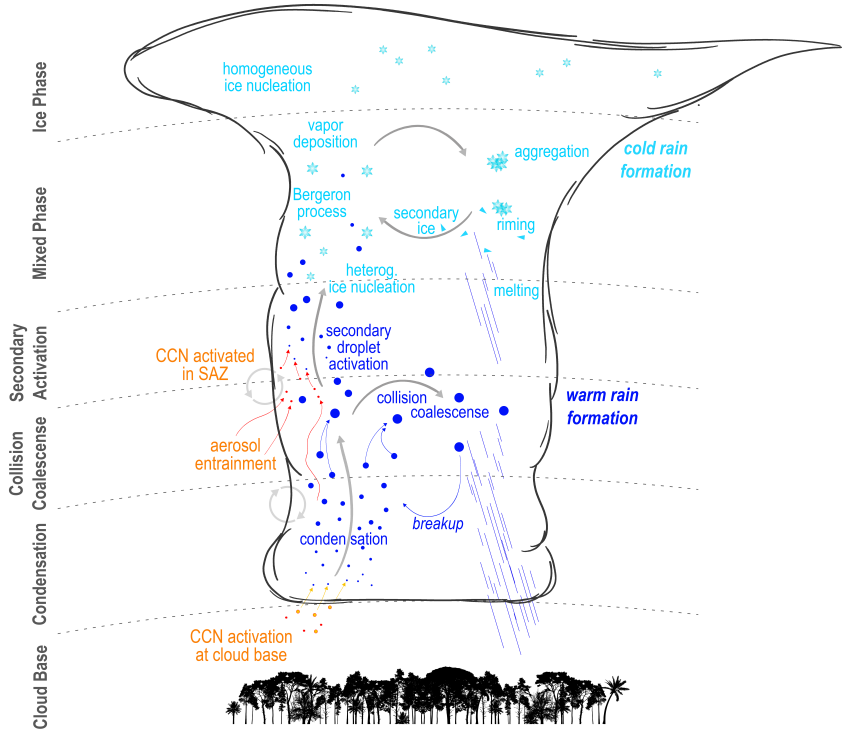


**Figure 1.** Illustration of basic microphysical processes and corresponding microphysical zones in Amazonian convective clouds. Refer also to related scheme in Lauer et al. (2022).

boundaries. The activation in this area is not as sharp as at cloud base and widens the droplet size distribution considerably. The **secondary droplet activation zone** (SAZ) at higher altitude also invigorates $w$ and releases further latent heat, which, in turn, extends the vertical cloud development and its longevity.

When the droplets reach altitudes with temperatures well below $0°C$, first ice particles start to form. This is typically gradual process described as **mixed phase** where liquid and frozen particles coexist. In clouds that formed in polluted regimes and have high $N_d$, the condensation zone can extend up to the freezing level without major coalescence. For comparatively narrow droplet size distributions, the most droplets freeze at a similar temperature, typically around $-10°C$, which reduces the mixed phase to a rather thin layer. For clouds that reach the freezing levels when coalescence is already happening, the wider droplet size distribution leads to a vertically more extended mixed phase and a lower initial freezing temperature at $\sim -5°C$ as a result of the bigger droplets present. Clouds that experienced secondary activation before reaching the freezing level, typically develop a vertically extended mixed phase as a result of the small droplets activated at high altitude. They freeze at much lower

temperatures than the comparatively large particles after coalescence. Extended mixed phases can reach from $-5$ to $-10\,-5$°C and will not reach full glaciation before $-25$ to $-30\,-5$°C. Over the mixed phase, the **ice phase** is located and defined as the microphysical zone where no liquid water is present any more. This is typically reached between $-15$ to $-30\,-5$°C. Large cumulonimbus anvil clouds with significant ice phases spawn cirrus clouds due to strong wind shear at the cloud top.

Satellite observations are a particularly valuable tool to investigate aerosol and cloud properties on large geographic scales. In this study we combined aerosol in situ observation with high-resolution remote sensing observations of cloud microphysical properties from the Visible Infrared Imaging Radiometer Suite (VIIRS) on the Suomi National Polar-orbiting Partnership (NPP) satellite. The VIIRS approach and data analysis has been outlined in Rosenfeld et al. (2014), Lauer et al. (2022), Yue et al. (2019), and Efraim et al. (2022b). The study was conducted in the Amazon rain forest, which is an ecosystem of particular importance in the Earth system .

## 2 Methods

### 2.1 Satellite data analysis

This study is based on the retrieval of so-called $T$-$r_e$ profiles, which estimate the vertical evolution of the effective cloud droplet radius ($r_e$) as a function of temperature ($T$) in a cluster of clouds. Satellite images were recorded by the VIIRS installed on the Suomi NPP satellite (Hillger et al., 2013, 2014). A detailed description of the data analysis can be found in the related study by Lauer et al. (2022). Further information can be found in Yue et al. (2019) and Efraim et al. (2022b).

$T$-$r_e$ profiles are a new approach to investigate aerosol cloud interactions and cloud micropysics and utilizes the high resolution of modern instrumentation of last generation meterological satellites like the SuomiNPP satellite, equipped with the VIIRS that provides a resolution of 325 m in its 5 main channels and a 750 m resolution in the other 17 channels. The main channels used for $T$-$r_e$ profiles area the 3.7 $\mu$m and the 11.7 $\mu$m infrared channels. While the first is used to retrieve $r_e$, the latter is the main channel for $T$ recording (Rosenfeld et al., 2014; Hillger et al., 2014). Afterwards all pixels in the investigated area got binned into temperature bins with 1°C width to prepare the raw data for the cloud mask that filters the raw data for cloud pixels. The homogeneous background of the dense vegetation in the Amazon improves the performance of this crucial task. The warmest temperature where 40 % of the pixels pass the cloud mask (Zhu et al., 2014) determines the cloud base temperature. It is essential to find an accurate cloud base height, since the CCN calculation is most sensitive to an accurately detected cloud base height. To determine the cloud base height, the constant lapse rate in the boundary layer of $9.8\,\mathrm{K\,km^{-1}}$ is utilized in combination with the $T$ difference between the the cloud base temperature and the 2 m above ground level air temperature received form reanalysis data (Rosenfeld et al., 2016). The SuomiNPP satellite is a polar orbiting satellite, therefore it is not possible to resolve diurnal trends and developments. All data was received between 12:15 and 12:45 local time.

The data was filtered to fit the limitations for $T$-$r_e$ profiles, including solar and viewing angles, and suitable cloud coverage. For every satellite overpass that fulfilled the requirements, several polygons were selected by hand following Lauer et al. (2022) with a standard test for outliers. With the goal of a conclusive and statistical robust picture on the seasonal difference and the influence of aerosols on cloud microphysics above the Amazon, 189 days comprising 881 $T$-$r_e$ profiles between the beginning of 2017 and the end of 2019 have been evaluated. The interpretation of the $T$-$r_e$ profiles has been automated with a dedicated algorithm that analyzes the geometrical shape of the profile, but also accounts for physical and meteorological limitations (Efraim et al., 2022b; Lauer et al., 2022).

### 2.2 Definition of cloud microphysical zone

Based on the $T$-$r_e$ profiles, the microphysical zones are define here as follows:

- **Condensation zone**: The condensation zone starts at the cloud base and extends vertically until coalescence occurs. To define the condensation zone, an adiabatic curve is fitted to the $T$-$r_e$ profile, excluding the lowest $r_e$ values, because of semitransparent cloud edges and resulting ground contamination of the measured $r_e$ values. To get the best possible fit, all $r_e$ values below $15\,\mu m$ that are not effected by ground contamination are considered for the adiabatic fit. For the final fit, a $N_d$ combination of at least 5 consecutive points that show the best fit to the satellite data were chosen to calculate the adiabatic curve. In case no 5 points in the defined size range were found, the fit was forced through the origin and the last $r_e$ value smaller than $15\,\mu m$. This case only occurs in very clean conditions with $N_{CCN}$ below $160\,cm^{-3}$ at cloud base. In this case, individual droplet growth is too fast to find enough points for a regular adiabatic fit curve.

- **Entrainment zone**: In some cases, on top of the condensation zone, the effective radius grows slower than expected by the adiabatic fit curve (Sup.: 4). A possible explanation is a wrong detected cloud base, when the actual cloud base was not found and the lowest detected $r_e$ is >10 $\mu$m. In many cases this cant be the possible explanation since the right cloud bases are detected indicated by the lowest $r_e$ being at a realistic value at $5\mu$m. This signature can be detected more frequently in clean conditions. A possible explanation is Entrainment near the cloud base caused by an low unstable updraft when the latent heat released at cloud base is not high enough to establish a stable updraft dry entrainment can occur. The entrained dry air can evaporate already activated droplets especially locally at the cloud edges reducing the surface area available and removing water form the cloud, if the air parcel rises further new condensation can occur leading to the unspecific $T$-$r_e$ profile.(reference)

- **Coalescense zone**: In the coalescence zone, droplet collision and coalescence into larger droplets causes growth rates higher than expected from adiabatic growth only (Sup.: 4). Droplets need to have a minimum $r_e$ of $12-15\,\mu m$ to collide efficiently. Depending on the best fit curve found in the condensation zone, the coalescence zone can start before $15\,\mu m$, but the starting point can not be at higher values. The start of the coalescence zone also marks the point where precipitation is initiated. The $N_d$ decreases sharply in the coalescence zone and can cause the updraft to stall as a result of insufficient condensation area, limiting the release of latent heat. In this case the top of the coalescence zone corresponds

to the cloud top. In case the updraft does not stall completely, the reduced condensation caused by the limited surface area at the top of the coalescence zone causes the $S$ to increase. In this area of the cloud, the $S$ can exceed the initial supersaturation at cloud base, with the effect of secondary droplet activation marking the beginning of the secondary activation zone (SAZ).

– **Secondary droplet activation zone (SAZ)**: The start of the secondary activation zone is indicated by a vertically constant or receding $r_e$. In any case the slope has to be steeper (or negative) compared to the adiabatic curve for a SAZ to be detected. This signature in the profile is cause by the new droplet nucleation. The additional droplets shift the median droplet size to smaller values, compared to the expected adiabatic growth. The effects of secondary activation and coalescence can cancel each other out. It is important to note that the algorithm can only detect zones correctly where one of the microphysical processes is dominating. The vertical height of the SAZ is no indicator for the intensity of the secondary activation. Neither the numerical nor the volumetric increase of droplets can be quantified. secondary activation and coalescence can overlap, therefore, the maximum $S$ does not have to be at the beginning of the SAZ. But since the absolute humidity is highest for warmer temperatures the higher the initial temperature of the SAZ is, the more potential it has for secondary activation. The droplet size distribution widens significantly due to the secondary activation and for the droplet size distribution a vertically bigger SAZ does increase the spread further as a result of the indistinct activation in the SAZ (Braga et al., 2022; Niedermeier et al., 2020). Secondary activation can also occur during condensation, only several hundred meters above the cloud base. When the initial maximum supersaturation at the cloud base is very low and, therefore, the $N_d$ is high, a scenario that typically happens on at high pollution during the dry season. In this cases, the sudden release of latent heat at the cloud base increases the updraft fast enough to cause a second, stronger maximum in supersaturation at higher altitude. Cases that show this behavior were filtered out, because they cause the fitting of the adiabatic curve to fail, making it impossible to determine the $N_d$ at cloud base and detect microphysical zones reliably. The mechanism is detailed in Efraim et al. (2022a). If secondary activation is detected before the first coalescence zone it is marked as entrainment (Sup. 7).

– **Mixed phase, comprising ice particle and water droplets**: The beginning of the mixed phase is the most challenging interface to determine. It is important to know that the biggest droplets that can be detected by the algorithm for the effective radius are 40 $\mu$m and ice particles get detected as particles >40 $\mu$m. The beginning of the mixed phase is the easiest to detect in polluted cases where the condensation zone reaches high enough to reach freezing level. In this case the very homogeneous droplet size distribution causes to freeze all droplets at nearly the same premature causing a rapid increase of the detected effective radius to the detection limit in only 2 to 3 degree. Detecting the beginning of the mixed phase after a large SAZ is not as clear cut and leaves room for interpretation. The effective radius increases gradually but starts to exceed droplet sizes that are not physically explainable indicating the introduction of ice particle that shift the median value of the detected effective radii to bigger sizes. The algorithm searches constantly for the points in the $T$-$r_e$ profile with the most pronounced local curvature. To determine the mixed phase by empirical testing a value of 28 $\mu$m at a temperature >0 °C indicates that ice nucleation started. to determine the start of the mixed phase the last local

maximum curvature before this value is chosen as the start of the mixed phase. if no local maximum curvature is found mixed phase starts at re > 30 $\mu$m or temperatures lower 0 °C.

– **Ice phase**: The ice phase starts when the median effective radius approaches the detection limit. If the median effective radius is > 39 $\mu$m full crystallisation completed. From this point to the top of the cloud the cloud only contains ice particles.

## 3 Results and Discussion

### 3.1 Vertical profiles of tropical cumulus clouds

Using T-Re profiles, coupled cumulus clouds can be split into different mycropysical zones in vertical direction. The zones differentiate by the dominant mycrophysical process dominant at the given altitude. The most important processes happening inside a cloud are phase changes of water, depending on temperature and pressure gradients, supplemented by coalescence, precipitation and entrainment. Starting from the base of the cloud where aerosols and moist air form the boundary layer enter the cloud with the updraft. Utilization of T-Re profiles allowes in depth investigation into cloud microphysics, besides calculating CCN at cloud base. The different zones and how they are determined is described in Efraim et al. (2022b).

As shown in Figure 2 the mycrophysical structure or clouds underlies drastic seasonal changes. The cloud base temperature is in average 1 °C warmer in the wet season in comparison to the dry season. When taking the on average higher surface temperature and lower humidity during the dry season into account the detected average cloud base height is more than 500 m higher in the dry season, than the cloud base height detected in the wet season, which is 675 m above ground. While the cloud base height is only determined by meteorological factors, the low aerosol loads during the wet season lead to an aerosol limited droplet activation at cloud base as showen in Lauer et al (2022). As a result we detect on average 3 times lower CCN numbers during the wet season which increase the growth rate of droplets. In the most extreme cases during may the CCN number at cloud base is below 150 cm-3 making it difficult to fit an adiabatic curve because the coalescence already starts 5 °C above cloud base. On average coalescence consistently occurs at much lower altitude than during the dry season, with a low precipitation onset producing warm rain-out during the wet season.

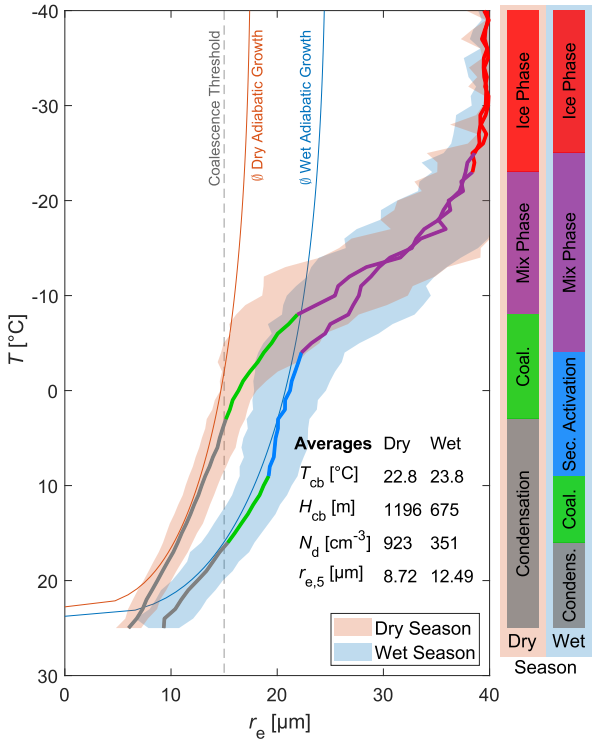


**Figure 2.** Averaged $T$-$r_e$-profiles for the wet and dry season, including the corresponding adiabatic curves and the limit for condensational growth at 15 $\mu$m. On the right Schematic vertical distribution of microphisical zones during the wet and dry season. The zones are automatically detected by different methods described in Efraim et al. (2022b). The table shows the average values for different cloud properties calculated from all cases found during the corresponding season. The colored shades show the standard distribution for all cases considered during the respective season.

### 3.2 Seasonality of micropysical zones in tropical cumulus clouds

175 Fig. 3 shows a high correlation between the cloud microphysical zones and the total aerosole load measured at ATTO. Warm rain-out enables a secondary droplet activation zone after most of the surface area available for condensation depleted with the droplets removed by precipitation. This causes the supersaturation to rise again to the point where it can exceed the supersaturation at cloud base leading to new particle activation of particles that were not able to activate at cloud base. Additionally particles entrained above cloud base contribute to the new droplet formation in the secondary activation zone (SAZ).

180 3 show the highest vertical expansion for the SAZ for a $N_d$ at cloud base between 250-500 cm-3. Clouds with higher droplet activation tend to reach the mixed phase before precipitation depletes the surface area to the point condensation gets limited.

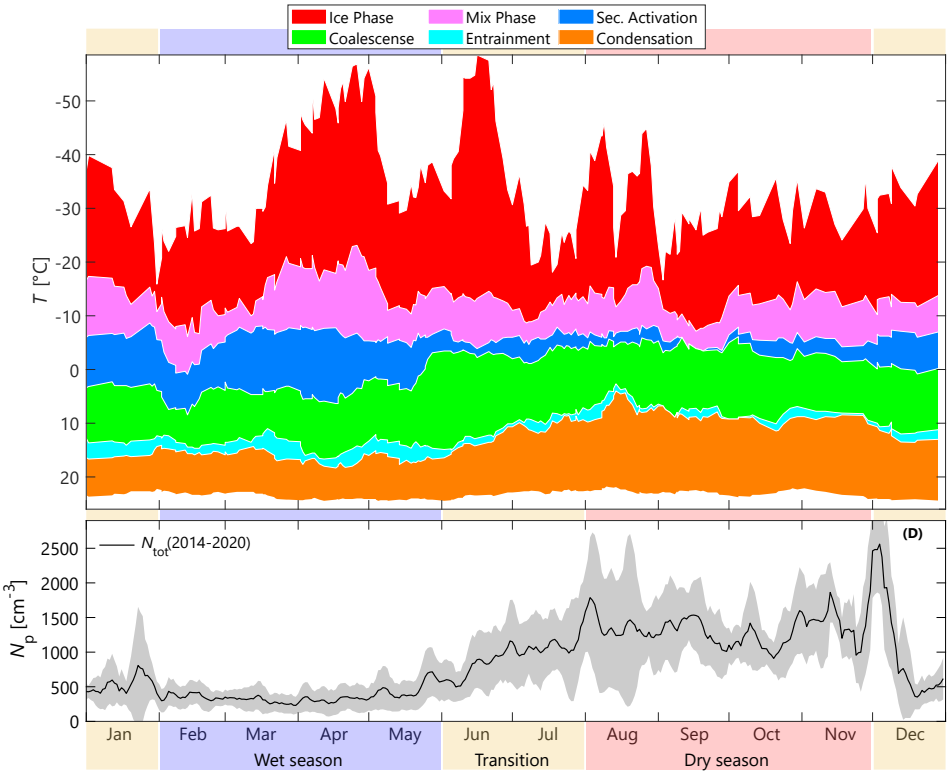


**Figure 3.** Microphysical structure of tropical cumulus clouds at ATTO. Much larger condensation zones in the dry season due to lower growth rate of the droplets. Entrainment is strongest during the wet season, low during dry season. Coalescence constant during the year if no entrainment detected. Secondary activation mostly during the Wet season, less during the transition season and nearly none during the dry season. Largest mix phase in the wet and transition season, potentially related to stronger secondary activation. The Ice phase starts below -20 °C in the wet season and above that temperature in the dry season. All data is plotted as 9-point-floating average to reduce noise and emphasize seasonal trends.the chart does not represent the vertical structure of the investigated cloud microphysical zones, but shows the combined vertical expansion of the different microphysic zones in the order they usually can be observed. Especially Coalescence and secondary activation can alter multiple times before reaching the mixed phase (Sup.: 5). The vertical size of the zones is no indicator for the intensity of the microplhysic processes that occur, they only show which process is dominant in the given region.

Clouds below 250 cm-3 often rain out at such low altitude that the latent heat released by condensation is not enough to maintain an updraft. Clouds that form in very clean conditions with initial $N_d$ at cloud base below 200 cm-3 can include a SAZ that is small in height but can invigorate the updraft enough to keep the cloud expanding into cumulonimbus anvil clouds.

Note that Fig. 3 combines all measured clouds, therefore clouds that dissipate at lower altitude contribute only to the low level of the mycrophysical zones stacked in this figure. Therefore, Fig. 3 does not represent the amount of secondary activation occurring. Neither the numerical nor the volumetric increase of droplets can be quantified, because other than at cloud base there is no sharp level of maximum supersaturation, but activation happens gradually. Also the number of droplets that didn't precipitate and are left over from initial cloud base activation can not be quantified. Therefore a larger vertical expansion of a SAZ is not synonymous with more secondary activation.

However, we Fig. 3 shows a relationship between the vertically extension of the SAZ and a more pronounced mixed phase. The gradual activation in the SAZ causes a wider droplet size distribution and freezing temperatures are strongly dependent on droplet radii. The wide droplet size distributions caused by vertically pronounced SAZs directly influences the vertical size of the mixed phase. This is likely to lead to wider ice particle distributions that can promote charge separation due to different aerodynamic drag and consequently more severe weather events. Besides the influence on the freezing processes the SAZ increases the liquid water content of the cloud as well as the longevity.

Especially coalescence zones and SAZ can alternate multiple times before reaching freezing altitudes. This happens when the newly activated particles quickly grow to a size the can start coalescence and additional war rain-out is triggered. Precipitation from the mixed or ice phase is not investigated since T-Re profiles do not provide the necessary insight.Coalescence is playing a significant role in the mixed phase as well but the microphysics in this region are complex ;therefore as soon as ice particles are detected all this processes are combined under mixed phase that expand vertically until full crystallization is reached at which point the ice phase starts.

During the dry season $N - d$ at cloud base can be so high that warm rain-out is suppressed before the droplets reach freezing temperatures. The higher number of droplets at cloud base cause a slower individual droplet growth postponing coalescence to higher altitudes. In very polluted conditions during the burning season and when wind direction changes more south the droplet growth is slow enough for the condensation zone to directly reach freezing levels before coalescence occurs. Compared to the wet season with rising aerosol loads clouds often do not reach the ice phase or coalescence zone at all, but dissipate at lower levels for the investigated time frame between 12:15 and 12:45 local time. When the satellite passes the investigated region used in this study.

Precipitation from the mixed or ice phase is not investigated since T-Re profiles do not provide the necessary insight.Coalescence is playing a significant role in the mixed phase as well but the microphysics in this region are complex ;therefore as soon as ice particles are detected all this processes are combined under mixed phase that expand vertically until full crystallization is reached at which point the ice phase starts.

## 4 Conclusions

We showed that the cloud microphysics can be regarded rather as aerosol-limited than updraft-limited, which means that central Amazonian clouds react sensitively to changes in the aerosol population. This paper shows that this finding is not only limiting the view on the cloud base droplet activation but also the role aerosols play in cloud mycrophysics at elevated altitudes. The influence of Aerosols on cloud development is manifold even during the majority of the dry season. Additionally at least 3 different mechanisms that result in additional droplet activation above the cloud base have been observed.

(1) Secondary droplet activation after warm rain-out happens frequently and is an important factor to retain buoyancy after warm rain-out in coupled cumulus clouds during the wet season. The resulting spread in droplet size distribution as a consequence of the new droplet formation strongly influences ice nucleation and mycrophysical processes in the ice phase as a whole.

(2) Dry entrainment can lead to a SAZ zone before rain-out and above condensation. This is most often observed during the cleanest annual condition end of April and the first half of may. The strong aerosol limitation hempen the release of latent heat and subsequently updraft stabilization at cloud base.This cal lead to a wider activation zone with no sharp horizon for the maximum supersaturation.

(3) For highly polluted conditions secondary activation happens already during condensation. It violates the principle of homogeneous growth during condensation and leads to gross overestimation of the detected Nd when using T-Re profiles and no adiabatic curve can be fitted. Therefore cases that showed this behavior had to be excluded from this study and were investigated in a separate study (Efraim et al. (2022a)).

The much stronger and more complex influence of aerosols and cloud mycrophysics found in this study raise additional concerns of the land use and the increasing deforestation efforts in the Amazon region. The methods used in this study can also serve as a blueprint to future satellite investigation of large scale investigation of regional cloud microphysics which are highly requested to improve regional and global cloud models.

*Data availability.* The data of the key results presented here have been deposited in supplementary data files for use in follow-up studies. The ATTO data used in this study are available via the ATTO data portal through https://www.attoproject.org/. For data requests beyond the available data, please refer to the corresponding authors.

*Author contributions.* TEXT

*Competing interests.* The authors declare that they have no conflict of interest.

*Disclaimer.* This paper contains results of research conducted under the Technical/Scientific Cooperation Agreement between the National Institute for Amazonian Research, the State University of Amazonas, and the Max-Planck-Gesellschaft e.V.; the opinions expressed are the entire responsibility of the authors and not of the participating institutions.

*Acknowledgements.* This research has been supported by the Max Planck Society, the Max Planck Graduate Center with the Johannes Gutenberg University Mainz (MPGC), the Bundesministerium für Bildung und Forschung (BMBF contracts 01LB1001A, 01LK1602B, and 01LK2101B), the Brazilian Ministério da Ciência, Tecnologia e Inovação (MCTI/FINEP contract 01.11.01248.00), the Conselho Nacional de Desenvolvimento Científico e Tecnológico (CNPq, Brazil) (process 200723/2015-4), the FAPESP (Fundação de Amparo à Pesquisa do Estado de São Paulo) (grant no. 2017/17047-0), the CNPq project (grant no. 169842/2017-7), the CAPES project (grant no. 88887.368025/2019-00), and the European Commission, H2020 Research Infrastructures (A-LIFE (grant no. 640458)). For the operation of the ATTO site, we acknowledge the support by the Max Planck Society, the German Federal Ministry of Education and Research and the Brazilian Ministério da Ciência, Tecnologia e Inovação as well as the Amazon State University (UEA), FAPEAM, LBA/INPA, and SDS/CEUC/RDS-Uatumã. We would like to especially thank all the people involved in the technical, logistical, and scientific support of the ATTO project.

**References**

Andreae, M. and Rosenfeld, D.: Aerosol–cloud–precipitation interactions. Part 1. The nature and sources of cloud-active aerosols, Earth-Science Reviews, 89, 13–41, 2008.

Braga, R. C., Rosenfeld, D., Andreae, M. O., Pöhlker, C., Pöschl, U., Voigt, C., Weinzierl, B., Wendisch, M., Pöhlker, M. L., and Harrison, D.: Detrainment Dominates CCN Concentrations Around Non-Precipitating Convective Clouds Over the Amazon, Geophysical Research Letters, 49, e2022GL100 411, e2022GL100411 2022GL100411, 2022.

Carslaw, K. S., Lee, L. A., Reddington, C. L., Pringle, K. J., Rap, A., Forster, P. M., Mann, G. W., Spracklen, D. V., Woodhouse, M. T., Regayre, L. A., and Pierce, J. R.: Large contribution of natural aerosols to uncertainty in indirect forcing, Nature, 2013.

Efraim, A., Campos Braga, R., Rosenfeld, D., Lauer, O., Franco, M. A., Kremper, L. A., Pöhlker, C., Andrerae, M. O., Dias-Junior, C. Q., and Pöhlker, M. L.: Satellite-based detection of secondary droplet activation during condensational growth in convective clouds, 2022a.

Efraim, A., Lauer, O., Rosenfeld, D., Braga, R. C., Franco, M. A., Kremper, L. A., Zhu, Y., Pöschl, U., Pöhlker, C., Andreae, M. O., Artaxo, P., de Araújo, A. C., and Pöhlker, M. L.: Satellite-Based Detection of Secondary Droplet Activation in Convective Clouds, Journal of Geophysical Research: Atmospheres, 127, e2022JD036 519, e2022JD036519 2022JD036519, 2022b.

Forster, P., Storelvmo, T., Armour, K., Collins, W., Dufresne, J.-L., Frame, D., Lunt, D., Mauritsen, T., Palmer, M., Watanabe, M., Wild, M., and Zhang, H.: The Earth's Energy Budget, Climate Feedbacks, and Climate Sensitivity, in: Climate Change 2021: The Physical Science Basis. Contribution of Working Group I to the Sixth Assessment Report of the Intergovernmental Panel on Climate Change, edited by Masson-Delmotte, V., Zhai, P., Pirani, A., Connors, S., Péan, C., Berger, S., Caud, N., Chen, Y., Goldfarb, L., Gomis, M., Huang, M., Leitzell, K., Lonnoy, E., Matthews, J., Maycock, T., Waterfield, T., Yelekçi, O., Yu, R., and Zhou, B., chap. 7, 2021.

Hillger, D., Kopp, T., Lee, T., Lindsey, D., Seaman, C., Miller, S., Solbrig, J., Kidder, S., Bachmeier, S., Jasmin, T., and Rink, T.: First-Light Imagery from Suomi NPP VIIRS, Bulletin of the American Meteorological Society, 94, 1019 – 1029, 2013.

Hillger, D., Seaman, C., Liang, C., Miller, S., Lindsey, D., and Kopp, T.: Suomi NPP VIIRS imagery evaluation, Journal of Geophysical Research, 119, 6440–6455, 2014.

Howell, W. E.: THE GROWTH OF CLOUD DROPS IN UNIFORMLY COOLED AIR, Journal of Atmospheric Sciences, 6, 134 – 149, 1949.

Köhler, H.: The nucleus in and the growth of hygroscopic droplets, Transactions of the Faraday Society, 1936.

Lauer, O., Kremper, L. A., Rosenfeld, D., Franco, Marco A.and Andreae, M. O., Artaxo, P., Campos Braga, R., Dias-Júnior, C. Q., de Araújo, A. C., Ditas, F., Efraim, A., Ervens, B., Holanda, B. A., Jungandreas, L., Krüger, O. O., Machado, L. A. T., Hernández Pardo, L., Pöschl, U., Pulik, G., Quaas, J., Zheng, Y., Zhu, Y., Pöhlker, C., and Pöhlker, M. L.: High aerosol sensitivity of Amazonian clouds throughout the seasons, 2022.

Mülmenstädt, J. and Feingold, G.: The radiative forcing of aerosol–cloud interactions in liquid clouds: Wrestling and embracing uncertainty, Curr. Clim. Change Rep., 4, 23–40, 2018.

Niedermeier, D., Voigtländer, J., Schmalfuß, S., Busch, D., Schumacher, J., Shaw, R. A., and Stratmann, F.: Characterization and first results from LACIS-T: a moist-air wind tunnel to study aerosol–cloud–turbulence interactions, Atmospheric Measurement Techniques, 13, 2015–2033, 2020.

Rosenfeld, D., Liu, G., Yu, X., Zhu, Y., Dai, J., Xu, X., and Yue, Z.: High-resolution (375 m) cloud microstructure as seen from the NPP/VIIRS satellite imager, Atmos. Chem. Phys., 2014.

Rosenfeld, D., Zheng, Y., Hashimshoni, E., Pöhlker, M. L., Jefferson, A., Pöhlker, C., Yu, X., Zhu, Y., Liu, G., Yue, Z., Fischman, B., Li, Z., Giguzin, D., Goren, T., Artaxo, P., Barbosa, H. M. J., Pöschl, U., and Andreae, M. O.: Satellite retrieval of cloud condensation nuclei concentrations by using clouds as CCN chambers, Proceedings of the National Academy of Sciences, 2016.

Yue, Z., Rosenfeld, D., Liu, G., Dai, J., Yu, X., Zhu, Y., Hashimshoni, E., Xu, X., Hui, Y., and Lauer, O.: Automated Mapping of Convective Clouds (AMCC) Thermodynamical, Microphysical, and CCN Properties from SNPP/VIIRS Satellite Data, Journal of Applied Meteorology and Climatology, 58, 887 – 902, 2019.

Zhu, Y., Rosenfeld, D., Yu, X., Liu, G., Dai, J., and Xu, X.: Satellite retrieval of convective cloud base temperature based on the NPP/VIIRS Imager, Geophysical Research Letters, 2014.

*Supplement of*

# Seasonality of microphysical zones in Amazonian convective clouds with particular focus on secondary droplet activation

**Oliver Lauer et al.**

*Correspondence to:* Mira L. Pöhlker (m.pohlker@mpic.de), Christopher Pöhlker (c.pohlker@mpic.de)

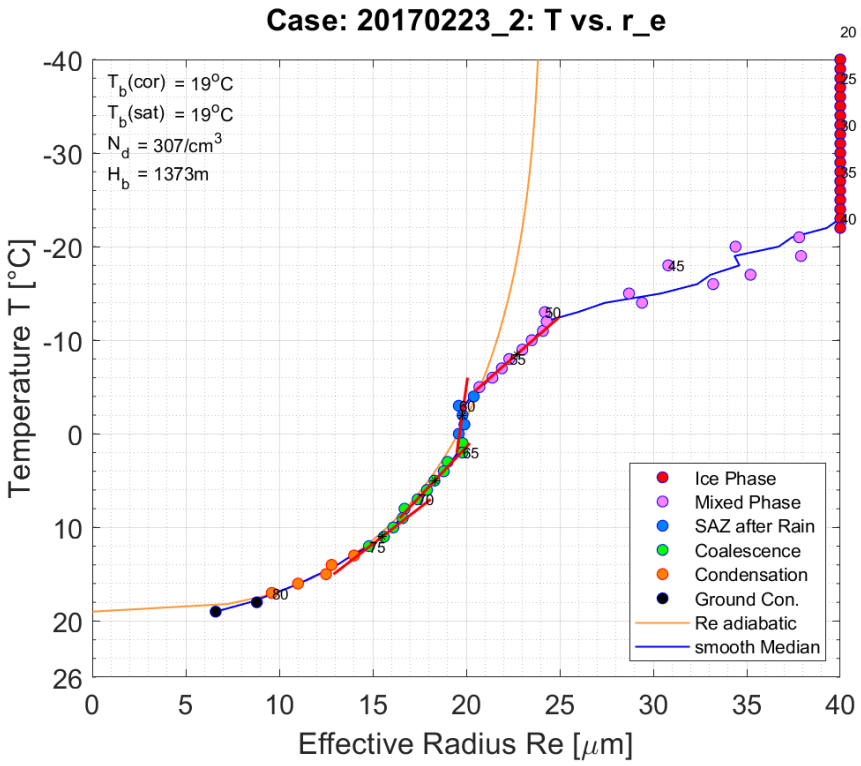


**Figure 4.** Illustration of the principle behind the automatized microphysic zone detection.The algorithm searches for local maxima in curvature of the 3 point floating average of the T-Re profile. They are set as potential zone borders and a slope is fitted. If the slope is shallower than the average slope of the adibatic curve at the same altitude it is determined a coalescence zone and if its steeper it is determined a secondary activation zone SAZ. In case a SAZ is detected before the first coalescence zone it is marked as entrainment. A sharp increase of the effective radius above 28 $\mu$m at a temperature >0 °C indicates the beginning of the mixed phase. If the median effective radius exceeds 39 $\mu$m it is considered full crystallisation in the ice phase.

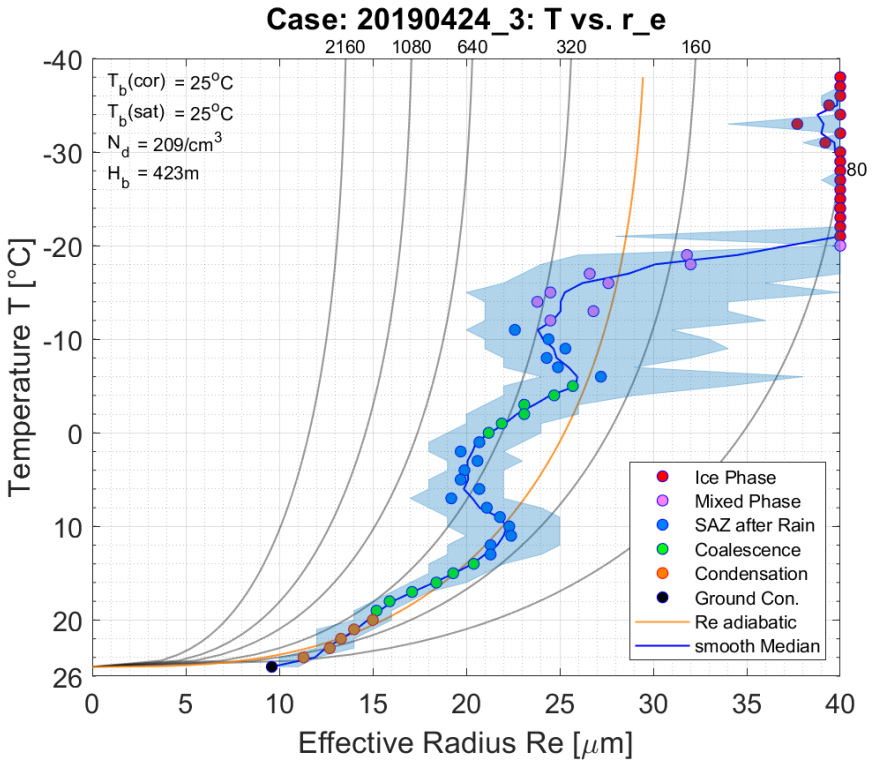


**Figure 5.** A typical profile as seen commonly during the wet season. When $r_e$ exceeds 15 $\mu$m coalescence starts. Coalescence and secondary activation zones (SAZ) can alternate between each other multiple times, when the newly activated droplets grow fast enough to trigger coalescence and subsequently precipitation, which will reset the cycle again. A vertically extended mixed phase is also typical for wet season clouds with secondary activation

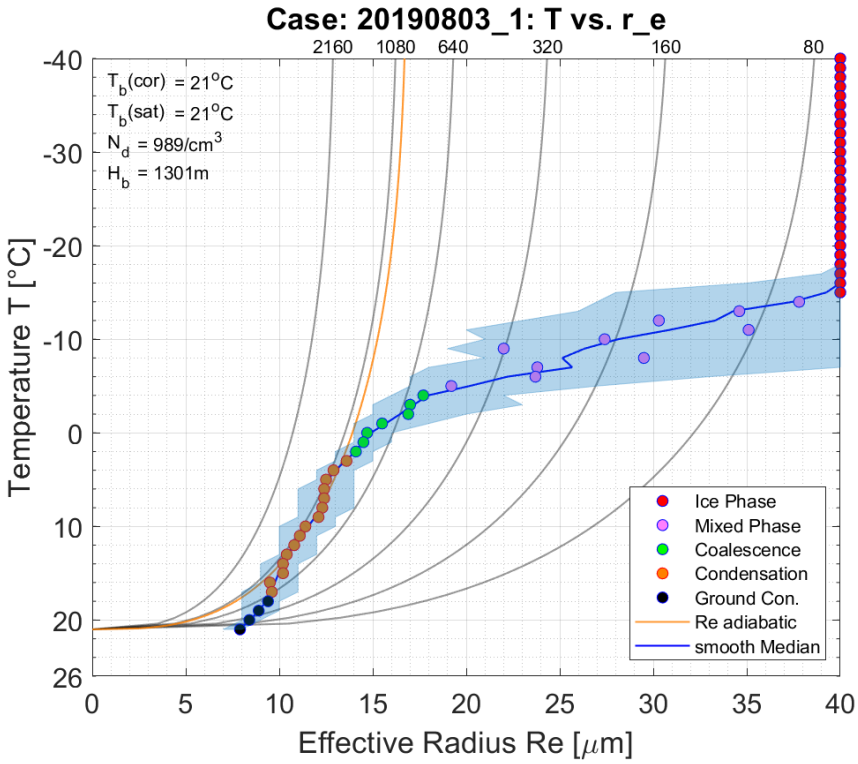


**Figure 6.** Exculpatory profile of dry season clouds including a vertically extended condensation zone with a short coalescence zone quickly reaching freezing level to convert into a vertically narrow mixed phase. and full crystallisation is reached before -20 °C. The quick freezing process is typical for dry season clouds wis a vertically extended condensation zone, which leads narrow droplet size distribution enabling all droplets to freeze in a narrow temperature window.

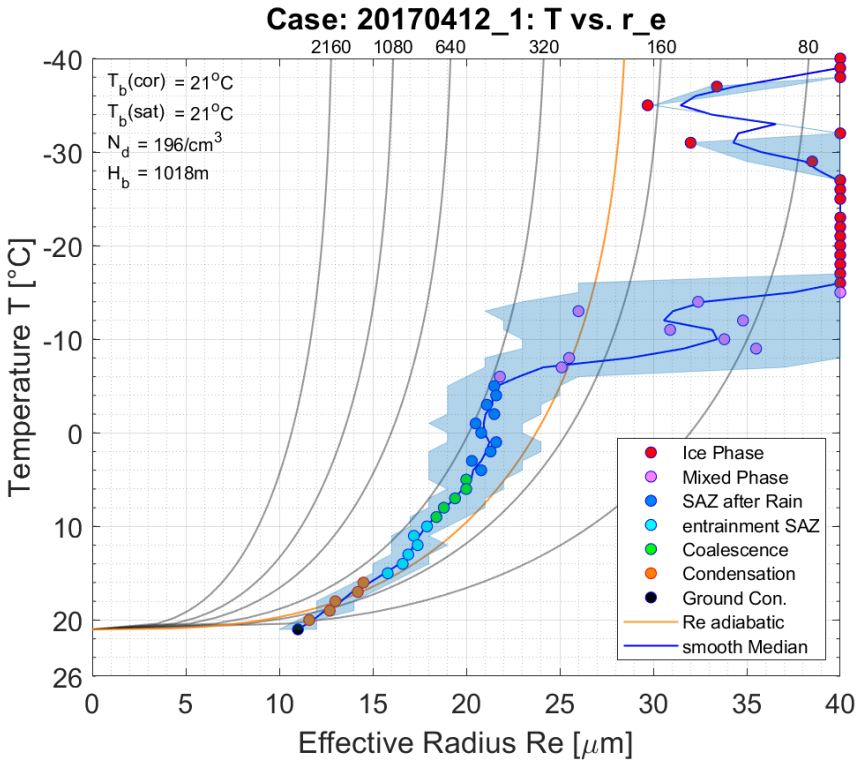


**Figure 7.** Entrainment can occur in clouds with weak updrafts at cloud base that can become unstable and introduce additional entrainment of dry air reducing the local supersaturation vaporize some already activated droplets and removing water from the cloud. the reduces surface area and high instability can lead to a surge in supersaturation leading to more activation above the initial activation at cloud base. This mostly can be observed in very clean environments during the dry season.

CHAPTER 3

# Conclusions and Outlook

**Conclusions and Future research perspectives**

The aerosol-induced effects on convective clouds in the Amazonian rain-forest are high even in the polluted dry season. A remarkably large fraction of aerosol particles act as cloud condensation nuclei (CCN) in the Amazonian clouds, not only during the pristine aerosol conditions during the wet season, but also during the dry season. The fraction of activated particles was higher than expected from previous studies. It was found that the cloud formation in the Amazon is both, aerosol- and updraft-sensitive, not just in the predominately low aerosol abundance during the wet season, as previously assumed, but also in the dry season with heavy biomass burning smoke present. The annual average aerosol load in the Amazon is representative for a large region on the globe. There are globally only few regions with a significantly larger CCN concentration. Follow-up studies on this finding should investigate how these results change our understanding of the aerosol effects on clouds and climate on a global scale. Simple equations are provided, which can be used in models and which can be compared to our current understanding using models with different aerosol and cloud parametrizations.

Furthermore, when extending the analysis of $T$-$r_{\mathrm{e}}$ profiles above the initial condensational droplet growth, cloud microphysical zones were determined and reliably detected. This provided a more detailed picture of the vertical distribution of cloud microphysical zones and confirmed the occurrence of secondary activation of aerosols, that were not activate at cloud base. Secondary activation appears to have a significant impact on cloud development, as shown by models and in-situ flight data before. It is shown that secondary activation enables clouds to extend their vertical height, due to additional release of latent heat after warm rain out, that invigorates updrafts and extends the total water content height and lifetime of the clouds. Secondary activation has the biggest impact during the transitional and rain season when the total aerosol load is low enough to initiate warm rain out. In contrast during the dry season, droplets often do not grow to the size necessary for rain out before reaching freezing temperatures. A result is an increased height of the mixed phase during the Amazonian transition periods and wet season compared the dry season, based on the newly developed approach for cloud zone detection via remote sensing.

# Bibliography


Andreae, M. O.: "Correlation between cloud condensation nuclei concentration and aerosol optical thickness in remote and polluted regions". *Atmospheric Chemistry and Physics*, 9, 2. (2009), pp. 543–556. URL: <GotoISI>://WOS:000263325700013.

Andreae, M. O.; Acevedo, O. C.; Araùjo, A.; Artaxo, P.; Barbosa, C. G. G.; Barbosa, H. M. J.; Brito, J.; Carbone, S.; Chi, X.; Cintra, B. B. L.; Silva, N. F. da; Dias, N. L.; Dias-Júnior, C. Q.; Ditas, F.; Ditz, R.; Godoi, A. F. L.; Godoi, R. H. M.; Heimann, M.; Hoffmann, T.; Kesselmeier, J.; Könemann, T.; Krüger, M. L.; Lavric, J. V.; Manzi, A. O.; Moran-Zuloaga, D.; Nölscher, A. C.; Santos Nogueira, D.; Piedade, M. T. F.; Pöhlker, C.; Pöschl, U.; Rizzo, L. V.; Ro, C. U.; Ruckteschler, N.; Sá, L. D. A.; Sá, M. D. O.; Sales, C. B.; Santos, R. M. N. D.; Saturno, J.; Schöngart, J.; Sörgel, M.; Souza, C. M. de; Souza, R. A. F. de; Su, H.; Targhetta, N.; Tóta, J.; Trebs, I.; Trumbore, S.; Eijck, A. van; Walter, D.; Wang, Z.; Weber, B.; Williams, J.; Winderlich, J.; Wittmann, F.; Wolff, S., and Yáñez-Serrano, A. M.: "The amazon tall tower observatory (atto): overview of pilot measurements on ecosystem ecology, meteorology, trace gases, and aerosols". *Atmos. Chem. Phys.*, 15. (2015), pp. 10723–10776. DOI: 10.5194/acp-15-10723-2015.

Andreae, M. O.; Afchine, A.; Albrecht, R.; Holanda, B. A.; Artaxo, P.; Barbosa, H. M. J.; Borrmann, S.; Cecchini, M. A.; Costa, A.; Dollner, M.; Fütterer, D.; Järvinen, E.; Jurkat, T.; Klimach, T.; Konemann, T.; Knote, C.; Krämer, M.; Krisna, T.; Machado, L. A. T.; Mertes, S.; Minikin, A.; Pöhlker, C.; Pöhlker, M. L.; Pöschl, U.; Rosenfeld, D.; Sauer, D.; Schlager, H.; Schnaiter, M.; Schneider, J.; Schulz, C.; Spanu, A.; Sperling, V. B.; Voigt, C.; Walser, A.; Wang, J.; Weinzierl, B.; Wendisch, M., and Ziereis, H.: "Aerosol characteristics and particle production in the upper troposphere over the amazon basin". *Atmos. Chem. Phys.*, 18, 2. (2018), pp. 921–961. DOI: 10.5194/acp-18-921-2018. URL: https://www.atmos-chem-phys.net/18/921/2018/.

Andreae, M. O. and Rosenfeld, D.: "Aerosol-cloud-precipitation interactions. part 1. the nature and sources of cloud-active aerosols". *Earth-Science Reviews*, 89, 1-2. (2008), pp. 13–41. DOI: 10.1016/j.earscirev.2008.03.001. URL: <GotoISI>://000257534400002.

Andreae, M. O.; Rosenfeld, D.; Artaxo, P.; Costa, A. A.; Frank, G. P.; Longo, K. M., and Silva-Dias, M. A. F.: "Smoking rain clouds over the amazon". *Science*, 303, 5662. (2004), pp. 1337–1342. DOI: 10.1126/science.1092779. URL: <GotoISI>://WOS:000189238600042.

Avissar, R.; Silva Dias, P. L.; Silva Dias, M. A. F., and Nobre, C.: "The large-scale biosphere-atmosphere experiment in amazonia (lba): insights and future research

needs". *Journal of Geophysical Research: Atmospheres*, 107, D20. (2002), LBA 54–1–LBA 54–6. DOI: 10.1029/2002JD002704. URL: https://doi.org/10.1029/2002JD002704.

Baustian, K. J.; Cziczo, D. J.; Wise, M. E.; Pratt, K. A.; Kulkarni, G.; Hallar, A. G., and Tolbert, M. A.: "Importance of aerosol composition, mixing state, and morphology for heterogeneous ice nucleation: a combined field and laboratory approach". *Journal of Geophysical Research-Atmospheres*, 117. (2012). DOI: 10.1029/2011jd016784. URL: <GotoISI>://WOS:000302237100003.

Bigg, E. K.: "The formation of atmospheric ice crystals by the freezing of droplets". *Quarterly Journal of the Royal Meteorological Society*, 79, 342. (1953), pp. 510–519. DOI: https://doi.org/10.1002/qj.49707934207. eprint: https://rmets.onlinelibrary.wiley.com/doi/pdf/10.1002/qj.49707934207. URL: https://rmets.onlinelibrary.wiley.com/doi/abs/10.1002/qj.49707934207.

Braga, R. C.; Rosenfeld, D.; Krüger, O. O.; Ervens, B.; Holanda, B. A.; Wendisch, M.; Krisna, T.; Pöschl, U.; Andreae, M. O.; Voigt, C., and Pöhlker, M. L.: "Linear relationship between effective radius and precipitation water content near the top of convective clouds: measurement results from acridicon–chuva campaign". *Atmospheric Chemistry and Physics*, 21, 18. (2021), pp. 14079–14088. DOI: 10.5194/acp-21-14079-2021. URL: https://acp.copernicus.org/articles/21/14079/2021/.

Braga, R. C.; Rosenfeld, D.; Weigel, R.; Jurkat, T.; Andreae, M. O.; Wendisch, M.; Pöhlker, M. L.; Klimach, T.; Pöschl, U.; Pöhlker, C.; Voigt, C.; Mahnke, C.; Borrmann, S.; Albrecht, R. I.; Molleker, S.; Vila, D. A.; Machado, L. A. T., and Artaxo, P.: "Comparing parameterized versus measured microphysical properties of tropical convective cloud bases during the acridicon–chuva campaign". *Atmos. Chem. Phys.*, 17, 12. (2017), pp. 7365–7386. DOI: 10.5194/acp-17-7365-2017. URL: https://www.atmos-chem-phys.net/17/7365/2017/.

Braham, R. R.: "What is the role of ice in summer rain-showers?" *Journal of Atmospheric Sciences*, 21, 6. (1964), pp. 640 –645. DOI: 10.1175/1520-0469(1964)021<0640:WITROI>2.0.CO;2. URL: https://journals.ametsoc.org/view/journals/atsc/21/6/1520-0469_1964_021_0640_witroi_2_0_co_2.xml.

Campos Braga, R.; Ervens, B.; Rosenfeld, D.; Andreae, M.; Förster, J.-D.; Fütterer, D.; Hernández Pardo, L.; Holanda, B.; Jurkat, T.; Krüger, O.; Lauer, O.; Machado, L.; Pöhlker, C.; Sauer, D.; Voigt, C.; Walser, A.; Wendisch, M.; Pöschl, U., and Pöhlker, M.: "Cloud droplet number closure for tropical convective clouds during the ACRIDICON–CHUVA campaign". *Atmospheric Chemistry and Physics Discussions*. (2021), pp. 1–17. DOI: 10.5194/acp-2021-80.

Carslaw, K. S.; Lee, L. A.; Reddington, C. L.; Pringle, K. J.; Rap, A.; Forster, P. M.; Mann, G. W.; Spracklen, D. V.; Woodhouse, M. T.; Regayre, L. A., and Pierce, J. R.: "Large contribution of natural aerosols to uncertainty in indirect forcing". *Nature*, 503, 7474. (2013), pp. 67–71. DOI: 10.1038/nature12674. URL: <GotoISI>://WOS:000326585600033.

Cecchini, M. A.; Machado, L. A. T.; Andreae, M. O.; Martin, S. T.; Albrecht, R. I.; Artaxo, P.; Barbosa, H. M. J.; Borrmann, S.; Fütterer, D.; Jurkat, T.; Mahnke, C.; Minikin, A.; Molleker, S.; Pöhlker, M. L.; Pöschl, U.; Rosenfeld, D.; Voigt, C.; Wenzierl, B., and Wendisch, M.: "Sensitivities of amazonian clouds to aerosols and

updraft speed". *Atmos. Chem. Phys. Discuss.*, 2017. (2017), pp. 1–23. DOI: 10.5194/acp-2017-89. URL: https://www.atmos-chem-phys-discuss.net/acp-2017-89/.

Colarco, P.; Silva, A. da; Chin, M., and Diehl, T.: "Online simulations of global aerosol distributions in the nasa geos-4 model and comparisons to satellite and ground-based aerosol optical depth". *Journal of Geophysical Research: Atmospheres*, 115, D14. (2010). DOI: 10.1029/2009jd012820. URL: https://agupubs.onlinelibrary.wiley.com/doi/abs/10.1029/2009JD012820.

D Rosenfeld WL Woodley, T. K. V. M.: "Aircraft microphysical documentation from cloud base to anvils of hailstorm feeder clouds in Argentina". *J. Appl. Meteorol. Climatol.*, 45, 9. (2006), pp. 1261–1281. DOI: 10.1175/jam2403.1.

Davidson, E. A.; Araujo, A. C. de; Artaxo, P.; Balch, J. K.; Brown, I. F.; Bustamante, M. M. C.; Coe, M. T.; DeFries, R. S.; Keller, M.; Longo, M.; Munger, J. W.; Schroeder, W.; Soares-Filho, B. S.; Souza Carlos M., J., and Wofsy, S. C.: "The amazon basin in transition". *Nature*, 481, 7381. (2012), pp. 321–328. DOI: 10.1038/nature10717. URL: <GotoISI>://WOS:000299210600034.

Derksen, J. W. B.; Roelofs, G. J. H., and Rockmann, T.: "Influence of entrainment of ccn on microphysical properties of warm cumulus". *Atmospheric Chemistry and Physics*, 9, 16. (2009), pp. 6005–6015. DOI: 10.5194/acp-9-6005-2009. URL: <GotoISI>://WOS:000269404000010.

Dusek, U.; Frank, G. P.; Curtius, J.; Drewnick, F.; Schneider, J.; Kürten, A.; Rose, D.; Andreae, M. O.; Borrmann, S., and Pöschl, U.: "Enhanced organic mass fraction and decreased hygroscopicity of cloud condensation nuclei (ccn) during new particle formation events". *Geophysical Research Letters*, 37, 3. (2010). DOI: 10.1029/2009gl040930. URL: https://agupubs.onlinelibrary.wiley.com/doi/abs/10.1029/2009GL040930.

Efraim, A.; Campos Braga, R.; Rosenfeld, D.; Lauer, O.; Franco, M. A.; Kremper, L. A.; Pöhlker, C., and Pöhlker, M. L.: "Satellite-based detection of secondary droplet activation during condensational growth in convective clouds". *Submitted to Journal of Geophysical Research: Atmospheres*. (2022).

Efraim, A.; Lauer, O.; Rosenfeld, D.; Braga, R. C.; Franco, M. A.; Kremper, L. A.; Zhu, Y.; Pöschl, U.; Pöhlker, C.; Andreae, M. O.; Artaxo, P.; Araújo, A. C. de, and Pöhlker, M. L.: "Satellite-Based Detection of Secondary Droplet Activation in Convective Clouds". *Journal of Geophysical Research: Atmospheres*, 127, 12. (2022). DOI: 10.1029/2022JD036519.

Fan, J.; Rosenfeld, D.; Zhang, Y.; Giangrande, S. E.; Li, Z.; Machado, L. A. T.; Martin, S. T.; Yang, Y.; Wang, J.; Artaxo, P.; Barbosa, H. M. J.; Braga, R. C.; Comstock, J. M.; Feng, Z.; Gao, W.; Gomes, H. B.; Mei, F.; Pöhlker, C.; Pöhlker, M. L.; Pöschl, U., and Souza, R. A. F. de: "Substantial convection and precipitation enhancements by ultrafine aerosol particles". *Science*, 359, 6374. (2018), pp. 411–418. DOI: 10.1126/science.aan8461. URL: http://science.sciencemag.org/content/sci/359/6374/411.full.pdf.

Fan, J.; Rosenfeld, D.; Zhang, Y.; Giangrande, S. E.; Li, Z.; Machado, L. A.; Martin, S. T.; Yang, Y.; Wang, J.; Artaxo, P.; Barbosa, H. M.; Braga, R. C.; Comstock, J. M.; Feng, Z.; Gao, W.; Gomes, H. B.; Mei, F.; Pöhlker, C.; Pöhlker, M. L.; Pöschl, U., and De Souza, R. A.: "Substantial convection and precipitation enhancements by

ultrafine aerosol particles". *Science*, 359, 6374. (2018), pp. 411–418. DOI: 10.1126/science.aan8461.

FISCH, G.; MARENGO, J. A., and NOBRE, C. A.: "The climate of Amazonia - a review". *Acta Amazonica*, 28, 2. (1998), pp. 101–101. DOI: 10.1590/1809-4392199828212 6. URL: http://www.scielo.br/j/aa/a/NVRbNSn7P5z4hjtFNmMjLjx/abstract/?lang=en.

Forster, P.; Storelvmo, T.; Armour, K.; Collins, W.; Dufresne, J.-L.; Frame, D.; Lunt, D.; Mauritsen, T.; Palmer, M.; Watanabe, M.; Wild, M., and Zhang, H.: "The earth's energy budget, climate feedbacks, and climate sensitivity". In: *Climate Change 2021: The Physical Science Basis. Contribution of Working Group I to the Sixth Assessment Report of the Intergovernmental Panel on Climate Change*. Ed. by V. Masson-Delmotte; P. Zhai; A. Pirani; S. Connors; C. Péan; S. Berger; N. Caud; Y. Chen; L. Goldfarb; M. Gomis; M. Huang; K. Leitzell; E. Lonnoy; J. Matthews; T. Maycock; T. Waterfield; O. Yelekçi; R. Yu, and B. Zhou. Cambridge, United Kingdom and New York, NY, USA: Cambridge University Press, 2021. Chap. 7.

Freud, E.; Rosenfeld, D.; Andreae, M. O.; Costa, A. A., and Artaxo, P.: "Robust relations between ccn and the vertical evolution of cloud drop size distribution in deep convective clouds". *Atmospheric Chemistry and Physics*, 8, 6. (2008), pp. 1661–1675. URL: <GotoISI>://WOS:000254416700014.

Hamilton, D. S.: "Natural aerosols and climate: understanding the unpolluted atmosphere to better understand the impacts of pollution". *Weather*, 70, 9. (2015), pp. 264–268. DOI: 10.1002/wea.2540. URL: <GotoISI>://WOS:000360806600009.

Hamilton, D. S.; Lee, L. A.; Pringle, K. J.; Reddington, C. L.; Spracklen, D. V., and Carslaw, K. S.: "Occurrence of pristine aerosol environments on a polluted planet". *Proceedings of the National Academy of Sciences of the United States of America*, 111, 52. (2014), pp. 18466–18471. DOI: 10.1073/pnas.1415440111. URL: <GotoISI>://WOS:000347444400030.

Heiblum, R. H.; Koren, I., and Feingold, G.: "On the link between amazonian forest properties and shallow cumulus cloud fields". *Atmospheric Chemistry and Physics*, 14, 12. (2014), pp. 6063–6074. DOI: 10.5194/acp-14-6063-2014. URL: <GotoISI>://WOS:000338438300013.

Heintzenberg, J.: "Properties of the log-normal particle size distribution". *Aerosol Science and Technology*, 21, 1. (1994), pp. 46–48. DOI: 10.1080/02786829408959695. URL: https://doi.org/10.1080/02786829408959695.

Holanda, B. A.; Pöhlker, M. L.; Walter, D.; Saturno, J.; Sörgel, M.; Ditas, J.; Ditas, F.; Schulz, C.; Franco, M. A.; Wang, Q.; Donth, T.; Artaxo, P.; Barbosa, H. M. J.; Borrmann, S.; Braga, R.; Brito, J.; Cheng, Y.; Dollner, M.; Kaiser, J. W.; Klimach, T.; Knote, C.; Krüger, O. O.; Fütterer, D.; Lavrič, J. V.; Ma, N.; Machado, L. A. T.; Ming, J.; Morais, F. G.; Paulsen, H.; Sauer, D.; Schlager, H.; Schneider, J.; Su, H.; Weinzierl, B.; Walser, A.; Wendisch, M.; Ziereis, H.; Zöger, M.; Pöschl, U.; Andreae, M. O., and Pöhlker, C.: "Influx of african biomass burning aerosol during the amazonian dry season through layered transatlantic transport of black carbon-rich smoke". *Atmos. Chem. Phys.*, 20, 8. (2020), pp. 4757–4785. DOI: 10.5194/acp-20-4757-2020. URL: https://www.atmos-chem-phys.net/20/4757/2020/.

Hoose, C.; Kristjansson, J. E., and Burrows, S. M.: "How important is biological ice nucleation in clouds on a global scale?" *Environmental Research Letters*, 5, 2. (2010). DOI: 10.1088/1748-9326/5/2/024009. URL: <GotoISI>://000279369500010.

Hoppel, W. A.; Frick, G. M., and Fitzgerald, J. W.: "Deducing droplet concentration and supersaturation in marine boundary layer clouds from surface aerosol measurements". *Journal of Geophysical Research-Atmospheres*, 101, D21. (1996), pp. 26553–26565. DOI: 10.1029/96jd02243. URL: <GotoISI>://WOS:A1996VW42100034.

Johnson, D. B.: "On the relative efficiency of coalescence and riming". *Journal of Atmospheric Sciences*, 44, 13. (1987), pp. 1671 –1680. DOI: 10.1175/1520-0469(1987)044<1671:OTREOC>2.0.CO;2. URL: https://journals.ametsoc.org/view/journals/atsc/44/13/1520-0469_1987_044_1671_otreoc_2_0_co_2.xml.

Khain, A. P.; Phillips, V.; Benmoshe, N., and Pokrovsky, A.: "The role of small soluble aerosols in the microphysics of deep maritime clouds". *Journal of the Atmospheric Sciences*, 69, 9. (2012), pp. 2787–2807. DOI: 10.1175/2011jas3649.1. URL: <GotoISI>://WOS:000308280400010.

Kristiansen, N. I.; Stohl, A.; Olivié, D. J. L.; Croft, B.; Søvde, O. A.; Klein, H.; Christoudias, T.; Kunkel, D.; Leadbetter, S. J.; Lee, Y. H.; Zhang, K.; Tsigaridis, K.; Bergman, T.; Evangeliou, N.; Wang, H.; Ma, P.-L.; Easter, R. C.; Rasch, P. J.; Liu, X.; Pitari, G.; Di Genova, G.; Zhao, S. Y.; Balkanski, Y.; Bauer, S. E.; Faluvegi, G. S.; Kokkola, H.; Martin, R. V.; Pierce, J. R.; Schulz, M.; Shindell, D.; Tost, H., and Zhang, H.: "Evaluation of observed and modelled aerosol lifetimes using radioactive tracers of opportunity and an ensemble of 19 global models". *Atmospheric Chemistry and Physics*, 16, 5. (2016), pp. 3525–3561. DOI: 10.5194/acp-16-3525-2016. URL: https://acp.copernicus.org/articles/16/3525/2016/.

Krüger, M. L.; Mertes, S.; Klimach, T.; Cheng, Y. F.; Su, H.; Schneider, J.; Andreae, M. O.; Pöschl, U., and Rose, D.: "Assessment of cloud supersaturation by size-resolved aerosol particle and cloud condensation nuclei (ccn) measurements". *Atmos. Meas. Tech.*, 7, 8. (2014), pp. 2615–2629. DOI: 10.5194/amt-7-2615-2014. URL: http://www.atmos-meas-tech.net/7/2615/2014/.

Kulmala, M.; Dal Maso, M.; Makela, J. M.; Pirjola, L.; Vakeva, M.; Aalto, P.; Miikkulainen, P.; Hameri, K., and O'Dowd, C. D.: "On the formation, growth and composition of nucleation mode particles". *Tellus Series B-Chemical and Physical Meteorology*, 53, 4. (2001), pp. 479–490. DOI: 10.1034/j.1600-0889.2001.530411.x. URL: <GotoISI>://WOS:000171133400011.

Kulmala, M.; Vehkamaki, H.; Petaja, T.; Dal Maso, M.; Lauri, A.; Kerminen, V. M.; Birmili, W., and McMurry, P. H.: "Formation and growth rates of ultrafine atmospheric particles: a review of observations". *Journal of Aerosol Science*, 35, 2. (2004), pp. 143–176. DOI: 10.1016/j.jaerosci.2003.10.003. URL: <GotoISI>://WOS:000188832200002.

Kunert, A. T.; Pöhlker, M. L.; Tang, K.; Krevert, C. S.; Wieder, C.; Speth, K. R.; Hanson, L. E.; Morris, C. E.; Schmale, D. G.; Pöschl, U., and Fröhlich-Nowoisky, J.: "Macromolecular fungal ice nuclei in Fusarium: Effects of physical and chemical

processing". *Biogeosciences*, 16, 23. (2019), pp. 4647–4659. DOI: 10.5194/BG-16-4647-2019.

Köhler, H.: "The nucleus in and the growth of hygroscopic droplets". *Transactions of the Faraday Society*, 32, 2. (1936), pp. 1152–1161. DOI: 10.1039/tf9363201152. URL: <GotoISI>://WOS:000202778200017.

Lauer, O.; Andreae, M. O.; Artaxo, P.; Campos Braga, R.; Efraim, A.; Kremper, L. A.; Franco Marco A.and Pöschl, U.; Zheng, Y.; Zhu, Y.; Rosenfeld, D., and Pöhlker, M. L.: "Cloud Microphysical Zones in the Amazon". *In Preparation*. (2022).

Lauer, O.; Kremper, L. A.; Rosenfeld, D.; Franco, M. A.; Andreae, M. O.; Artaxo, P.; Campos Braga, R.; Dias-Júnior, C. Q.; Araújo, A. C. de; Ditas, F.; Efraim, A.; Ervens, B.; Holanda, B. A.; Jungandreas, L.; Krüger, O. O.; Machado, L. A. T.; Hernández Pardo, L.; Pöschl, U.; Pulik, G.; Quaas, J.; Zheng, Y.; Zhu, Y.; Pöhlker, C., and Pöhlker, M. L.: "High aerosol sensitivity of Amazonian clouds throughout the seasons". *To be submitted*. (2022).

Lohmann, U. and Feichter, J.: "Global indirect aerosol effects: a review". *Atmospheric Chemistry and Physics*, 5. (2005), pp. 715–737. URL: <GotoISI>://000227375000002.

Lohmann, U.: "Anthropogenic Aerosol Influences on Mixed-Phase Clouds". *Current Climate Change Reports*, 3, 1. (2017), pp. 32–44. DOI: 10.1007/S40641-017-0059-9/FIGURES/4. URL: https://link.springer.com/article/10.1007/s40641-017-0059-9.

Machado, L. A. T.; Calheiros, A. J. P.; Biscaro, T.; Giangrande, S.; Dias, M.; Cecchini, M. A.; Albrecht, R.; Andreae, M. O.; Araujo, W. F.; Artaxo, P.; Borrmann, S.; Braga, R.; Burleyson, C.; Eichholz, C. W.; Fan, J. W.; Feng, Z.; Fisch, G. F.; Jensen, M. P.; Martin, S. T.; Poschl, U.; Pohlker, C.; Pohlker, M. L.; Ribaud, J. F.; Rosenfeld, D.; Saraiva, J. M. B.; Schumacher, C.; Thalman, R.; Walter, D., and Wendisch, M.: "Overview: precipitation characteristics and sensitivities to environmental conditions during goamazon2014/5 and acridicon-chuva". *Atmospheric Chemistry and Physics*, 18, 9. (2018), pp. 6461–6482. DOI: 10.5194/acp-18-6461-2018. URL: <GotoISI>://WOS:000431588500005.

McFiggans, G.; Artaxo, P.; Baltensperger, U.; Coe, H.; Facchini, M. C.; Feingold, G.; Fuzzi, S.; Gysel, M.; Laaksonen, A.; Lohmann, U.; Mentel, T. F.; Murphy, D. M.; O'Dowd, C. D.; Snider, J. R., and Weingartner, E.: "The effect of physical and chemical aerosol properties on warm cloud droplet activation". *Atmospheric Chemistry and Physics*, 6. (2006), pp. 2593–2649. URL: <GotoISI>://WOS:000238823900001.

Molion, L.: "Amazonian Rainfall and Its Variability". *Hydrology and water Management in the Humid Tropics*. (1993).

Moran-Zuloaga, D.; Ditas, F.; Walter, D.; Saturno, J.; Brito, J.; Carbone, S.; Chi, X.; Angelis, I. Hrabě de; Baars, H.; Godoi, R. H. M.; Heese, B.; Holanda, B. A.; Lavrič, J. V.; Martin, S. T.; Ming, J.; Pöhlker, M. L.; Ruckteschler, N.; Su, H.; Wang, Y.; Wang, Q.; Wang, Z.; Weber, B.; Wolff, S.; Artaxo, P.; Pöschl, U.; Andreae, M. O., and Pöhlker, C.: "Long-term study on coarse mode aerosols in the amazon rain forest with the frequent intrusion of saharan dust plumes". *Atmos. Chem. Phys.*, 18, 13. (2018), pp. 10055–10088. DOI: 10.5194/acp-18-10055-2018. URL: https://www.atmos-chem-phys.net/18/10055/2018/.

Nölscher, A. C.; Yanez-Serrano, A. M.; Wolff, S.; Araujo, A. C. de; Lavric, J. V.; Kesselmeier, J., and Williams, J.: "Unexpected seasonality in quantity and composition of amazon rainforest air reactivity". *Nature Communications*, 7. (2016), pp. 1–12. DOI: 10.1038/ncomms10383. URL: <GotoISI>://WOS:000369019200002.

Penner, J.: *Carbonaceous aerosols influencing atmospheric radiation: Black and organic carbon*. Report. 1994. URL: http://www.osti.gov/energycitations/servlets/purl/10118242-yeKNsw/webviewable/.

Petters, M. D. and Kreidenweis, S. M.: "A single parameter representation of hygroscopic growth and cloud condensation nucleus activity". *Atmospheric Chemistry and Physics*, 7, 8. (2007), pp. 1961–1971. URL: <GotoISI>://WOS:000246455500005.

Pinsky, M.; Khain, A.; Mazin, I., and Korolev, A.: "Analytical estimation of droplet concentration at cloud base". *Journal of Geophysical Research-Atmospheres*, 117. (2012). DOI: 10.1029/2012jd017753. URL: <GotoISI>://WOS:000309417700002.

Pinsky, M. and Khain, A.: "Some effects of cloud turbulence on water–ice and ice–ice collisions". *Atmospheric Research*, 47-48. (1998), pp. 69–86. DOI: https://doi.org/10.1016/S0169-8095(98)00041-6. URL: https://www.sciencedirect.com/science/article/pii/S0169809598000416.

Pöhlker, M. L.; Zhang, M.; Campos Braga, R.; Krüger, O. O.; Pöschl, U., and Ervens, B.: "Aitken mode particles as CCN in aerosol- And updraft-sensitive regimes of cloud droplet formation". *Atmospheric Chemistry and Physics*, 21, 15. (2021), pp. 11723–11740. DOI: 10.5194/ACP-21-11723-2021.

Pruppacher, H. R. and Klett, J. D.: *Microphysics of Clouds and Precipitation, 2nd Edition*. Dordrecht: Kluwer Academic Publishers, 1997.

Pöhlker, C.; Walter, D.; Paulsen, H.; Könemann, T.; Rodríguez-Caballero, E.; Moran-Zuloaga, D.; Brito, J.; Carbone, S.; Degrendele, C.; Després, V. R.; Ditas, F.; Holanda, B. A.; Kaiser, J. W.; Lammel, G.; Lavrič, J. V.; Ming, J.; Pickersgill, D.; Pöhlker, M. L.; Praß, M.; Löbs, N.; Saturno, J.; Sörgel, M.; Wang, Q.; Weber, B.; Wolff, S.; Artaxo, P.; Pöschl, U., and Andreae, M. O.: "Land cover and its transformation in the backward trajectory footprint region of the amazon tall tower observatory". *Atmos. Chem. Phys.*, 19, 13. (2019), pp. 8425–8470. DOI: 10.5194/acp-19-8425-2019. URL: https://www.atmos-chem-phys.net/19/8425/2019/.

Pöhlker, M. L.; Ditas, F.; Saturno, J.; Klimach, T.; Angelis, I. Hrabě de; Araùjo, A. C.; Brito, J.; Carbone, S.; Cheng, Y.; Chi, X.; Ditz, R.; Gunthe, S. S.; Holanda, B. A.; Kandler, K.; Kesselmeier, J.; Könemann, T.; Krüger, O. O.; Lavrič, J. V.; Martin, S. T.; Mikhailov, E.; Moran-Zuloaga, D.; Rizzo, L. V.; Rose, D.; Su, H.; Thalman, R.; Walter, D.; Wang, J.; Wolff, S.; Barbosa, H. M. J.; Artaxo, P.; Andreae, M. O.; Pöschl, U., and Pöhlker, C.: "Long-term observations of cloud condensation nuclei over the amazon rain forest – part 2: variability and characteristics of biomass burning, long-range transport, and pristine rain forest aerosols". *Atmos. Chem. Phys.*, 18, 14. (2018), pp. 10289–10331. DOI: 10.5194/acp-18-10289-2018. URL: https://www.atmos-chem-phys.net/18/10289/2018/.

Pöhlker, M. L.; Pöhlker, C.; Klimach, T.; Angelis, I. Hrabe de; Barbosa, H. M. J.; Brito, J.; Carbone, S.; Cheng, Y.; Chi, X.; Ditas, F.; Ditz, R.; Gunthe, S. S.; Kesselmeier, J.; Könemann, T.; Lavrič, J. V.; Martin, S. T.; Moran-Zuloaga, D.; Rose, D.; Saturno, J.; Su, H.; Thalman, R.; Walter, D.; Wang, J.; Wolff, S.; Artaxo, P.; Andreae, M. O., and Pöschl, U.: "Long-term observations of cloud condensation nuclei in the amazon rain forest – part 1: aerosol size distribution, hygroscopicity, and new model parameterizations for ccn prediction". *Atmos. Chem. Phys.*, 16. (2016), pp. 15709–15740. DOI: 10.5194/acp-2016-519. URL: http://www.atmos-chem-phys-discuss.net/acp-2016-519/.

Pöschl, U.: "Atmospheric aerosols: composition, transformation, climate and health effects". *Angewandte Chemie-International Edition*, 44, 46. (2005), pp. 7520–7540. DOI: 10.1002/anie.200501122. URL: <GotoISI>://WOS:000233694800004.

Quaas, J.; Arola, A.; Cairns, B.; Christensen, M.; Deneke, H.; Ekman, A. M.; Feingold, G.; Fridlind, A.; Gryspeerdt, E.; Hasekamp, O.; Li, Z.; Lipponen, A.; Mülmenstädt, J.; Nenes, A.; Penner, J. E.; Rosenfeld, D.; Schrödner, R.; Sinclair, K.; Sourdeval, O.; Stier, P.; Tesche, M.; Van Diedenhoven, B., and Wendisch, M.: "Constraining the Twomey effect from satellite observations: Issues and perspectives". *Atmospheric Chemistry and Physics*, 20, 23. (2020), pp. 15079–15099. DOI: 10.5194/ACP-20-15079-2020.

Reutter, P.; Su, H.; Trentmann, J.; Simmel, M.; Rose, D.; Gunthe, S. S.; Wernli, H.; Andreae, M. O., and Poschl, U.: "Aerosol- and updraft-limited regimes of cloud droplet formation: influence of particle number, size and hygroscopicity on the activation of cloud condensation nuclei (ccn)". *Atmospheric Chemistry and Physics*, 9, 18. (2009), pp. 7067–7080. URL: <GotoISI>://WOS:000270131400025.

Rosenfeld, D.; Andreae, M. O.; Asmi, A.; Chin, M.; Leeuw, G. de; Donovan, D. P.; Kahn, R.; Kinne, S.; Kivekas, N.; Kulmala, M.; Lau, W.; Schmidt, K. S.; Suni, T.; Wagner, T.; Wild, M., and Quaas, J.: "Global observations of aerosol-cloud-precipitation-climate interactions". *Reviews of Geophysics*, 52, 4. (2014), pp. 750–808. DOI: 10.1002/2013rg000441. URL: <GotoISI>://WOS:000348452000005.

Rosenfeld, D.; Liu, G.; Yu, X.; Zhu, Y.; Dai, J.; Xu, X., and Yue, Z.: "High-resolution (375 m) cloud microstructure as seen from the npp/viirs satellite imager". *Atmospheric Chemistry and Physics*, 14, 5. (2014), pp. 2479–2496. DOI: 10.5194/acp-14-2479-2014. URL: https://acp.copernicus.org/articles/14/2479/2014/.

Rosenfeld, D.; Fishman, B.; Zheng, Y.; Goren, T., and Giguzin, D.: "Combined satellite and radar retrievals of drop concentration and ccn at convective cloud base". *Geophysical Research Letters*, 41. (May 2014). DOI: 10.1002/2014GL059453.

Rosenfeld, D.; Lahav, R.; Khain, A., and Pinsky, M.: "The role of sea spray in cleansing air pollution over ocean via cloud processes". *Science*, 297, 5587. (2002), pp. 1667–1670. DOI: 10.1126/science.1073869.

Rosenfeld, D. and Lensky, I. M.: "Satellite-Based Insights into Precipitation Formation Processes in Continental and Maritime Convective Clouds". *Bulletin of the American Meteorological Society*, 79, 11. (1998), pp. 2457–2476. DOI: 10.1175/1520-0477(1998)079<2457:SBIIPF>2.0.CO;2.

Rosenfeld, D.; Zheng, Y.; Hashimshoni, E.; Pöhlker, M. L.; Jefferson, A.; Pöhlker, C.; Yu, X.; Zhu, Y.; Liu, G.; Yue, Z.; Fischman, B.; Li, Z.; Giguzin, D.; Goren, T.; Artaxo, P.; Barbosa, H. M. J.; Pöschl, U., and Andreae, M. O.: "Satellite retrieval of cloud condensation nuclei concentrations by using clouds as ccn chambers". *Proceedings of the National Academy of Sciences*, 113, 21. (2016), pp. 5828–5834. DOI: 10.1073/pnas.1514044113. URL: http://www.pnas.org/content/113/21/5828.abstract.

Saturno, J.; Pöhlker, C.; Massabò, D.; Brito, J.; Carbone, S.; Cheng, Y.; Chi, X.; Ditas, F.; Angelis, I. Hrabě de; Morán-Zuloaga, D.; Pöhlker, M. L.; Rizzo, L. V.; Walter, D.; Wang, Q.; Artaxo, P.; Prati, P., and Andreae, M. O.: "Comparison of different aethalometer correction schemes and a reference multi-wavelength absorption technique for ambient aerosol data". *Atmos. Meas. Tech.*, 10, 8. (2017), pp. 2837–2850. DOI: 10.5194/amt-10-2837-2017. URL: https://www.atmos-meas-tech.net/10/2837/2017/.

Schnell, R. C. and Vali, G.: "Atmospheric ice nuclei from decomposing vegetation". *Nature*, 236, 5343. (1972), pp. 163–&. URL: <GotoISI>://A1972L964100021.

Shinozuka, Y.; Clarke, A. D.; DeCarlo, P. F.; Jimenez, J. L.; Dunlea, E. J.; Roberts, G. C.; Tomlinson, J. M.; Collins, D. R.; Howell, S. G.; Kapustin, V. N.; McNaughton, C. S., and Zhou, J.: "Aerosol optical properties relevant to regional remote sensing of ccn activity and links to their organic mass fraction: airborne observations over central mexico and the us west coast during milagro/intex-b". *Atmos. Chem. Phys.*, 9, 18. (2009), pp. 6727–6742. DOI: 10.5194/acp-9-6727-2009. URL: https://www.atmos-chem-phys.net/9/6727/2009/.

Spracklen, D. V. and Heald, C. L.: "The contribution of fungal spores and bacteria to regional and global aerosol number and ice nucleation immersion freezing rates". *Atmos. Chem. Phys.*, 14, 17. (2014), pp. 9051–9059. DOI: 10.5194/acp-14-9051-2014. URL: https://www.atmos-chem-phys.net/14/9051/2014/.

Stevens, B. and Feingold, G.: "Untangling aerosol effects on clouds and precipitation in a buffered system". *Nature*, 461, 7264. (2009), pp. 607–613. DOI: 10.1038/nature08281. URL: <GotoISI>://WOS:000270302600031.

Tobo, Y.; Prenni, A. J.; DeMott, P. J.; Huffman, J. A.; McCluskey, C. S.; Tian, G.; Pöhlker, C.; Pöschl, U., and Kreidenweis, S. M.: "Biological aerosol particles as a key determinant of ice nuclei populations in a forest ecosystem". *Journal of Geophysical Research: Atmospheres*. (2013), n/a–n/a. DOI: 10.1002/jgrd.50801. URL: http://dx.doi.org/10.1002/jgrd.50801.

Twomey, S.: "The nuclei of natural cloud formation—part ii: the supersaturation in natural clouds and the variation of cloud droplet concentration". *Geofis Pura e Appl*, 43. (1959), 243–249.

Wendisch, M.; Pöschl, U.; Andreae, M. O.; Machado, L. A. T.; Albrecht, R.; Schlager, H.; Rosenfeld, D.; Martin, S. T.; Abdelmonem, A.; Afchine, A.; Araùjo, A. C.; Artaxo, P.; Aufmhoff, H.; Barbosa, H. M. J.; Borrmann, S.; Braga, R.; Buchholz, B.; Cecchini, M. A.; Costa, A.; Curtius, J.; Dollner, M.; Dorf, M.; Dreiling, V.; Ebert, V.; Ehrlich, A.; Ewald, F.; Fisch, G.; Fix, A.; Frank, F.; Fütterer, D.; Heckl, C.; Heidelberg, F.; Hüneke, T.; Jäkel, E.; Järvinen, E.; Jurkat, T.; Kanter, S.; Kästner, U.; Kenntner, M.; Kesselmeier, J.; Klimach, T.; Knecht, M.; Kohl, R.; Kölling, T.; Krämer, M.; Krüger, M.; Krisna, T. C.; Lavric, J. V.; Longo, K.; Mahnke, C.; Manzi, A. O.; Mayer,

B.; Mertes, S.; Minikin, A.; Molleker, S.; Münch, S.; Nillius, B.; Pfeilsticker, K.; Pöhlker, C.; Roiger, A.; Rose, D.; Rosenow, D.; Sauer, D.; Schnaiter, M.; Schneider, J.; Schulz, C.; Souza, R. A. F. d.; Spanu, A.; Stock, P.; Vila, D.; Voigt, C.; Walser, A.; Walter, D.; Weigel, R.; Weinzierl, B.; Werner, F.; Yamasoe, M. A.; Ziereis, H.; Zinner, T., and Zöger, M.: "Acridicon–chuva campaign: studying tropical deep convective clouds and precipitation over amazonia using the new german research aircraft halo". *Bulletin of the American Meteorological Society*, 97, 10. (2016), pp. 1885–1908. DOI: 10.1175/bams-d-14-00255.1. URL: http://journals.ametsoc.org/doi/abs/10.1175/BAMS-D-14-00255.1.

Williamson, C. J.; Kupc, A.; Axisa, D.; Bilsback, K. R.; Bui, T.; Campuzano-Jost, P.; Dollner, M.; Froyd, K. D.; Hodshire, A. L.; Jimenez, J. L.; Kodros, J. K.; Luo, G.; Murphy, D. M.; Nault, B. A.; Ray, E. A.; Weinzierl, B.; Wilson, J. C.; Yu, F.; Yu, P.; Pierce, J. R., and Brock, C. A.: "A large source of cloud condensation nuclei from new particle formation in the tropics". *Nature*, 574, 7778. (2019), pp. 399–403. DOI: 10.1038/s41586-019-1638-9. URL: https://doi.org/10.1038/s41586-019-1638-9.

Yue, Z.; Rosenfeld, D.; Liu, G.; Dai, J.; Yu, X.; Zhu, Y.; Hashimshoni, E.; Xu, X.; Hui, Y., and Lauer, O.: "Automated Mapping of Convective Clouds (AMCC) thermodynamical, microphysical, and CCN properties from SNPP/VIIRS satellite data". *Journal of Applied Meteorology and Climatology*, 58, 4. (2019), pp. 887–902. DOI: 10.1175/JAMC-D-18-0144.1.

# Personal List of Publications


Yue, Z.; Rosenfeld, D.; Liu, G.; Dai, J.; Yu, X.; Zhu, Y.; Hashimshoni, E.; Xu, X.; Hui, Y., and Lauer, O.: "Automated Mapping of Convective Clouds (AMCC) thermodynamical, microphysical, and CCN properties from SNPP/VIIRS satellite data". *Journal of Applied Meteorology and Climatology*, 58, 4. (2019), pp. 887–902. DOI: 10.1175/JAMC-D-18-0144.1

Efraim, A.; Lauer, O.; Rosenfeld, D.; Braga, R. C.; Franco, M. A.; Kremper, L. A.; Zhu, Y.; Pöschl, U.; Pöhlker, C.; Andreae, M. O.; Artaxo, P.; Araújo, A. C. de, and Pöhlker, M. L.: "Satellite-Based Detection of Secondary Droplet Activation in Convective Clouds". *Journal of Geophysical Research: Atmospheres*, 127, 12. (2022). DOI: 10.1029/2022JD036519

Campos Braga, R.; Ervens, B.; Rosenfeld, D.; Andreae, M.; Förster, J.-D.; Fütterer, D.; Hernández Pardo, L.; Holanda, B.; Jurkat, T.; Krüger, O.; Lauer, O.; Machado, L.; Pöhlker, C.; Sauer, D.; Voigt, C.; Walser, A.; Wendisch, M.; Pöschl, U., and Pöhlker, M.: "Cloud droplet number closure for tropical convective clouds during the ACRIDICON–CHUVA campaign". *Atmospheric Chemistry and Physics Discussions*. (2021), pp. 1–17. DOI: 10.5194/acp-2021-80

Efraim, A.; Campos Braga, R.; Rosenfeld, D.; Lauer, O.; Franco, M. A.; Kremper, L. A.; Pöhlker, C., and Pöhlker, M. L.: "Satellite-based detection of secondary droplet activation during condensational growth in convective clouds". *Submitted to Journal of Geophysical Research: Atmospheres*. (2022)

Lauer, O.; Kremper, L. A.; Rosenfeld, D.; Franco, M. A.; Andreae, M. O.; Artaxo, P.; Campos Braga, R.; Dias-Júnior, C. Q.; Araújo, A. C. de; Ditas, F.; Efraim, A.; Ervens, B.; Holanda, B. A.; Jungandreas, L.; Krüger, O. O.; Machado, L. A. T.; Hernández Pardo, L.; Pöschl, U.; Pulik, G.; Quaas, J.; Zheng, Y.; Zhu, Y.; Pöhlker, C., and Pöhlker, M. L.: "High aerosol sensitivity of Amazonian clouds throughout the seasons". *To be submitted*. (2022)

Lauer, O.; Andreae, M. O.; Artaxo, P.; Campos Braga, R.; Efraim, A.; Kremper, L. A.; Franco Marco A.and Pöschl, U.; Zheng, Y.; Zhu, Y.; Rosenfeld, D., and Pöhlker, M. L.: "Cloud Microphysical Zones in the Amazon". *In Preparation*. (2022)

# Curriculum Vitae


## Oliver Lauer

Date of birth: 24/05/1988
Place of birth: Frankenthal, Germany
E-mail: oliver.lauer@mpic.de


## Education

12/2016 – present **Doctoral researcher in atmospheric science**
*Max Planck Institute for Chemistry (Mainz, Germany)*
*Project*: "Influence of aerosols on cloud microphysical properties in the Amazon"

10/2017 – 11/2018 **Visiting doctoral researcher**
*Institute of Earth Sciences, The Hebrew University of Jerusalem (Jerusalem, Israel)*

10/2007 – 09/2015 **Diploma as Chemical Engineer**
*Karlsruhe Institute for Technology (KIT, Germany)*
*Project*: "Experimentelle Untersuchung der monoselektiven Elektrodialyse als Methode zur Reduktion der Scalingbildner in hochaufkonzentrierenden Entsalzungsverfahren"

## Teaching Experience

03/2021 – 04/2021 **Grundpraktikum Analytische Chemie**
*Johannes Guthenberg University Mainz, Chemistry Department, Germany*

02/2010 – 03/2010 **Grundlagen der Wasserchemie, Praktikum**
*Karlsruhe Institute of Technology (KIT), Engler Bunte Institute, Germany*